Molecular Modeling and Experimental Insights in the Application of Hydrophobic Deep Eutectic Solvents for Remediation of Micropollutant from Aqueous Systems

A Thesis

Submitted in Partial Fulfilment of the Requirement for the Degree *of*

DOCTOR OF PHILOSOPHY

in

Chemical Engineering

By

Nabendu Paul

Department of Chemical Engineering

Indian Institute of Technology Guwahati

Guwahati-781039, Assam, India

May, 2023

Molecular Modeling and Experimental Insights in the Application of Hydrophobic Deep Eutectic Solvents for Remediation of Micropollutant from Aqueous Systems

A Thesis

Submitted in Partial Fulfilment of the Requirement for the Degree *of*

DOCTOR OF PHILOSOPHY

in

Chemical Engineering

By

Nabendu Paul

Department of Chemical Engineering

Indian Institute of Technology Guwahati

Guwahati-781039, Assam, India

May, 2023

Dedicated to My Parents, Teachers, and Friends

Indian Institute of Technology Guwahati

Department of Chemical Engineering

Statement

I, hereby declare that the content embodied in this thesis entitled **"Molecular Modeling and Experimental Insights in the Application of Hydrophobic Deep Eutectic Solvents for Remediation of Micropollutant from Aqueous Systems"** is the result of investigations carried out by me at the Department of Chemical Engineering, Indian Institute of Technology Guwahati, Guwahati, India, under the supervision of **Prof. Tamal Banerjee.**

In keeping with the general practice of reporting scientific observations, due acknowledgements have been made wherever the work described is based on the findings of other investigators.

Guwahati,

May, 2023 Nabendu Paul

Indian Institute of Technology Guwahati

Department of Chemical Engineering

Certificate

It is certified that the work described in this thesis entitled **"Molecular Modeling and Experimental Insights in the Application of Hydrophobic Deep Eutectic Solvents for Remediation of Micropollutant from Aqueous Systems"** by Mr. Nabendu Paul for the award of degree of Doctor of Philosophy is an authentic record of the results obtained from the research work carried out under my supervision at the Department of Chemical Engineering, Indian Institute of Technology Guwahati, Guwahati, India, and this work has not been submitted elsewhere for a degree.

Dr. Tamal Banerjee
Professor
Department of Chemical Engineering
IIT Guwahati, Guwahati – 781039
Assam, India

ACKNOWLEDGEMENTS

My doctoral dissertation would not have come to a successful completion without the help of several people. I would like to take this opportunity to express my sincere gratitude to all of them.

First and foremost, I express my profound sense of gratitude and respect to my thesis supervisor **Prof. Tamal Banerjee** Sir, Department of Chemical Engineering, for his unparalleled and unwavering guidance. This thesis would not have been possible without his wise supervision, unflinching support and encouragement at every stage of my work. I could always reach him to clarify my doubts and he was always very kind and helpful in clarifying my doubts despite his busy schedule. His punctuality, discipline and relentless dedication always left me flabbergasted. I feel extremely blessed that he gave me the opportunity to work under his precious guidance. I shall be forever grateful for his love and care for me.

I would like to thank my doctoral committee members **Prof. Chandan Das, Prof. Ashok Kumar Dasmahapatra,** and **Dr. Uttam Manna** for their valuable suggestions and comments during all assessments of the Ph. D. program. I would like to also thank my comprehensive committee members **Prof. Kaustubha Mohanty, Dr. Anki Reddy Katha,** and **Dr. Pankaj Kalita.**

I would like to thank the external reviewers of my doctoral thesis, **Prof. Sreedevi Upadhyayula** of Department of Chemical Engineering, IIT Delhi and **Prof. Ana Rita C. Duarte** of Nova School of Science and Technology, Portugal for their time along with very constructive comments on my thesis. I would also like to acknowledge the members of the Viva-Voce Examination Board, **Prof. Chandan Das, Prof. Sreedevi Upadhyayula, Prof. Sandip Paul, Prof. V. V. Goud,** and **Prof. Tamal Banerjee** for the evaluation of my Viva-Voce examination.

I would like to acknowledge **Prof. Isabel Maria Marrucho** and her laboratory from Instituto Superior Técnico under Universidade de Lisboa for providing me the opportunity to work under her valuable guidance. Her valuable knowledge and insights were incredibly useful in carrying out the experiments.

I am thankful to **Dr. Partho Sarathi Gooh Pattader, and Dr. Omkar S. Deshmukh**, Department of Chemical Engineering, IIT Guwahati for giving me useful suggestions and

doubt clarification during my research work. I also thank **Prof. Kaustubha Mohanty**, Head, Department of Chemical Engineering, for his administrative support. Furthermore, I would like to thank other faculty members, research scholars, supporting staff of the Department of Chemical Engineering, IIT Guwahati for their kind cooperation in all aspects.

I acknowledge Ministry of Human Resource Development (MHRD) and our institute for providing fellowship throughout the Ph. D. program. I would also like to acknowledge the Scheme for Promotion of Academic and Research Collaboration (SPARC), (Project Code: P848) under Ministry of Human Resource Development (MHRD), Government of India for sanctioning the financial grant in the project titled "Hydrophobic Deep Eutectic Solvent for Remediation of Antifungal and Antibiotics in Waste water" to financially support my visit to the Instituto Superior Técnico, Lisbon.

I extend my sincere thanks to Dr. Papu Kumar Naik and Dr. Mood Mohan for helping me to learn molecular dynamics simulation.

I would also like to thank Central Instruments Facility (CIF), IIT Guwahati and analytical laboratory of Chemical Engineering, IIT Guwahati for providing the characterizations analysis. PARAM-ISHAN supercomputer (162 nodes and 3024 cores in each node) is duly acknowledged for providing the enormous computational requirement to carry out the simulation and computational works.

Special thanks to academic people, Library facilities and staff and Core I-IV people for their necessary support in every aspect. I would like to acknowledge Barak hostel, IIT Guwahati for becoming almost my second home during my doctoral journey.

I deeply acknowledge my past lab seniors, colleagues and collaborators Dr. Debashis Kundu, Dr. Mood Mohan, Dr. Rima Biswas, Dr. Rupesh Verma, Dr. Basudhrity Banerjee, Dr. Papu Naik, Dr. Pyarimohan Dehury, Dr. Upasana Mahanta, Dr. Sunil K. Singh, Dr. Dhirendra K. Mishra, Swetha, Diksha, G. Harish, Sambita, Dileep, Somtirtha and my present lab colleagues Dr. Venkateshwara Rao, Nikhil, Arindam, Nipu, Raghibul, Mangal, Rajib, Uday, Anushka for providing a co-operative research environment.

I am especially thankful to my friends during my doctoral journey Kuldeep, Barnali, Nirmal, Nayan, Mahula, Ananya, Tanusree, Ritesh, Purnima, Bibari, Kumari, Swapna and

Bittu; my B. Tech and M. Tech friends Saptarshi, Bitang, Suman, Sutapa, Deba, Raja, Gautam, Pankaj, Bibhash; and my school friends Rupam, Monoj, Rajdeep, Debajit, Abhijit, Suman, and Manish, for being a part of a wonderful journey throughout the time.

I extend my sincere love and affection towards my cousins Tantu, Guddu, Roni, Bhutan, Ramu, Dulal, Shamu, Dhrubha, Kuti, Pinky, Samrat, Soni, Keya, Rim, Ritu, and many more.

Last but not least, I want to convey my sincere gratitude and unfathomable sense of indebtedness to my mother **Mrs. Arati Paul** and my father **Mr. Narayan Paul**, for all their eternal love, invaluable support and sacrifices throughout my life. Special thanks to my elder sister **Saswati**, her husband **Arup** dadabhai and my younger brother **Biltu** who always strengthened my morale by supporting me and standing by me in all situations. I would like to mention my nephew (**Arohan**) and wish him a healthy and happy life ahead. I will be thankful to them and I promise I shall never forget their uncountable help and encouragement. Whatever I have achieved till date and whatever I will achieve in future, everything is and will be possible because of the love and support of my parents and I feel truly indebted to them and they are always in my heart. I wish to thank many other people whose names are not mentioned here but this does not mean that I have forgotten their help. Above all, I am thankful to GOD for giving me a wonderful and healthy life.

"Do everything you have to do, but not with greed, not with ego, not with lust, not with envy but with love, compassion, humility and devotion".

- Lord Krishna to Arjun (Bhagavad Gita)

NABENDU PAUL

ABSTRACT

Micropollutants have emerged as a new class of pollutants due to their harmful effects on humans and livestock, even at low concentrations. The frightening consequences of micropollutants compelled the environmental research fraternity to consider these as a contemporary division of pollutants. Even if present in low quantities, micropollutants have been associated with a range of detrimental impacts on humans and livestock, including poisoning, neurotoxicity, endocrine-disrupting effects, and microorganism antibiotic resistance. Antibiotic overuse and improper use have contributed to the emergence of microorganisms that are resistant to these drugs, making treatment of bacterial infections increasingly difficult. This takes place when bacteria undergo a process of evolution in which they acquire the ability to withstand the effects of antibiotics. Reformed and modified wastewater treatment processes such as oxidative degradation, biological and photo-catalytic degradation processes and a combination of these methods have emerged to be beneficial in the removal of pesticides from water supplies as compared to the traditional treatment processes such as adsorption, ozonation, chlorination, membrane filtration. Green solvents, especially deep eutectic solvents (DESs), especially hydrophobic DESs (HDESs) through liquid-liquid extraction and microextraction (LLE/LLME) can have a revolutionary impact in achieving the efficient pharmaceutical removal pathway.

The formation mechanism and stability of HDESs in aqueous environment were studied through molecular dynamics (MD) simulation and quantum chemical (QC) calculations. The DES integrity and the disruption through water penetration, the structural arrangements at the microscopic level, compactness of the hydrogen bond acceptor (HBA) and hydrogen bond donor (HBD) within the DES, interaction energies (IE), relative stability, structural properties, hydrogen bonding (H-bonds) and transport properties (diffusivity), and the characteristics of the non-bonded interactions were thoroughly evaluated. To observe the behaviour of the hydrophobic DESs in aqueous system-based applications, solvation studies of the DESs have been carried out employing both explicit as well as implicit solvation models. MD and QC studies for two pesticide extraction (acetamiprid & imidacloprid) from an aqueous environment via HDES. Higher interaction was witnessed between pesticide and DESs to form hydrogen bonding between the molecules. The extraction efficiency of 75% and 69% by the MD simulation was close enough to that of the experiments. The non-bonded interaction distances attained between the DES and pesticide in the optimized clusters were ranging from 2.896 to 3.77 Å for imidacloprid, and from 1.724 to 2.03 Å for acetamiprid. Charge transfer (CT)

occurred in the direction of DES to the pesticide molecule in each system as per the natural bonding orbital (NBO) analysis. Frontier molecular orbital (FMO) study indicated a relatively stronger DES-pesticide complex with higher band-gap energy.

The experimental batch-type extraction of enoxacin from the aqueous environment with three hydrophobic DESs achieved 82.6%, 79.6% and 69.1% extraction efficiency three DESs. Different recycling schemes have been implemented to assess the reuse and recovery of DESs to achieve higher net extraction efficiency (NEE) ensuring a sustainable and circular approach to solvent regeneration via adsorption on activated carbon (AC). The QC calculation elucidated the strength of the DES-enoxacin interaction and provided insights regarding the interaction mechanism with structural arrangement combined with charge transfer behaviour. Non-covalent interaction (NCI) with atoms-in molecules calculation (AIM) highlighted the multiple interacting components in the formation of the DES-enoxacin complex.

PDMS (Polydimethylsiloxane) microchannel-based continuous extraction of ciprofloxacin (antibiotic) and fluconazole (antifungal) from an aqueous environment by liquid-liquid extraction using two HDESs. The influence of flow rate, residence time and DES/water mass ratio on extraction efficiency (%EE) have been evaluated through experiments. QC calculation and MD simulation results generated atomistic and molecular-level insights into the drug-DES complexes. CT, FMO, non-bonded interaction energy, and hydrogen bonding analysis explained the stability and interactive nature of the components. Non-covalent interaction (NCI) associated with reduced density gradient (RDG) analysis was incorporated to understand the noncovalent interactions such as hydrogen bonding and dispersion interactions (van der Waals) that prevailed within the drug-DES complexes.

Table of Contents

List of Figures

List of Tables

List of Abbreviations and Symbols

	Abbreviations
AIM	Atoms-in-molecules
ABS	Aqueous biphasic system
AMBER	Assisted Model Building with Energy Refinement
BCP	Bond critical points
B3LYP	Becke three-parameter, Lee-Yang-Parr
BSSE	Basis Set Superposition Error
CDF	Combined Distribution Functions
CHARMM	Chemistry at Harvard Macromolecular Mechanics
CHELPG	CHarges from Electrostatic Potentials using a Grid based method
CN	Coordination Number
COSMO-RS	COnductor like Screening MOdel for Real Solvents
CT	Charge Transfer
D3BJ	Becke-Johnson damping (Three Parameter)
DES	Deep Eutectic Solvent
DFT	Density Functional Theory
FMO	Frontier Molecular Orbital
GAFF	Generalized AMBER Force Field
HBA	Hydrogen Bond Acceptor
HBD	Hydrogen Bond Donor
HF	Hartree–Fock
HOMO	Higher Occupied Molecular Orbital
IE	Interaction Energy
IL	Ionic Liquid
LLE	Liquid Liquid Extraction
LUMO	Lower Unoccupied Molecular Orbitals
MD	Molecular Dynamics
MSD	Mean Squared Displacement
NAMD	Nanoscale Molecular Dynamics
NBO	Natural Bonding Orbitals
NCI	Non-covalent Interaction
NMR	Nuclear Magnetic Resonance
PCM	Polarizable Continuum Model

QC	Quantum Chemical
QTAIM	Quantum Theory of Atoms in Molecules
RDF	Radial Distribution Functions
RDG	Reduced Density Gradient
RESP	Restrained Electrostatic Potential
SCRF	Self-Consistent Reaction Field
SDF	Spatial Distribution Functions
SLE	Solid-Liquid Equilibrium
SMD	Solvation model based on density
THEDES	Therapeutic DESs
VMD	Visual Molecular Dynamics

List of Symbols	
T_f	Freezing point
ΔG_{solv}	Gibbs free energy of solvation
G_{sol}	Gibbs free energy in the solvent
G_{vacuum}	Vacuum or gas phase Gibbs free energy
ρ_{BCP}	Electron density at BCP
$\nabla\rho_{BCP}^2$	Laplacian of electron density
G_{BCP}	Kinetic energy density
V_{BCP}	Potential energy density
λ_2	Electron density Hessian second eigenvalue
S	Relative Stability Factor
D	Self-diffusion coefficient
β	Distribution coefficient
S)	Selectivity
%EE	Extraction efficiency
η	Chemical hardness
μ	Chemical potential

Chapter- 1

Introduction and Literature Review for the Stability of Hydrophobic Deep Eutectic Solvents (DES) and its Applications in Remediation of Pharmaceutical Drugs from Waste-water Systems

1 Introduction to Remediation of Pharmaceutical Drugs from Waste-water Systems

1.1. Pharmaceutical Micropollutants in Aqueous Systems of Wastewater

Ensuring general access to safe drinking water is one of the challenges faced by modern society. This requires the development of effective wastewater treatment facilities and the reduction of pollution risks associated with residential, commercial, and agricultural water usage. Micropollutants have emerged as a new class of pollutants due to their harmful effects on humans and livestock, even at low concentrations.[1] The frightening consequences of micropollutants compelled the environmental research fraternity to consider these as a contemporary division of pollutants. Even if present in low quantities, micropollutants have been associated with a range of detrimental impacts on humans and livestock, including poisoning, neurotoxicity, endocrine-disrupting effects, and microorganism antibiotic resistance.[2–4]

Research conducted by Larsson's group in the neighbourhood surrounding a wastewater treatment plant in Hyderabad, India revealed alarming levels of pharmaceutical contamination in local surface water bodies, which seeped into the groundwater and drinking water facilities despite the presence of an industrial treatment process.[5] Antibiotics and fluoroquinolones like enoxacin, ofloxacin, and enrofloxacin contribute to the majority of these, along with antihistamines like cetirizine and beta-adrenoreceptor antagonists like metoprolol at concentrations in the range of ng L^{-1} to μg L^{-1}. This investigation reveals a critical environmental and health risk to aquatic and subsurface creatures. The animals are directly affected, and the surrounding farmland gets contaminated as a result. There is no doubt that humans and other livestock will suffer long-term consequences. Antibiotic resistance is a direct result of the disruption of the ecological balance of microorganisms in their environment caused by the long-term persistent presence of antibiotics. A rising public health crisis is this antibiotic resistance. Antibiotic overuse and improper use have contributed to the emergence of microorganisms that are resistant to these drugs, making treatment of bacterial infections increasingly difficult. This takes place when bacteria undergo a process of evolution in which they acquire the ability to withstand the effects of antibiotics. As antibiotics become less effective against bacteria, they pose a serious risk to public health because untreated bacterial infections can extend hospital admissions, increase medical costs, and even be fatal. Along with responsive handling and judicious usage of antibiotics, pharmaceutical wastewater from different sources needs to be properly treated to lower the levels to the permissible limit. As a

result, eliminating these micropollutants is crucial at either the upstream or the downstream stages. Table 1.1 presents the findings of Larsson's group in detecting various kinds of active pharmaceuticals ingredients (APIs) and drugs at surprisingly higher levels from their respective permissible limits near the investigated plant (Patancheru Enviro Tech Ltd.; PETL) situated in Patancheru, near Hyderabad.

For the top 11 pharmaceutical compounds tested in PETL effluent samples, detection levels were all greater than 100 µg/L. All of these drugs were found in quantities that exceeded the previous record for any sewage discharge. Ciprofloxacin, the most used antibiotic, can reach toxicity levels over a thousand times higher than those at which it is hazardous to bacteria (up to 31,000 µg/L).[5]

Table 1.1: Active pharmaceuticals found in effluent near treatment plant in Hyderabad, India (Larsson et al. (2007))[5]

Active ingredient	Type of drug	Range (µg/L)
Ciprofloxacin	Antibiotic-fluoroquinolone	28,000–31,000
Losartan	Angiotensin II receptor antagonist	2,400–2,500
Cetirizine	H_1-receptor antagonist	1,300–1,400
Metoprolol	β_1-adrenoreceptor antagonist	800–950
Enrofloxacin	Antibiotic-fluoroquinolone (veterinary use)	780–900
Citalopram	Serotonin reuptake inhibitor	770–840
Norfloxacin	Antibiotic-fluoroquinolone	390–420
Lomefloxacin	Antibiotic-fluoroquinolone	150–300
Enoxacin	Antibiotic-fluoroquinolone	150–300
Ofloxacin	Antibiotic-fluoroquinolone	150–160
Ranitidine	H_2-receptor antagonist	90–160

In a study by Fick et al., the environmental fate of active pharmaceutical ingredients in a major production area for the global bulk drug market was investigated.[6] Samples of water were collected from a common effluent treatment plant near Hyderabad, India, which receives

process water from around 90 bulk drug manufacturers. In addition, surface water was analyzed from two lakes that are not contaminated by the treatment plant and from the recipient stream. Furthermore, water samples were collected from wells in six nearby villages. The researchers used liquid chromatography-mass spectrometry to analyze the presence of 12 pharmaceuticals in the samples. The results showed that all wells were contaminated with drugs, with several wells containing high levels of ciprofloxacin, enoxacin, cetirizine, terbinafine, and citalopram (over 1 mg/L). Very high concentrations of ciprofloxacin (14 mg/L) and cetirizine (2.1 mg/L) were found in the effluent of the treatment plant, along with seven additional pharmaceuticals. In addition, the two lakes contained high levels of ciprofloxacin (up to 6.5 mg/L), cetirizine (up to 1.2 mg/L), norfloxacin (up to 0.52 mg/L), and enoxacin (up to 0.16 mg/L). These findings indicate that the investigated area has additional sources of industrial waste that are not adequately treated. This inadequate wastewater management in one of the world's largest centres for bulk drug production leads to unprecedented drug contamination of surface, ground, and drinking water, which raises serious concerns regarding the development of antibiotic resistance.[6]

1.2. Treatment Processes Available for Micropollutant Removal

Traditional drinking water treatment processes such as adsorption, ozonation, chlorination, membrane filtration and physicochemical processes like coagulation-flocculation and floatation are widely used for water purification processes.[7] Despite this, the effective removal of pharmaceuticals and pesticide agents was not specifically covered by these processes. Removal of pharmaceutical ingredients from water bodies is necessary to prevent the pathogens from being drug-resistive hence the persistent presence of a small quantity of the drugs could be detrimental. Reformed and modified processes such as oxidative degradation, biological and photo-catalytic degradation processes and a combination of these methods have emerged to be beneficial in the removal of pesticides from water supplies.[8,9] Reverse osmosis, membrane distillation and electrodialysis-based operations were effectively used in reducing salts and other contaminants from drinking water sources.[10] However, the intensive energy consumption and high set-up expenses associated with these processes have become a hindrance to the economic and efficient utilization of these treatment processes in pesticide removal. Each of these processes is associated with several advantages and drawbacks depending on their respective operational aspects.

Nevertheless, adsorption can be considered the most extensively-exercised pharmaceutical removal method in waste-water treatment plants.[11] Low cost, ease of operation and high performance are some advantages of the adsorption process whereas, weak selectivity

and the build-up of waste materials are some of the major shortcomings of this method. Among all the different types of adsorbents, activated carbon is considered one of the most commonly used products in water treatment plants.[12] High capacity to adsorb, a faster rate of adsorption, easy assimilation and cost-effectiveness are a few of the excellent properties of activated carbon.[12] Pesticide removal performance with the help of activated carbon as an adsorbent media were investigated and productive findings have been obtained.[13] However, activated carbon gets depleted after a certain period and the process of regeneration or reactivation is inefficient with respect to time, energy as well as cost. In addition, various classes of complex functionalized pesticides with distinctive structural appearances and the ineffectiveness to inhibit pathogen growth in the filter media are some challenging aspects of pesticide removal from an aqueous environment by these generic processes. [14,15]

Consequently, other alternate methods and innovative ways of water decontamination are being explored such as Ionic Liquids (ILs) and their application in liquid membrane technology[16,17] and aqueous biphasic systems (ABS).[18] Liquid membrane treatment processes are advantageous due to high selectivity, low solvent consumption and non-equilibrium mass transfer whereas ABS can provide a high distribution ratio due to the presence of a salt-rich phase in an aqueous two-phase system where hydrophilic ILs are utilized. ILs being very costly and highly viscous at room temperature are quite challenging to be applied in waste-water treatment. Additionally, the arduous purification and recovery/recycling process of the ILs is quite a hindrance to the effective removal of pesticides from water sources. Researchers have come up with various hydrogel-based water treatment processes for the removal of metal ions such as Co, Cr, Fe, Mn, Ni, Zn etc, but these are not very effective in removing pesticides from water.[19] Deep eutectic solvents (DESs) are an affordable, eco-friendly, and sustainable alternative to ILs that can be used to reduce the aforementioned drawbacks. Figure 1.1 is a schematic representation of the conventional water treatment processes for micropollutant removal and their new-age counterparts with enhanced and superior advantages. Green solvents, especially DESs through liquid-liquid extraction and microextraction (LLE/LLME) can have a revolutionary impact in achieving the efficient pharmaceutical removal pathway combined with the other water treatment processes by complementing and enhancing the clean water drive and requirement of society.

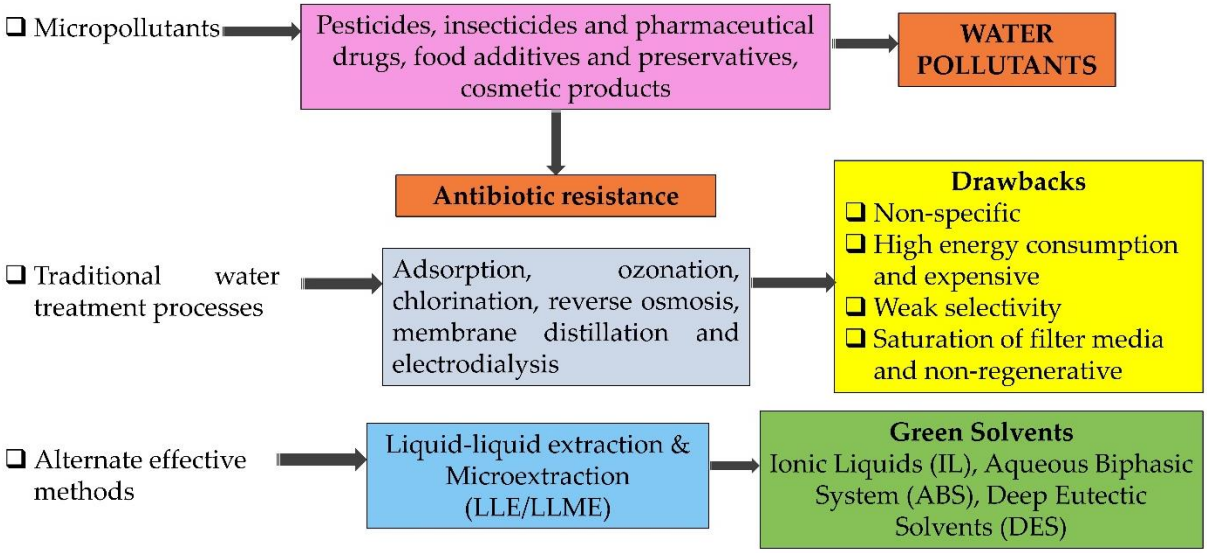

Figure 1.1: Schematic of the traditional and new-age treatment processes available for the removal of micropollutants from wastewater with the application of green solvents.

1.3. Eutectic Solvents in Pharmaceutical Micropollutant Removal

The breakthrough discovery of Deep Eutectic Solvents (DESs) by mixing two or more different compounds at a specific composition has emerged to be a remarkable introduction in connection with an alternative class of 'green' solvents.[20] Since its emergence by Abbott et al in 2003 in the form of choline chloride-urea DES,[20,21] numerous classifications of DESs has been unearthed by various research groups.

A DES is generally composed of two or three cheap and safe components capable of associating with each other through hydrogen bond interactions to form a eutectic mixture. Melting points lower than that for each element characterizes the resulting DES. DESs usually have very significant freezing point depression and most DESs are in a liquid state at room temperatures up to 70°C.[22] Figure 1.2 depicts the binary phase diagram of a mixture of A and B at varying compositions to observe the melting point of the mixture as a function of mole fractions of individual components. Upon mixing, the melting point of the mixture gradually decreases to finally reach a minimum melting point composition to be called a 'eutectic point' and the resultant mixture is termed a 'deep' eutectic solvent (DES). The eutectic point is pointed out in Figure 1.2 with the red arrow and the formation of a clear liquid can be seen. The largest drop in freezing point ΔT_f is associated with the eutectic point.

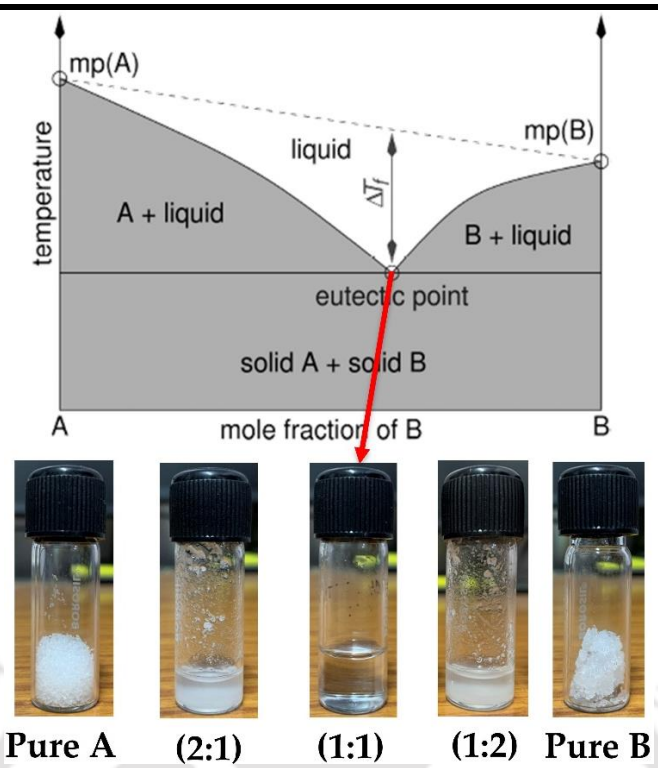

Figure 1.2: Solid-liquid schematic phase diagram of a binary mixture of two compounds A and B showing eutectic behaviour.

One can operate above the eutectic point line as per one's requirement and application and not necessarily at the eutectic point, however, the composition of the eutectic point is unique between two specific compounds and cannot be altered. Since its inception, four types of DESs (type I, type II, type III and type IV) have been broadly classified based on the property and categories of the precursor materials. However, in recent research advancements, one new class of DESs have been unearthed consisting of non-ionic compounds as precursor components termed type-V DES as presented in Figure 1.3.

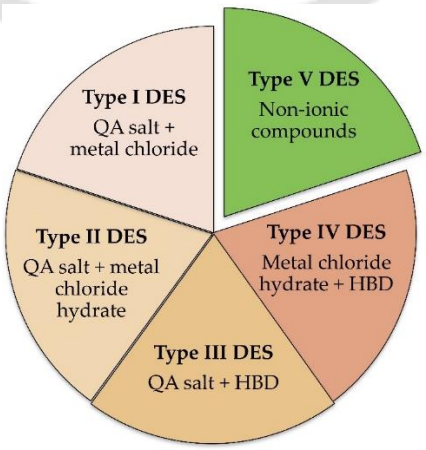

Figure 1.3: Classification of deep eutectic solvents based on precursor compounds.

This type of DESs largely contains environmentally benign and harmless compounds that are easily accessible and thus have greater prospects.[22]

In the earlier works, largely metal salt and their hydrates; and organic salts combined with neutral compounds were utilized for the formation of DESs. These materials were preferred as they were inexpensive and easy to handle and would possess various other attractive attributes such as low volatility, lesser toxicity, enhanced biocompatibility and bio-degradability and non-corrosive nature which were desirable for a solvent.[21] As a result, the number of publications has increased by a great deal in recent years using DESs in different applications such as metal ions extraction and removal, metal treating,[21,23–27] de-aromatization, desulfurization[28–30], denitrification of fuel,[31,32] protein, amino acids and biomaterials extraction,[33,34] and electrochemistry[35–37]. Figure 1.4 shows how DESs can be used effectively in a variety of scientific domains thanks to their many attractive solvent characteristics. However, the earlier DESs mostly belonged to the hydrophilic class which was not very promising concerning the applications exposed to aqueous interaction.

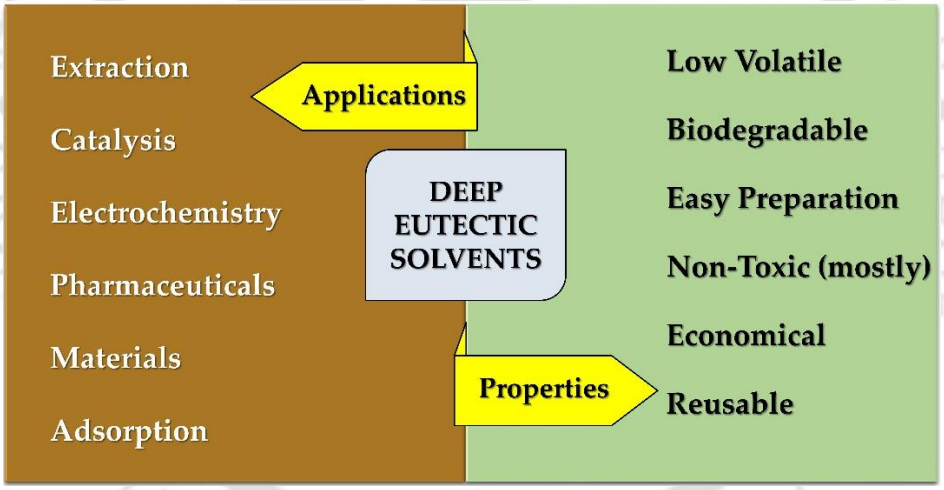

Figure 1.4: Solid-liquid schematic phase diagram of a binary mixture of two compounds A and B showing eutectic behaviour.

During the recent few years, a new class of DES namely hydrophobic deep eutectic solvents (HDESs) have emerged where naturally occurring hydrophobic compounds were applied as hydrogen bond donor (HBD) and acceptor (HBA) to form a DES having water-deterring property.[38,39] These HDESs were widely used in the field of water treatment and purification, natural component extraction from plants, CO2 capture and organic materials synthesis.[38,40] The very first instance of HDES was reported in the synthesis of six quaternary ammonium salt- decanoic acid-based HDESs. The water-leaching tendency of the ammonium salts as a function of carbon chain length was measured.[39] Since then, the number of scientific

research publications on hydrophobic DESs has increased at a good rate across different disciplines of scientific research. One can refer to Figure 1.5 for the latest data on the number of publications relating to DES and HDES. The growing interest in utilizing HDESs has been associated with the remarkable exposure of these solvents in research related to aqueous system-based applications. The experimental investigation on the hydrophobic nature of DL-menthol and carboxylic acid-based DESs was further used to extract four neonicotinoid pesticides from water-based solutions using DL-menthol as HBA and long-chain fatty acids (C_8 to C_{12}) as HBD.[40]

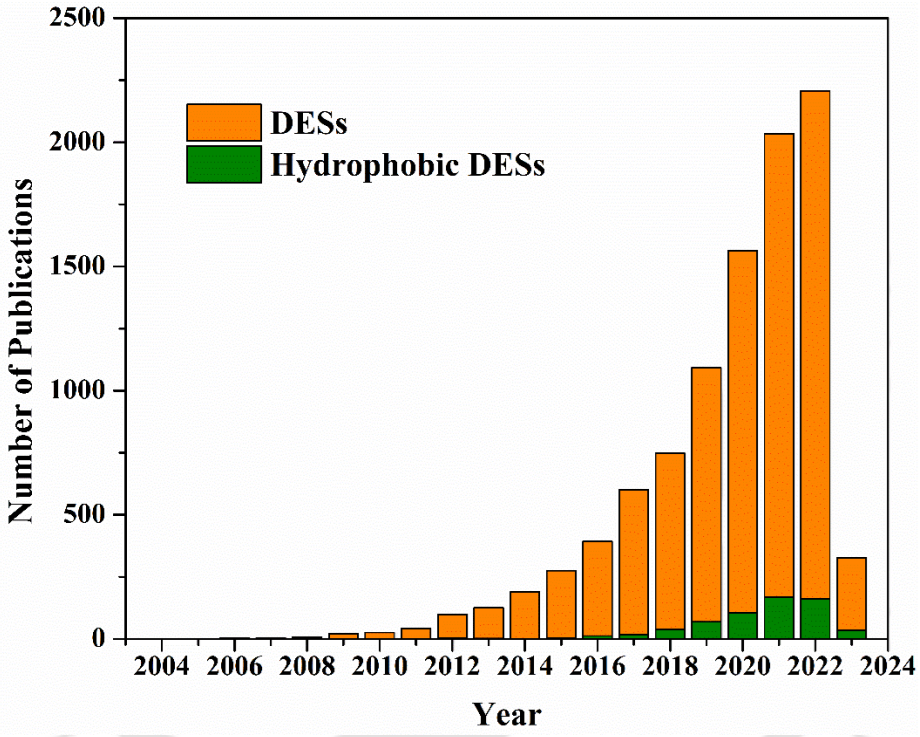

Figure 1.5: The number of scientific published papers on HDESs and DESs from 2004 to March 2023 acquired from the source of the web of science. (Keywords for the search were: DES and HDES; accessed on 05th March 2023)

Morrison et al. (2009) investigated the dissolution of several poorly soluble drugs including benzoic acid, griseofulvin, danazol, itraconazole and AMG517 in ChCl/urea and ChCl/malonic acid DESs. Tested drugs are found 5–22000 folds more soluble in pure DESs (i.e., ChCl/urea and ChCl/malonic acid) than in pure water as the DESs can be utilized as a vehicle for oral administration in rats during preclinical pharmacokinetic studies.[41] Weiyang et al. (2018) investigated a rapid vortex-assisted LLME technique using fatty acid/alcohol-based hydrophobic DESs for quickly extracting levofloxacin and ciprofloxacin from common water samples with extraction recoveries of levofloxacin and ciprofloxacin exceeding 94.8%. The proposed hydrophobic DES-based LLME method provides high precision, good linearity, an

acceptable limit of detection (LOD) and limit of quantification (LOQ), and satisfactory recoveries for the targets. These results support the potential of this method as a new type of extraction medium to replace conventional hydrophobic organic solvents in various applications.[42]

Florindo et al. (2017) focused on the development of hydrophobic deep eutectic solvents (DESs), as cheap extractants for the removal of four neonicotinoids (imidacloprid, acetamiprid, nitenpyram and thiamethoxam), from diluted aqueous solutions. In particular, two different families of DESs, one based on natural neutral ingredients (DL-Menthol and natural organic acids) and the other based on quaternary ammonium salts and organic acids were prepared and their water stability was carefully studied through ^{1}H NMR. Only the chemically stable DESs were selected to be used as solvents in the extraction of the four neonicotinoids so that no contamination of the water cycle is attained, while the reuse of the DES is possible. The final results were compared with those obtained for liquid-liquid extraction using hydrophobic imidazolium-based ionic liquids as solvents. The water stability of the DESs was analyzed and it was found that long-chain acids constitute more hydrophobic and stable DESs.[40]

Alina et al. (2018) developed a dispersive liquid-liquid microextraction method for the simultaneous determination of 11 (eleven) pharmaceuticals. The method is based on a microextraction procedure applied to wastewater samples from different regions of Hungary followed by high-performance liquid chromatography with mass spectrometry. The effect of the nature of the extractant, dispersive solvent, different additives, and extraction time were examined on the extraction efficiency of the dispersive liquid-liquid microextraction method. Under optimal conditions, the linearity for determining the pharmaceuticals was in the range of 1–500 ng/mL, with the correlation coefficients ranging from 0.9922 to 0.9995. The limits of detection and limits of quantification were in the range of 0.31–6.65 and 0.93–22.18 ng/mL, respectively.[43] Zawadzki et al. (2016) developed a sustainable process for the recovery of valuable drugs from pharmaceutical wastes using ionic liquid (IL)-based aqueous biphasic systems (ABS). ABS composed of phosphonium and quaternary ammonium-based ILs together with distinct phosphate-based salts and buffers were selected to ascertain the partitioning behaviour of amitriptyline hydrochloride. The effects of different process parameters, namely the IL nature, pH and mixture composition used in the extraction system, were studied and the process was optimized to maximize the extraction of the antidepressant from pharmaceutical wastes. In addition to this, an analysis was done to determine the maximum amount of amitriptyline that could be handled utilizing such systems. The set of ABS investigated herein revealed a high extraction performance, as indicated by the

outstanding logarithmic functions of the amitriptyline partition coefficients ranging from 2.41 ± 0.05 to > 2.5 and extraction efficiencies between 66% ± 1% and 100%. The best ABS and conditions were considered in the development of an integrated multi-step purification process.[44]

Francisca et al. (2014) investigated ammonium-based ILs, reported as being cost-effective ILs of low toxicity, and as promising biocompatible solvents to stabilize biomolecules, to extract active substances from pharmaceutical wastes. Here, paracetamol served as a model drug to evaluate the extraction capabilities of the IL-based ABS. Six short-chain quaternary ammonium compounds (tetraethylammonium bromide $[N_{2222}]Br$, tetraethylammonium chloride $[N_{2222}]Cl$, tetrapropylammonium bromide $[N_{3333}]Br$, tetrapropylammonium chloride $[N_{3333}]Cl$, tetrabutylammonium bromide $[N_{4444}]Br$ and tetrabutylammonium chloride $[N_{4444}]Cl$) and three different salts (potassium citrate buffer, potassium carbonate and potassium phosphate buffer) were used to prepare the ABS, aiming at investigating the influence of the alkyl chain of the cation and the anion effect. A systematic analysis of the aptitude of ammonium compounds to form ABS was performed by changing the salt, the ammonium type and the medium pH. All the studied systems, employing both the model compound and real matrix revealed a great aptitude to recover paracetamol from pharmaceutical wastes, presenting extraction efficiencies ranging from around 80% up to 100%.[45]

Almeida et al. (2017) used aqueous biphasic systems (ABS) composed of ionic liquids (ILs) and aluminium-based salts for the removal of diclofenac, ibuprofen, naproxen, and ketoprofen. With these systems, extraction efficiencies of non-steroidal anti-inflammatory drugs (NSAIDs) up to 100% into the IL-rich phase were obtained in a single step. Further, the recovery of NSAIDs from the IL medium and the recyclability of the IL-rich phase were ascertained aiming at developing a more sustainable and cost-effective strategy. Based on the remarkable increase of the NSAIDs solubility in the IL-rich phase (from 300 to 4100-fold when compared with pure water), water was used as an effective antisolvent, where recovery percentages of NSAIDs from the IL-rich phase up to 91% were obtained. After the "cleaning" of the IL-rich phase by the induced precipitation of NSAIDs, the phase-forming components were recovered and reused in four consecutive cycles, with no detected losses on both the extraction efficiency and recovery of NSAIDs.[46]

Table 1.2 represents the compilation of the various applications of ILs/DESs as extraction solvents of micropollutants from aqueous streams carried out by different research groups. These works cover a wide variety of micropollutants such as pesticides, antibiotics,

heavy metal ions, phenolic compounds, pharmaceutical extracts, industrial dyes and paints. The extraction techniques include LLE (liquid-liquid extraction), LLME (liquid-liquid microextraction), LPME (liquid phase microextraction) and DLLME (dispersive liquid-liquid microextraction) to extract micropollutants from water medium with very promising recovery (%).

Table 1.2: Summary of the application of DESs and ILs for the removal of different water micropollutants

Micropollutant	DES/IL (molar ratio)	Sample matrix	Extraction technique	Recovery (%)	Ref.
bisphenol-A, bisphenol-AF, tetrabromobisphenol-A,4-tert-octyl phenol	Fatty acid-based DESs	water	LLME	87.4-106.6	[47]
β-agonists	$[N_{4444}]$ Cl: DecA (1:3)	environmental water	DLLME	56-91	[48]
chlorophenols	$[N_{8881}]$ Cl: OctA (1:2)	wastewater	DLLME	90.8-93	[49]
PAHs	$[N_{4444}]$ Br: DecA (1:2)	environmental water	SFD-DLLME	83-117	[50]
anti-depressant drugs	ChCl: Ph (1:4)	pharmaceutical wastewater	AA-DLLME	42-68	[51]
pyrethroid insecticides	THTDP-Cl: DodecA (1:2)	environmental water	UA-DLLME	81-110	[52]
PAHs	Thymol: ±camphor (1:1)	industrial wastewater	UA-DLLME	74-126	[53]
Antibiotics (levofloxacin, ciprofloxacin)	$[N_{8881}]$ Cl:1-OctOH (1:4)	environmental water	VA-LLME	87.5-94.5	[42]
Hg^{2+}, CH_3Hg^+	ChCl: Ph (1:3)	water	UA-DLLME	84-114	[54]
Cr^{3+}, Cr^{6+}	ChCl: Ph (1:2)	environmental water	UA-DLLME	93-94	[55]

ciprofloxacin	Menthol: fatty acid DESs	aqueous samples	LLE	76 (at neutral Ph)	[56]
Zn^{2+}, Cd^{2+}, and Fe^{3+}	$[MTOA^+][Cl^-]$, $[omim^+][BF4^-]$	aqueous hydrochloride solutions	LLE	> 90	[57]

LLE: Liquid-liquid extraction

DLLME: Dispersive liquid-liquid microextraction

UA-DLLME: ultrasound-assisted dispersive liquid-liquid microextraction

VA-LLME: vortex-assisted liquid phase microextraction

For futuristic potential, the upgradation of the batch process to a sustainable continuous process could be significant with a regeneration and recycling approach embedded within. One such approach is presented in the schematic in Figure 1.6. Here, a complete regenerative and sustainable cyclic approach to pharmaceutical removal from wastewater is presented.[58] This process could work for ABS as well as the HDES approach for water decontamination with an added advantage of high recycling efficiency of the solvents. The extraction unit is developed for the mixing of wastewater (containing pharmaceuticals) and DESs, and for intimate mixing, stirring could be added. Connecting this unit, one phase separation unit has been attached for the settlement of two phases and effective separation of the DES-rich phase and the salt-/aqueous-rich phase. The drug separation unit is the final compartment where the recovery of the drug from the DES phase is carried out and the regenerated DES solvents are directed back to the first unit, that is, the extraction unit. In the case of the ABS, an additional salt-rich phase is formed and the hydrophilic DES forms the other phase. After careful separation of both phases, the DES-rich phase then goes through a solvent (mainly water) for washing out the drugs, later to be precipitated, and the regenerated DES–aqueous solution is again sent back to the extraction unit for the next run. This process is termed the antisolvent method. Thus, a continuous large-scale setup can be developed for the productive separation of pesticides from wastewater sources, which could be effective in terms of both cost and energy consumption.

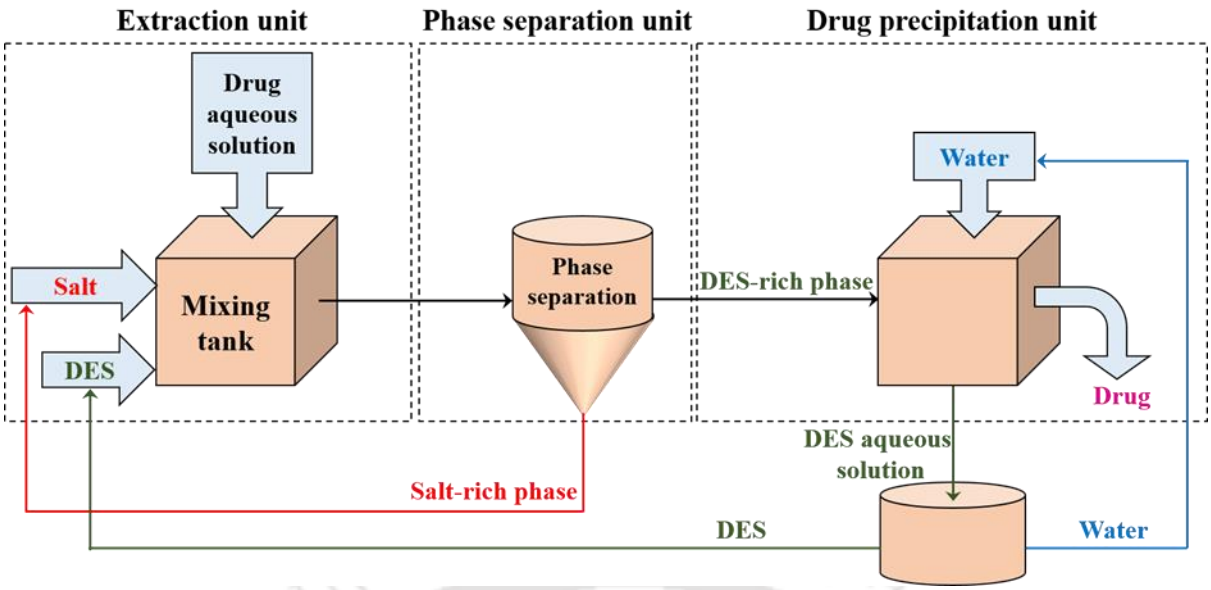

Figure 1.6: Schematic of the proposed futuristic model for a continuous sustainable water treatment process with DES as the extractant medium.[58]

1.4. Computational Approaches towards Deep Eutectic Solvents as Green Solvent for Remediation Applications

Classical MD simulations are considered to be beneficial for achieving satisfactory results for both conventional as well as experiments in severe conditions. Given the complexity of eutectic systems and the high cost of several DES precursor materials, simulation approaches can be immensely effective in reducing the time and cost requirements for the screening process of these components.[59–61] MD simulation analysis may be conducted at the atomic level and recorded at the nanosecond level.[62] Thermodynamic properties of DES along with transport and structural ones can be obtained by MD simulation via trajectory analysis. In general, experiments and simulations may be conducted concurrently to generate more accurate and efficient pure component and phase equilibria data. Naik et al. investigated the extraction of poly-aromatic hydrocarbon (quinoline) from fuel oil (heptane) using methyl triphenylphosphonium bromide- ethylene glycol (1:4) DES experimentally and numerically.[63] Additionally, the solubility of glucose in tetrabutylammonium bromide-based deep eutectic solvents was investigated by Mohan et al.[60] Ray et al. studied the influence of four structurally similar cations based on pyrrolidinium and piperidinium on the anion named as bis(trifluoromethane sulfonyl)imide ($[NTf2]^-$) by MD simulation.[64] They determined the influence of increasing ring size and the addition of an alkyl chain on the physicochemical parameters of three protic ILs and one aprotic IL. They observed the weakening of inter-ionic interactions and ordering when alkyl groups are added to the cation.

While MD simulation can provide valuable insights into a system at a molecular level with bulk system properties, quantum chemical (QC) calculations in the form of density functional theory (DFT) on the other hand offer significant information at the atomic-molecular level. Information regarding structure, charge transfer behaviour, molecular level energies, thermochemistry, bonding and anti-bonding orbitals can be immensely valuable for DESs. Wagle et al. investigated the desulfurization of aromatic sulfur compounds (ASCs) based on benzothiophene, dibenzothiophene and their oxides via extraction with reline and ethaline DESs.[65] They obtained the ASC-DES complex structure and the charge transfer (CT) process along with the solvation thermodynamics of the systems. They also observed multiple weak non-bonded interactions to be dominant in case of charge transfer between the ASCs and the DES components. Mishra et al. probed the release of hydrogen from chemical hydrides in the presence of ionic liquids (ILs), both experimentally and with DFT analysis.[66] They carried out the frontier molecular orbital (FMO) analysis of the IL-hydride complex to understand the selectivity of the solvents and the CT process within the components.

Understanding interactive pathways, mobility and electron cloud delocalization, ground and excited state orbital participation, and prevention of disruption of own structural arrangement against the penetration by an outside entity require observation at the molecular and atomic level. Panda et al. studied the effect of two different hydrogen bond donors (HBDs) namely, glycerol and ethylene glycol, and tetrabutylammonium chloride as HBA, to explore the effect of HBDs on the structure of DESs. Structural property analysis suggested dominant interaction between the anion and the HBD. Long-range structural ordering has been witnessed among the DES components with the existence of electrostatic as well as hydrogen bonding.[67] Kivelä et al. investigated the effect of low water content on the hydrophobic DES, tetrabutylammonium chloride: decanoic acid (1:2), through MD simulation and spectroscopic characterization techniques. They observed that the low water content had an effect on changing the density, viscosity and electrical conductivity of the DES. A network of intermolecular non-bonded interactions was observed between the DES components in the form of chloride−carboxylic acid hydrogen bonding and the introduction of water broke the interactions by hydrating the carboxylic acid groups and chloride ions leading to dynamic nanoscale phase segregation.[68] Abbas et al. investigated the density profile, dipole moment, and hydrogen bonds of DES-aqueous interfaces of eight hydrophobic DES composed of four organic compounds: decanoic acid, menthol, thymol, and lidocaine using molecular dynamics simulations. Hydrogen bond connectivity between the HBA and HBD had been observed for all the DESS along with a moderate number and lower stability of the DES-water hydrogen bond in the interface. They also observed the variation of the dipole fluctuation and

heterogeneous hydrogen bonds at the liquid-liquid interface for all eight DES systems.[69] Malik et al. performed an MD simulation to investigate the dynamics of DL-menthol (DLM) based HDESs with hexanoic (C6), octanoic (C8), and decanoic (C10) acids as HBDs to reveal the hydrogen bond relaxation with time and the lifetime associated with the strong and weak hydrogen bonding interactions present in these HDESs. It was also revealed that the translational dynamics of the species in the HDES become slower with an increasing tail length of the organic acid, while slightly enhanced caging was also observed for the HDES with a longer tail length of the acids.[70] A proper combination of experimental and theoretical studies such as MD simulation and QC calculations can provide useful insights to understand the formation, stability and dynamics of DL-menthol: carboxylic acid-based HDESs.

1.5. Objectives of the Thesis

The current thesis aims at the molecular-level understanding of the formation mechanism and stability of hydrophobic DESs in water with MD simulation and QC calculation. Detailed analysis in understanding the driving force for DES formation, hydrogen bonding, structural properties, transport properties, charge transfer process, molecular level energies, thermochemistry, and non-covalent interactions are addressed in this work. Computational evaluation of extraction of pesticides (nitenpyram, acetamiprid and imidacloprid) have been carried out to understand the mechanism of the extraction and to study the viability of the computational approach. Both experimental and theoretical aspects of DES-based solvent extraction of some primary drugs (enoxacin, ciprofloxacin and fluconazole) have been studied in batch-type extraction process along with the extension towards microchannel-based extraction (for ciprofloxacin and fluconazole) to enhance the extraction performance of the type V DESs. Recycling schemes have been implemented to assess the reuse and recovery of DESs to achieve sustainable and effective regenerative continuous processes with higher separation efficiency and performance.

The following objectives have been specified for the thesis work:

(a) *Initiate* molecular dynamics (MD) simulation and quantum chemical (QC) calculations to investigate the water stability of hydrophobic deep eutectic solvents (HDESs).
(b) *Employ* theoretical study on hydrophobic deep eutectic solvents-aided extraction of pesticides (nitenpyram, acetamiprid and imidacloprid) from an aqueous environment.

(c) *Apply* HDESs in experimental decontamination of enoxacin containing aqueous phase with solvent regeneration. This shall further involve quantum chemical insights and non-covalent interaction (NCI) studies.

(d) *Formulate* a continuous approach in the removal of ciprofloxacin and fluconazole from water with microfluidic device-based extraction by hydrophobic deep eutectic solvents (HDESs). This shall further involve MD simulation and NCI analysis.

1.6. Outline of Thesis

The current thesis is organized into the following chapters.

Chapter 2 investigates the formation mechanism and stability of the Type-V DESs comprised of DL-menthol: carboxylic acid and tetrabutylammonium chloride: carboxylic acid through molecular dynamics (MD) simulation in an aqueous medium. Later on, quantum chemical (QC) studies were performed for the menthol-based DESs. It is found that the menthol-based DESs consisting of acetic acid, butanoic acid and hexanoic acid are very less water-stable. The stability of the DESs in the aqueous phase was evaluated via interaction energies (IE), relative stability, structural properties, hydrogen bonding (H-bonds) and transport properties (diffusivity) through MD simulation. The DES integrity and the disruption of DESs through water penetration were investigated by QC calculation. The structural arrangements at the microscopic level, compactness of the hydrogen bond acceptor (HBA) and hydrogen bond donor (HBD) within the DES were demonstrated in this chapter followed by the non-covalent interaction (NCI) analysis to understand the characteristics of the non-bonded interactions responsible for DES formation and stability.

After establishing the hydrophobic nature of the DESs as a stable entity in water, the extraction mechanism of extract pesticides (acetamiprid and imidacloprid) via DL-menthol: carboxylic acid DESs have been investigated in **Chapter 3.** The molecular dynamics (MD) simulation is followed by quantum chemical (QC) calculation involving both the pesticides to highlight the molecular level insights about the DES-pesticide complex formation. Structural properties have been obtained in the form of radial, combined and spatial distribution functions (RDF, CDF and SDF, respectively) to understand the presence of DES components around pesticide molecules along with hydrogen bonding (H-bonds). Mean square displacement (MSD) analysis is carried out to observe the higher affinity of the pesticides towards the DES-rich phase for both systems. The QC calculations provide the optimized geometrical arrangements of the DESs and the DES-pesticide complex formations. The stable form of the

DES-pesticide complex has been evaluated via frontier molecular orbital analysis (FMO) interactions among the components of DES as well as pesticides have been established.

After the successful implementation of theoretical studies as described in chapter 3, we focus on the experimental framework to extract a drug (enoxacin) from the aqueous phase through batch-type liquid-liquid extraction using three hydrophobic deep eutectic solvents (DES) namely, (a) DL-menthol: decanoic acid (1:1), (b) DL-menthol: dodecanoic acid (2:1), and (c) dodecanoic acid: decanoic acid (1:2). **Chapter 4** addresses the extraction of enoxacin with experimental investigations followed by quantum chemical (QC) studies. The experiment investigates the effect of DES/ water mass ratio, and initial drug concentration at each of these DESs followed by recycling schemes to assess the reuse and recovery of DESs to achieve sustainable and a circular approach to solvent regeneration. The interactive framework of the DES-enoxacin complex has been investigated in quantum chemical (QC) studies via interaction energy (IE), natural bonding orbital (NBO), frontier molecular orbital (FMO) and non-covalent interaction NCI) analysis.

In chapter 4, we successfully implemented DL-menthol-based hydrophobic DESs in a batch-type extraction process. To develop a continuous process along with higher achievable extraction performance, we have employed a PDMS-based microchannel to extract a fluoroquinolone drug (ciprofloxacin) and an antifungal drug (fluconazole) using DL-menthol: carboxylic acid-based DESs, as addressed in **Chapter 5**. This chapter combines experimental findings with theoretical investigations to support and validate the obtained results. In the experimental study, the effect of contact time in the microchannel, the flow rate of the phases within the channel and the DES/ water mass ratio, on the extraction efficiency for both pharmaceutical drugs have been examined. The quantification of the compositions is carried out by the UV-vis spectroscopy method. The mechanism of the extraction has been thoroughly evaluated by theoretical studies. While interaction energy (IE), structural properties and hydrogen bonding (H-bonds) are the findings of the molecular dynamics (MD) simulation, the quantum chemical (QC) study highlights the atomistic level insights on the structural arrangements of the DES-drug complexes and their stability via HOMO-LUMO (highest occupied molecular orbital- lowest unoccupied molecular orbital) energy gap analysis. Further in this chapter, atoms-in-molecules (AIM) and non-covalent interaction (NCI) analysis have been performed to display the involvement of closed-shell weak interactions in forming a strong interactive framework in maintaining the stability of the DES-drug complex structure. Finally, **Chapter 6** summarizes the key findings of the thesis work and also presents a discussion on future directions.

References

(1) Abdel-Raouf, N.; Al-Homaidan, A. A.; Ibraheem, I. B. M. Microalgae and Wastewater Treatment. *Saudi J. Biol. Sci.* **2012**, *19* (3), 257–275. https://doi.org/10.1016/j.sjbs.2012.04.005.

(2) Fent, K.; Weston, A. A.; Caminada, D. Ecotoxicology of Human Pharmaceuticals. *Aquat. Toxicol.* **2006**, *76* (2), 122–159. https://doi.org/10.1016/j.aquatox.2005.09.009.

(3) Luo, Y.; Guo, W.; Ngo, H. H.; Nghiem, L. D.; Hai, F. I.; Zhang, J.; Liang, S.; Wang, X. C. A Review on the Occurrence of Micropollutants in the Aquatic Environment and Their Fate and Removal during Wastewater Treatment. *Sci. Total Environ.* **2014**, *473–474*, 619–641. https://doi.org/10.1016/j.scitotenv.2013.12.065.

(4) Sontheimer, H.; Brauch, H. J.; Kühn, W. Impact of Different Types of Organic Micropollutants Present on Sources of Drinking Water on the Quality of Drinking Water. *Sci. Total Environ.* **1985**, *47*, 27–44. https://doi.org/10.1016/0048-9697(85)90317-1.

(5) Larsson, D. G. J.; de Pedro, C.; Paxeus, N. Effluent from Drug Manufactures Contains Extremely High Levels of Pharmaceuticals. *J. Hazard. Mater.* **2007**, *148* (3), 751–755. https://doi.org/https://doi.org/10.1016/j.jhazmat.2007.07.008.

(6) Fick, J.; Söderström, H.; Lindberg, R. H.; Phan, C.; Tysklind, M.; Larsson, D. G. J. Contamination of Surface, Ground, and Drinking Water from Pharmaceutical Production. *Environ. Toxicol. Chem.* **2009**, *28* (12), 2522–2527. https://doi.org/10.1897/09-073.1.

(7) Rodriguez, D.; Van Buynder, P.; Lugg, R.; Blair, P.; Devine, B.; Cook, A.; Weinstein, P. Indirect Potable Reuse: A Sustainable Water Supply Alternative. *Int. J. Environ. Res. Public Health* **2009**, *6* (3), 1174–1209. https://doi.org/10.3390/ijerph6031174.

(8) Muga, H. E.; Mihelcic, J. R. Sustainability of Wastewater Treatment Technologies. *J. Environ. Manage.* **2008**, *88* (3), 437–447. https://doi.org/10.1016/j.jenvman.2007.03.008.

(9) Hannah, S. A.; Austern, B. M.; Eralp, A. E.; Wise, R. H. Comparative Removal of Toxic Pollutants by Six Wastewater Treatment Processes. *J. Water Pollut. Control Fed.* **1986**, *58* (1), 27–34.

(10) Ebro, H.; Kim, Y. M.; Kim, J. H. Molecular Dynamics Simulations in Membrane-Based Water Treatment Processes: A Systematic Overview. *J. Memb. Sci.* **2013**, *438*, 112–125. https://doi.org/https://doi.org/10.1016/j.memsci.2013.03.027.

(11) Grassi, M.; Kaykioglu, G.; Belgiorno, V.; Lofrano, G. Removal of Emerging Contaminants from Water and Wastewater by Adsorption Process. In *Emerging Compounds Removal from Wastewater: Natural and Solar Based Treatments*; Lofrano, G., Ed.; Springer Netherlands: Dordrecht, 2012; pp 15–37. https://doi.org/10.1007/978-94-007-3916-1_2.

(12) Ali, I.; Gupta, V. K. Advances in Water Treatment by Adsorption Technology. *Nat. Protoc.* **2007**, *1* (6), 2661–2667. https://doi.org/10.1038/nprot.2006.370.

(13) Gupta, V. K.; Gupta, B.; Rastogi, A.; Agarwal, S.; Nayak, A. Pesticides Removal from Waste Water by Activated Carbon Prepared from Waste Rubber Tire. *Water Res.* **2011**, *45* (13), 4047–4055. https://doi.org/10.1016/j.watres.2011.05.016.

(14) Carballa, M.; Omil, F.; Lema, J. M. Issn : 1579-4377 Removal of Pharmaceuticals and Personal Care Products (Ppcps) From Municipal Wastewaters By Physico-Chemical Processes. **1999**, 309–313.

(15) López-Montilla, J. C.; Pandey, S.; Shah, D. O.; Crisalle, O. D. Removal of Non-Ionic Organic Pollutants from Water via Liquid-Liquid Extraction. *Water Res.* **2005**, *39* (9), 1907–1913. https://doi.org/10.1016/j.watres.2005.02.018.

(16) Fortuny, A.; Coll, M. T.; Sastre, A. M. Ionic Liquids as a Carrier for Chloride Reduction from Brackish Water Using Hollow Fiber Renewal Liquid Membrane. *Desalination*

2014, *343*, 54–59. https://doi.org/10.1016/j.desal.2013.10.029.

(17) Lozano, L. J.; Godínez, C.; de los Ríos, A. P.; Hernández-Fernández, F. J.; Sánchez-Segado, S.; Alguacil, F. J. Recent Advances in Supported Ionic Liquid Membrane Technology. *J. Memb. Sci.* **2011**, *376* (1–2), 1–14. https://doi.org/10.1016/j.memsci.2011.03.036.

(18) Moscoso, F.; Deive, F. J.; Esperança, J. M. S. S.; Rodríguez, A. Pesticide Removal from Aqueous Solutions by Adding Salting out Agents. *Int. J. Mol. Sci.* **2013**, *14* (10), 20954–20965. https://doi.org/10.3390/ijms141020954.

(19) Tassanapukdee, Y.; Prayongpan, P.; Songsrirote, K. Removal of Heavy Metal Ions from an Aqueous Solution by CS/PVA/PVP Composite Hydrogel Synthesized Using Microwaved-Assisted Irradiation. *Environ. Technol. Innov.* **2021**, *24*, 101898. https://doi.org/https://doi.org/10.1016/j.eti.2021.101898.

(20) Abbott, A. P.; Capper, G.; Davies, D. L.; Rasheed, R. K.; Tambyrajah, V. Novel Solvent Properties of Choline Chloride/Urea Mixtures. *Chem. Commun.* **2003**, No. 1, 70–71. https://doi.org/10.1039/b210714g.

(21) Abbott, A. P.; Boothby, D.; Capper, G.; Davies, D. L.; Rasheed, R. K. Deep Eutectic Solvents Formed between Choline Chloride and Carboxylic Acids: Versatile Alternatives to Ionic Liquids. *J. Am. Chem. Soc.* **2004**, *126* (29), 9142–9147. https://doi.org/10.1021/ja048266j.

(22) Papu Kumar Naik, Nikhil Kumar, Nabendu Paul, T. B. *Deep Eutectic Solvents in Liquid–Liquid Extraction Correlation and Molecular Dynamics Simulation*; Taylor & Francis, 2022. https://doi.org/10.1201/9781003231158.

(23) Amphlett, J. T. M.; Choi, S. Metal Oxide Solubility in Deep Eutectic Solvents ± Applications in Decontamination in Decommissioning. **2019**, *3*, 287–288.

(24) Ivanova, N.; Gugleva, V.; Dobreva, M.; Pehlivanov, I.; Stefanov, S.; Andonova, V. Silver Nanoparticles as Multi-Functional Drug Delivery Systems. In *Nanomedicines*; Farrukh, M. A., Ed.; IntechOpen: Rijeka, 2019. https://doi.org/10.5772/intechopen.80238.

(25) Söldner, A.; Zach, J.; König, B. Deep Eutectic Solvents as Extraction Media for Metal Salts and Oxides Exemplarily Shown for Phosphates from Incinerated Sewage Sludge Ash. *Green Chem.* **2019**, *21* (2), 321–328. https://doi.org/10.1039/c8gc02702a.

(26) Abbott, A. P.; Alhaji, A. I.; Ryder, K. S.; Horne, M.; Rodopoulos, T. Electrodeposition of Copper-Tin Alloys Using Deep Eutectic Solvents. *Trans. Inst. Met. Finish.* **2016**, *94* (2), 104–113. https://doi.org/10.1080/00202967.2016.1148442.

(27) Jenkin, G. R. T.; Al-Bassam, A. Z. M.; Harris, R. C.; Abbott, A. P.; Smith, D. J.; Holwell, D. A.; Chapman, R. J.; Stanley, C. J. The Application of Deep Eutectic Solvent Ionic Liquids for Environmentally-Friendly Dissolution and Recovery of Precious Metals. *Miner. Eng.* **2016**, *87*, 18–24. https://doi.org/10.1016/j.mineng.2015.09.026.

(28) Li, C.; Li, D.; Zou, S.; Li, Z.; Yin, J.; Wang, A.; Cui, Y.; Yao, Z.; Zhao, Q. Extraction Desulfurization Process of Fuels with Ammonium-Based Deep Eutectic Solvents. *Green Chem.* **2013**, *15* (10), 2793–2799. https://doi.org/10.1039/c3gc41067f.

(29) Zhao, H.; Baker, G. A. Oxidative Desulfurization of Fuels Using Ionic Liquids: A Review. *Front. Chem. Sci. Eng.* **2015**, *9* (3), 262–279. https://doi.org/10.1007/s11705-015-1528-0.

(30) Zhao, H.; Baker, G. A.; Wagle, D. V.; Ravula, S.; Zhang, Q. Tuning Task-Specific Ionic Liquids for the Extractive Desulfurization of Liquid Fuel. *ACS Sustain. Chem. Eng.* **2016**, *4* (9), 4771–4780. https://doi.org/10.1021/acssuschemeng.6b00972.

(31) Hizaddin, H. F.; Ramalingam, A.; Hashim, M. A.; Hadj-Kali, M. K. O. Evaluating the Performance of Deep Eutectic Solvents for Use in Extractive Denitrification of Liquid Fuels by the Conductor-like Screening Model for Real Solvents. *J. Chem. Eng. Data* **2014**, *59* (11), 3470–3487. https://doi.org/10.1021/je5004302.

(32) Lima, F.; Dave, M.; Silvestre, A. J. D.; Branco, L. C.; Marrucho, I. M. Concurrent

Desulfurization and Denitrogenation of Fuels Using Deep Eutectic Solvents. *ACS Sustain. Chem. Eng.* **2019**, *7* (13), 11341–11349. https://doi.org/10.1021/acssuschemeng.9b00877.

(33) Zhao, H.; Zhang, C.; Crittle, T. D. Choline-Based Deep Eutectic Solvents for Enzymatic Preparation of Biodiesel from Soybean Oil. *J. Mol. Catal. B Enzym.* **2013**, *85–86*, 243–247. https://doi.org/10.1016/j.molcatb.2012.09.003.

(34) Gutiérrez, M. C.; Ferrer, M. L.; Mateo, C. R.; Monte, F. Del. Freeze-Drying of Aqueous Solutions of Deep Eutectic Solvents: A Suitable Approach to Deep Eutectic Suspensions of Self-Assembled Structures. *Langmuir* **2009**, *25* (10), 5509–5515. https://doi.org/10.1021/la900552b.

(35) Tran, M. K.; Rodrigues, M. T. F.; Kato, K.; Babu, G.; Ajayan, P. M. Deep Eutectic Solvents for Cathode Recycling of Li-Ion Batteries. *Nat. Energy* **2019**, *4* (4), 339–345. https://doi.org/10.1038/s41560-019-0368-4.

(36) Whitehead, A. H.; Pölzler, M.; Gollas, B. Zinc Electrodeposition from a Deep Eutectic System Containing Choline Chloride and Ethylene Glycol. *J. Electrochem. Soc.* **2010**, *157* (6), D328. https://doi.org/10.1149/1.3364930.

(37) Ruggeri, S.; Poletti, F.; Zanardi, C.; Pigani, L.; Zanfrognini, B.; Corsi, E.; Dossi, N.; Salomäki, M.; Kivelä, H.; Lukkari, J.; Terzi, F. Chemical and Electrochemical Properties of a Hydrophobic Deep Eutectic Solvent. *Electrochim. Acta* **2019**, *295*, 124–129. https://doi.org/10.1016/j.electacta.2018.10.086.

(38) Ribeiro, B. D.; Florindo, C.; Iff, L. C.; Coelho, M. A. Z.; Marrucho, I. M. Menthol-Based Eutectic Mixtures: Hydrophobic Low Viscosity Solvents. *ACS Sustain. Chem. Eng.* **2015**, *3* (10), 2469–2477. https://doi.org/10.1021/acssuschemeng.5b00532.

(39) Van Osch, D. J. G. P.; Zubeir, L. F.; Van Den Bruinhorst, A.; Rocha, M. A. A.; Kroon, M. C. Hydrophobic Deep Eutectic Solvents as Water-Immiscible Extractants. *Green Chem.* **2015**, *17* (9), 4518–4521. https://doi.org/10.1039/c5gc01451d.

(40) Florindo, C.; Branco, L. C.; Marrucho, I. M. Development of Hydrophobic Deep Eutectic Solvents for Extraction of Pesticides from Aqueous Environments. *Fluid Phase Equilib.* **2017**, *448*, 135–142. https://doi.org/10.1016/j.fluid.2017.04.002.

(41) Morrison, H. G.; Sun, C. C.; Neervannan, S. Characterization of Thermal Behavior of Deep Eutectic Solvents and Their Potential as Drug Solubilization Vehicles. *Int. J. Pharm.* **2009**, *378* (1–2), 136–139. https://doi.org/10.1016/j.ijpharm.2009.05.039.

(42) Tang, W.; Dai, Y.; Row, K. H. Evaluation of Fatty Acid/Alcohol-Based Hydrophobic Deep Eutectic Solvents as Media for Extracting Antibiotics from Environmental Water. *Anal. Bioanal. Chem.* **2018**, *410* (28), 7325–7336. https://doi.org/10.1007/s00216-018-1346-6.

(43) Diuzheva, A.; Balogh, J.; Jekő, J.; Cziáky, Z. Application of Liquid–Liquid Microextraction for the Effective Separation and Simultaneous Determination of 11 Pharmaceuticals in Wastewater Samples Using High-Performance Liquid Chromatography with Tandem Mass Spectrometry. *J. Sep. Sci.* **2018**, *41* (14), 2870–2877. https://doi.org/https://doi.org/10.1002/jssc.201800309.

(44) Zawadzki, M.; e Silva, F. A.; Domańska, U.; Coutinho, J. A. P.; Ventura, S. P. M. Recovery of an Antidepressant from Pharmaceutical Wastes Using Ionic Liquid-Based Aqueous Biphasic Systems. *Green Chem.* **2016**, *18* (12), 3527–3536. https://doi.org/10.1039/C5GC03052H.

(45) e Silva, F. A.; Sintra, T.; Ventura, S. P. M.; Coutinho, J. A. P. Recovery of Paracetamol from Pharmaceutical Wastes. *Sep. Purif. Technol.* **2014**, *122*, 315–322. https://doi.org/https://doi.org/10.1016/j.seppur.2013.11.018.

(46) Almeida, H. F. D.; Marrucho, I. M.; Freire, M. G. Removal of Nonsteroidal Anti-Inflammatory Drugs from Aqueous Environments with Reusable Ionic-Liquid-Based Systems. *ACS Sustain. Chem. Eng.* **2017**, *5* (3), 2428–2436. https://doi.org/10.1021/acssuschemeng.6b02771.

(47) Yang, D.; Wang, Y.; Peng, J.; Xun, C.; Yang, Y. A Green Deep Eutectic Solvents Microextraction Coupled with Acid-Base Induction for Extraction of Trace Phenolic Compounds in Large Volume Water Samples. *Ecotoxicol. Environ. Saf.* **2019**, *178*, 130–136. https://doi.org/https://doi.org/10.1016/j.ecoenv.2019.04.021.

(48) Liu, Y.; Xu, W.; Zhang, H.; Xu, W. Hydrophobic Deep Eutectic Solvent-Based Dispersive Liquid–Liquid Microextraction for the Simultaneous Enantiomeric Analysis of Five β-Agonists in the Environmental Samples. *Electrophoresis* **2019**, *40* (21), 2828–2836. https://doi.org/https://doi.org/10.1002/elps.201900149.

(49) An, Y.; Ma, W.; Row, K. H. Preconcentration and Determination of Chlorophenols in Wastewater with Dispersive Liquid–Liquid Microextraction Using Hydrophobic Deep Eutectic Solvents. *Anal. Lett.* **2020**, *53* (2), 262–272. https://doi.org/10.1080/00032719.2019.1646754.

(50) Yousefi, S. M.; Shemirani, F.; Ghorbanian, S. A. Hydrophobic Deep Eutectic Solvents in Developing Microextraction Methods Based on Solidification of Floating Drop: Application to the Trace HPLC/FLD Determination of PAHs. *Chromatographia* **2018**, *81* (8), 1201–1211. https://doi.org/10.1007/s10337-018-3548-7.

(51) Moghadam, A. G.; Rajabi, M.; Asghari, A. Efficient and Relatively Safe Emulsification Microextraction Using a Deep Eutectic Solvent for Influential Enrichment of Trace Main Anti-Depressant Drugs from Complicated Samples. *J. Chromatogr. B* **2018**, *1072*, 50–59. https://doi.org/https://doi.org/10.1016/j.jchromb.2017.09.042.

(52) Liu, X.; Liu, C.; Qian, H.; Qu, Y.; Zhang, S.; Lu, R.; Gao, H.; Zhou, W. Ultrasound-Assisted Dispersive Liquid-Liquid Microextraction Based on a Hydrophobic Deep Eutectic Solvent for the Preconcentration of Pyrethroid Insecticides Prior to Determination by High-Performance Liquid Chromatography. *Microchem. J.* **2019**, *146*, 614–621. https://doi.org/https://doi.org/10.1016/j.microc.2019.01.048.

(53) Makoś, P.; Przyjazny, A.; Boczkaj, G. Hydrophobic Deep Eutectic Solvents as "Green" Extraction Media for Polycyclic Aromatic Hydrocarbons in Aqueous Samples. *J. Chromatogr. A* **2018**, *1570*, 28–37. https://doi.org/10.1016/j.chroma.2018.07.070.

(54) Thongsaw, A.; Udnan, Y.; Ross, G. M.; Chaiyasith, W. C. Speciation of Mercury in Water and Biological Samples by Eco-Friendly Ultrasound-Assisted Deep Eutectic Solvent Based on Liquid Phase Microextraction with Electrothermal Atomic Absorption Spectrometry. *Talanta* **2019**, *197*, 310–318. https://doi.org/https://doi.org/10.1016/j.talanta.2019.01.018.

(55) Yilmaz, E.; Soylak, M. Ultrasound Assisted-Deep Eutectic Solvent Based on Emulsification Liquid Phase Microextraction Combined with Microsample Injection Flame Atomic Absorption Spectrometry for Valence Speciation of Chromium(III/VI) in Environmental Samples. *Talanta* **2016**, *160*, 680–685. https://doi.org/https://doi.org/10.1016/j.talanta.2016.08.001.

(56) Florindo, C.; Lima, F.; Branco, L. C.; Marrucho, I. M. Hydrophobic Deep Eutectic Solvents: A Circular Approach to Purify Water Contaminated with Ciprofloxacin. *ACS Sustain. Chem. Eng.* **2019**, *7* (17), 14739–14746. https://doi.org/10.1021/acssuschemeng.9b02658.

(57) de los Ríos, A. P.; Hernández-Fernández, F. J.; Lozano, L. J.; Sánchez, S.; Moreno, J. I.; Godínez, C. Removal of Metal Ions from Aqueous Solutions by Extraction with Ionic Liquids. *J. Chem. Eng. Data* **2010**, *55* (2), 605–608. https://doi.org/10.1021/je9005008.

(58) Paul, N.; Banerjee, T. Study on the Extraction of Acetamiprid and Imidacloprid from an Aqueous Environment Using Menthol-Based Hydrophobic Eutectic Solvents: Quantum Chemical and Molecular Dynamics Insights. *ACS Sustain. Chem. Eng.* **2022**, *10* (13), 4227–4246. https://doi.org/10.1021/acssuschemeng.2c00023.

(59) Eike, D. M.; Maginn, E. J. Atomistic Simulation of Solid-Liquid Coexistence for Molecular Systems: Application to Triazole and Benzene. *J. Chem. Phys.* **2006**, *124* (16). https://doi.org/10.1063/1.2188400.

(60) Mohan, M.; Naik, P. K.; Banerjee, T.; Goud, V. V.; Paul, S. Solubility of Glucose in Tetrabutylammonium Bromide Based Deep Eutectic Solvents: Experimental and Molecular Dynamic Simulations. *Fluid Phase Equilib.* **2017**, *448*, 168–177. https://doi.org/10.1016/j.fluid.2017.05.024.

(61) Paul, S.; Paul, S. The Influence of Trehalose on Hydrophobic Interactions of Small Nonpolar Solute: A Molecular Dynamics Simulation Study. *J. Chem. Phys.* **2013**, *139* (4). https://doi.org/10.1063/1.4816521.

(62) Naik, P. K.; Paul, S.; Banerjee, T. Physiochemical Properties and Molecular Dynamics Simulations of Phosphonium and Ammonium Based Deep Eutectic Solvents. *J. Solution Chem.* **2019**, *48* (7), 1046–1065. https://doi.org/10.1007/s10953-019-00903-0.

(63) Naik, P. K.; Mohan, M.; Banerjee, T.; Paul, S.; Goud, V. V. Molecular Dynamic Simulations for the Extraction of Quinoline from Heptane in the Presence of a Low-Cost Phosphonium-Based Deep Eutectic Solvent. *J. Phys. Chem. B* **2018**, *122* (14), 4006–4015. https://doi.org/10.1021/acs.jpcb.7b10914.

(64) Ray, P.; Elfgen, R.; Kirchner, B. Cation Influence on Heterocyclic Ammonium Ionic Liquids: A Molecular Dynamics Study. *Phys. Chem. Chem. Phys.* **2019**, *21* (8), 4472–4486. https://doi.org/10.1039/c8cp07683a.

(65) Wagle, D. V.; Zhao, H.; Deakyne, C. A.; Baker, G. A. Quantum Chemical Evaluation of Deep Eutectic Solvents for the Extractive Desulfurization of Fuel. *ACS Sustain. Chem. Eng.* **2018**, *6* (6), 7525–7531. https://doi.org/10.1021/acssuschemeng.8b00224.

(66) Mishra, D. K.; Banerjee, B.; Pugazhenthi, G.; Banerjee, T. Metal-Free, Ionic Liquid-Mediated Hydrogen Release from Amine Borane Complexes: An Experimental and Density Functional Theory Investigation. *Ind. Eng. Chem. Res.* **2021**, *60* (27), 9764–9776. https://doi.org/10.1021/acs.iecr.1c01507.

(67) Panda, D. K.; Bhargava, B. L. Intermolecular Interactions in Tetrabutylammonium Chloride Based Deep Eutectic Solvents: Classical Molecular Dynamics Studies. *J. Mol. Liq.* **2021**, *335*, 116139. https://doi.org/https://doi.org/10.1016/j.molliq.2021.116139.

(68) Kivelä, H.; Salomäki, M.; Vainikka, P.; Mäkilä, E.; Poletti, F.; Ruggeri, S.; Terzi, F.; Lukkari, J. Effect of Water on a Hydrophobic Deep Eutectic Solvent. *J. Phys. Chem. B* **2022**, *126* (2), 513–527. https://doi.org/10.1021/acs.jpcb.1c08170.

(69) Abbas, U. L.; Qiao, Q.; Nguyen, M. T.; Shi, J.; Shao, Q. Structure and Hydrogen Bonds of Hydrophobic Deep Eutectic Solvent-Aqueous Liquid–Liquid Interfaces. *AIChE J.* **2021**, *67* (12), e17427. https://doi.org/https://doi.org/10.1002/aic.17427.

(70) Malik, A.; Kashyap, H. K. Multiple Evidences of Dynamic Heterogeneity in Hydrophobic Deep Eutectic Solvents. *J. Chem. Phys.* **2021**, *155* (4), 44502. https://doi.org/10.1063/5.0054699.

Chapter- 2

Computational Studies on the Water Stability of Hydrophobic Deep Eutectic Solvents

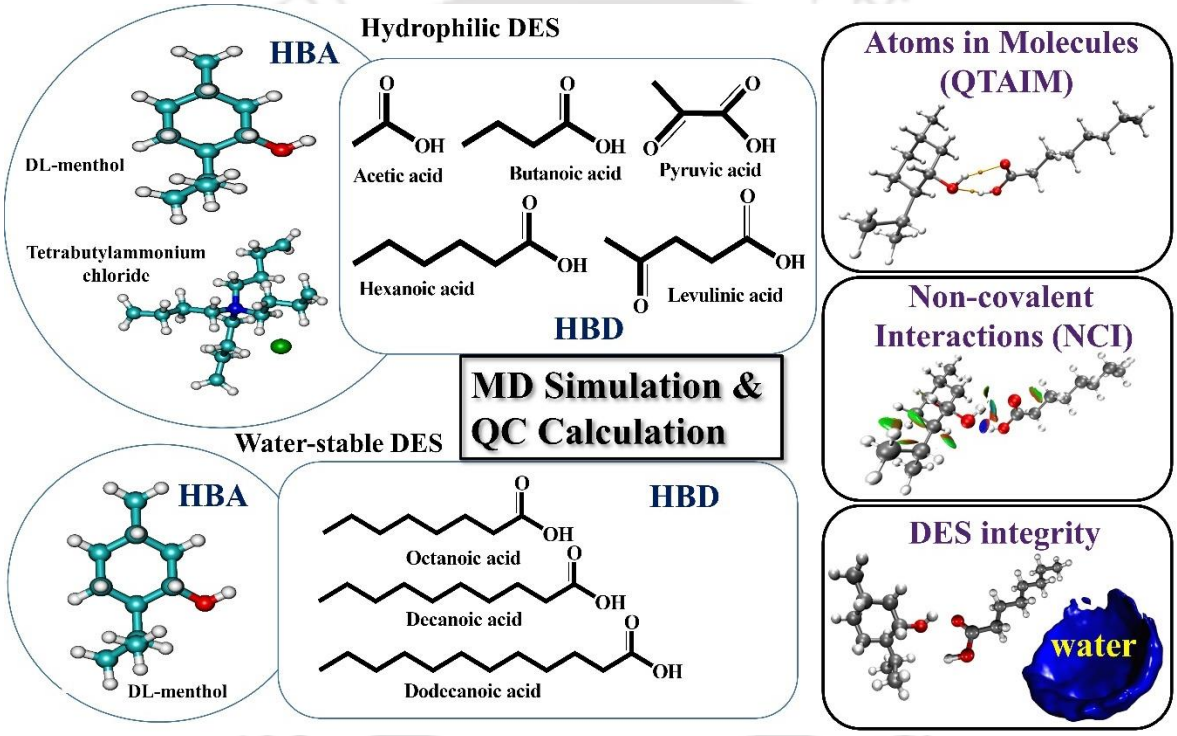

Published Article:

N. Paul, P.K. Naik, B.D. Ribeiro, P.S.G. Pattader, I.M. Marrucho, T. Banerjee, Molecular Dynamics Insights and Water Stability of Hydrophobic Deep Eutectic Solvents Aided Extraction of Nitenpyram from an Aqueous Environment, J. Phys. Chem. B., 124 (34) (2020) 7405–7420.

N. Paul, T. Banerjee, Stability Mechanism of Menthol and Fatty Acid Based Hydrophobic Eutectic Solvents: Insights from Nonbonded Interactions, ACS Sustain. Chem. Eng., 11 (2023) 3539−3556.

2 Computational Studies on the Water Stability of Hydrophobic Deep Eutectic Solvents

The current chapter reports the computational evaluation of the formation mechanism and stability of type-V DESs comprised of DL-menthol and tetrabutylammonium chloride as HBAs, and carboxylic acids (acetic, butanoic, hexanoic, octanoic, nonanoic, decanoic and dodecanoic acid) as HBDs through MD simulation followed by QC calculation. The formation mechanism can immensely help in understanding the applicability of these DESs. The non-bonded interaction energy, structural properties, hydrogen bonding and charge transfer analysis are a useful application of MD simulation that has been implemented here. The QC study combined with the QTAIM analysis has been carried out to reveal the closed-shell non-bonded interactions present within the DES system. To observe the behaviour of the hydrophobic DESs in aqueous system-based applications, solvation studies of the DESs have been carried out employing both explicit as well as implicit solvation models. The QTAIM-based non-covalent interaction (NCI) analysis has been performed to reveal the extent of hydrogen bonding and dispersion interactions among the components for pure as well as solvated state of the DESs

2.1 Introduction

The term 'ionic liquid' (IL) has been around for the past 25 years, beginning in the early 1990s.[1,2] It has been responsible for revolutionizing the entire green chemistry associated fields due to its excellent properties, including high thermal and chemical stability, lower vapour pressure, and recyclability.[3–6] Despite these excellent properties, ionic liquids have serious drawbacks, such as high toxicity, poor biodegradability for a certain class of ILs, high cost of precursors, and complexity of the recycling process.[7,8] In search of new and improved quality solvents, researchers have come up with a new class of IL-analogous green solvents, namely ‘deep eutectic solvent’ (DES) having proficiencies such as excellent biodegradability and biocompatibility, lower vapour pressure and lesser toxicity, less expensive and ease of preparation as compared to the ILs, thus addressing the shortcomings of the ILs.[9] Since the advent of the first DES, choline chloride-urea DES, in 2003 by Abbott et al. several types of DESs have been discovered by researchers all over the globe.[10] It was simply obtained by the mixing of choline chloride acting as a hydrogen bond acceptor (HBA) and urea as hydrogen

bond donor (HBD) at a specific temperature and suitable molar ratio that can be termed as 'eutectic composition', the resultant deep eutectic mixture (DES) obtained a melting point comfortably below than that of the pure precursors.[10] Over a decade or so, several classes of DESs have been utilized in different fields of application such as electrochemistry, chemical and biomedical applications, extraction, purification, catalytic processes, and so forth.[11–23] Different combinations of HBAs and HBDs can be adopted to fine-tune DESs for a specific application. The most recent class of DESs are type V DES, mainly associated with selecting naturally occurring benign compounds (non-ionic compounds) as HBA and HBD components, termed NADES (natural deep eutectic solvents).

The DES's affinity for its surroundings is a potentially game-changing factor in how the solvent functions as a whole. While hydrophilic DESs have been the majority in the past, hydrophobic alternatives, namely hydrophobic deep eutectic solvents (HDESs) have emerged in the recent decade or so to assist in aqueous system-based applications including metal ion extraction, pharmaceutical remediation, and so on.[24,25] Quaternary ammonium salt−decanoic acid-based HDESs, among the earliest identified HDESs, along with DL-menthol and carboxylic acid-based HDESs have been implemented in the aqueous-based extraction experiments.[24] The study performed by Florindo et al. explored the durability of the menthol-fatty acid-based, as well as ammonium salt-based DES systems,[26] to analyze their aqueous-phase stability via experiments. However, a detailed molecular-level understanding of the formation mechanism of the DES and the HBA-HBD interactive frameworks is yet quite insufficient.

The hydrogen bonding network in conjunction with the electrostatic and dispersion interactions may prove to be crucial in the formation of DESs and in modulating the extraction performance of the DES, as well. The mechanism of interaction and formation of type I and type III DES has been the subject of several studies. Computational approaches have been utilized by Ashworth et al.,[27] Zhekenov et al.,[28], Zahn et al.,[29] Sun et al.[30] and Yang's group[31] to understand the hydrogen bonding, charge delocalization, effect of the HBA and the HBD in melting point and freezing point depression in DES systems along with some experimentation. The correlation between melting temperatures and electron density was predicted by García et al. using quantum chemistry calculations and atom-in-molecule (AIM) analysis in ChCl-based DES systems.[32]

On the other hand, there aren't quite adequate computational studies that investigate the formation mechanism of type V DES. In our prior works, we implemented molecular dynamics (MD) modelling[33] and quantum chemistry (QC)[34] to gain a better

knowledge of the behaviour and extraction performance of several hydrophobic DESs in an aqueous environment. While the MD simulation has been utilized to obtain the thermodynamic characteristics of the bulk system, the density functional theory (DFT) study addressed the analysis of the charge transfer (CT), orbital energies, and molecular reactivity of the systems. Extraction studies involving the water phase have shown that menthol-carboxylic acid-based DESs are the most adaptable solvents during their development. Understanding interactive pathways, mobility and electron cloud delocalization, ground and excited state orbital participation, and prevention of disruption of own structural arrangement against the penetration by an outside entity require observation at the molecular and atomic level. Panda et al. studied the effect of two different hydrogen bond donors (HBDs) namely, glycerol and ethylene glycol, and tetrabutylammonium chloride as HBA, to explore the effect of HBDs on the structure of DESs. Structural property analysis suggested dominant interaction between the anion and the HBD. Long-range structural ordering has been witnessed among the DES components with the existence of electrostatic as well as hydrogen bonding.[35] Kivelä et al. investigated the effect of low water content on the hydrophobic DES, tetrabutylammonium chloride: decanoic acid (1:2), through MD simulation and spectroscopic characterization techniques. They observed that the low water content affected changing the density, viscosity and electrical conductivity of the DES. A network of intermolecular non-bonded interactions was observed between the DES components in the form of chloride−carboxylic acid hydrogen bonding and the introduction of water broke the interactions by hydrating the carboxylic acid groups and chloride ions leading to dynamic nanoscale phase segregation.[36] Abbas et al. investigated the density profile, dipole moment, and hydrogen bonds of DES-aqueous interfaces of eight hydrophobic DES composed of four organic compounds: decanoic acid, menthol, thymol, and lidocaine using molecular dynamics simulations. Hydrogen bond connectivity between the HBA and HBD had been observed for all the DESS along with a moderate number and lower stability of the DES-water hydrogen bond in the interface. They also observed the variation of the dipole fluctuation and heterogeneous hydrogen bonds at the liquid-liquid interface for all eight DES systems.[37] Malik et al. performed an MD simulation to investigate the dynamics of DL-menthol (DLM) based HDESs with hexanoic (C_6), octanoic (C_8), and decanoic (C_{10}) acids as HBDs to reveal the hydrogen bond relaxation with time and the lifetime associated with the strong and weak hydrogen bonding interactions present in these HDESs. It was also revealed that the translational dynamics of the species in the HDES become slower with increasing tail length of the organic acid, while slightly enhanced caging was also observed for the HDES with a longer tail length of the acids.[38] A proper combination of

experimental and theoretical studies such as MD simulation and QC calculations can provide useful insights to understand the formation, stability and dynamics of DL-menthol: carboxylic acid-based HDESs.

Density functional theory (DFT) calculations have been used throughout this study to investigate the formation mechanism of DL-menthol and carboxylic acid (acetic, butanoic, hexanoic, octanoic, nonanoic, decanoic, and dodecanoic acid) based DESs in their pure state along with the solvated state calculations of the same DESs. The optimized geometries, electronic structures, molecular orbitals, charge transfer and delocalization, angular distributions, interaction energy and solvation properties of the DESs, have all been investigated in this work. In addition to this, the MD simulation-derived spatial distribution function, also known as SDF, was generated to comprehend the three-dimensional density distribution of the components. The DFT-based explicit as well as implicit solvation model has been implemented to observe the changes that occurred in the intermolecular interaction frameworks due to the presence of an aqueous environment and also for obtaining the dissolution dynamics of the DESs. In addition, Bader's quantum theory of atoms in molecules[39], commonly known as QTAIM, as well as noncovalent interactions, also known as the reduced density gradient (RDG) or NCI approach, have been employed in studies to investigate the interaction mechanism. The DFT study, in conjunction with the results of the MD simulations, has been followed by an analysis of the non-covalent interactions, which collectively present multifaceted investigative insights into the formation and stability mechanism of DL menthol-carboxylic acid-based DESs, which represent type V DES.

2.2 Computational Details

2.2.1 Quantum Chemical Calculation

Initially, the DES-optimized structures were generated by inserting the individual carboxylic fatty acids (acetic acid, butanoic acid, hexanoic acid, octanoic acid, decanoic acid and dodecanoic acid) around multiple possible orientations around the DL-menthol moiety using GaussView 6. Geometry optimization was carried out primarily employing B3LYP density functional in combination with 6-311+G(d,p) basis set, for the DES components using Gaussian 16.[40] Grimme and coworkers' atom-pair-wise correction techniques with Becke-Johnson damping (D3BJ) were used to accounting for the long-range dispersion effects between the HBA and the HBD.[41,42] The BJ-damping requires one fit parameter more for each functional (three instead of two) but has the advantage of avoiding repulsive interatomic forces

at shorter distances. With BJ-damping better results for non-bonded distances and clear effects of intramolecular dispersion in the molecular systems can be obtained with higher precision in calculating the non-bonded interaction.[42] Energy minima were identified as the consequent stationary points on the hypersurface of potential energy by vibrational frequency analysis as triggered by the 'freq' keyword in Gaussian at the same level of theory. Subsequently, the geometries are re-optimized again at the M06-2X functional[43] with the same basis set, i.e., 6-311+G(d,p) for a comparative study considering the suitability of this functional in analyzing similar systems. The counterpoise approach in eliminating the basis set superposition error is exercised for the interaction energy and other subsequent quantum chemical calculations.[44] Natural bond orbital (NBO) analysis[45] and CHELPG partial charge analysis designed for the charge distribution and transfer in eutectic systems, and frontier molecular orbital (FMO) analysis,[46] for the molecular electronic structure based on the frontier orbital overlap and the electronic transition were carried out. NBO study elucidated the charge transfer (CT) profile of the DES systems based on the distribution of charges over the components. The implicit solvation study was performed by employing the SMD solvation model developed by the Truhler group on the optimized DES structures to calculate the Gibbs free energy of solvation (ΔG_{solv}), selecting water as the solvent medium[47] and the explicit solvation was performed with two water molecules explicitly positioned around each of the DESs and optimizing those structures. All the calculations were performed using the Gaussian 16 package.[40] The chemical structures of the components and the composition of the DESs have been presented in Figure 2.1 and Table 2.1, respectively.

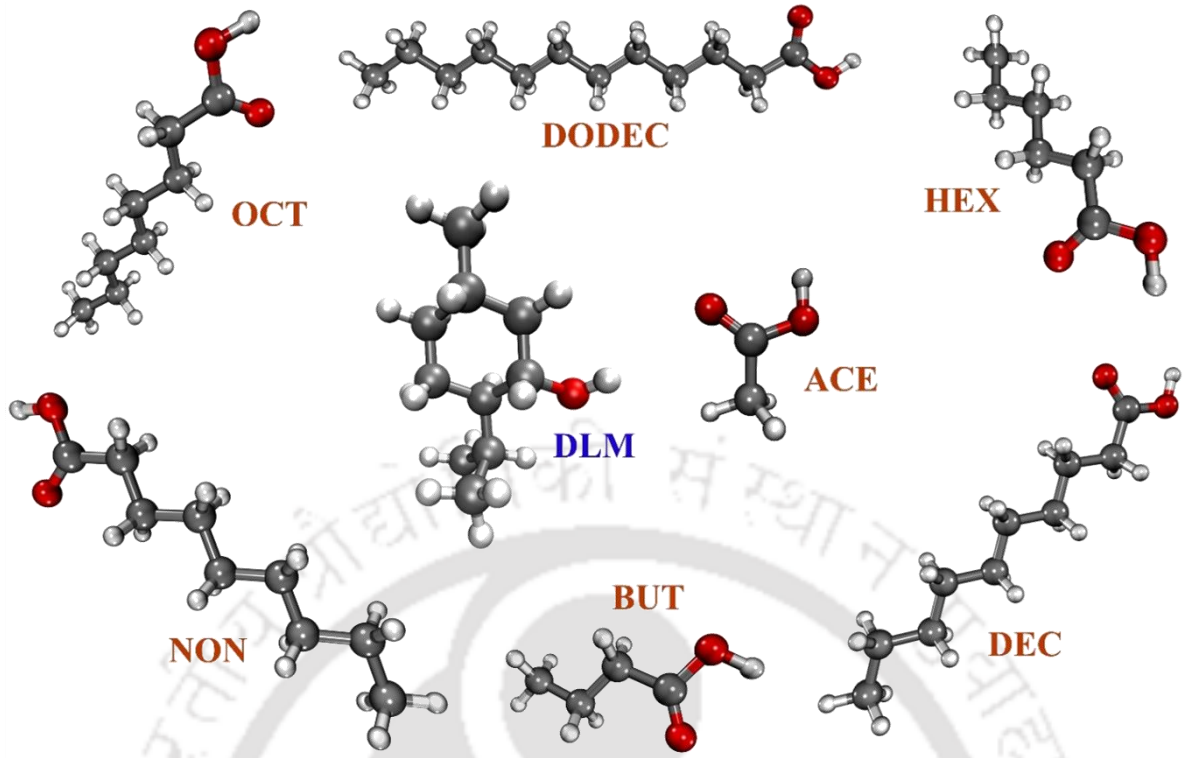

Figure 2.1: Ball and stick representation of the DES components for the quantum chemical study (DLM: DL-menthol, ACE: acetic acid, BUT: butanoic acid, HEX: hexanoic acid, OCT: octanoic acid, NON: nonanoic acid, DEC: decanoic acid, DODEC: dodecanoic acid).

Table 2.1: Studied hydrophobic DESs with molar ratios for the quantum chemical analysis

DES	Abbreviation	HBA	HBD	Molar ratio (HBA: HBD)
DES1	DLM-ACE	DL- menthol	acetic acid	1:1
DES2	DLM-BUT	DL- menthol	butanoic acid	1:1
DES3	DLM-HEX	DL- menthol	hexanoic acid	1:1
DES4	DLM-OCT	DL- menthol	octanoic acid	1:1
DES5	DLM-NON	DL- menthol	nonanoic acid	1:1
DES6	DLM-DEC	DL- menthol	decanoic acid	1:1
DES7	DLM-DODEC	DL- menthol	dodecanoic acid	1:1

2.2.2 QTAIM Calculation

To comprehensively investigate the intermolecular interactions between the HBA and the HBD, Bader's QTAIM approach[39] supported by non-covalent interaction (NCI) and RDG (Reduced Density Gradient) analysis[48,49] were implemented using the MultiWFN code.[50] The electron density at the bond critical points (BCP), (ρ_{BCP}) and its Laplacian ($\nabla\rho_{BCP}^2$) were obtained which provided valuable insights regarding the strength and the character of the

interactions. The NCI analysis can be exercised in identifying different interaction regions within the DES and the electron density distribution of DESs containing low density and gradient of density. The detailed calculation protocol of the NCI and QTAIM analysis have been presented in the upcoming sections of the Quantum Theory of "Atoms in Molecules" (QTAIM) Analysis and the "Non-Covalent Interaction Analysis".

2.2.3 Molecular Dynamics Simulation

The MD simulation scheme starts with firstly drawing the structures of the individual HBA, HBD, and water molecules in GaussView 6 with geometry optimization using Gaussian 16 at the B3LYP/6-31G* level of theory.[40] Figure B.1 and Figure B.2 (Appendix B) present the chemical structures of all the molecules along with atomic notations. The partial atomic charges of the molecules were obtained by the restricted electrostatic potential (RESP)[51] module of AMBER 14[52] and the partial charges were fitted. Table 2.2 represents the compound name and composition of various hydrophobic DES studied.

Table 2.2: Composition and nomenclature of various hydrophobic DESs in MD simulation

Sl. No.	Name of DES	DES		Molar ratio
		HBA	HBD	
1	DES1	DL-menthol	Acetic acid	1:1
2	DES2	DL-menthol	Butanoic acid	1:1
3	DES3	DL-menthol	Hexanoic acid	1:1
4	DES4	DL-menthol	Octanoic acid	1:1
5	DES5	DL-menthol	Decanoic acid	1:1
6	DES6	DL-menthol	Dodecanoic acid	2:1
7	DES7	DL-menthol	Pyruvic acid	1:2
8	DES8	DL-menthol	Levulinic acid	1:1
9	DES9	$N_{4444}Cl$	Acetic acid	1:1
10	DES10	$N_{4444}Cl$	Octanoic acid	1:2

The final partial charges for different atomic sites of all the molecules are provided in Table B.1 (Appendix B). The generalized amber force field[53] functional of the ANTECHAMBER[54] module of AMBER 14,[52] was applied to generate all force field parameters. The validation of

the generated force field parameters was done by comparing the simulated density of DES1 (0.929 gm/cm^3) at 298.15 K temperature and 1 atm pressure condition with that of the experimental density (0.931 gm/cm^3) at the same temperature-pressure condition. The experimental compositions were used from an earlier work by Florindo et al.[26] The composition of the different systems has been presented in Table 2.3.

Table 2.3: Composition of different systems considering the 1:1 mass ratio of DES and water and the number of molecules considered for MD simulation

System No	DES		Number of molecules				Periodic Box Size
	HBA	HBD	HBA	HBD	Water	Total	(Å × Å × Å)
S1	DL-menthol	Acetic acid	30	30	181	241	35.38 × 21.23 × 21.23
S2	DL-menthol	Butanoic acid	30	30	204	264	36.89 × 22.13 × 22.13
S3	DL-menthol	Hexanoic acid	30	30	227	287	38.61 × 23.17 × 23.17
S4	DL-menthol	Octanoic acid	25	25	209	259	37.62 × 22.57 × 22.57
S5	DL-menthol	Decanoic acid	30	30	274	334	41.67 × 25.00 × 25.00
S6	DL-menthol	Dodecanoic acid	50	25	238	313	43.71 × 26.22 × 26.22
S7	DL-menthol	Pyruvic acid	30	60	185	275	38.49 × 23.09 × 23.09
S8	DL-menthol	Levulinic acid	30	30	227	287	38.10 × 22.86 × 22.86
S9	$N_{4444}Cl$	Acetic acid	30	30	282	342	40.49 × 24.29 × 24.29
S10	$N_{4444}Cl$	Octanoic acid	30	60	315	405	45.35 × 28.86 × 28.86

Initially, a specific number of the DES components (HBA, HBD) and water molecules were packed in a simulation box using PACKMOL.[55]. Following that, the MD simulation for each system was carried out in NAMD 2.10 package[56] at 298.15 K and atmospheric pressure. NAMD simulation was carried out with a 6 ns minimization run, followed by heating at 298.15 K for 0.5 ns and an equilibration run for 10 ns. NPT ensemble was employed to equilibrate the

system where the simulation box size was equilibrated. A uniform system energy has been obtained to confirm the successful completion of the equilibration step and to continue the production run. Lastly, a 100 ns production run employing the NVT ensemble at 298.15 K and 1 atm pressure was carried out. The periodic boundary condition (PBC) was applied for maintaining the system continuum. To obtain the spatial density function (SDF) data, TRAVIS package[57] was used, where the parameter file and the final trajectory file were utilized. VMD 1.9.3 trajectory analyzer visualization tool was used to obtain the SDF iso-surfaces and MD simulation-driven angular distribution findings.[58] Specific reference and observed molecules were selected to obtain the SDF coordinate file. Proper iso-values were set to display the three-dimensional SDF plots of the DES-water systems.

2.2.3.1 Binary Systems

The binary systems were considered for studying the stability of the DESs in water. Those systems consisted of two components i.e., DES and water. Initially, the HBA and HBD molecules were inserted in a cubical box, while water molecules were packed in a separate cubic box. Thereafter the two boxes were placed close to each other to mimic a two-phase system having a DES-rich phase and a water-rich phase respectively. All the MD simulations were carried out in NAMD 2.10 package.[56] The systems were initially minimized for 6 ns in an NVE ensemble, thereafter all the systems were gradually heated from 0 K to 298.15 K within 0.5 ns. The systems were then subjected to an equilibration step for 10 ns in an NPT ensemble at 298.15 K and atmospheric pressure.

The Langevin dynamics method[59] with a collision frequency of 1 ps^{-1} was used for maintaining the desired temperature. The Nosé–Hoover Langevin piston was used for pressure-control with an oscillation period of 100 fs and a damping factor of 50 fs.[60] Subsequently, the production runs were carried out for 100 ns for each of the systems with the NVT ensemble. The trajectory data were saved at every 5ps. The SHAKE algorithm was considered to restrain the bonds involving hydrogen atoms.[61] VMD 1.9.3 package was used for visualizing the trajectory of the molecules within the systems.[58] The particle mesh Ewald method was used for the calculation of the long-range intermolecular electrostatic interactions.[62] A cutoff distance of 12 Å was considered for short-range interactions. Periodic boundary condition (PBC) was applied in each system.[63] The box size of the individual systems is provided in Table 2.3. Each system was initiated with three different starting configurations to ensure successful completion and reproducibility of the simulation that can provide a realistic estimate of the

trajectory and the thermodynamic properties. This was performed to remove any numerical or modelling bias in the simulation procedure.

The percentage loss of the DES components (HBA, HBD) to the aqueous phase was obtained by calculating the number of the molecules present in the water-rich phase after 100 ns which initially were present in the DES phase. Later, the number was averaged out from all three simulation runs carried out for each system and then subsequently divided by the total number of molecules of that species. It was then converted to percentage to obtain percentage loss.

2.2.3.2 Ternary System

In the case of the extraction of the pesticide, the system is 'ternary' with the addition of a pesticide component to the binary system. Water-DES-nitenpyram ternary system was prepared for the simulation study of pesticide extraction from the corresponding mole fraction inline with the respective molecules of the experiment. The exact mimicking of the experimental number of molecules was not possible due to the computational limit. As a result, we have considered the equal mass of DES and water for the simulated system with 5 molecules of nitenpyram initially present in the aqueous phase. We have kept the mass of the DES and water-rich phase, similar to that of the experiment. The simulation was carried out with a 6 ns minimization run in the NVE ensemble, followed by heating at 298.15 K for 0.5 ns. It was then equilibrated for 10 ns with an NPT ensemble. Finally, the 100 ns production run with NVT ensemble at 298.15 K and 1 atm pressure was carried out. Periodic Boundary Condition (PBC) is applied with a system box dimension of 68.10 Å × 34.10 Å × 34.10 Å.

2.2.3.3 Analysis Details

After the successful completion of the production run, a trajectory file was obtained which contains the trajectory of the molecules of the system. The parameter file and the trajectory files were then inserted into the VMD software package.[58] The non-bonded interaction energy, average hydrogen bonding and radial distribution function on the specification of the requisite criteria were obtained directly using the tools provided in VMD. TRAVIS package[57] was used to obtain the CDF and the SDF where the final coordinate file was used as the input. Specific molecules and atoms along with required criteria such as reference molecule and observed molecule were selected to get the CDF datasheet SDF coordinate file. The data ware then plotted on a graph sheet. Proper isovalue was set to view the three-dimensional SDF. The mean square displacement (MSD) curve were obtained by solving the Einstein equation of self-

diffusivity through VMD. The diffusion coefficient was obtained from the linear slope of the MSD curve.

2.3 Results and Discussion

2.3.1 Water Stability of Hydrophobic DESs

2.3.1.1 QC Analysis

2.3.1.1.1 Geometry Optimization

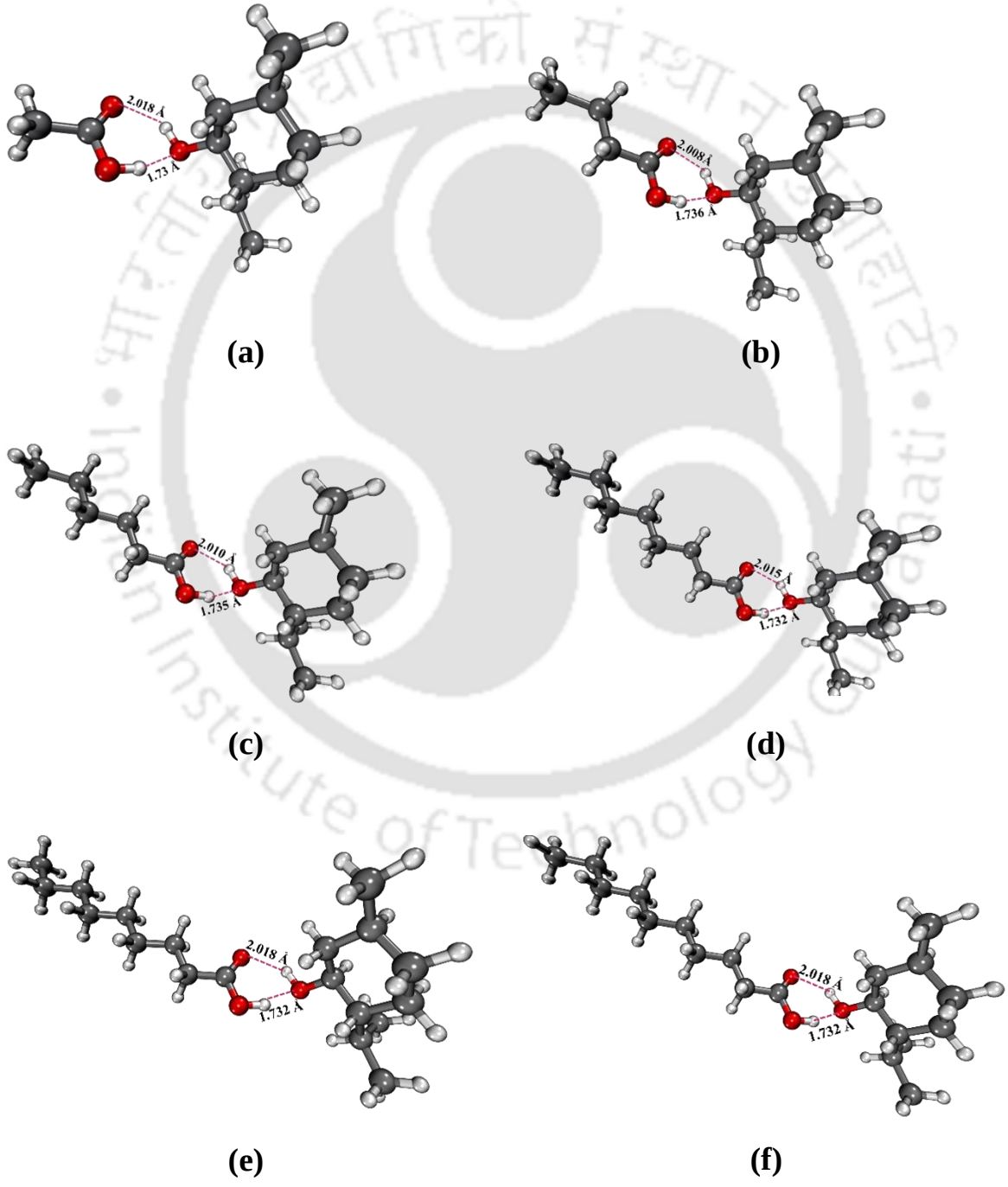

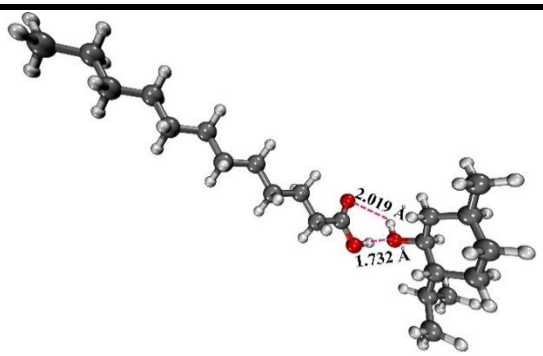

(g)

Figure 2.2: Optimized structures of (a) DL-menthol/ acetic acid, (b) DL-menthol/ butanoic acid, (c) DL-menthol/ hexanoic acid, (d) DL-menthol/ octanoic acid, (e) DL-menthol/ nonanoic acid, (f) DL-menthol/decanoic acid and (g) DL-menthol/ dodecanoic acid DESs at the B3LYP/6-311+G (d,p) level of theory with D3BJ dispersion correction.

Optimized geometries of the DESs were obtained using the B3LYP/6-311+G(d,p)-D3BJ[64] and the M06-2X/6-311+G(d,p) level of theory and presented in Figure 2.2 and Figure B.3 (Appendix B), respectively. Harmonic vibration analysis confirmed the absence of any imaginary frequency. Exploring the optimized geometries, the following significant observations can be acknowledged:

(i) DESs are formed purely on the foundation of the non-bonded interactions between the DL-menthol and the respective carboxylic fatty acids. The most possible interactive sites are the –OH group of DL-menthol and the –COOH group of the organic acids, where opposite partial charges on the atoms extend the favourable non-bonded interactions between the O and H atoms of the respective components.

(ii) Short to medium-range interaction is observed around the intermolecular region of the HBA and the HBD. The O (menthol)…H (organic acid) distance appeared to be in the range of 1.730 to 1.735 Å, for the B3LYP-D3BJ method and between 1.762 to 1.769Å, for the M06-2X method. This distance is shortest in the case of acetic acid (1.73 Å) as shown in Figure 2.2a, suggesting a close and stronger interaction leading to higher compactness. The other O (organic acid) … H (menthol) distance ranges between 2.008 to 2.019 Å for the B3LYP-D3BJ method and between 2.06 to 2.07 Å, for the M06-2X method. The former shorter interaction i.e., the O (menthol)…H (organic acid) indicates the possible O…H hydrogen bonding in all the DESs or probable electrostatic interaction for short-chain fatty acids. The medium-range interactions i.e., the O (organic acid) … H (menthol) interactions have indicated

the possible occurrence of van der Waals or dispersion interactions collectively responsible for the stable DES formation.

2.3.1.1.2 Charge Transfer

To have a thorough understanding of the charge transfer (CT) process and delocalization of charge in the DES systems, the NBO charge and the CHELPG partial charge analysis were carried out using the B3LYP as well as the M06-2X method as presented in Table 2.4 and Table B.2 (see Appendix B). There was a slight variation of charges obtained in both the charge analysis schemes due to their different mechanism of charge evaluation, however, that did not have any significant deviation and the general consistency of the results was observed in both schemes. The precursor HBA and HBD molecules were neutral compounds and thus each of those contained zero charges. However, upon mixing charge transfer took place between them developing non-zero partial charges on the respective components preserving the overall neutrality of the DES. The interaction between DL-menthol and acetic acid leads to higher charge transfer than other DESs. The closer structural framework of DES1 assisted the charge transfer between DL-menthol and acetic acid, however, not the dominating factor in the interactions of the DES components.

In NBO analysis, it is observed that the DL-menthol molecule acquired a net positive charge acting as an HBA, whereas the HBD acquired an equal amount of negative charge. The negative charge acquired by the carboxylic acids after DES formation followed a certain trend in general, where the smaller HBD attains higher CT than that of the larger HBDs. Charge transfer for acetic acid is highest (−0.0239e), while the least amount of charge transfer took place in dodecanoic acid (−0.0222e) for B3LYP calculation, as presented in Table 2.4. Similarly, for the M06-2X calculation, the charges were reduced from acetic acid to dodecanoic acid (from −0.0272 to −0.0259e). Even being not so significant in the degree of CT, DES1 still reveals higher charge transfer as compared to DES4, DES5, DES6 and DES7. In the CHELPG scheme with M06-2X functional, a similar charge transfer scenario was observed as acetic acid (−0.0243e) showed the highest charge transfer as compared to the lowest value of dodecanoic acid (−0.0207e) as presented in Table B.2 (Appendix B). To understand the CT mechanism precisely, the charges on $-OH_{HBA}$ and $-COOH_{HBD}$ were obtained as these are the possible active sites responsible for the formation of the DES. The individual groups interacted with each other via the favourable orientation of the positively charged H atom and negatively charged O atom contributing from the opposite molecule. The difference between these two

charges is listed in Table 2.4 as presented by $CD_{-OH/-COOH}$. The higher the $CD_{-OH/-COOH}$ value, the higher will be the resistance to charge transfer. Accordingly, DES7 revealed higher resistance to charge transfer as compared to DES1.

The presence of –COOH and –OH groups in acetic acid and DL-menthol, respectively, is responsible for superior electrostatic interaction along with hydrogen bonding between the HBA and HBD. Thus, electrostatic interaction along with hydrogen bonding acts as the driving force responsible for the stability of DL menthol: acetic acid DES. However, both the HBA and the HBD are neutral compounds and thus direct charge transfer between the HBA and the HBD is not the dominating factor due to the non-covalent interactions. With the increase in the alkyl chain length in DES4 to DES7, the dispersion interactions become dominant as compared to the electrostatic interactions. The presence of the non-polar long carbon-chains present in octanoic, decanoic and dodecanoic acid restricts the mobility of the HBD molecules and the increased van der Waals/ dispersion interactions between the HBA and HBD act as the driving force responsible for the stability of these DESs.

Thus, the driving force between the HBA and HBD is a combination of different non-bonded interactions present within the components and the characteristics of these non-covalent interactions are determined by the interactive nature of the HBA and HBD. Ionic compounds lead to electrostatic interaction, non-ionic compounds give rise to van der Waals and dispersion interactions, and electronegative elements present within the components result in hydrogen bonding.

Table 2.4: Calculated NBO charges (in a.u.) on the different components before and after the formation of the DESs [DLM (HBA): DL-menthol, acid (HBD): different fatty acids corresponding to the respective DESs, $-OH_{HBA}$: −OH group of DL-menthol and $-COOH_{HBD}$: −COOH group of different HBDs] ($CD_{-OH/-COOH}$: charge difference between $-OH_{HBA}$ and $-COOH_{HBD}$)

DES systems	B3LYP					M06-2X				
	DLM (HBA)	Acid (HBD)	$-OH_{HBA}$	$-COOH_{HBD}$	$CD_{-OH/-COOH}$	DLM (HBA)	Acid (HBD)	$-OH_{HBA}$	$-COOH_{HBD}$	$CD_{-OH/-COOH}$
DES1	0.02391	−0.0239	−0.29386	−0.03249	0.26137	0.02726	−0.02724	−0.289180	−0.03598	0.253200
DES2	0.02313	−0.02314	−0.29352	−0.0255	0.26802	0.02604	−0.02604	−0.289510	−0.02681	0.262700
DES3	0.02282	−0.02283	−0.29375	−0.02455	0.2692	0.02609	−0.02608	−0.289460	−0.02587	0.263590
DES4	0.02259	−0.02259	−0.29395	−0.02443	0.26952	0.02605	−0.02606	−0.289410	−0.02591	0.263500
DES5	0.02242	−0.02246	−0.29406	−0.02434	0.26972	0.02608	−0.0261	−0.289340	−0.02597	0.263370
DES6	0.02235	−0.02236	−0.29411	−0.02429	0.26982	0.02593	−0.02596	−0.289450	−0.02587	0.263580
DES7	0.02224	−0.0222	−0.2941	−0.02427	0.26983	0.02599	−0.02598	−0.289440	−0.02596	0.263480
pure component	0.00	0.00	-	-	-	0.00	0.00	-	-	-

2.3.1.1.3 Interaction Energy

Interaction energy refers to the reduction or release of energy from the system due to the interaction between two or more molecules. The calculation of interaction energy involves finding the difference between the energy of the system or complex formed and the sum of energy of the individual molecules which are involved in the interaction. The interaction energy of the DES is calculated by the following equation:

$$\Delta E_{DES}\ (IE) = E_{DES} - (E_{HBA} + E_{HBD}) \qquad (2.1)$$

Where, E_{DES} is the total energy of the DES and E_{HBA} and E_{HBD} are the individual energies of the HBA and HBD, respectively. A negative value of the interaction energy points towards favourable interaction between molecules in the system suggesting a more stable structural arrangement.

The interaction energy is a measure of the compactness of a molecule. For a multi-component system such as ILs or DESs, higher interaction energy leads to tighter molecular structure suggesting higher compactness of the molecules and vice versa. This is important in the dissolution or extraction of incoming solute molecules such as drugs, pesticides etc. molecules by allowing a facile restructuring of the DES i.e., rearrangement of the HBA and the HBD orientation.

Based on the interaction energy calculated for the DL menthol- carboxylic fatty acid-based DESs as presented in Figure 2.3, acetic acid-based DES (DES1) reported the highest interaction energy whereas, dodecanoic acid-based DES (DES7) reported the lowest having a difference of 1.4 kcal/mol and 2.07 kcal/mol for B3LYP-D3BJ and M062X functionals, respectively. DES1 developed a compact structure due to its smaller size as compared to DES7. Similar phenomena occurred in the case of DES4, DES5 and DES6, as the HBD size effect comes into play. The decreasing order interaction energy is as follows: DES1 > DES2 > DES3 > DES4 > DES5 > DES6 > DES7. Small differences in the interaction energy values for DES4 to DES8 are noticed due to the negligible correlation of the interaction energy beyond six-membered straight-chain fatty acids as HBDs. In general, DESs with higher interaction energy have a closer distance between the HBA and the HBD. This distance-interaction energy criterion was evident in charged DESs because of the dominant CT process. However, in the case of Type-V DESs, where naturally occurring neutral compounds were used as the DES forming constituents (HBA/ HBD), largely the non-bonded forces applied to

the molecules such as electrostatic, H-bonding, van der Waals and steric forces separately or in combination, define the strength of the interactions. The molecular structure, functional groups and size of the molecules also have a decisive influence on the facilitation of these non-bonded.

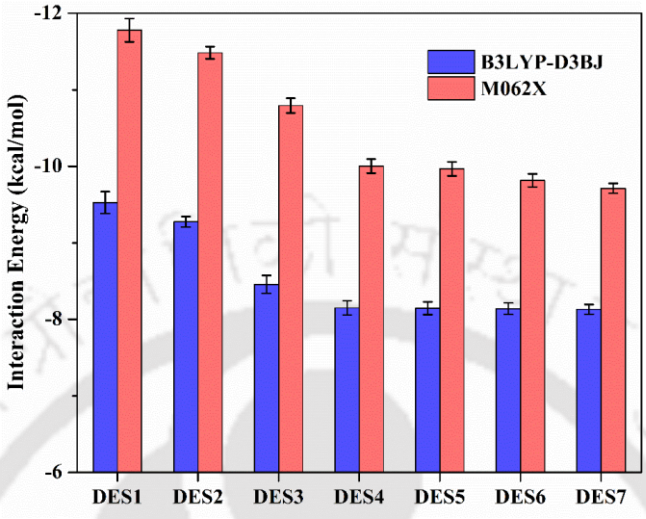

Figure 2.3: Non-bonded interaction energy of DES systems from QC calculation

From a perspective of the formation stability of the DES, DES1 was more stable than the others as the components released more energy when the DES is formed. Although, based on the studies,[26,33] for applications involving the dissolution of drugs or any other solutes, one should select the DESs comprising the properties like less compactness, lower interaction energy, higher restructuring ability and higher affinity towards the solute such as DES4, DES5, DES6 and DES7.

2.3.1.1.4 Solvation Study of the DESs in an Aqueous Environment

For an effective extracting media, the performance of the hydrophobic DES should be superior in terms of the dissolution of those impurities and resistance to interact with the adjacent aqueous environment as well. The solvation study can be immensely effective in selecting the potential candidates for the hydrophobic DESs in search of a strong and stable extraction agent. Our previous work shed light on the stability[33] of the DESs in a water medium with the help of MD simulation followed by experimental validation. In our present work, QC calculation is implemented along with several MD simulation calculations to dig deeper into the solvation mechanism and dynamics for the menthol-carboxylic acid-based hydrophobic DESs to understand the systems at a molecular level.

2.3.1.1.4.1 Gibbs Free Energy of Solvation (Implicit Solvation)

The Gibbs free energy of solvation (ΔG_{solv}) was calculated using Equation 2.2 for all the DES systems to explore the stability of the DES in an aqueous environment employing the SMD solvation model.[47]

$$\Delta G_{solv} = G_{vacuum} - G_{sol} \quad (2.2)$$

The schematic has been presented in Figure 2.4a. Firstly, the vacuum or gas phase Gibbs free energy of DES (G_{vacuum}) is obtained. Afterwards, the optimized DES molecule is placed in a solvent (here water) following the SMD solvation model formulated by a dielectric medium of the said solvent properties and the Gibbs free energy in the solvent (water) (G_{sol}) is obtained. The obtained Gibbs free energy of solvation (ΔG_{solv}) data for all the DESs has been presented in Figure 2.4b, calculated in B3LYP-D3BJ and M06-2X functional, as well. A negative ΔG_{solv} value indicates the favourable nature of solvation which means the solute releases energy to be involved with the solvent to promote dissolution. A more negative ΔG_{solv} value implies higher dissolution or solubility of the solute in the respective solvent. DES1 exhibited the highest ΔG_{solv} value (−7.98 kcal/mol) and thus was the least stable in an aqueous environment. As we keep on increasing the carbon numbers of the straight-chain fatty acids, ΔG_{solv} gradually decreased and DES7 displayed the lowest ΔG_{solv} value (−2.06 kcal/mol). DES4 (−3.14 kcal/mol), DES5 (−3.09 kcal/mol) and DES6 (−2.89 kcal/mol) exhibit closer ΔG_{solv} values suggesting similar dissolution properties.

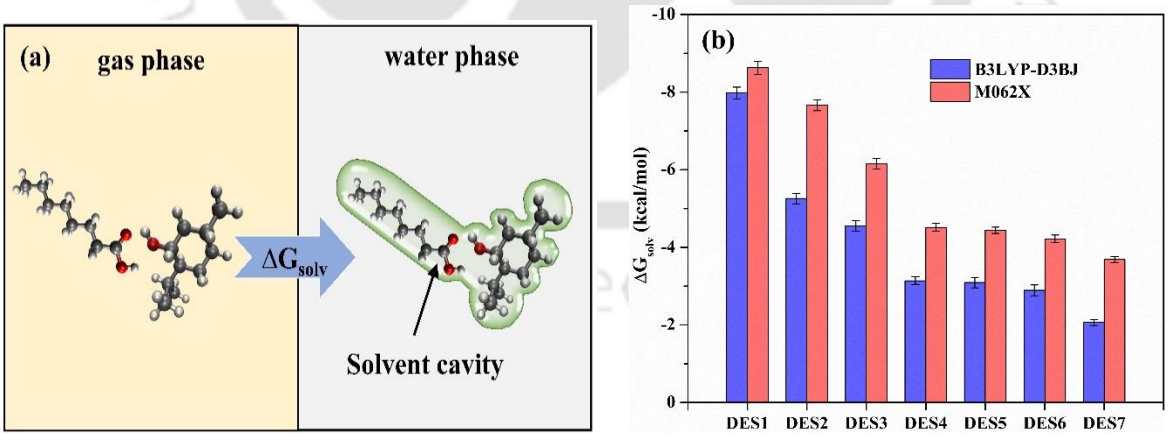

Figure 2.4: (a) Schematic representation of the Gibbs free energy of solvation calculation for a DES for transfer from the gas phase to the water phase, Modified version of the scheme, reprinted (adapted) with permission from {Durgesh V. Wagle , Hua Zhao, Carol A. Deakyne, and Gary A. Baker, Quantum Chemical Evaluation of Deep Eutectic Solvents for the

Extractive Desulfurization of Fuel, ACS Sustainable Chemistry & Engineering, 2018, 6 (6), 7525–7531}.[65] Copyright {2018} American Chemical Society. (b) Gibbs free energy of solvation of DES systems using SMD solvation model.

From the findings mentioned above, DES4 to DES7 can be considered more stable in an aqueous environment than DES1 to DES3. DES1 to DES3 displayed a strong affinity towards water molecules due to the hydrophilic nature of the HBDs and thus are not suitable for any applications that require prolonged presence in an aqueous environment. On the contrary, DES4 to DES7 contain long-chain fatty acids as HBDs each of which possessed superior hydrophobic characteristics and thus is much more suitable in separation or extraction applications involving a water environment. The experimental results of Florindo et al.[26] suggested similar findings.

2.3.1.1.4.2 Explicit Solvation Study.

The stability of the DESs was studied through an explicit solvation model. Two external water molecules were placed around each DES molecule and each system was optimized at the B3LYP-D3BJ and M06-2X/6-311+G (d,p) levels of theory. The idea behind the selection of two explicit water molecules was to maintain the same number of molecules of DES and water within the system. Furthermore, the number of active functional groups present in the DES system being two (−OH & −COOH) have made it appropriate to use two explicit water molecules for feasible interaction. The explicit water molecules present in the system have participated in developing non-bonded interactions, mainly hydrogen bonding, primarily with the fatty acids (HBD) and thus the overall structure of the DESs has been influenced or distorted based on the intermolecular interactions with water. Figures B.3 (Appendix B) and Figure 2.5 demonstrate the pure state and solvated geometries (explicit) optimized at the Minnesota functional, respectively. The O (organic acid) … H (menthol) distance increased to the highest value of 3.12 Å from 2.07 Å for DES1, and from 2.06 to 2.54 Å for DES2, unambiguously indicating the disruption of the HBA-HBD construction. However, this distance tends to decrease as we move towards longer chain fatty acid-based DESs, such as DES4 (2.2 Å), DES6 (2.15 Å), and DES7 (2.08 Å) as in Figures 2.5 (c), (d) and (e) respectively, suggesting a definitive strong HBA-HBD interaction resisting the disruption in the presence of water molecules. Although the water molecules have placed themselves closer to the carboxyl part of the HBDs due to their polar nature, the interaction was ineffective

for DES4 to DES7. The increasing distance between HBD and water (1.84 Å for DES1 to 1.99 Å for DES7) suggests the declining affinity of long-chain fatty acids towards water. For DES1 and DES2, the water molecules managed to break into the HBA-HBD assembly disrupting the structure through the enhanced development of non-covalent interactions with the HBDs. Thus, the long-chain fatty acid-based DESs have demonstrated superior hydrophobic nature which is evident from the experimental as well as the MD simulation studies. DES1 to DES3 have revealed greater relaxation between the HBA and HBD thus increasing the distance between the components and hence are less stable in an aqueous environment. Figure 2.6 is an excellent schematic representation of the distinctive miscible nature of two DESs.

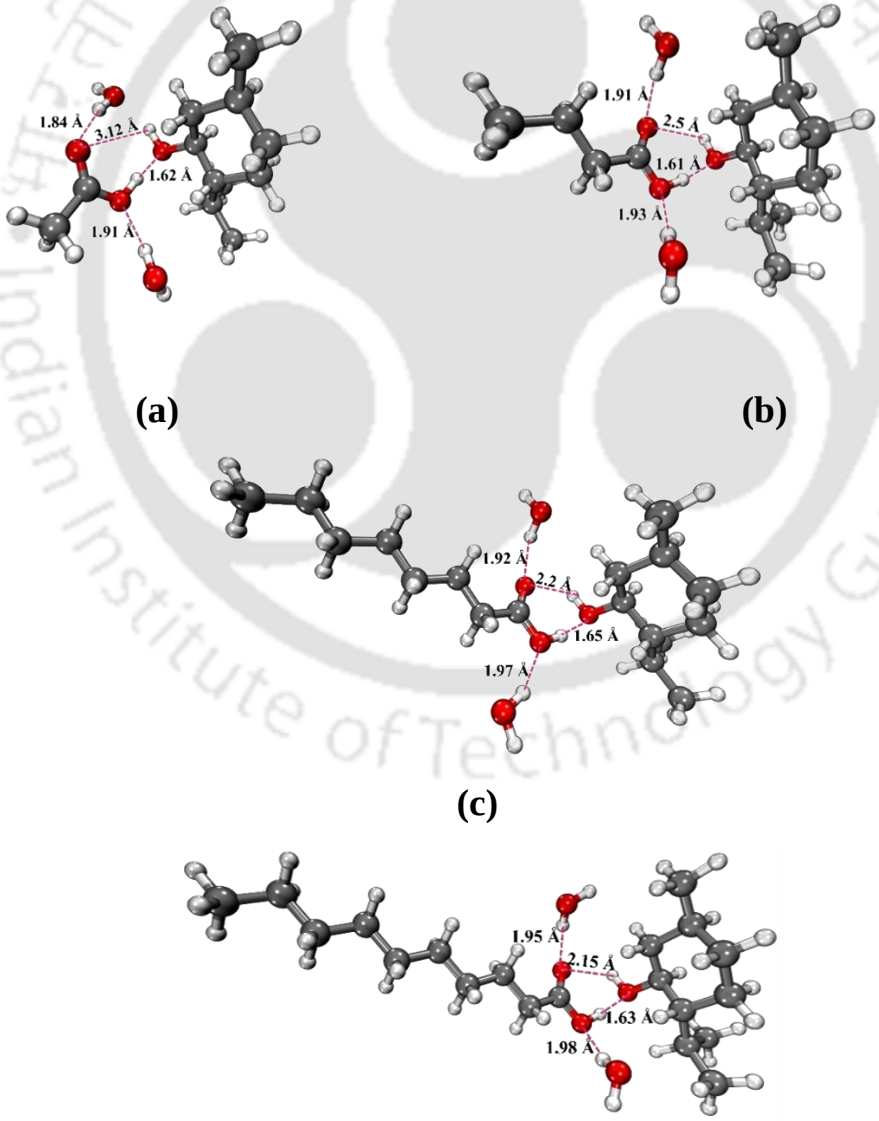

(d)

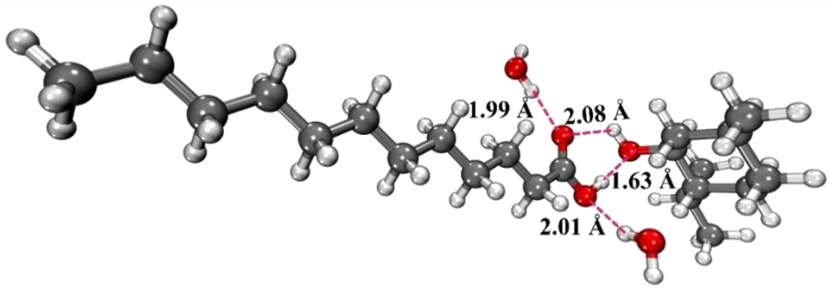

(e)

Figure 2.5: Solvated Structures of (a) DL-menthol/ acetic acid, (b) DL-menthol/ butanoic acid, (c) DL-menthol/ octanoic acid, (d) DL-menthol/decanoic acid and (e) DL-menthol/ dodecanoic acid DESs at the M06-2X/6-311+G (d,p) level of theory.

Figure 2.6: Schematic representation of the experimental water miscibility study for DES1 (DL-menthol: acetic acid) and DES4 (DL-menthol: octanoic acid) before and after mixing with water.

DES1 turned out to be highly miscible in water within 2-3 hours of mixing due to the transport of the hydrophilic acetic acid to the water phase, while DL-menthol still formed a small yet distinct phase quite separate from the water. DES4, having been constituted through the integration of hydrophobic octanoic acid and DL-menthol, resulted in an immiscible phase

formation in the presence of water. The QTAIM analysis can provide significant information regarding the non-covalent interactive network developed within the DES systems, which is addressed in the upcoming section.

2.3.1.1.5 Angular Distribution Analysis.

Figure 2.7 represents the illustrations of the angles of non-bonded interactions present between the active sites of the HBA and the HBDs for pure as well as solvated DES. The respective angles for the intermolecular non-covalent interactions were identified as O-H (DLM)…..O (acid) and O-H (acid)…..O (DLM), where the latter can be identified as a strong H-bond. In pure DES molecular structure, the angle of this type of distribution ranged from 159.3 to 159.6° whereas, the O-H (DLM)…..O (acid) distribution ranged within the angle from 134.65 to 135.58°. Similar angular distributions were obtained correspondingly from the SMD solvation model analysis. This relaxation of the intermolecular non-covalent interactions was agreeably noticeable in Figures 2.7b and 2.7d in the case of DES1 and DES2 where the non-bonded interactive arrangement was disrupted the most. The O-H (DLM)…..O (acid) angle changed from 134.93° and 135.58° to 96.43° and 98.6°, respectively for DES1 and DES2 in solvated structure as compared to the pure structure due to hydrophilic nature. It means that the HBA-HBD assembly opened up the structural arrangement to accommodate water molecules. This adjustment propagates by the relative affinity of the smaller fatty acids with water.

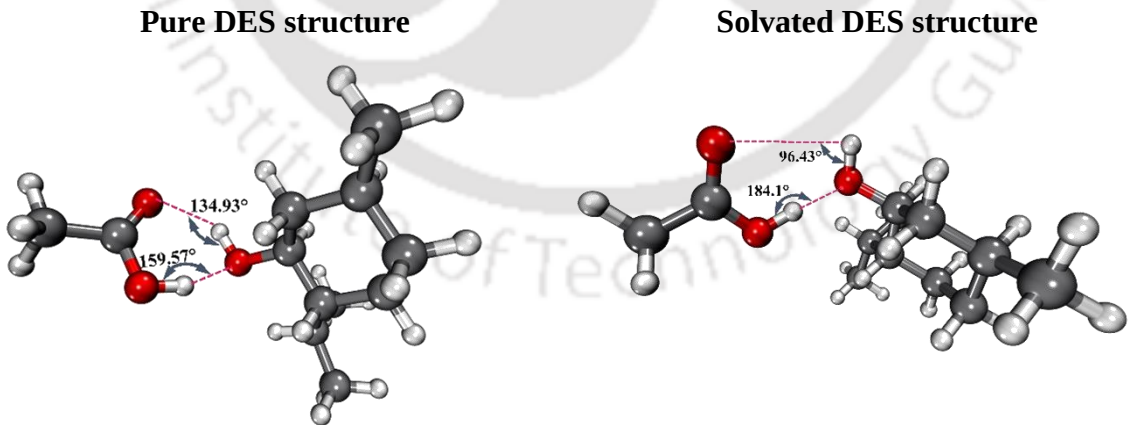

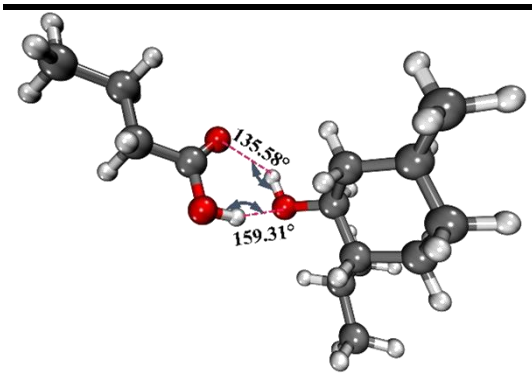

c

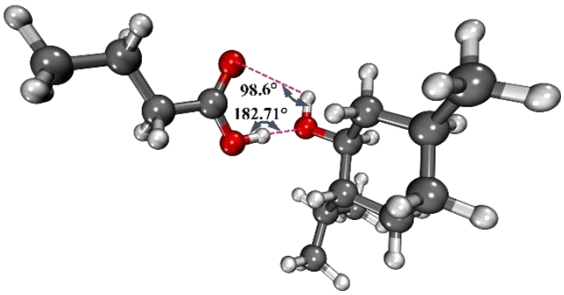

d

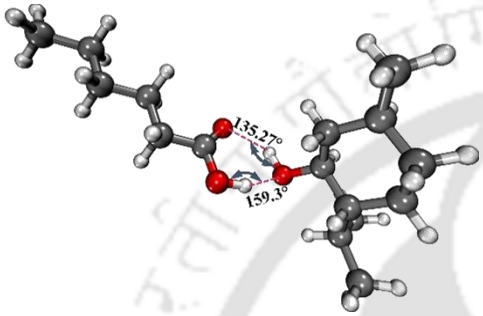

e

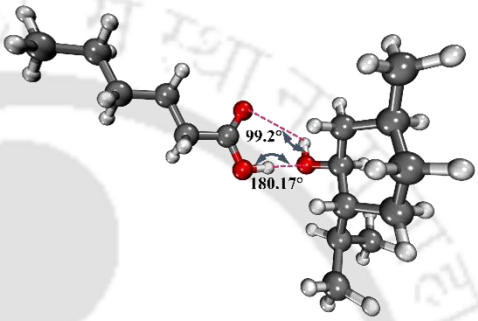

f

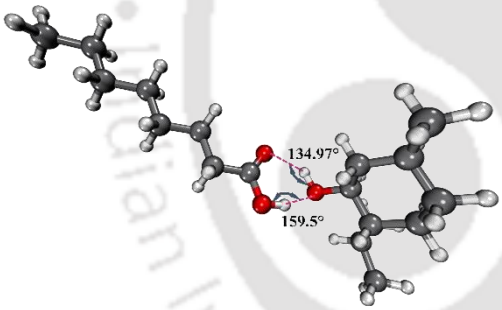

g

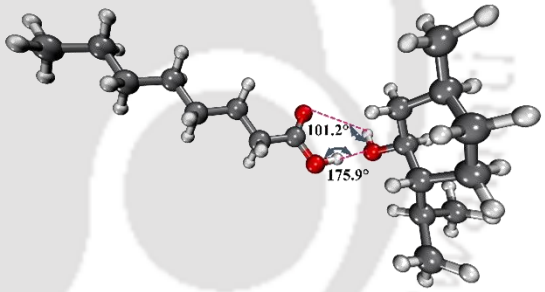

h

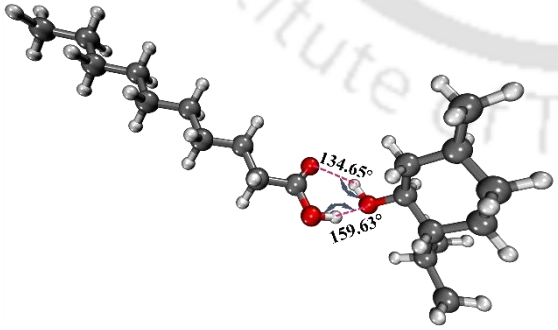

i

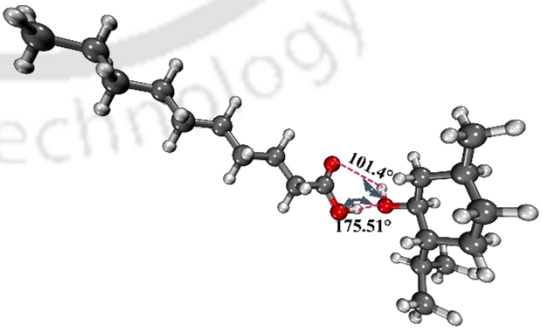

j

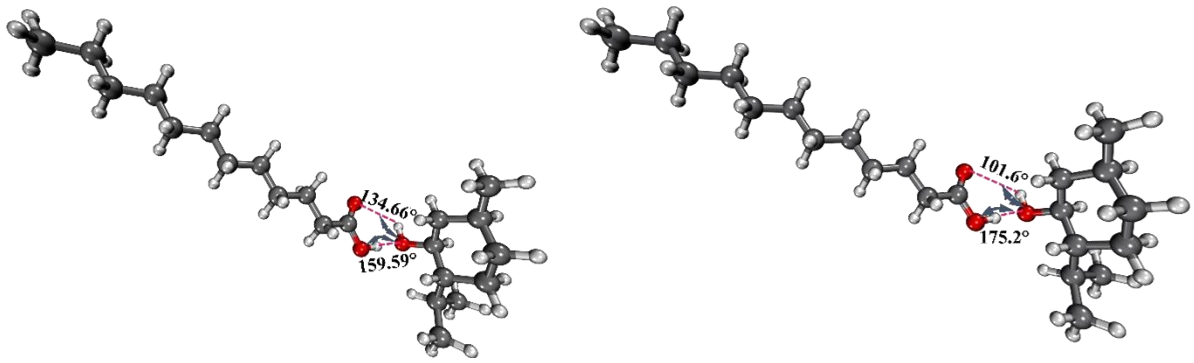

k **l**

Figure 2.7: Angular representation of the O-H…O interactions between the HBA (DL-menthol) and the HBD (carboxylic acids) of different DESs at normal ground state (pure DES) orientation and solvated state orientation. (a), (c), (e), (g), (i) and (k) display ground state optimized structures of DL menthol- acetic acid, DL menthol- butanoic acid, DL menthol-hexanoic acid, DL menthol- octanoic acid, DL menthol- decanoic acid and DL menthol-dodecanoic acid, respectively, whereas, (b), (d), (f), (h), (j) and (l) display solvated state optimized structures of the respective DESs.

However, smaller changes in the angles of the solvated DES structures can be observed for DES4, DES6 and DES7 presented in Figures 2.7 h, k and l. Higher O-H (DLM)…..O (acid) angle in the range of 101.6° has been observed for all three DESs suggesting a minimal disruption in the presence of water molecules. All the three DESs contained HBDs with superior hydrophobic character thus preventing the destruction of HBA-HBD interactions. Interestingly, the O-H (acid)…..O (DLM) angular distributions adhered to be in the range of 175.2 to 175.9° indicating a relatively stronger H-bond.

To substantiate the above findings, we have obtained the O-H (DLM)…..O (acid) angles for different DES systems solvated with water through MD simulation and plotted as a function of simulation time as displayed in Figure 2.8 as an explicit solvation study for comparative analysis. In this case, also, the higher carbon chain length of the HBDs can be viewed as a distinguishing factor for the repulsion of water molecules and the angular distribution suggests the same. DL menthol: octanoic acid, DL menthol: decanoic acid and DL menthol: dodecanoic acid based DESs displayed almost similar O-H (DLM)…..O (acid) angular distributions from 103.2 to 103.7°, fairly close to that of QC calculation as discussed above. Thus, the solvation study with MD and QC combined revealed the relaxation of the

DES structure and possible disruption of small-chain fatty acid-based DESs in contact with water.

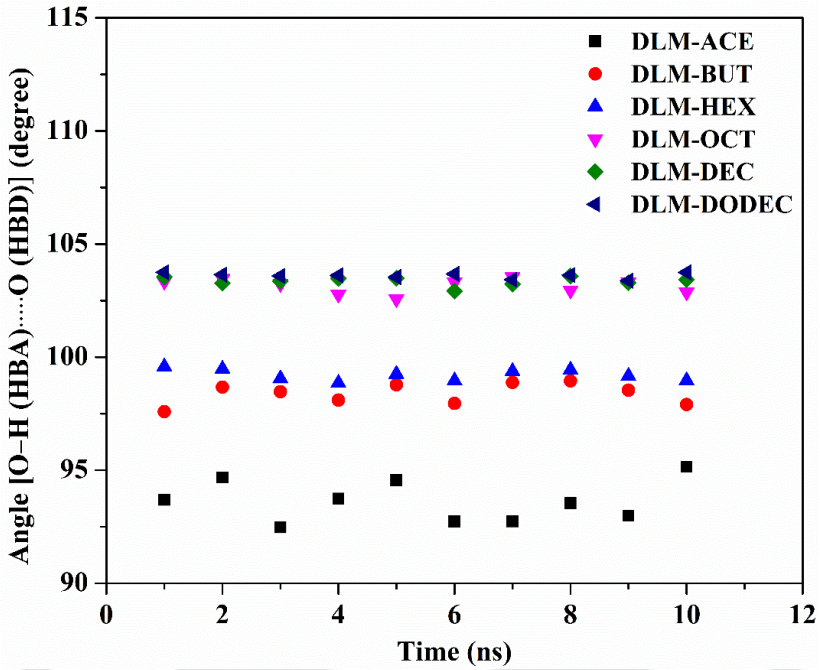

Figure 2.8: Angle of the O-H…O interaction (in degree) between the HBA (DL-menthol) and the HBD (carboxylic acids) obtained from MD simulation of different DL menthol (HBA) - carboxylic acid (HBD) - water systems, as a function of simulation time for 90 to 100 ns. (DLM: DL-menthol, ACE: acetic acid, BUT: butanoic acid, HEX: hexanoic acid, OCT: octanoic acid, DEC: decanoic acid, DODEC: dodecanoic acid).

2.3.1.1.6 FMO Analysis of the DESs.

Frontier Molecular Orbital (FMO) analysis has been performed, recognized to be an extremely efficient method for determining the acceptor-donor interaction, as well as molecular stability and reactivity, using HOMO-LUMO orbital exploration. 'HOMO' and 'LUMO' are the abbreviated forms of 'Highest Occupied Molecular Orbital' and 'Lowest Unoccupied Molecular Orbital', respectively. HOMO is associated with the nucleophilic or electron-donating tendency of a species, whereas LUMO describes the electrophilic or electron-accepting tendency of a species. The energy needed for a species to transit from its ground state to an excited energy state, achieved by the addition or removal of electrons, can be determined by the HOMO-LUMO energy gap that provides valuable information regarding the chemical and kinetic stability of a molecule.[66] The larger the HOMO-LUMO energy gap,

the more the molecular kinetic stability, and the lower the chemical reactivity and greater resistance to CT.

The FMO diagrams of the pure DL menthol-carboxylic acid-based hydrophobic DESs as a function of the HOMO and LUMO species are illustrated in Figure 2.9. The HOMO species were primarily localized around the DL-menthol (HBA) moiety suggesting the nucleophilic nature, while LUMOs were predominantly contributed from the carboxylic fatty acids (HBD) indicating the electron-withdrawing character suggesting a stronger HBA-HBD collaboration.

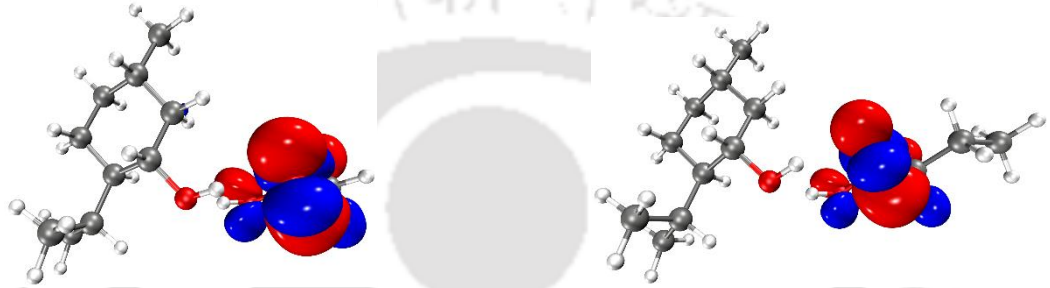

LUMO LUMO

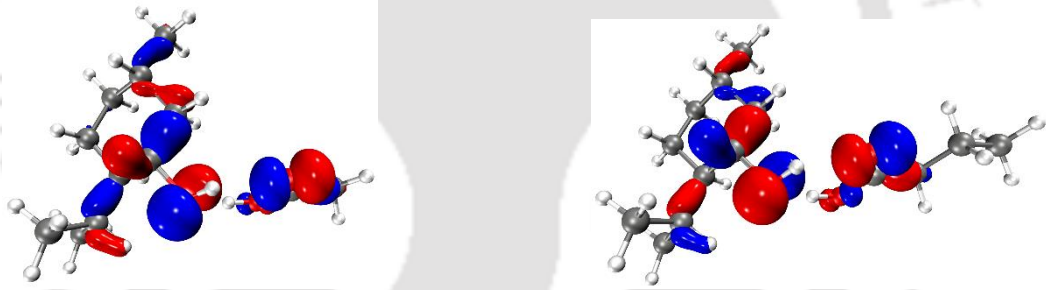

HOMO **HOMO**

(a) **(b)**

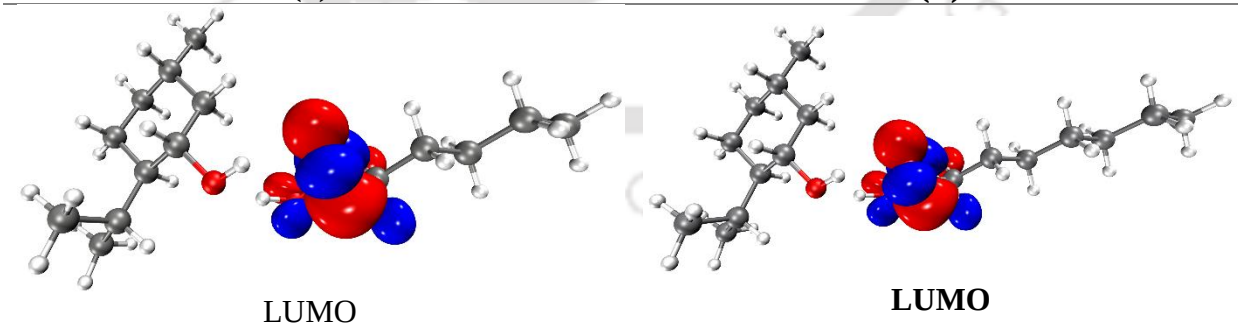

LUMO **LUMO**

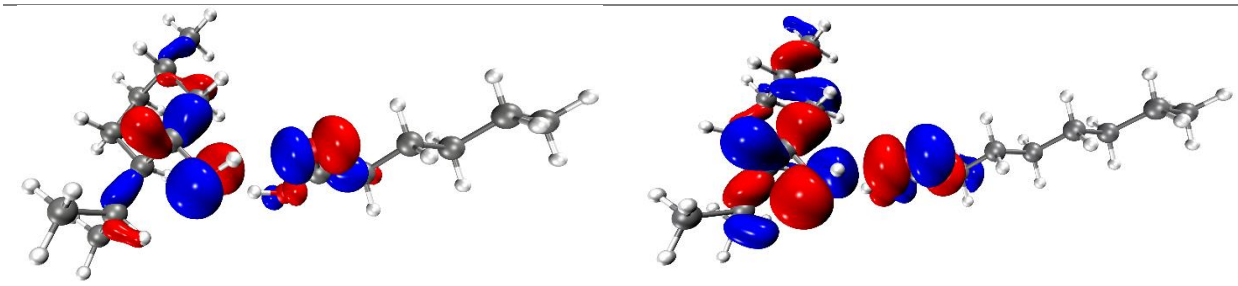

HOMO **HOMO**

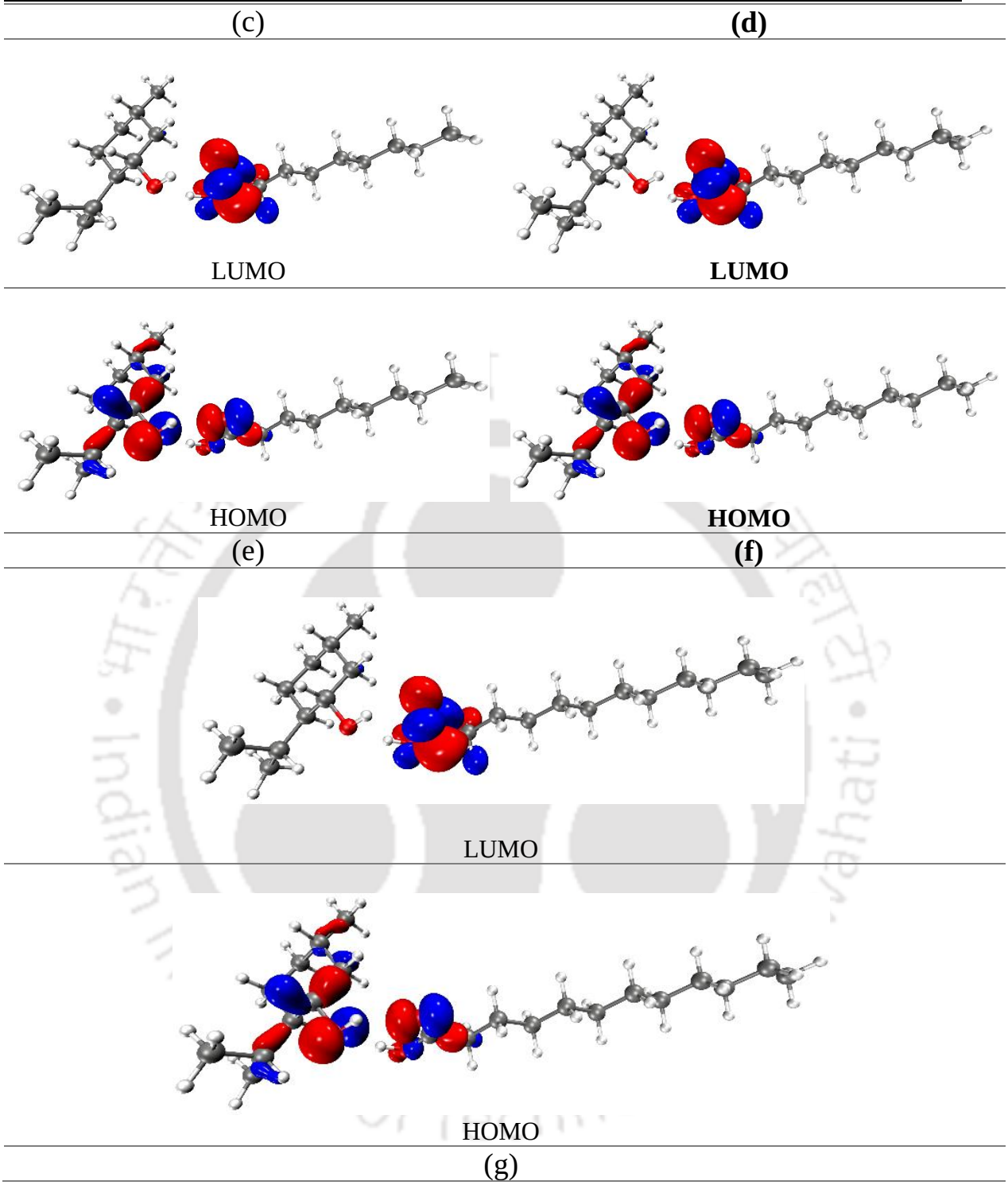

Figure 2.9: HOMO−LUMO iso-surfaces of DESs, (a) DL-menthol/ acetic acid, (b) DL-menthol/ butanoic acid, (c) DL-menthol/ hexanoic acid, (d) DL-menthol/ octanoic acid, (e) DL-menthol/ nonanoic acid, (f) DL-menthol/decanoic acid and (g) DL-menthol/ dodecanoic acid.

The HOMO-LUMO energy gap for the different DESs follows the order of DES1 (0.27294 Hartree) < DES2 (0.27398 Hartree) < DES3 (0.27464 Hartree) < DES4

(0.27494 Hartree) < DES5 (0.27511 Hartree) < DES6 (0.27547 Hartree) < DES7 (0.27697 Hartree), as can be referenced from Table B.3 (Appendix B) and Figure 2.10.

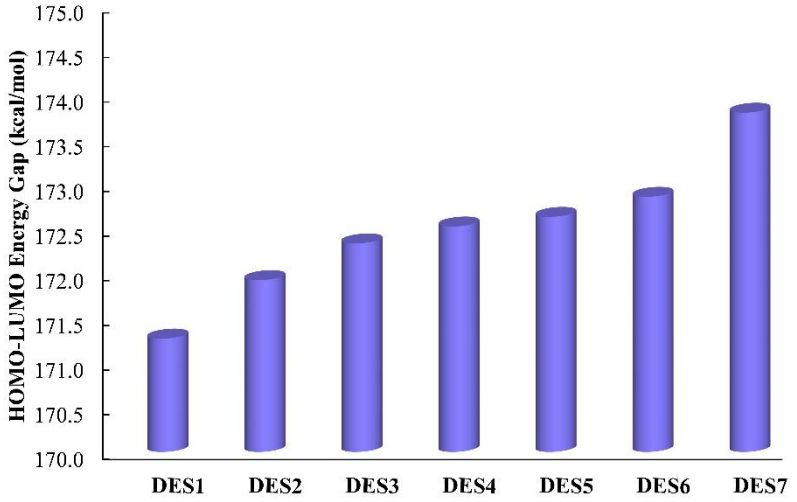

Figure 2.10: HOMO-LUMO energy gap data for various DESs using the DFT-B3LYP-D3BJ method.

DL menthol-dodecanoic acid DES exhibited the highest HOMO-LUMO band gap energy suggesting higher stability and lesser reactivity. Chemical hardness (η), following Koopmann's theorem[67], was evaluated. The higher (η) value associated with this DES (0.1384 Hartree) implied that DES7 possessed higher global hardness and higher resistance to charge transfer (CT) as compared to DL menthol-acetic acid DES, where the least energy gap and global hardness (0.1365 Hartree) was observed. The difference in the HOMO-LUMO energy gap between DES1 and DES7 is 2.53 kcal/mol, whereas, in the case of the global hardness (η), the difference is 1.20 kcal/mol for the same two systems. Thus, DES1 became less stable and displayed less resistance to CT and more polarizability. The stability referred to here is the chemical stability of a molecule, where more energy is required to move electrons from the ground state to an excited state. DES4, DES5 and DES6 were more stable as compared to DES1, DES2 and DES3 due to their superior HOMO-LUMO gap energy and higher η values as well. Similar findings were obtained in the sections consisting of interaction energy and the NBO charge transfer analysis.

2.3.1.2 Quantum Theory of "Atoms in Molecules" (QTAIM) Analysis

The QTAIM analysis, or the Quantum Theory of "Atoms in Molecules," was implemented as a potent approach for comprehending the various intermolecular interactions between the constituents of the DL menthol-carboxylic acid-based DES systems in both their optimized ground-state and also the solvated forms. By studying the electron density

distribution at the so-called bond critical points i.e., the BCPs (3, −1), one can understand the numerous non-covalent interactions (NCI) between molecules or atoms using Bader's QTAIM scheme[39]. Bond critical points (BCPs) appear as a saddle point between two nearby atoms, with maximum electron density in two directions and minimum in one direction perpendicular to the others defining a bonded interaction. To understand the nature, mechanism, and strength of the interaction in a better way, it is helpful to look at the electron density at BCP (ρ_{BCP}) and its Laplacian ($\nabla\rho_{BCP}^2$).[48] The sign of ($\nabla\rho_{BCP}^2$) determines the characteristic of the interaction, and (ρ_{BCP}) correlates to the interaction's intensity. A smaller ρ_{BCP} implies weaker bonds and more interatomic distance.[68] Covalent bonds are denoted by a negative value of the Laplacian of electron density ($\nabla\rho_{BCP}^2$), whereas closed-shell interaction features like ionic, van der Waals, or hydrogen bonds are indicated by a positive value.[69] In addition to these two characteristics, energetic parameters such as the electron energy density at BCP (H_{BCP}), which combines the kinetic (G_{BCP}) and potential (V_{BCP}) energy density components, can help identify the interaction type. When noncovalent contact is present, generally the ($-G_{BCP}/V_{BCP}$) value appears to be more than 1.

All these calculated values associated with the BCPs for different DES systems are presented in Table 2.5 and the molecular graphs of the DESs are reported in Figure B.4 (see Appendix B). The AIM analysis revealed that all the values of ρ_{BCP} and the $\nabla\rho_{BCP}^2$ at different BCPs of the studied DESs were positive confirming the closed-shell noncovalent interactions. In each of the DES systems, two types of BCPs were observed as presented in Figure B.4 (Appendix B) which signified the interactive involvement of the active chemical groups present in the HBAs and the HBDs, i.e., −OH and −COOH groups, respectively.

Table 2.5: Electron density (ρ_{BCP}), the Laplacian of electron density ($\nabla\rho_{BCP}^2$) and the energetic components at the relevant BCPs for DL-menthol- acetic acid, DL-menthol- octanoic acid, and DL-menthol- decanoic acid DESs in the ground state. [DLM: DL menthol, ACE: acetic acid, HEX: hexanoic acid, OCT: octanoic acid, NON: nonanoic acid, DEC: decanoic acid, DODEC: dodecanoic acid]

Component pair	BCP interaction	Distance (Å)	ρ_{BCP} (a.u.)	$\nabla\rho_{BCP}$ (a.u.)	G_{BCP} (a.u.)	V_{BCP} (a.u.)	$-G_{BCP}/V_{BCP}$
DLM-ACE	BCP1a: H_{31}-O_{33}	2.0185	0.0234	0.0808	0.0187	−0.0172	1.088
	BCP1b: O_{30}-H_{35}	1.7303	0.0429	0.1276	0.0354	−0.0389	0.909

DLM-BUT	BCP2a: H_{31}-O_{39}	2.008	0.0239	0.0826	0.0192	−0.0177	1.085
	BCP2b: O_{30}-H_{41}	1.7365	0.0424	0.1266	0.0350	−0.0382	0.915
DLM-HEX	BCP3a: H_{31}-O_{45}	2.010	0.0238	0.0824	0.0191	−0.0162	1.084
	BCP3b: O_{30}-H_{47}	1.735	0.0425	0.1271	0.0351	−0.0387	0.906
DLM-OCT	BCP4a: H_{31}-O_{51}	2.0154	0.0235	0.0816	0.0189	-0.0174	1.086
	BCP4b: O_{30}-H_{53}	1.7324	0.0428	0.1276	0.0353	−0.0387	0.912
DLM-NON	BCP5a: H_{31}-O_{54}	2.018	0.0234	0.0810	0.0188	-0.0173	1.087
	BCP5b: O_{30}-H_{56}	1.732	0.0428	0.1275	0.0353	−0.0388	0.911
DLM-DEC	BCP6a: H_{31}-O_{51}	2.018	0.0234	0.0811	0.0188	-0.0173	1.087
	BCP6b: O_{30}-H_{53}	1.732	0.0428	0.1277	0.0353	-0.0388	0.911
DLM-DODEC	BCP7a: H_{31}-O_{51}	2.019	0.0234	0.0810	0.0187	-0.0172	1.087
	BCP7b: O_{30}-H_{53}	1.732	0.0429	0.1276	0.0354	-0.0388	0.911

Higher electron densities and Laplacian of electron densities are observed for DL menthol (O) - fatty acid (H) BCPs (BCP 1b, 2b, 3b, 4b, 5b, 6b and 7b) with electron density values (from 0.0424 to 0.0429 a.u.) due to the lesser distance between the interactive atoms (from 1.7303 to 1.7365 Å) forming a stronger interaction. The other BCPs (BCP 1a, 2a, 3a, 4a, 5a, 6a and 7a) formed between DL menthol (H) - fatty acid (O) acquired less electron density ranging from 0.0234 to 0.0239 a.u. owing to the marginally longer interaction distance (from 2.008 to 2.019 Å) as compared to the previously mentioned BCPs. The ($-G_c/V_c$) value of greater than 1 has been obtained in the BCPs 1a-7a predominantly suggesting non-covalent interactions between the positively charged H_{31} atom (DL-menthol) and an electronegative O atom (carboxylic acids). The other BCPs (BCP 1b-7b) attained slightly lesser ($-G_c/V_c$) ranging from 0.909 to 0.915, which suggested a stronger interaction was present between DL-menthol (O_{30}) and carboxylic acids (H) that imparted higher covalency in the closed-shell interaction as a result of shorter interaction distance. The presence of these non-covalent interactions comprising hydrogen bonding, van der Waals as well as dispersion interactions are responsible for the stable formation of the DESs, supporting a superior HBA-HBD interaction responsible for the larger melting point depression.

(a)

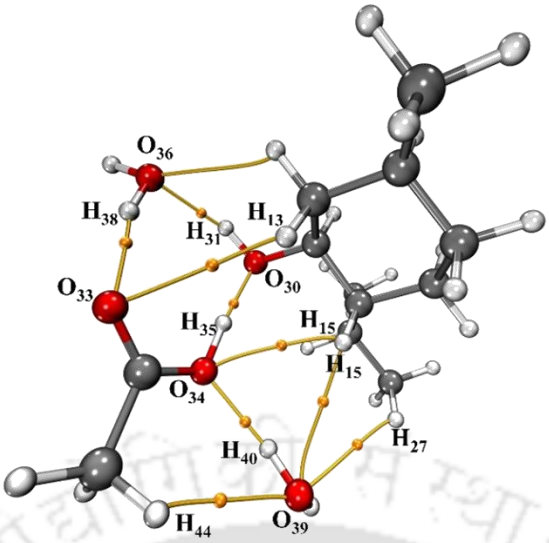

(b)

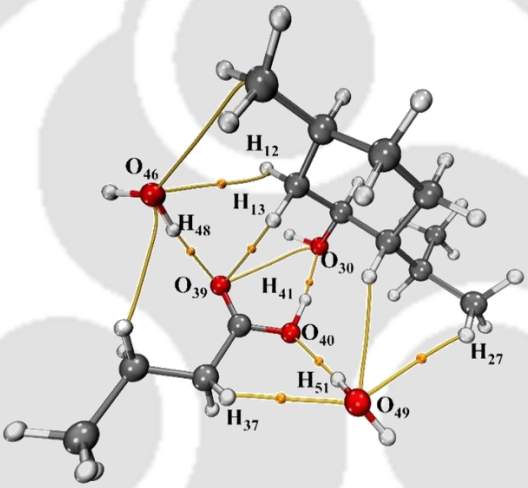

(c)

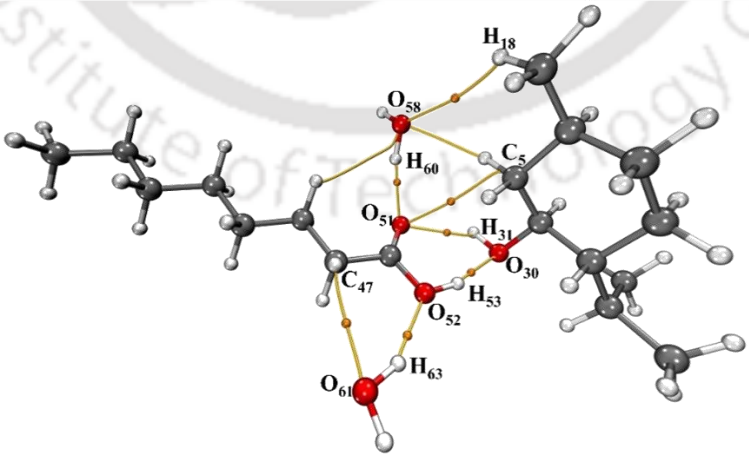

(d)

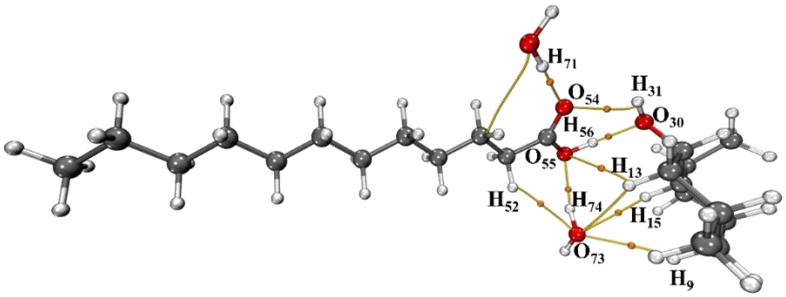

Figure 2.11: Molecular graphs of the explicitly solvated structures of (a) DES1; (b) DES2; (c) DES4; and (d) DES7, at the B3LYP/6-311+G(d,p) level with D3BJ dispersion correction revealing bond critical points (BCPs) and their corresponding paths.

To explore the solvated state geometries of the DESs, the QTAIM analysis for four DESs (DES1, DES2, DES4 and DES7) was carried out and their BCP components are presented in Table B.4 (Appendix B) and Figure 2.11. For DES1, BCP1b of the solvated structure had an increase in the electron density (ρ_{BCP}) owing to a reduction in the interaction distance from 1.73 to 1.62 Å. However, BCP1a: H_{31}-O_{33} of the pure DES1 was destroyed in the solvated structure suggesting interference of the water molecules to penetrate through the DES assembly. The increased HBD-water interactions can be verified by the BCPs 1d, 1e and 1f, newly formed between acetic acid and water, as presented in Table B.4 (see Appendix B). The ($-G_{BCP}/V_{BCP}$) values for these BCPs are greater than 1 and the $\nabla\rho_{BCP}^2$ values are positive, implying closed-shell interactions such as hydrogen bonding between acetic acid and water molecules. Similar occurrences were observed for DES2, where BCP2a: H_{31}-O_{39} was destroyed in the presence of water molecules. Higher HBD-water interactions were observed through multiple BCPs between butanoic acid and water. Both of these DESs encountered destruction of HBA-HBD contacts to a greater extent and the disintegration of HBA-HBD assembly can be confirmed.

On contrary, DES4 and DES7, generally claimed as hydrophobic DESs, exhibited quite the opposite results from the hydrophilic DESs. Both DES 4 and DES7 retained the pure state BCPs even in the solvated state claiming significant HBA-HBD interactions. BCP4a: O_{51}-H_{31}, and BCP4b: H_{53}-O_{30} were very much intact in the solvated DES state. Higher ρ_{BCP} was observed in the case of BCP4b due to a smaller interaction distance, whereas the ρ_{BCP} value slightly decreased for BCP4a because of the slight relaxation of the interaction. However, the overall DES assembly is strong enough to withstand the water environment with a stronger intermolecular interactive framework between the HBA and the HBD. Much stronger HBA-

HBD interactions were observed for DES7, where the aqueous phase around the DES assembly was almost ineffective in disrupting the DES structure with almost negligible relaxation of the HBA-HBD framework as displayed in Figures 2.5(e) and 2.11(d). The outcome is quite obvious and consistent with the hydrophobic nature of these DESs confirmed through experiments as well as computational study. The NCI analysis can comprehensively illustrate the detailed non-covalent interactions responsible for the formation of the DES and its stability in an aqueous environment as investigated in the upcoming section.

2.3.1.2.1 Non-Covalent Interaction Analysis

The following equation expresses the concept of "reduced density gradient" (RDG) analysis, which is based on examining the electron density distribution in areas with low electron density and low gradient values.

$$RDG = \frac{1}{2(3\pi^2)^{1/3}} \frac{|\nabla\rho|}{\rho^{4/3}} \qquad (2.3)$$

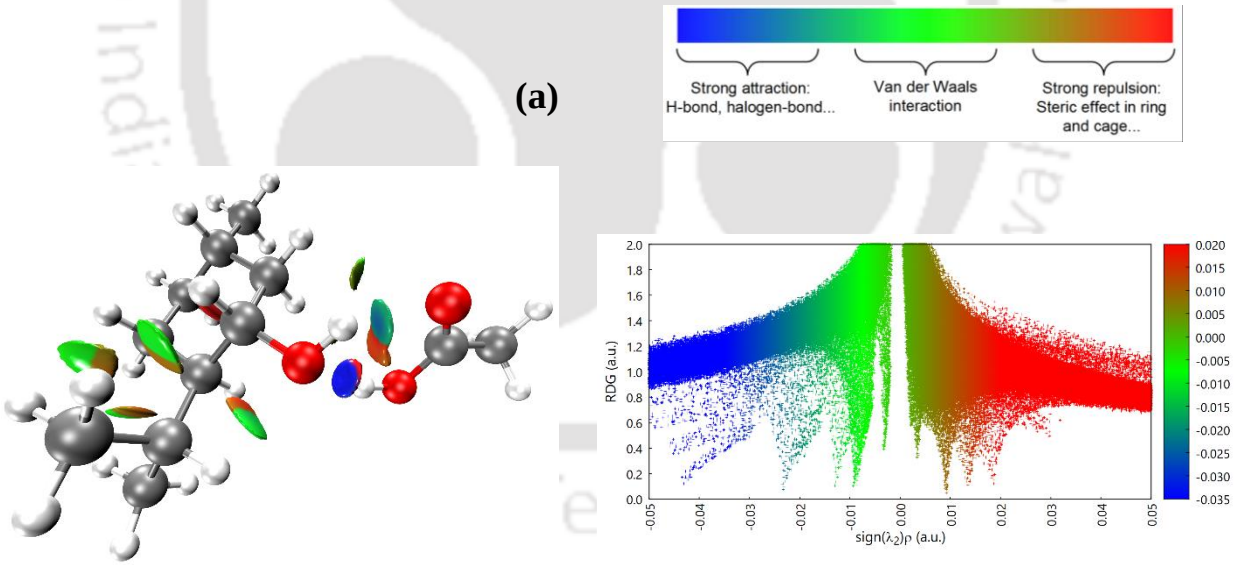

(a)

(b)

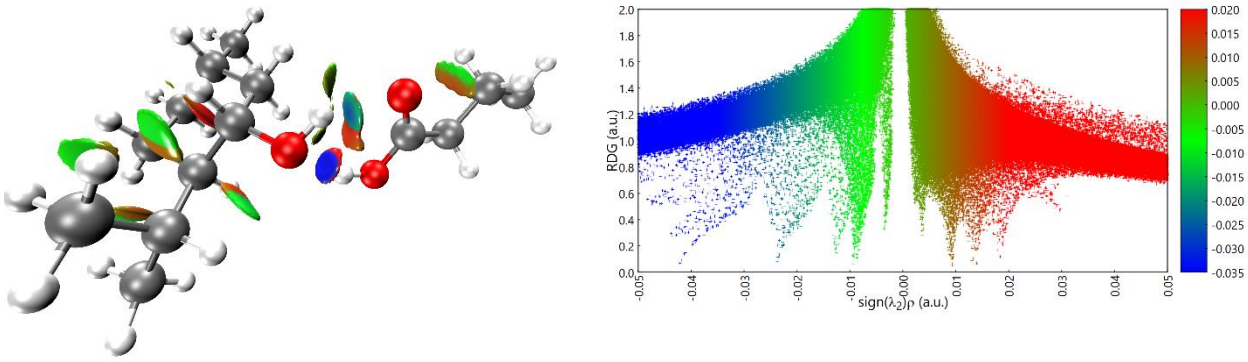
RDG (a.u.)
sign(λ2)ρ (a.u.)

(c)

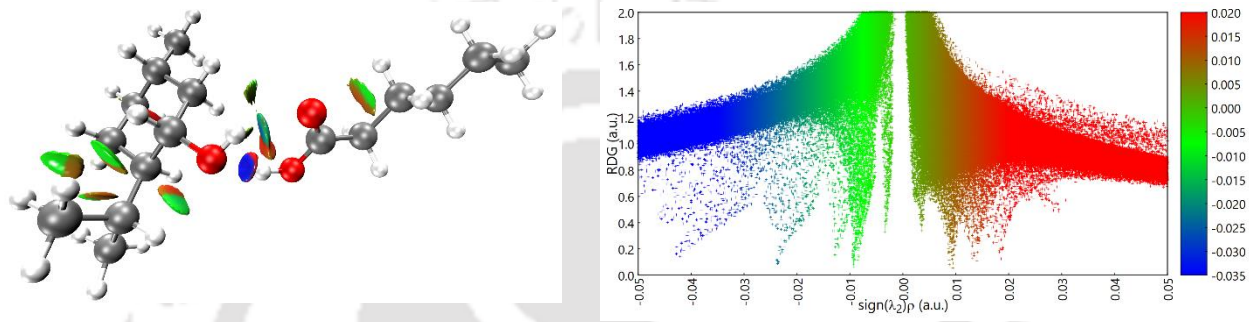
RDG (a.u.)
sign(λ2)ρ (a.u.)

(d)

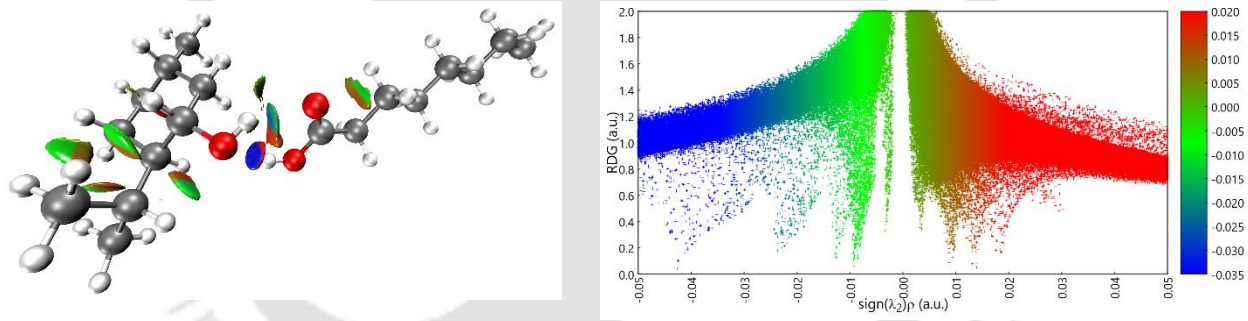
RDG (a.u.)
sign(λ2)ρ (a.u.)

(e)

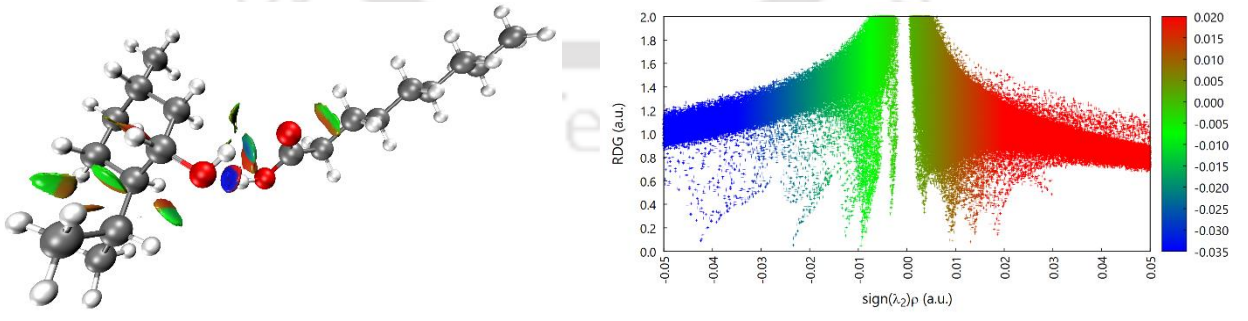
RDG (a.u.)
sign(λ2)ρ (a.u.)

(f)

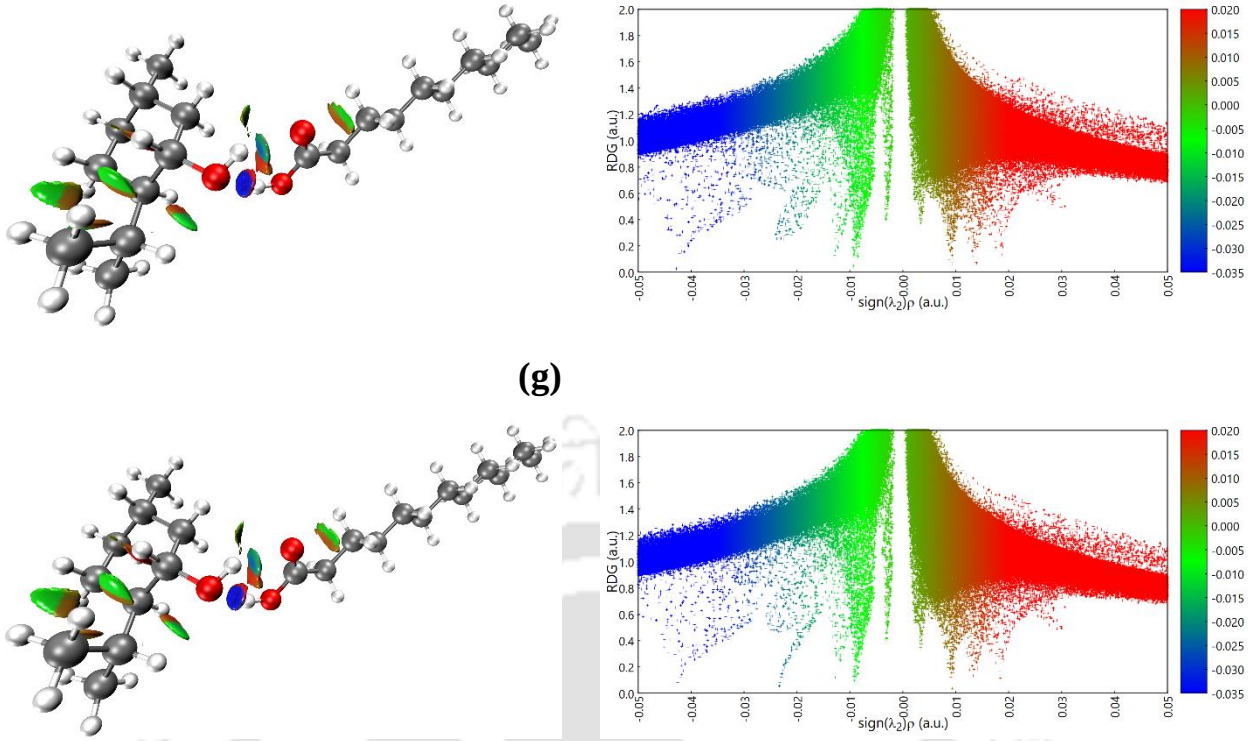

Figure 2.12: RDG isosurfaces and scatter graphs of RDG for (a) DES1, (b) DES2, (c) DES3, (d) DES4, (e) DES5, (f) DES6, and (g) DES7, at the B3LYP/6-311+G(d,p) level with D3BJ dispersion correction.

The insightful NCI analysis is based on the interpretation of RDG spikes.[48,49] The NCI analysis using the RDG approach may uncover and quantify a variety of weak interactions, including hydrogen bonding, van der Waals, and dispersion interactions. The RDG scatter graph is plotted as a function of electron density multiplied by the sign of the electron density Hessian second eigenvalue [sign(λ_2)ρ]. Figure 2.12 shows the RDG isosurfaces and the RDG scatter plots revealing various weak interactions ranging from positive to negative [sign(λ_2)ρ] values for DES1 to DES7 at the B3LYP/6-311+G(d,p) level with D3BJ dispersion correction. Amenable results ascertaining the consistency were obtained for the M06-2X/6-311+G(d,p) level of theory. Different Colored spikes indicate a specific kind of interaction (blue: H-bonds or halogen bonds ($\lambda_2 < 0$); green: van der Waals or dispersion interaction ($\lambda_2 \cong 0$); and red: steric effect due to ring or cage formation ($\lambda_2 > 0$)). To figure out what each colour means in the NCI plots, you could think of strong, attractive interactions like hydrogen bonds, halogen bonds, and electrostatic interactions as being in the blue areas. The red regions show strong repulsion caused by non-bonded overlap, while the transitions region contains information on vdW interactions like dispersion interaction, dipole-dipole interaction, and so on.

The present RDG study of the DESs revealed the presence of the combination of hydrogen bonding and dispersion interactions (vdW) as multiple RDG spikes were witnessed between 0 to −0.05 a.u. in Figure 2.12a-g. The blue spikes present between −0.01 to −0.05 a.u. were indicative of the existence of hydrogen bonds between the O (menthol) and H (carboxylic acid) of the DESs. The blue flake present in the NCI plots in Figure 2.12 indicated the same. Spikes were also obtained in the transition region between 0 to −0.01 a.u. evidenced by the green flake regions of the NCI diagrams suggesting vdW and dispersion interactions. The presence of bulky groups in the molecular system gave rise to steric hindrance evidenced by the RDG peaks obtained in the range > 0.005 a.u. The long-chain hydrophobic part of the higher organic acids also exhibited steric repulsive identity. Comprehensively established was the fact that these DESs were formed with multiple weak interactions among the HBAs and the HBDs in the form of hydrogen bonds and dispersion interactions and in combination they influence the stability of the DES structures leading to the depression in freezing temperature and enhanced overall interactive network between the components.

The NCI plots for the explicitly solvated structures of the DESs are presented in Figure 2.13. Two hydrophilic (DES1 and DES2) and two hydrophobic DESs (DES4 and DES7) were selected for this comparison study based on the short and long-chain fatty acids. In DES1, blue flakes can be observed between acetic acid and water molecules revealing hydrogen bonding among the components. The multiple blue spikes present between −0.025 to −0.04 a.u. in Figure 2.13a confirmed the increased closed-shell interaction between HBD and water. The inclusion of water molecules enhanced the dispersion interaction within the system as more spikes can be witnessed in the vdW interaction region (green region) due to water-DES non-covalent interaction. The increased non-covalent interactions (green and blue spike regions) largely occurred due to hydrophilic HBD and polar water molecule interactions containing higher electron density (ρ) already discussed in the QTAIM analysis. The HBA-HBD non-covalent interactions were affected greatly as evidenced by the low ρ values. The spike present in the blue region of pure DES1 between −0.04 to −0.05 a.u. in Figure 2.12a disappeared in the solvated state as can be seen in Figure 2.13a, suggesting the destruction of O (acetic acid)…H (DL-menthol) hydrogen bonding. Similar nature of the non-covalent interactions was observed for DES2 with slightly better HBA-HBD interaction as can be observed by the green and blue regions in Figure 2.13b. The hydrophilic nature of DES1 and DES2 can thus be established by the NCI and the RDG analysis.

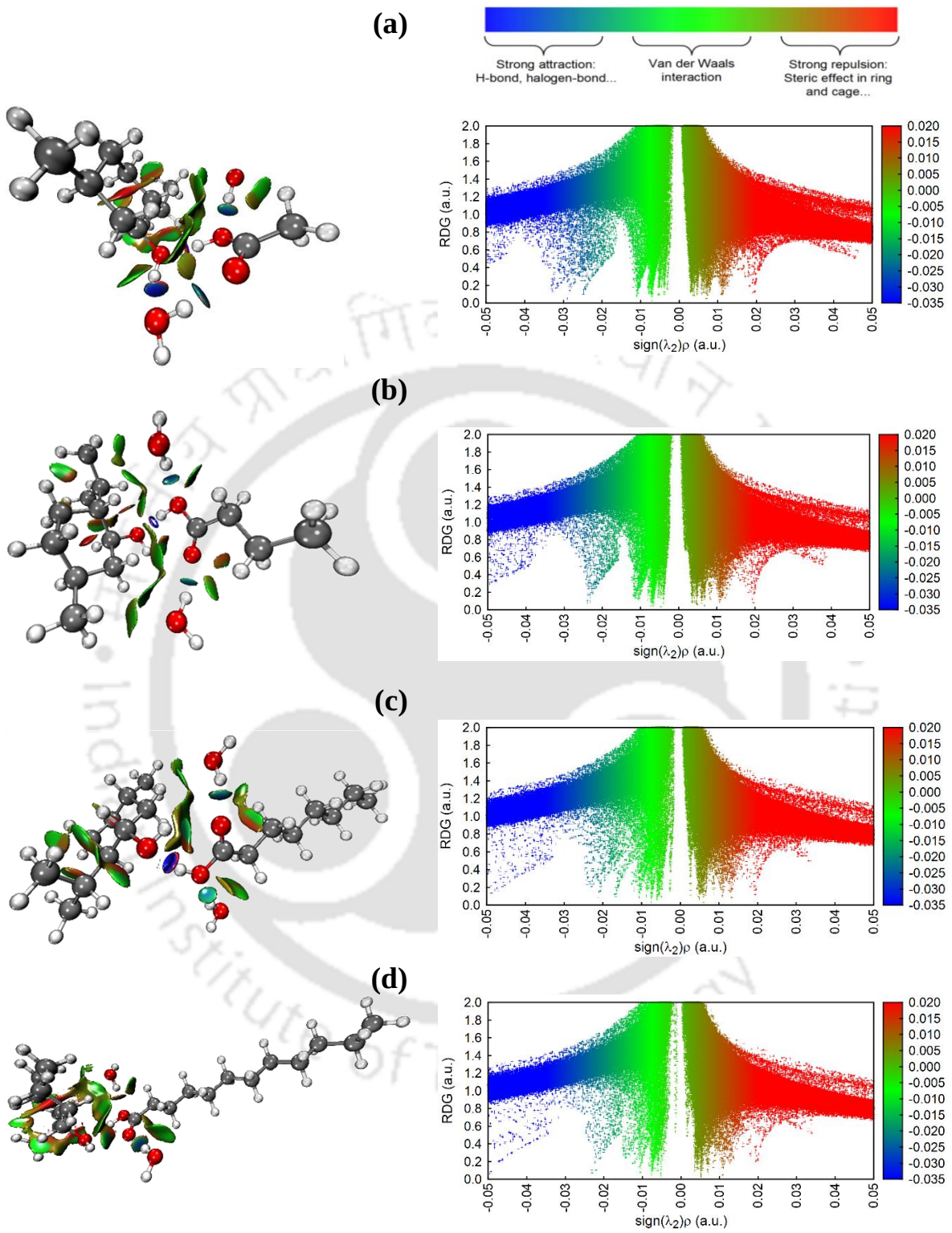

Figure 2.13: RDG iso-surfaces and scatter graphs of explicitly solvated structures of (a) DES1; (b) DES2; (c) DES4; and (d) DES7 at the B3LYP/6-311+G (d,p) level of theory with D3BJ dispersion correction.

In the case of DES4 and DES7, one can witness the improved non-covalent network within the HBA and HBD in Figure 2.13c-d. In the presence of water around DES4, the combined water-repelling character of octanoic acid and DL-menthol resulted in a higher and denser network of hydrogen bonding and vdW interactions between the DES-forming components. This was quite evident from the denser network of green flakes in the intermolecular region of DL-menthol and octanoic acid/dodecanoic acid for DES4 and DES7, respectively (Figure 2.13c-d). One distinguishing factor between the NCI and RDG plots of hydrophilic and hydrophobic DESs was the evolution of dispersion interactions in the vdW interaction region (green region). While, in the case of the hydrophilic DESs (e.g, DES1 and DES2), the higher HBD-water interaction was responsible for this, it was the superior HBA-HBD network that gave rise to this dense emergence of vdW interactions. Not only the hydrogen bonding network within the HBA-HBD sustained the water penetration by strong repulsion but also gained strength as can be observed by the increased ρ values (0.0489 and 0.049, for DES4 and DES7, respectively) presented in Table B.4 (Appendix B). Interaction of octanoic acid and dodecanoic acid with water at a lesser extent was also observed, however, the strength of these interactions was very low as evident from the low ρ values signifying the ineffective nature of water in disrupting the DES framework. Some spikes in the red region were observed in the RDG plots of all the DESs in Figure 2.13 largely due to the steric effect of DL-menthol and the ring-type formation of the molecules. In summary, the NCI and the RDG analysis showed that the DL-menthol: carboxylic acid DESs contain hydrogen bonding as well as vdW dispersion interactions for their formation. Upon mixing with water the short-chain fatty acid-based DESs get involved in enhanced non-covalent interaction (mainly H-bonding, and dispersion effects) with water molecules resulting in the disruption of the DES structures. However, long-chain fatty acid-based DESs withstand their structural integrity with a larger extent of dispersion as well as H-bonding interactions among the HBA and the HBD in the presence of external water molecules maintaining coherence with the experimental as well as MD simulation analysis.

2.3.1.3 MD Simulation Analysis

In our MD simulations, DL-menthol and tetrabutylammonium chloride were taken as hydrogen bond acceptors (HBA) and organic acids such as acetic acid, pyruvic acid, butanoic acid, hexanoic acid, levulinic acid, octanoic acid, decanoic acid and dodecanoic acid were taken as hydrogen bond donors (HBD) respectively, with appropriate compositions. Each system consisted of a 1:1 mass ratio of DES and water which was the same as the experiments.[26] The

number of molecules for each system considered for the simulation is presented in Table 2.3. The snapshots were captured at 0 ns and 100 ns of production run respectively for each system to compare the initial and the final molecular arrangements. The snapshots of the systems S1 to S10 at 0 ns and 100 ns were provided in Figures 2.14(a-t).

Water-stability of DES or DES stability in water can be explained as whether one DES could maintain its chemical and physical integrity when placed in an aqueous or other environments while retaining its identity or structure. A DES can be termed 'water-stable' if it can sustain itself in the presence of an aqueous environment and significantly did not leach to the aqueous phase or allow water molecules to disrupt its structure.

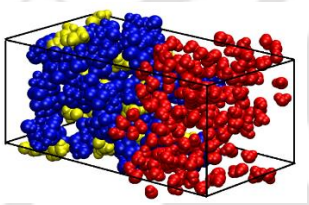

(a) DLM-ACE-WTR (0 ns) **(S1)**

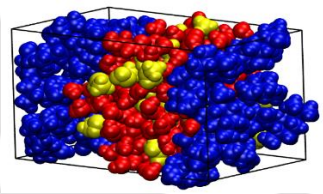

(b) DLM-ACE-WTR (100 ns) **(S1)**

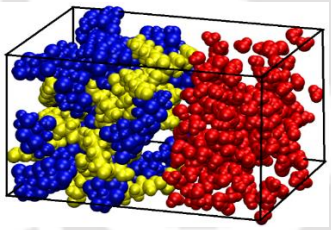

(c) DLM-BUT-WTR (0 ns) **(S2)**

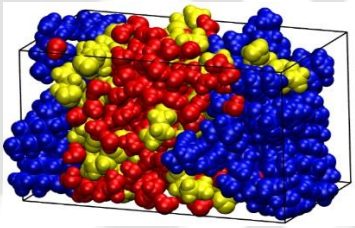

(d) DLM-BUT-WTR (100 ns) **(S2)**

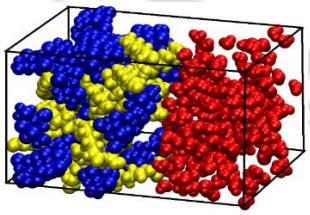

(e) DLM-HEX-WTR (0 ns) **(S3)**

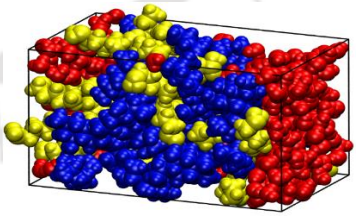

(f) DLM-HEX-WTR (100 ns) **(S3)**

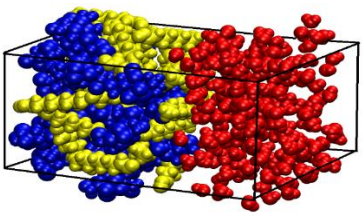

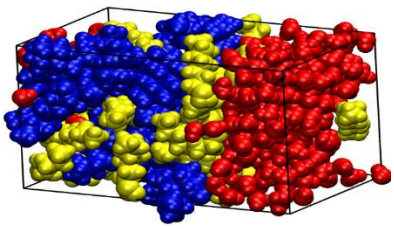

(g) DLM-OCT-WTR (0 ns) **(S4)**

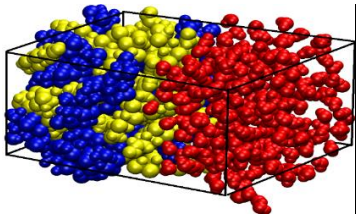

(h) DLM-OCT-WTR (100 ns) **(S4)**

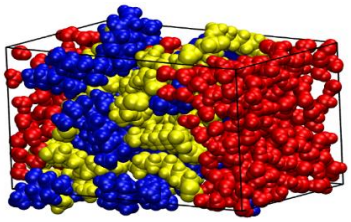

(i) DLM-DEC-WTR (0 ns) **(S5)**

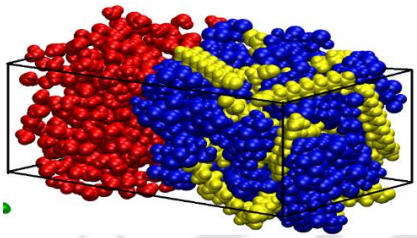

(j) DLM-DEC-WTR (100 ns) **(S5)**

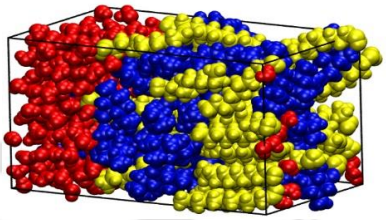

(k) DLM-DODEC-WTR (0 ns) **(S6)**

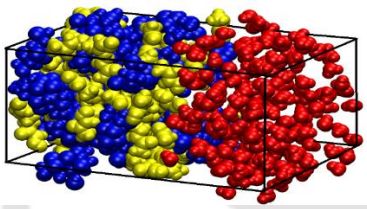

(l) DLM-DODEC-WTR (100 ns) **(S6)**

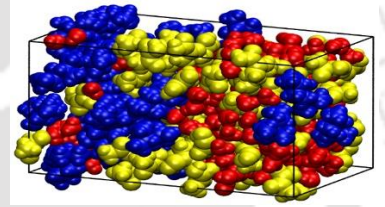

(m) DLM-PYR-WTR (0 ns) **(S7)**

(n) DLM-PYR-WTR (100 ns) **(S7)**

(o) DLM-LEV-WTR (0 ns) **(S8)**

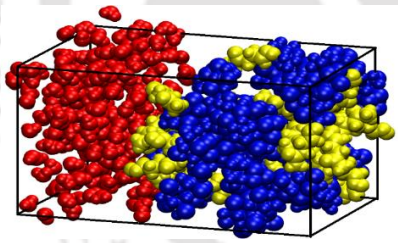

(p) DLM-LEV-WTR (100 ns) **(S8)**

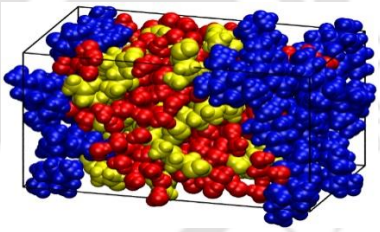

(q) TBACl-ACE-WTR (0 ns) **(S9)**

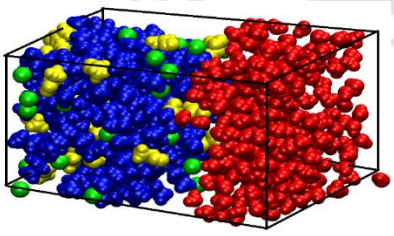

(r) TBACl-ACE-WTR (100 ns) **(S9)**

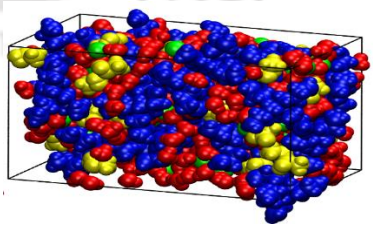

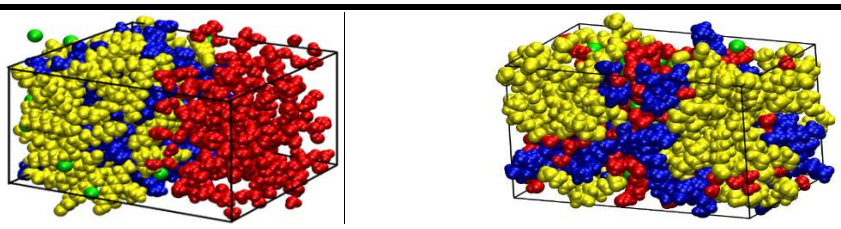

(s) TBACl-OCT-WTR (0 ns) **(S10)** (t) TBACl-OCT-WTR (100 ns) **(S10)**

Figure 2.14: Distribution snapshots of different DES- water systems at 0 ns and 100 ns for (a), (b) system S1; (c), (d) system S2; (e) (f) system S3; (g), (h) system S4; (i), (j) system S5; (k), (l) system S6; (m), (n) system S7; (o), (p) system S8; (q), (r) system S9 and (s), (t) system S10; (DLM and TBACl denote DL-menthol and tetrabutylammonium molecules, respectively, both in blue colour, chloride ions in green colour; WTR denotes water molecules in red colour; ACE, BUT, HEX, OCT, DEC, DODEC, PYR and LEV denote acetic acid, butanoic acid, hexanoic acid, octanoic acid, decanoic acid, dodecanoic acid, pyruvic acid and levulinic acid molecules, respectively, in yellow colour).

From Figure 2.14, it can be observed that the menthol-based DESs consisting of acetic acid, butanoic acid and hexanoic acid are very less water-stable. The order of stability of the DESs based on the distribution of HBD molecules in the water phase can be witnessed as DES1 < DES8 < DES2 < DES7 < DES3 < DES4 < DES5 < DES6. In system S1, disruption of the DES integrity was witnessed in contact with water, where around 95% loss of acid takes place towards the water-rich phase. On a similar note, the loss of acid decreases to around 35% and 15% for systems S2 and S3, respectively. These can be visualized from the molecular arrangements captured at 0 ns and 100 ns of the simulation run in Figures 2.14a to 2.14f.

Among all the systems containing DL-menthol as HBA, DES4, DES5 and DES6 have shown hydrophobic nature (Figure 2.14g to 2.14l) with low contamination of the hydrophobic long-chain organic acids (HBDs) in the water-rich phase. On the contrary, the systems containing DES1, DES2, DES3, DES7 and DES8 were unstable in contact with water because of the presence of hydrophilic organic groups as HBDs. In the case of $N_{4444}Cl$-based DESs, all the DESs such as DES9 and DES10 were found to be water-miscible because of the hydrophilic nature of $N_{4444}Cl$ (Figure 2.14q to 2.14t). In contrast to the menthol- based DESs where hydrophilic HBDs played a major role in its leaching towards the water-rich phase, the hydrophilic $N_{4444}Cl$ got transported primarily to the water-rich phase in the case of $N_{4444}Cl$-based DESs. This is, in fact, the main reason behind the instability of ammonium-based DESs

in contact with water. From the snapshots of the systems S9 (Figure 2.14q, 2.14r), it can be visualized that both HBA (tetrabutylammonium chloride) and HBD (acetic acid) were miscible with the water molecules, turning the whole system unstable with water. System S10 confirmed the transport of only hydrophilic ammonium salt to the water-rich phase, whereas the contamination of the HBDs such as octanoic acid to the water-rich phase was very negligible (Figure 2.14s, 2.14t).

When compared to experiments, Florindo et al. studied the water stability of different DESs by comparing the ^{1}H NMR spectra for the DES-rich phase and water-rich phase.[26] They confirmed the presence of the hydrophilic HBDs (such as acetic acid, butanoic acid, and hexanoic acid) in the water-rich phase for the systems S1, S2 and S3. With detailed scrutiny of the ^{1}H NMR data for acetic acid, butanoic acid and levulinic acid- based DESs, it was observed that the acid molecules (HBD) leached out to the water phase while the menthol molecules kept themselves isolated from the water phase. Similar results can be viewed in Figures 2.14(a,b), 1(c,d) and 1(o,p), respectively. However, in the case of octanoic acid and dodecanoic acid-based systems, no transport of menthol, as well as acid molecules (HBA and HBD), were observed. This has been confirmed and depicted in Figures 2.14(g,h) and 2.14(k,l). From the analysis of the tetrabutylammonium chloride- octanoic acid-based system, it was observed that the ammonium salt molecules have a strong affinity towards the water phase, whereas the octanoic acid molecules maintained their hydrophobic characteristic (Figures 2.14s, 2.14t). The experimental results hence can be seen in excellent agreement with the simulation results that were obtained in the present work. We further analysed the non-bonded interaction energy, average hydrogen bonding, radial distribution function, combined distribution function and the mean square displacement self-diffusion coefficient to have an insight into the molecular-level understanding within the different systems.

2.3.1.3.1 Non-bonded Interaction Energy

Table 2.6 represents the non-bonded interaction energies, subdivided further into electrostatic and van der Waals (vdW) interactions, among the different components in each system. To study the interaction energies, we have compared short-chain organic acids such as acetic acid with long-chain organic acids such as octanoic acid, decanoic acid and dodecanoic acid as HBD. Interaction between acetic acid and water was much more favourable (-3.17 kcal/mol) (system S1) than that of octanoic acid-water (-2.40 kcal/mol), decanoic acid-water (-1.94 kcal/mol) and dodecanoic acid-water (-1.83 kcal/mol) (system S4, S5 and S6, respectively). It

implied that when in contact with water, acetic acid would have a higher affinity towards the water-rich phase than the longer carboxylic acids such as C_8 to C_{12}. A further breakup of the interaction energy into electrostatic and van der Waals components of system S1 revealed that the electrostatic interaction between acetic acid and water (-2.75 kcal/mol) was more dominant than the van der Waals interaction (-0.42 kcal/mol). However, an opposite trend was seen between menthol and acetic acid as the van der Waals component (-2.48 kcal/mol) between the HBA and HBD molecule was higher than the electrostatic part (-1.72 kcal/mol). A probable explanation for this could be the large size of the menthol molecule as compared to that of acetic acid which leads to steric hindrance between the molecules, thus reducing the electrostatic effect. It should be noted that the HBA and the HBD were non-ionic compounds, for which electrostatic interactions were less likely to dominate and entropic effects predominate. The hydroxyl (-OH) group present in the menthol structure was more likely to participate in H-bonding with the polar carboxyl (-COOH) group present in the acetic acid.

DES2, DES3, DES7 and DES8 also appeared to be hydrophilic. For systems S2 and S3, we observed the distribution of the HBD molecules i.e., butanoic acid and hexanoic acid towards the water-rich phase, though the numbers drastically reduced in the case of hexanoic acid. Whereas both the HBA and the HBD molecules showed affinity towards the aqueous phase for systems S7 and S8. Interestingly, the stability of DES2 and DES3 in water was higher as compared to DES1 even though all possessed hydrophilic nature as the total HBA-HBD interaction was higher than the HBD-water interaction which thereby improved the overall hydrophobicity.

Table 2.6: MD simulated non-bonded interaction energies (kcal/mol) between the different Pairs of HBA-HBD-water for the different systems calculated at 298.15 K and 1 atm pressure

System No	Component pairs	Electrostatic interactions (E_{elec})	Vander Waals interactions (E_{vdW})	Total nonbonded interactions (E_{total})	Relative Stability Factor (S)
S1	Menthol- water	-1.18	-0.21	-1.39	
	Menthol- acetic acid	-1.72	-2.48	-4.20	0.92

	Acetic acid- water	-2.75	-0.42	-3.17	
S2	Menthol- water	-1.08	-0.15	-1.23	1.94
	Menthol- butanoic acid	-2.65	-5.44	-8.09	
	Butanoic acid-water	-2.44	-0.50	-2.94	
S3	Menthol- water	-0.87	-0.15	-1.02	3.21
	Menthol- hexanoic acid	-3.32	-8.15	-11.47	
	Hexanoic acid-water	-2.14	-0.41	-2.55	
S4	Menthol- water	-0.84	-0.15	-0.99	3.70
	Menthol- octanoic acid	-3.01	-9.51	-12.52	
	Octanoic acid-water	-2.04	-0.36	-2.40	
S5	Menthol- water	-0.90	-0.19	-1.09	4.61
	Menthol- decanoic acid	-2.56	-11.40	-13.96	
	Decanoic acid-water	-1.69	-0.25	-1.94	
S6	Menthol- water	-1.68	-0.24	-1.92	6.10
	Menthol- dodecanoic acid	-4.10	-18.77	-22.87	
	Dodecanoic acid-water	-1.57	-0.26	-1.83	
S7	Menthol- water	-0.99	-0.14	-1.13	2.48
	Menthol- pyruvic acid	-4.97	-7.35	-12.32	
	Pyruvic acid-water	-3.43	-0.40	-3.83	
S8	Menthol- water	-1.16	-0.17	-1.33	1.22
	Menthol- levulinic acid	-2.11	-4.07	-6.18	
	Levulinic acid-water	-3.14	-0.61	-3.74	
S9	$N_{4444}Cl$- water	-13.42	-0.28	-13.70	1.57
	$N_{4444}Cl$- acetic acid	-16.76	-6.08	-22.84	
	Acetic acid- water	-0.72	-0.12	-0.84	
S10	$N_{4444}Cl$- water	-13.81	-0.18	-13.99	

$N_{4444}Cl$- octanoic acid	-15.25	-16.11	-31.36	2.00
Octanoic acid- water	-1.46	-0.24	-1.70	

This can be explained based on total non-bonded energies as presented in Table 2.6. Here the menthol-organic acid energies are always greater than the water-organic acid systems. However, the difference is the lowest in acetic acid while the highest in dodecanoic acid. This implies that the higher the difference, the more strongly it is attached to the HBA (menthol). So, acetic acid has almost equal magnitude indicating its higher preference in leaching out to the water phase. Among all the menthol-based DESs studied in this work, DESs based on octanoic acid, decanoic acid and dodecanoic acid depicted very low HBD-water interaction. This explains why DES4, DES5 and DES6 are stable in water. The hydrophobic tail of the HBD molecules (higher carboxylic acids with C_8 to C_{12}) pushes the water molecules owing to steric hindrance, and hence contributes to a strong interaction between the HBA and HBD.

It can be observed from Table 2.6 for systems S1 to S6, that the total non-bonded interaction energy (E_{total}) between the HBD (carboxylic acids) and water gradually decreased (system S1 to S6) with an increase in the chain length of the organic acids (from C_1 to C_{12}). This happens because, with the increase in chain length, the HBA-HBD interaction also increased continuously. The total nonbonded HBA-HBD interaction (-4.20 kcal/mol) for system S1 increased to (-22.87 kcal/mol) for system S6, whereas, the HBD-water interaction for system S1 (-3.17 kcal/mol) reduced to (-1.83 kcal/mol) for system S6 (Table 2.6). For systems S9 and S10, it can be noticed that the $N_{4444}Cl$-octanoic acid interaction (-31.36 kcal/mol) is much greater than that of $N_{4444}Cl$ –acetic acid (-22.84 kcal/mol). The effect of individual properties of HBA and HBD on the stability of DES in a specific medium can be explained in terms of their interactions with the molecules of that medium. Systems S4 and S10 does follow this behaviour (Table 2.6). In both the systems, octanoic acid was present as the HBD whereas, DL-menthol and $N_{4444}Cl$ were present as HBA for S4 and S10, respectively. Octanoic acid showed higher interaction with $N_{4444}Cl$ (-31.36 kcal/mol) than DL-menthol (-12.52 kcal/mol) which could imply greater stability of DES10 than that of DES4. However, when the HBA- water interaction of both the systems was compared, it was observed that $N_{4444}Cl$ had greater interaction energy (-13.99 kcal/mol) with water than that of DL-menthol (-0.99 kcal/mol). For both systems, octanoic acid exhibited very low interactions with water. From the above observations, it can be concluded that $N_{4444}Cl$- octanoic acid DES did not

maintain its chemical and physical integrity in an aqueous environment largely due to the hydrophilic character of the HBA molecules suggesting a possible disruption of DES structure. Figures 2.14 (s), and (t) visually suggest the same for DES10. The difference in the relative stability factor of DES4 (3.70) and DES10 (2.0) can be justified by the above explanation. Here, the HBA characteristic determined the overall stability of the DES in the aqueous medium.

Based on the non-bonded interaction energy among different species in a system, the stability of the eutectic systems in an aqueous environment can be predicted. For that, we have introduced a new term called 'Relative Stability Factor' to evaluate the relative stability of a eutectic system.

2.3.1.3.2 Relative Stability Factor

Here we introduce a relative measure to analyse the stability of the hydrophobic DESs in an aqueous environment. The relative stability of hydrophobic DESs in water can be obtained from the ratio of the interaction energies between HBA-HBD and the sum of interaction energies between HBA-water and HBD-water. Here electrostatic interactions and van der Waals interactions were considered as the two components of non-bonded interaction. This factor revealed the order of stability of different DES systems in contact with an aqueous environment. It does not exactly quantify the stability of a system. Since the interaction between HBA-water was almost constant in the case of menthol-based DESs, the stability factor was primarily a function of the HBD-water interaction. Hence, we defined the same as below:

Relative stability factor of hydrophobic DES

$$(S) = \frac{IE(HBA-HBD)}{IE(HBA-WATER)+IE(HBD-WATER)} \qquad (2.4)$$

The factor was presented in Table 2.6. The higher the stability factor (S), the higher the stability of DES in water. From the experimental work of Florindo et al.,[26] long-chain organic acid-based DESs were found to be more stable than the short-chain ones (menthol based), whereas all the ammonium-based DESs were found to be hydrophilic. This can be verified by examining the relative stability factor (S) obtained with the help of MD simulation (Table 2.6). Initially, we compared the stability factor values obtained in this work (Table 2.6) to the experimental findings of the stability of DESs in water by Florindo et al.[26] It was discovered that a stability factor ranging from 0 to 3.30 can be labelled as 'miscible in water' or 'unstable in water'.

According to this assessment of the water-stability of menthol-based DESs, acetic acid (S= 0.92) was found to be the 'most unstable'. Butanoic acid (S= 1.94), hexanoic acid (S= 3.21), pyruvic acid (S= 2.48) and levulinic acid (S= 1.22) is also termed as 'unstable in water'. However, octanoic acid (S= 3.70), decanoic acid (S= 4.60) and dodecanoic acid (S= 6.10) emerged to be 'stable in water' (for menthol-based DESs). For $N_{4444}Cl$-based DESs, both acetic acid (S= 1.57) and Octanoic acid (S= 2.00) were 'unstable in water'. Overall, from the observation of the relative stability factor data (Table 2.6), the order of stability of menthol-based DESs in an aqueous medium in terms of HBD was found to be in the order: dodecanoic acid > decanoic acid > octanoic acid > hexanoic acid > pyruvic acid > butanoic acid > levulinic acid > acetic acid. The ammonium based DESs it was found to be in the order of octanoic acid > acetic acid.

2.3.1.3.3 Radial and Combined Distribution Functions

Radial distribution functions (RDFs) provided insight into the structural properties of the different eutectic systems and their interactions in the presence of water. The RDFs presented useful information regarding the overall structural properties of a molecule with different species in the system as shown in Figure 2.15, Figure B.5 and Figure B.6 (see Appendix B). Figure 2.15 presented the comparative analysis of the RDFs between HBD-water (Figure 2.15a) and HBA-HBD (Figure 2.15b). Figures B.5 and B.6 (Appendix B) depicted the individual RDFs of HBA-HBD and HBD-water, respectively for the menthol-based systems. The respective atomic sites that were selected for the RDFs are H24 and O2 for acetic acid, O2 for butanoic acid, H46 and O4 for octanoic acid, H40 and O2 for decanoic acid, O6 for water and H20 for DL-menthol (refer to Figure B.1 and B.2 for detailed notations of all the molecules; and Figure B.5 and Figure B.6 for the rest of the DESs, in Appendix B). From Figure 2.15a, it can be observed that acetic acid had the most favourable interaction with water among all the HBD molecules. It gave a significantly sharp peak indicating the first solvation shell at around 3.15 Å. With an increase in the alkyl chain length of the HBD molecules, the subsequent reduction in the g(r) values of the RDFs was observed. This comparative plot suggested that acetic acid had significant interaction with the water molecules and lower organic acid-based DESs were not stable with water as they tend to interact favourably with water. Conversely, higher organic acids have shown reduced interaction with water molecules as shown in Figure 2.15a.

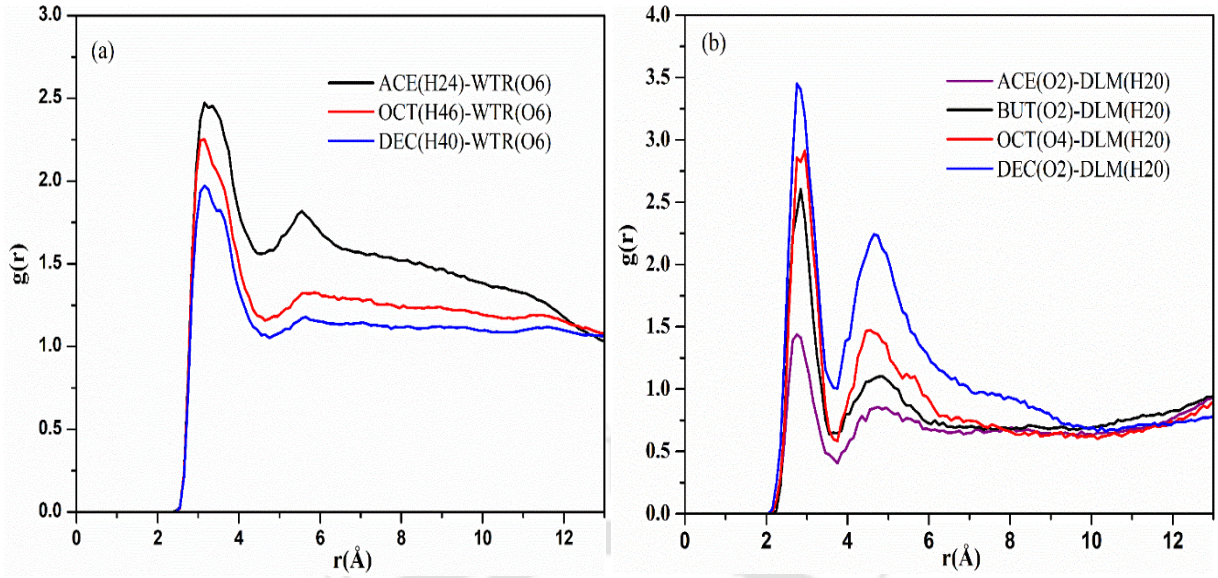

Figure 2.15: Comparison among atom-specific radial distribution function plots between the different molecular pairs present in the different DES-water systems (a) Acetic acid-water, octanoic acid-water and decanoic acid-water, for systems S1, S4 and S5, respectively; (b) DL-menthol-acetic acid, DL-menthol-butanoic acid, DL-menthol-octanoic acid, and DL-menthol-decanoic acid, for system S1, S2, S4 and S5, respectively, at 100 ns.

Further, from Figure 2.15b, we observed a sharp first solvation shell between DL-menthol and organic acids within 3Å. Interestingly, the maximum g(r) value sharply increased with an increase in the chain length of the organic acids. The maximum g(r) for decanoic acid, octanoic acid and acetic acid were 3.5, 2.9 and 1.4, respectively (Figure 2.15b). It signified that the interaction of acetic acid and DL-menthol was less as compared to acetic acid-water, thus DES1 became unstable in water. On the other hand, octanoic acid and decanoic acid have shown increased interaction with DL-menthol and less with water. This initiated higher stability to both the DESs towards an aqueous environment. The respective coordination numbers were shown in Table B.5 (Appendix B) which also validated the analysis of the RDFs.

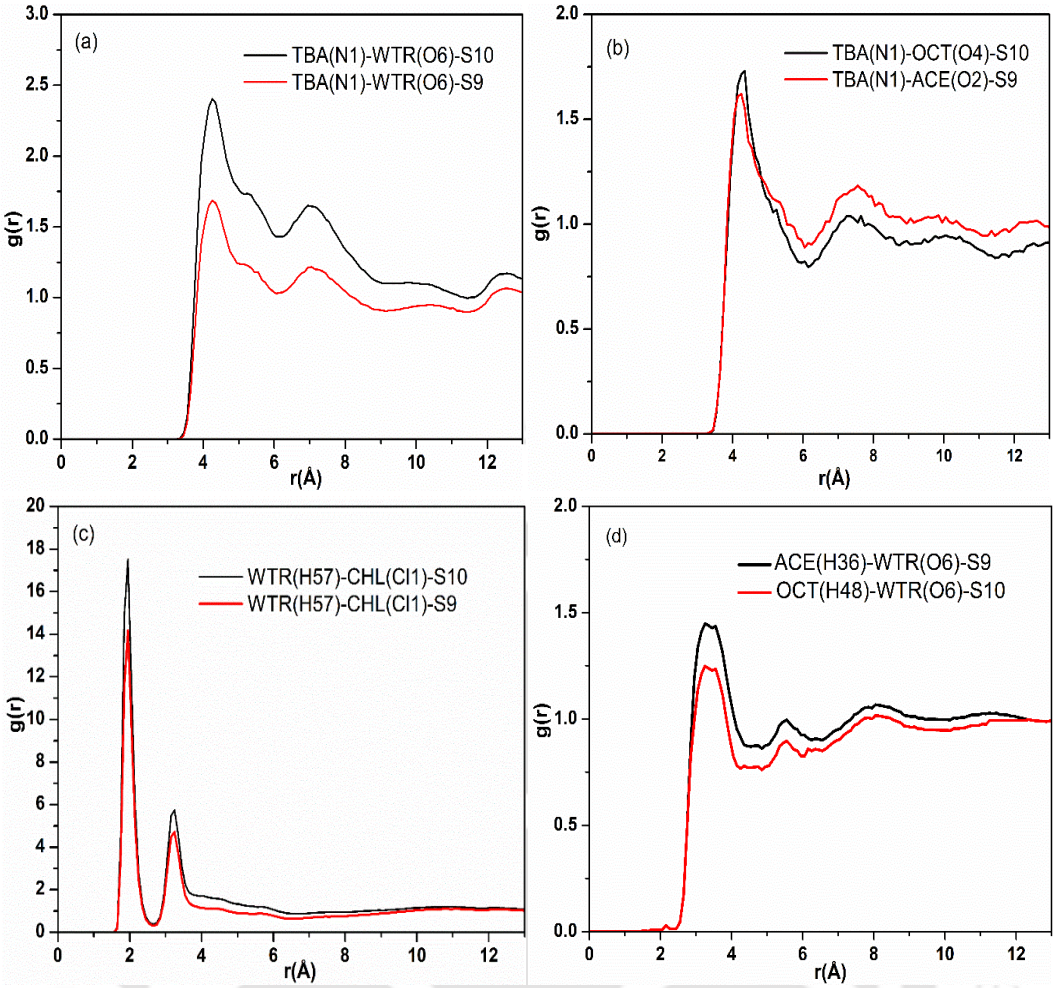

Figure 2.16: Comparison among atom-specific radial distribution function plots for different DES-water systems for the different molecular pairs between (a) tetrabutylammonium cation-water, for systems S9 and S10; (b) tetrabutylammonium cation- acetic acid, for system S9 and tetrabutylammonium cation- octanoic acid, for system S10; (c) water-chloride ion for system S9 and S10, at 100 ns; (d) acetic acid-water, for system S9 and octanoic acid-water, for system S10.

For tetrabutylammonium chloride-based DESs, we obtained the atom-atom RDF plots and tried to formulate a comparison among the species present, as shown in Figure 2.16. The ammonium cation exhibited higher interaction with water for system S10 as compared to system S9. For both cases, the maximum intensity g(r) peak appeared at ~ 4.15 Å, but the peak intensity differed (Figure 2.16a). We observed increased interaction of acetic acid-water as compared to octanoic acid-water as shown in Figure 2.16d. As water displayed less favourable interaction with octanoic acid (system S10), the ammonium cation present in the system exhibited higher interaction with water. It was also observed that ammonium cation displayed similar interaction with acetic acid and octanoic acid as well (Figure 2.16b). A very sharp g(r)

peak of 14 and 17.8 was obtained between chloride ion and water for S9 and S10, respectively (Figure 2.16c) at ~ 2.0 Å. Overall, the RDFs in Figure 2.16 suggested that both DES9 and DES10 had favourable interaction with water mainly because of the presence of hydrophilic moieties such as ammonium cation, chloride ion and acetic acid. This revealed the fact that DES components got disrupted in the presence of water which disturbed the DES- integrity and exposed the instability of ammonium-based DESs in the aqueous environment.

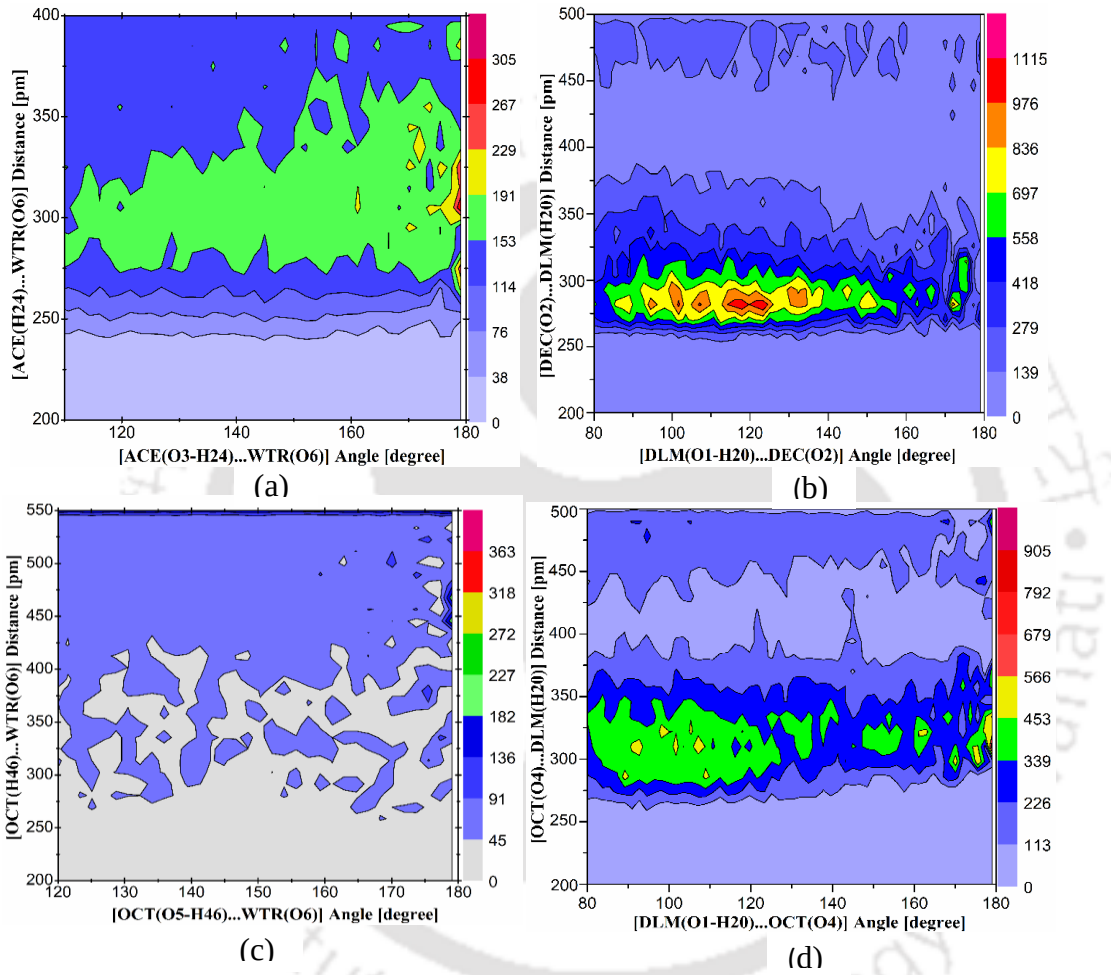

Figure 2.17: CDFs obtained by plotting the hydrogen bond distance (RDF) vs the hydrogen bond angle (ADF) for (a) O3-H24…O6 angle against H24…O6 distance (acetic acid-water); (b) O1-H20…O2 angle against H20…O2 distance (DL-menthol-decanoic acid); (c) O5-H46…O6 angle against H46…O6 distance (octanoic acid-water); and (d) O1-H20…O4 angle against H20…O4 distance (DL-menthol-octanoic acid).

Furthermore, for the confirmation of the hydrogen bonding, we have obtained the combined distribution function (CDF) (angular and radial). The CDF was evaluated as a function of hydrogen bond donor-hydrogen bond acceptor distance and donor-acceptor angle as shown in Figure 2.17. The TRAVIS package[57] was used to obtain the CDF. The CDF

confirmed the presence of hydrogen bonding among molecules and also helps us in verifying the observations of RDFs. From Figure 2.17a, it was observed that acetic acid formed O-H…O bond with water at a distance of around 3.15 Å. It also had an angle between 160° to 180°, which followed the criteria of hydrogen bonding. Thus the –OH group of acetic acid formed a hydrogen bond with the O atom of the water molecule with a distance of 3.15 Å and the bond was formed at an angle of 160° to 180° (for system S1). Similarly, Figure 2.17b pointed out the fact that DL-menthol formed O-H…O bond with decanoic acid at 3 Å keeping the angle between the bonds ranging from 120-160°. This confirms the results obtained by the RDFs and also the possible hydrogen bonding between DL-menthol and decanoic acid (for system S5). Similar to menthol-decanoic acid, DL-menthol displayed a possible O-H…O hydrogen bond with octanoic acid (for system S4) (Figure 2.17d). No significant interaction such as hydrogen bonding and molecular distribution were observed between octanoic acid and water (for system S4) as per Figure 2.17c. A significantly higher degree of hydrogen bonding was observed for decanoic acid and octanoic acid than acetic acid which is shown in Figures 2.17a, 2.17b and 2.17c. A higher value of the colour code suggests a higher degree of hydrogen bonding. We did not observe hydrogen bonding between decanoic acid and water. It signified that there was very little interaction between decanoic acid and water. Similar results were also obtained for octanoic acid and water.

2.3.1.3.4 Spatial Distribution Function (SDF)

To further substantiate the solvation findings from the QC results, MD simulation was carried out to mainly obtain the spatial distribution function (SDF) plots of DL menthol (HBA) and water molecules around the individual HBDs (carboxylic acids) of the respective DESs are presented in Figure 2.18 and Figure B.7 (Appendix B). The iso-values for specific components are mentioned alongside the figures. The affinity of the HBDs towards the water phase can be examined by the orientation of the water iso-surfaces around the central HBD molecules. The HBDs studied in this work are acetic acid (Figure 2.18a), butanoic acid (Figure 2.18b), hexanoic acid (Figure 2.18c), octanoic acid (Figure 2.18d), decanoic acid (Figure 2.18e) and dodecanoic acid (Figure 2.18f). The probability spots of water molecules were found in the region of space closer to the carboxylic group of the organic acids (HBDs) illustrating the possible interactive sites between organic acids and water molecules. The denser arrangement of water molecules confined around the HBD molecules indicated elevated interactions among them for the DESs consisting of acetic acid, butanoic acid and hexanoic acid as HBDs as shown in Figures 2.18a-c with the order of acetic acid > butanoic acid > hexanoic acid. Surprisingly,

the DL-menthol species are located away from the carboxylic acids as compared to water moiety because of the confinement of HBDs by water indicating the disintegration of DES-forming constituents. Water molecules penetrate the non-bonded interactive network present between the HBA and the HBD leading to DES disruption. Acetic, butanoic and hexanoic acids predominantly involve in non-bonded interactions with water due to their favourable electronic structure that facilitates O…H−O hydrogen bonding.

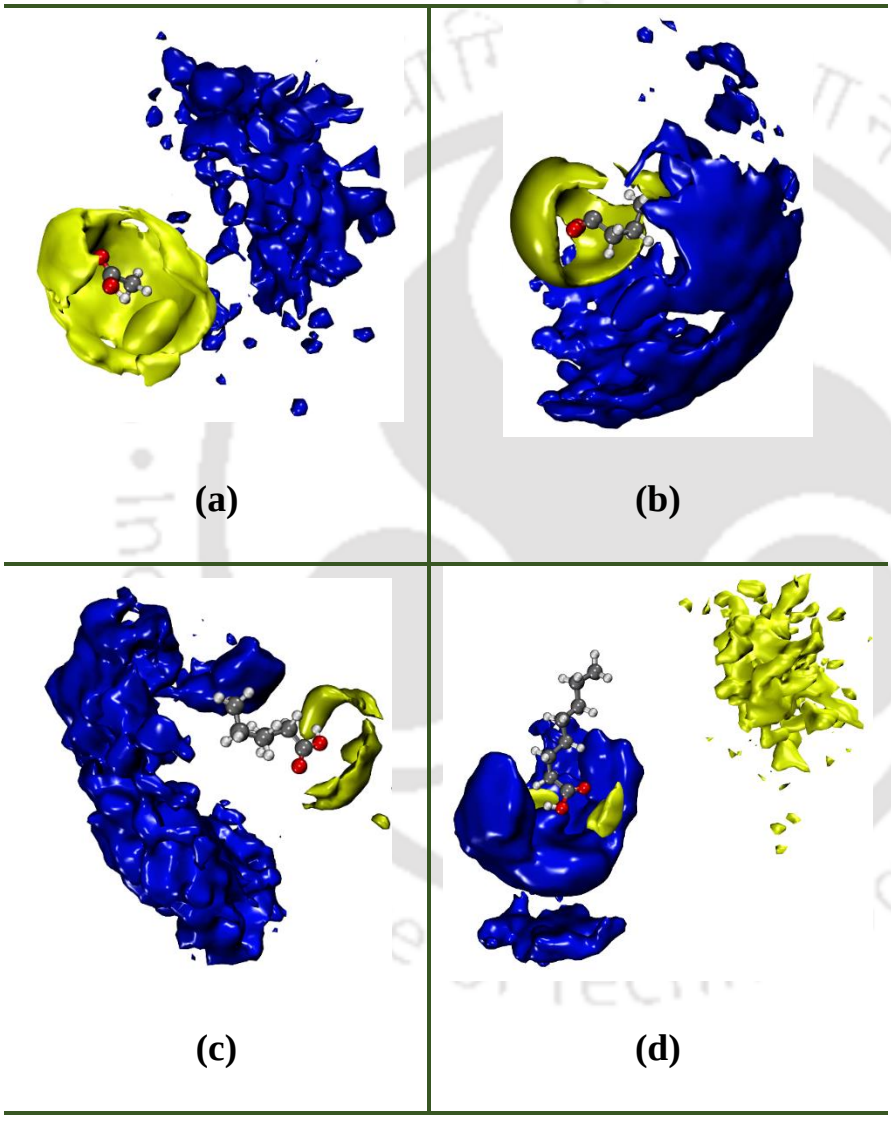

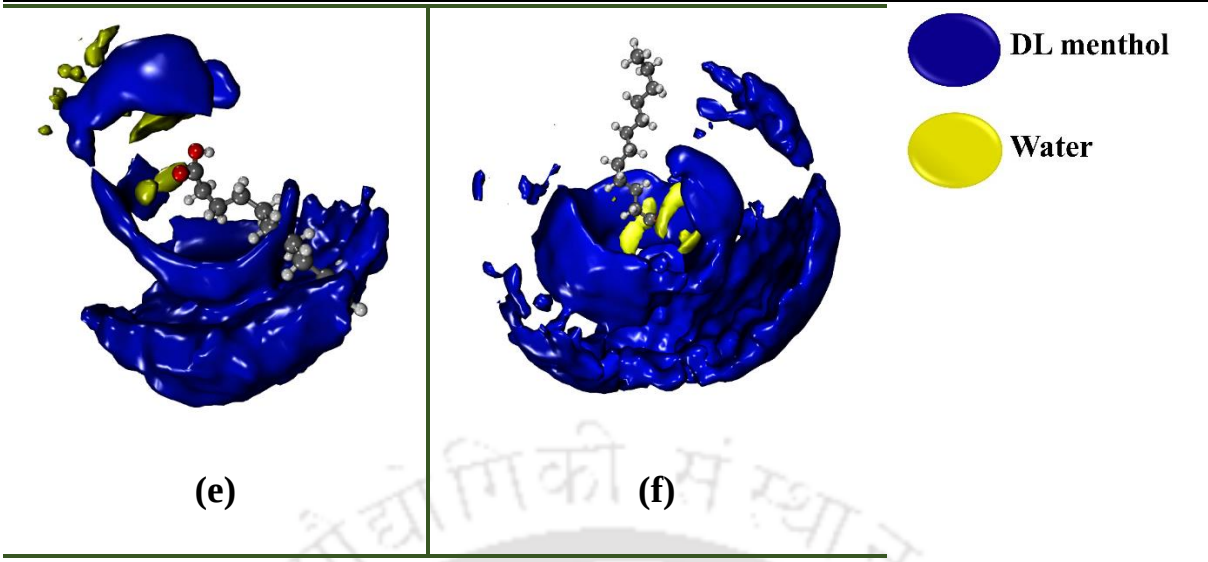

Figure 2.18: Spatial distribution functions (SDFs) of DL-menthol (HBA) and water molecules around respective carboxylic acids (HBDs) of different DESs calculated from the MD simulations of the DL menthol- carboxylic acid (DES)-water system. Menthol (in blue) and water (in yellow) around (a) acetic acid, (b) butanoic acid, (c) hexanoic acid, (d) octanoic acid, (e) decanoic acid, and (f) dodecanoic acid. [menthol around carboxylic acid: iso-value of 2.1 particle nm^{-3}; the water around carboxylic acid: iso-value of 20 particles nm^{-3}].

However, a different scenario can be witnessed in the case of the DESs consisting of the long-chain carboxylic acids such as octanoic, decanoic and dodecanoic acid, where the probability spots of DL-menthol species are located in the region of space near the carboxyl group of the HBDs suggesting a prominent HBA-HBD interaction. Although the presence of some water entity near the carboxyl group of the HBDs in the 3-D space has been observed in Figures 2.18d-f, the lower magnitude of the same indicated that very few spaces were available for the water molecules to interact with the O−H and the C=O groups of DES supported by the hydrophobic nature of the components. The SDF iso-surfaces of these three DESs suggest that these DESs with a higher carbon chain length (HBDs) can successfully resist the penetration of water molecules owing to a strong network of HBA-HBD non-bonded interactions signifying the validation of the non-covalent interaction study.

2.3.1.3.5 Hydrogen Bond Properties

Figure 2.19 represents the average number of HBD-water hydrogen bonds per HBD molecule and Figure 2.19b represents the average number of HBA-HBD hydrogen bonds per

DES molecule, both as a function of simulation time. The geometric criteria for hydrogen bonding were considered based on the literature.[70] The criteria were defined by a cut-off value for distance and angles between the atoms that were involved in hydrogen bonding. It can be observed that the hydrogen bond donors (carboxylic acids) form O-H---O hydrogen bonds with water at an average distance of ~3.1 Å (Figure 2.17a). Additionally, the HBD molecules formed O...H-O bonds with DL-menthol at an average distance of ~3 Å (Figure 2.17b). Because of this, 3.5 Å was considered as the cut-off distance, while the cut-off angle was considered from 120° to 180° for all the systems. The menthol-water hydrogen bonding for the systems S1, S2, S4 and S5 were shown in Figure 2.19c. The degree of hydrogen bonding between menthol and water was almost the same for all the systems and the value was quite less indicating minimum interaction between them. In Figure B.8 (see Appendix B), averaged value of the average number of hydrogen bonds was obtained between HBD- water, HBA-HBD and HBA- water, for the DL-menthol-based systems (S1 to S8), as a function of simulation time.

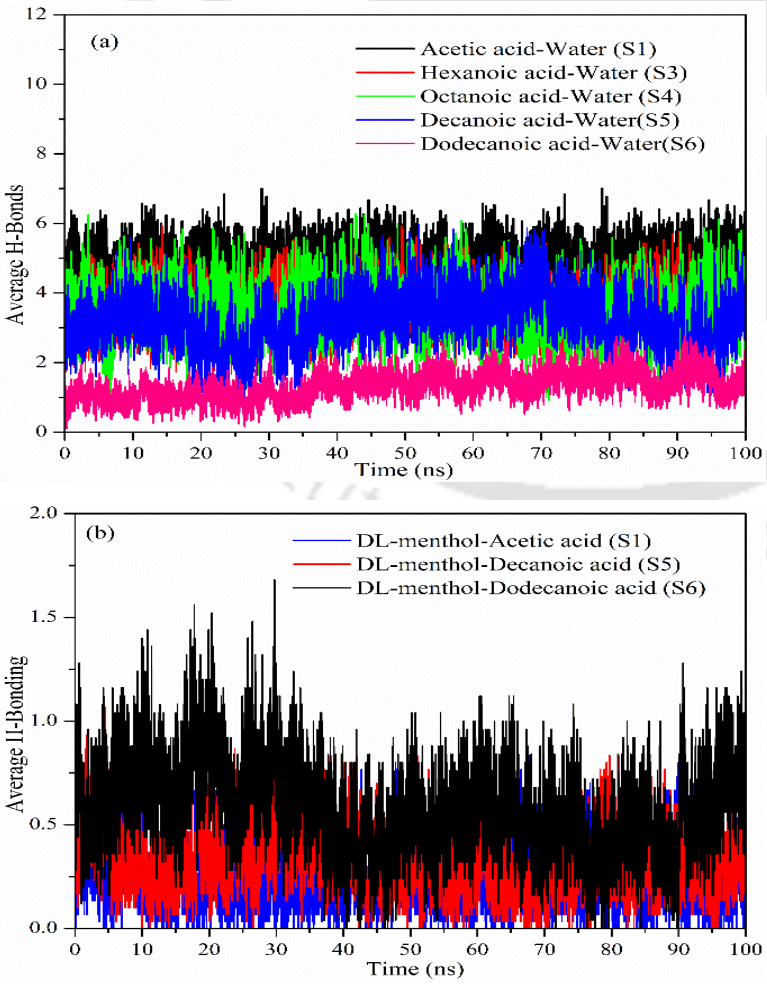

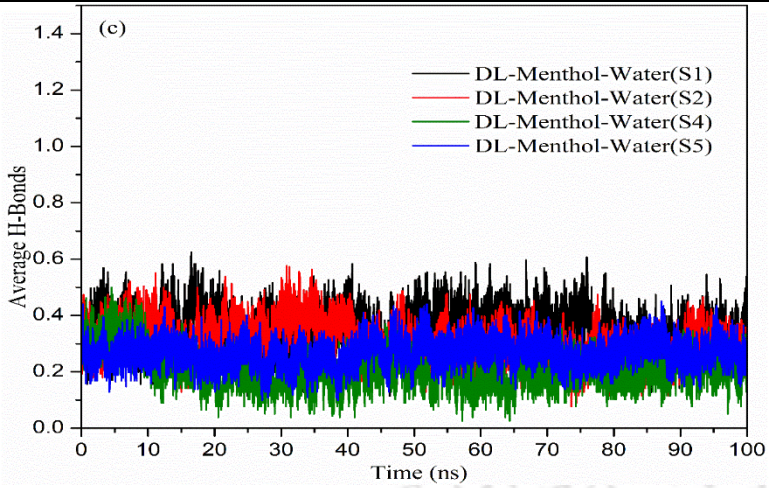

Figure 2.19: Average number of hydrogen bonds between (a) HBD- water per HBD molecule, for systems S1, S3, S4, S5, and S6; (b) HBA-HBD per DES molecule, for systems S1, S5 and S6; and (c) HBA- water per HBA molecule, for system S1, S2, S4, S5; as a function of simulation time.

In Figure 2.19a, it can be observed that the average number of hydrogen bonds between HBD and water decreased from the acetic acid system to the dodecanoic acid system in the case of DL-menthol-based DESs. It can be deduced that dodecanoic acid-based DES is more stable than that acetic acid-based DES in an aqueous medium. The degree of hydrogen bonding between HBD-water can be presented as acetic acid > levulinic acid > butanoic acid > pyruvic acid > hexanoic acid > octanoic acid > decanoic acid > dodecanoic acid. Exactly opposite order of the hydrogen bonding can be witnessed between HBA-HBD in Figure B.8b (Appendix B)**.** Lesser number of hydrogen bonding was witnessed between menthol and water for all the systems (Figure B.8c) (Appendix B)**.**

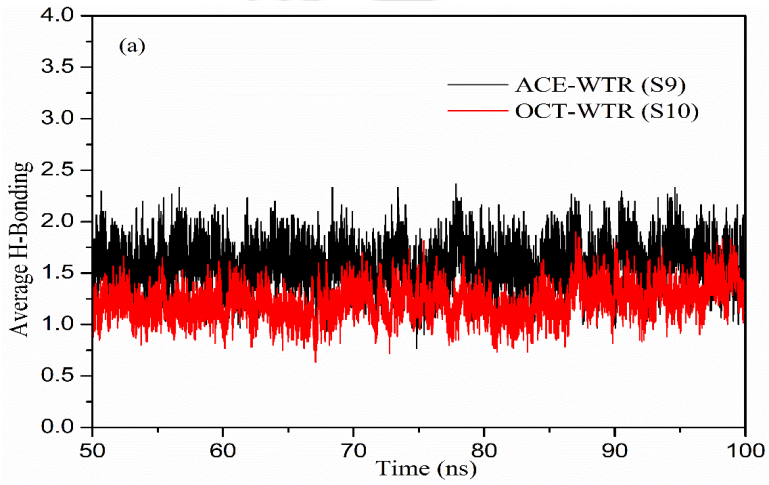

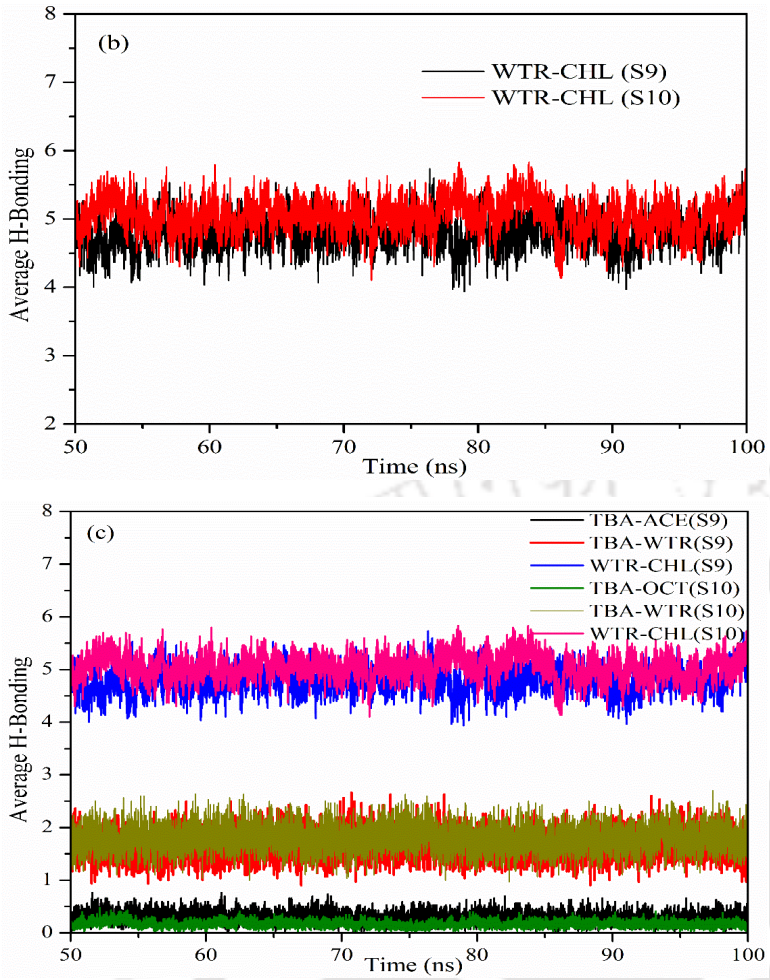

Figure 2.20: Average number of hydrogen bonds between (a) HBD- water per HBD molecule, for systems S9 and S10; (b) chloride anion- water per chloride ion, for systems S9 and S10; (c) various combinations among tetrabutylammonium cation, water, acetic acid, octanoic acid and chloride ion for system S9 and S10; as a function of simulation time.

The hydrogen bonding between the different species for the $N_{4444}Cl$-based systems was obtained as shown in Figure 2.20 and Figure B.9 (Appendix B). It can be noticed that acetic acid formed a higher number of hydrogen bonds with water as compared to octanoic acid (Figure 2.20a). Also, a very high degree of hydrogen bonding was observed between water molecules and chloride ions (Figure 2.20b) leading to the fact that DES- integrity was compromised as breakage of hydrogen bonding was witnessed between the ammonium cation and chloride anion. Here, hydration by chlorine atoms through water molecules was automatically addressed in the calculation of the average H-bonding ion. The overall nature of hydrogen bonding between the various components in the system S9 and S10 are plotted in Figure 2.20c. From this plot, one can observe the following order of hydrogen bonding in both

the systems S9 and S10, such as chloride ion-water molecule > tetrabutylammonium cation-water molecule > tetrabutylammonium cation- HBD molecule. The change in integral values of the ^{1}H-NMR spectra obtained by Florindo et al.[26] suggested that a large quantity of TBA cation was lost to the water phase. In contrast, octanoic acid remained intact even after mixing with water. The hydrogen bonding analysis of those systems shown in Figure B.9c (Appendix B) indicated the same finding. Overall, they were found to be in excellent support with that of the experiment.[26]

2.3.1.3.6 Mean Square Displacement

Estimation of the self-diffusion coefficient (D) is carried out by using the Einstein equation (Eq- 2.5)[71,72] which involves the mean square displacement (MSD) of the molecule. It is a useful parameter to measure the overall mobility of various species in a system. It can be expressed by eq 2 as follows:

$$\mathrm{D} = \frac{1}{6}\lim_{t\to\infty}\frac{d}{dt}\langle\sum_{i=1}^{N}|r_i(t) - r_i(0)|^2\rangle \qquad (2.5)$$

Here, $r_i(0)$ and $r_i(t)$ are the positions of the i^{th} atom at time 0 and *t*, respectively. The bracketed part in Equation 2.5 is considered the MSD of the molecular species. From the slope of the MSD curve obtained by the simulation, we can calculate the self-diffusion coefficient for each species. From Figure 2.21, the linear trend of the MSD plots can be observed. From Figures 2.21a and 2.21b, one can note that the acetic acid and water curves have come close to one another both indicating higher mobility within the system. The menthol curve is also shifted at 90-100 ns (Figure 2.21b) as compared to 0-10 ns (Figure 2.21a). One possible explanation for this can be a disruption of DES structure as acetic acid might leach through the DES phase. Due to this, we have observed the movement of the menthol molecule along with it. Figure 2.21c and Figure 2.21d depict less movement for both menthol and octanoic acid molecule. As both the components are hydrophobic, accordingly less mobility is observed. This certainly leads to the fact that both DES components are quite stable within the system. The self-diffusivity coefficient data for different systems are provided in Table B.6 (Appendix B).

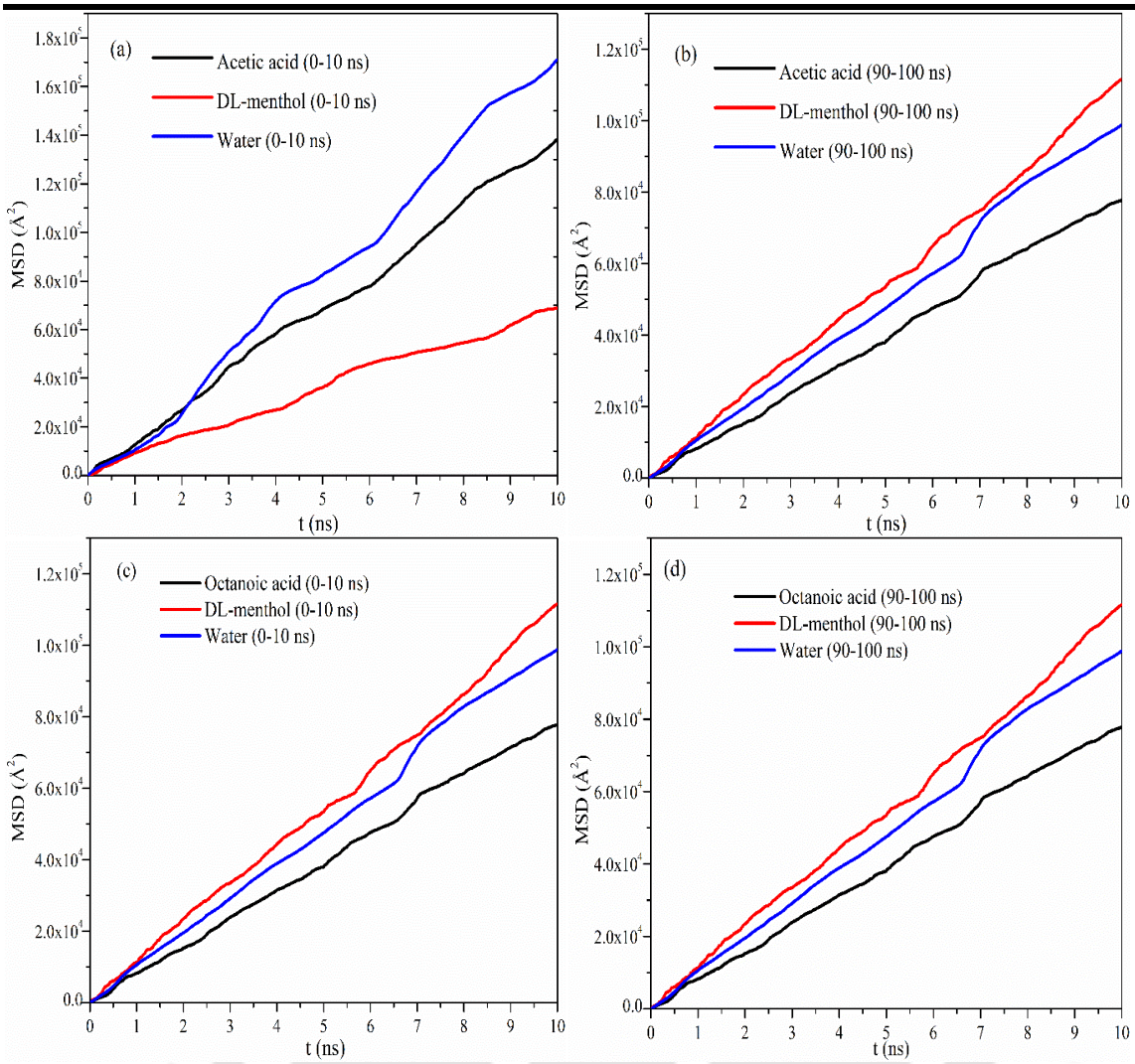

Figure 2.21: MSD plot at (a) 0-10 ns and (b) 90-100 ns, respectively for system S1 and at (c) 0-10 ns and (d) 90-100 ns, respectively for system S4.

From the self-diffusivity values of the species the following conclusions can be drawn:

(i) with an increase in simulation time, the diffusion coefficient values of both acetic acid and water are lowered. The increased movement and transport tendency of acetic acid and water molecules is suggested as both of the molecules follow a similar trend in diffusivity (System S1). Similar trends are observed between butanoic acid-water and pyruvic acid-water for the systems S2 and S7, respectively (Table B.6) (see Appendix B). Similar diffusivity values trigger the higher movement of molecules with a possibility to move through the phases.

(ii) Octanoic acid and DL-menthol have a significant difference in their self-diffusion coefficient with water both at the start as well as at the end of the production run. Furthermore, the diffusivity values for both molecules do not

change much throughout the simulation (system S4). Similar results are observed for DL-menthol- dodecanoic acid system (system S6) with similar self-diffusion coefficient values between these two species. Overall, it suggests that these DESs are quite stable in the DES phase and do not tend to move freely through the phases.

(iii) The diffusion coefficient values of acetic acid, chloride ion and water are very close to one another and in addition to that, the diffusivity value of TBA cation (System S9) decreases in the last 90-100 ns run (Table B.6) (Appendix B). This suggests a high diffusive property of all the molecular species. In the case of system S10, though octanoic acid is present in the system, similar results are observed as compared to system S9. Additionally, the diffusion coefficients of octanoic acid and DL-menthol are very close to unity implying a very stable assembly of the species.

From all the above findings, the following outcomes can be suggested : (i) DL-menthol-based DESs with acetic acid, butanoic acid, hexanoic acid, and pyruvic acid are not stable in an aqueous environment as they possess similar diffusivity to water and also high mobility within the system. Also, the transfer of acetic acid and butanoic acid to the water phase starts at the beginning of the simulation and happens at a similar rate throughout the simulation; (ii) DL-menthol-based DES with octanoic acid and higher organic acids have shown higher stability in water and can be utilised as hydrophobic solvents; (iii) Tetrabutylammonium chloride-based DESs are very hydrophilic as observed from the self-diffusivity values and the transport of the ions to the water phase was seen from 0 to 40 ns of the simulation run.

2.3.2 Nitenpyram Extraction

The extraction efficiency and selectivity of the pesticide nitenpyram were compared and validated with Florindo et al.[26] with DL-menthol-octanoic acid DES in a molar ratio 1:1. The simulation protocol is the same as mentioned earlier; albeit with a different simulation box configuration due to the addition of a new drug species (nitenpyram). Table 2.7 described the number of molecules considered for the simulation. Figure A.10S8 displayed the structures with atomic notations of the molecules present in the system and Figure 2.22 demonstrated the snapshots of the system at two different time steps 0 ns and 100 ns. After the successful completion of the simulation, the nonbonded interaction energy, radial and combined distribution function, spatial distribution function, hydrogen bonding properties, extraction

efficiency and selectivity of the pesticide, were obtained and compared with the experimental results. All the simulations were carried out in triplicate for minimizing the error. For the calculation of the distribution coefficient (β) and selectivity (S), the following equations were used:

$$\beta = \frac{x^{E}\text{nitenpyram}}{x^{R}\text{nitenpyram}} \tag{2.6}$$

$$S = \beta\text{nitenpyram} / \beta\text{water} = \frac{\frac{x^{E}\text{nitenpyram}}{x^{R}\text{nitenpyram}}}{\frac{x^{E}\text{water}}{x^{R}\text{water}}} \tag{2.7}$$

Here, x^{E}nitenpyram and x^{R}nitenpyram denoted the mole fractions of nitenpyram in DES-rich and water-rich phases, respectively. x^{E}water and x^{R}water denoted the mole fractions of water in DES-rich and water-rich phases, respectively.

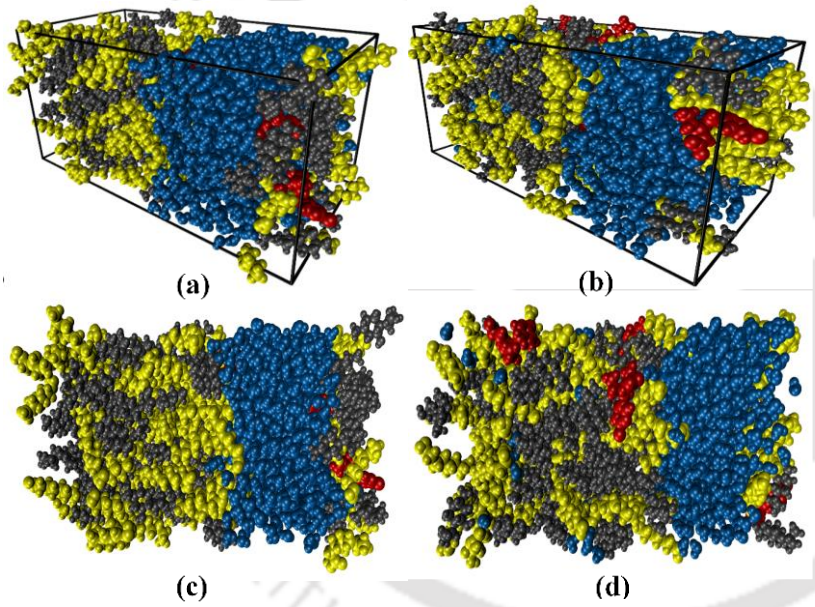

Figure 2.22: Distribution snapshots of nitenpyram in the solvent at different times: (a) and (b) 0 ns; (c) and (d) 100 ns, respectively (grey: menthol molecules; yellow: octanoic acid molecules; blue: water molecules; red: nitenpyram molecules).

A higher β value normally indicates a higher distribution of nitenpyram from the water phase to the DES phase. The higher the selectivity (S), the greater the ability of DES in extracting nitenpyram from water. From Table 2.8, it can be concluded that the DES can be used for the extraction of nitenpyram from the water phase and MD simulation confirmed the experimental nitenpyram extraction as shown in the table. To evaluate the extraction efficiency

of nitenpyram from water, the concentrations of nitenpyram in the aqueous phase before (C_o) and after extraction (C) can be used in Equation 2.8 as follows:

$$\%\text{EE} = [(C_0 - C)/C_0] \times 10 \qquad (2.8)$$

The extraction efficiency (%EE) calculated based on simulated results ranged between 42 to 46.7%, whereas the experimental efficiency is 39.6%.[26] The slight variation in the simulated result occurred due to the presence of the molecules in the interfacial region leading to numerical inaccuracy in calculating the exact number of molecules present in that region. The simulated distribution ratio was also calculated, which is defined as the ratio of the concentration of the pesticide in the DES phase to the concentration in the water phase. Experimental distribution ratio[26] (0.67) was found to be very close to that of the simulated distribution ratio (0.72) as shown in Table 2.8.

Table 2.7: Composition of the system considering the 1:1 mass ratio of DES and the aqueous solution of nitenpyram and the number of molecules considered for MD simulation

Name of pesticide	DES				Number of molecules		
	HBA	HBD	HBA	HBD	Nitenpyram	Water	Total
Nitenpyram	DL-menthol	Octanoic acid	100	100	5	835	1040

Table 2.8: MD simulated results in the calculation for distribution coefficient and selectivity at 1 atm pressure and 298.15 K temperature

System	DES-rich phase			Water-rich phase			Distribution Coefficient (*β*)	Selectivity (S)	Distribution ratio	
	X_{DES}	X_{nit}	X_{water}	X_{DES}	X_{nit}	X_{water}			Experimental [a]	Simulated
DES+ Nitenpyram + water	0.888	0.019	0.093	0.006	0.004	0.990	5.19	55.25	0.67	0.72

[a] The experimental value taken from Florindo et al.[26] X_{DES}, X_{nit} and X_{water} are the mole fraction of DES, nitenpyram and water respective

2.3.2.1 Non-bonded Interaction Energy

To study the interactions between the different molecules, we have quantified the total nonbonded interaction energies in terms of electrostatic and van der Waals interactions as shown in Table 2.9. From the data, it can be noticed that the nonbonded interactions between nitenpyram-menthol and nitenpyram-octanoic acid were more favourable than that of nitenpyram-water and menthol-water. A further investigation revealed that the van der Waals (vdW) interactions were higher than electrostatic interactions between nitenpyram and DES components (menthol and octanoic acid). However, in the case of nitenpyram-water and menthol-water, the electrostatic interactions were more dominant than the van der Waals (vdW) interactions. The total nonbonded interaction energy between DES and nitenpyram was −1.49 kcal/mol, where the electrostatic contribution was an order to magnitude lesser. This was contrary to that observed for nitenpyram and water. The total nonbonded interaction energy (−12.78 kcal/mol) between the DES components was much higher than that of the other component pairs which indicated higher stability of the DES in the water system. Further evaluation of the interactions of DES, nitenpyram and water suggested that nitenpyram-octanoic acid interaction (−0.81 kcal/mol) was the most favourable, followed by nitenpyram-menthol (−0.68 kcal/mol). Interaction between nitenpyram and water was the least favourable (−0.11 kcal/mol).

Table 2.9: MD simulated interaction energies (kcal/mol) between the different component pairs of menthol-octanoic acid-nitenpyram in 298.15 K and 1 atm pressure

Component Pairs	Electrostatic interactions (E_{elec})	Vander Waals interactions (E_{vdW})	Total nonbonded interactions (E_{total})
Nitenpyram- water	−0.07	−0.03	−0.11
Nitenpyram- octanoic acid	−0.27	−0.54	−0.81
Nitenpyram-DL-menthol	−0.08	−0.60	−0.68
DL-menthol- octanoic acid	−4.35	−8.42	−12.77

DES- nitenpyram	−0.35	−1.13	−1.49

$E_{total} = E_{elec} + E_{vdW}$

2.3.2.2 Radial and Combined Distribution Functions

RDFs were shown in Figure 2.23, where the selected atoms for different molecular species were the O1 atom of nitenpyram, H51 and O5 atom of octanoic acid, H35 atom of DL-menthol and H57 atom of the water molecule (notations as in Figure B.10 in Appendix B). It appeared that the well-defined first solvation shell for the DL-menthol and nitenpyram molecules was at 2 Å suggesting higher interaction between these two species (Figure 2.23a). The presence of water molecules at the first solvation shell (1.95 Å) was also observed suggesting an interaction between nitenpyram and water, however, a coordination number (1.50) being lower than DL-menthol (1.90) indicated a weaker interaction among them. For octanoic acid, it was at 3.35 Å (Figure 2.23a) justifying relatively weaker interaction as compared to nitenpyram- DL-menthol. A sharp peak was observed for DL-menthol and an octanoic acid moiety at 2.05 Å (Figure 2.23b) reflecting a very strong HBA-HBD interaction leading to the fact that the DES did not disintegrate in the presence of an aqueous environment. The coordination number presented in Table B.5 (see Appendix B) indicated similar coordination of menthol, octanoic acid and water molecules around the nitenpyram moiety. Moreover, a higher coordination number of HBA-HBD (5.50) compared to a very low value of HBD-water (0.75) strongly supported the higher stability of the DES in an aqueous medium.

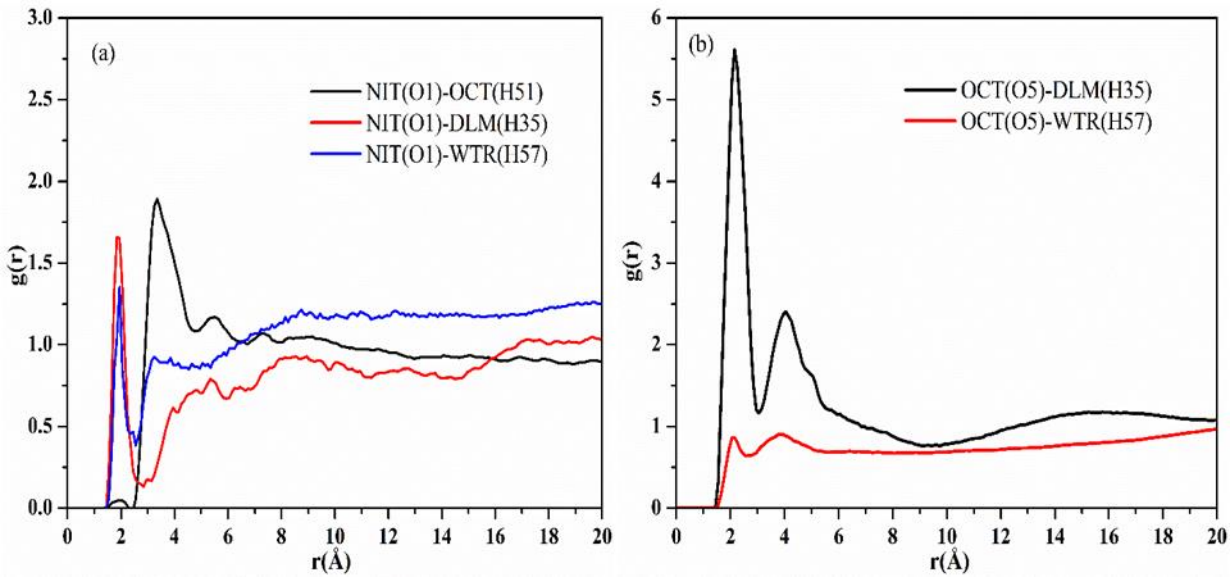

Figure 2.23: Comparison among atom-specific radial distribution function plots between the different molecular pairs present in the system (a) Nitenpyram-octanoic acid, nitenpyram-DL-

menthol and nitenpyram-water and (b) DL-menthol-octanoic acid and octanoic acid- water at 100 ns.

In addition to the RDFs, CDFs were presented in Figure 2.24 to incorporate the angular structural analysis. CDF confirmed the formation of hydrogen bonding between donor and acceptor atoms. Figure 2.24a and Figure 2.24b represent the CDF plots for nitenpyram- DL-menthol and nitenpyram- water, respectively to identify possible hydrogen bonding between the species. The –NOO site of the nitenpyram molecule acquired a negative charge density due to the presence of a highly electronegative element and can be considered an active site for other species containing a positive charge. Hence, we observed that of N-O...H bond was formed for both nitenpyram- DL-menthol and nitenpyram- water at a distance of~2 Å (Figure 2.24). These bonds were formed with an angle ranging from 140° to 180°. Both interactions justify the criteria for the formation of hydrogen bonding. Comparing the colour code values for both interactions, it can be observed that nitenpyram- menthol hydrogen bonding was higher than nitenpyram- water. Figure 2.24 confirmed the positions of the RDF peaks obtained in Figure 2.23. The presence of hydrogen bonding can further be analyzed by calculating the average hydrogen bond between the molecular species.

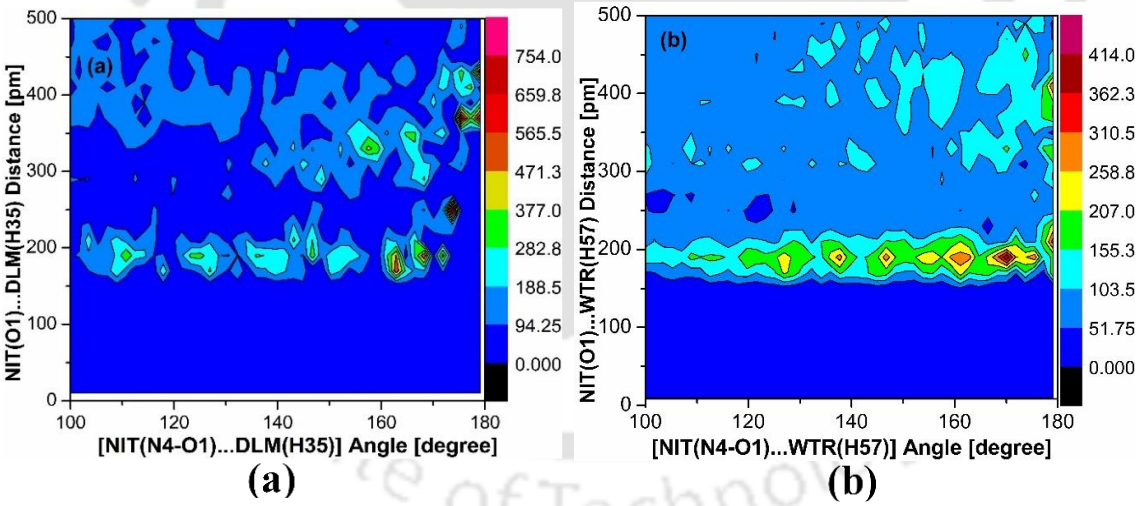

Figure 2.24: CDFs obtained by plotting the hydrogen bond distance (RDF) vs the hydrogen bond angle (ADF) for (a) N4-O1(nitenpyram)…H35 (DL-menthol) angle against O1…H35 distance, (b) N4-O1(nitenpyram)…H57(water) angle against O1…H57 distance.

2.3.2.3 Spatial Distribution Functions

SDFs were generated to indicate the average density distribution of different molecules around a reference nitenpyram molecule in Figure 2.25. The iso values employed for the SDFs corresponding to DES−nitenpyram were 1.5 Å, while that for nitenpyram−water was 0.05 Å.

It can be observed that the nitenpyram molecule was closely surrounded by water (blue colour) and menthol molecules (green colour) at ~2 Å (Figure 2.25a). It justified the findings from the RDFs and CDFs as mentioned before (Figure 2.23 and Figure 2.24). The smaller size of the water molecule and reasonably good interaction with nitenpyram made it feasible for higher distribution. Higher distribution of water was observed primarily around the N-O-O region of nitenpyram, which can be considered probable active sites. Figure 2.25c certainly confirmed the higher density distribution of water molecules around nitenpyram. All the components displayed relatively comparable density distribution around nitenpyram. Octanoic acid molecules (yellow colour) were distributed around nitenpyram at a distance of ~3.3 Å. The appearance of the density distribution of menthol closer to the active site revealed its slightly higher interaction with nitenpyram as compared to the octanoic acid molecule (Figure 2.25b) despite the higher interaction energy of the latter. One important aspect to be noticed here was the non-presence of water around the DES moieties implying the DES integrity and overall hydrophobic nature of this DES.

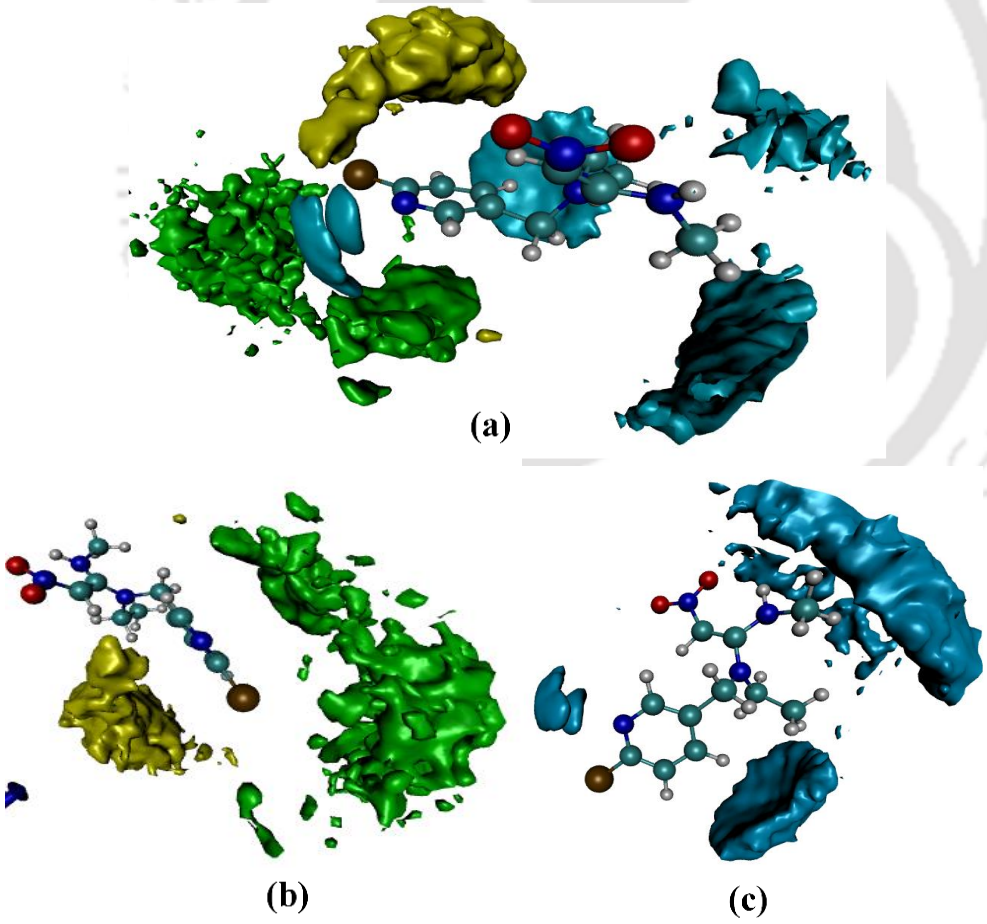

Figure 2.25: SDFs obtained for the system (a) DLM, OCT, and water around NIT; (b) DES around NIT; (c) water around NIT molecule. Green, yellow and blue surfaces refer to DL-menthol, octanoic acid and water, respectively.

2.3.2.4 Hydrogen Bond Properties

The average number of hydrogen bonds between nitenpyram and other molecular species present in the system as a function of simulation time was shown in Figure B.11 (Appendix B). The cutoff donor-acceptor distance was taken as 3.5 Å and the cutoff angle as 135° to 180° considering the results obtained in the RDF and the CDF as shown in Figure 2.23 and Figure 2.24, respectively. Earlier in the CDF calculation section, we performed a qualitative analysis because of the probable formation of H-bonding between molecules. Here, we obtained the quantitative analysis of the hydrogen bonding of nitenpyram with DES molecules and water molecules. As revealed in Figure 2.26, the number of average hydrogen bonding between the two species was found to be in the order of nitenpyram-octanoic acid (0.18) > nitenpyram-DL menthol (0.14) > nitenpyram-water (0.12). The presence of the carboxyl group (-COOH) in octanoic acid also aided in the formation of a hydrogen bond with the active site (-NOO) of nitenpyram. Meanwhile, it is to be mentioned that, as expected, we do not observe any significant hydrogen bonding interaction between DES and water.

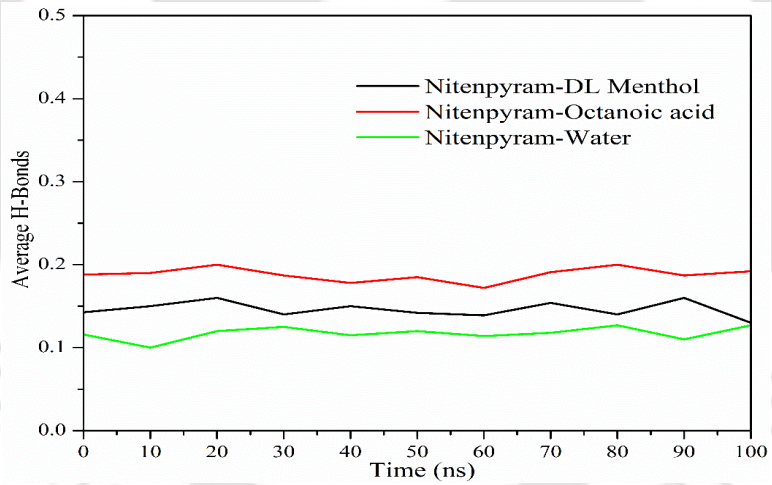

Figure 2.26: Averaged out plot of the average number of NIT-DLM, NIT-OCT and NIT-water hydrogen bonds as a function of simulation time.

2.3.2.5 Mean Square Displacement

A detailed description of MSD and the self-diffusivity coefficient was mentioned in the earlier section. Figure 2.27 represents the MSD plots for the DES-nitenpyram-water system at 0-10 ns and 90-100 ns, respectively. Linearity can be observed in all the plots. Initially, at the start of the simulation, the diffusivity of all the species is similar (Figure 2.27a), it diverges only at the end i.e 90 to 100 ns, whereas for water it took a gradual shift (Figure 2.27b). The similar curves other than water indicate suitable transport properties among the molecules. From this,

it can be assumed that the drug diffusivity is relatively higher in the DES. However, the water curve in both figures also suggests that water molecules maintained their mobility throughout the simulation period implying favourable transport properties with nitenpyram. Table B.7 (Appendix B) presents the diffusion coefficient of the species among each other in the system. From the data, it can be observed that the diffusion coefficients of DL- menthol and nitenpyram are close enough and both indicate a similar trend. Overall the following can be inferred: (i) the change in the diffusion coefficient of water is associated primarily with nitenpyram and (ii) from the diffusion coefficient data and the MSD plots it can be confirmed that the nitenpyram molecules have sufficient mobility towards the DES phase. Both these counter-effective phenomena are responsible for the moderate extraction of nitenpyram from an aqueous environment.

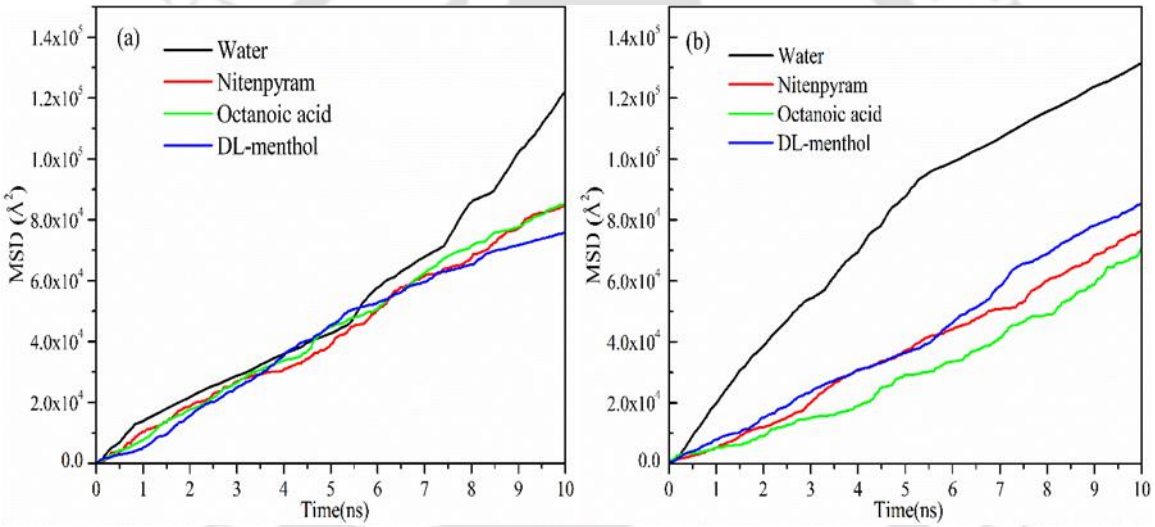

Figure 2.27: MSD plot at (a) 0-10 ns and (b) 90-100 ns, respectively for DL-menthol- octanoic acid- nitenpyram- water system.

2.4 Conclusion

In the present study, DFT calculations and MD simulation have been implemented to investigate the mechanism of formation, stability and compactness in an aqueous medium, structural integrity, the CT analysis and the non-covalent and intermolecular interactions among the components of DL menthol-carboxylic fatty acid based DESs at the molecular level. The following are the significant conclusions:

(i) Short to medium-range interactions ranging from 1.730 to 2.07 Å are observed between the −OH (DL-menthol) and −COOH (organic acid) group indicating the occurrence

of a network of non-bonded interactions such as hydrogen bonds and van der Waals or dispersion interactions between the HBA and the HBD to achieve stable DES formation. The interaction energy of the DESs follows the order as such: DL menthol- acetic acid (DES1) > DL menthol- butanoic acid (DES2) > DL menthol- hexanoic acid (DES3) > DL menthol- octanoic acid (DES4) > DL menthol- nonanoic acid (DES5) > DL menthol- decanoic acid (DES6) > DL menthol- dodecanoic acid (DES7).

(ii) The DFT-based solvation study suggests that DES1, DES2 and DES3 are not stable in water media as higher ΔG_{solv} values have been obtained, whereas the hydrophobicity of the long-chain fatty acids results in lower ΔG_{solv} values for DES4 to DES7 and a stable DES formation. SDF study combined with the angular distribution analysis revealed similar findings.

(iii) A higher HOMO-LUMO energy gap observed in DES7 (173.80 kcal/mol) indicates greater chemical stability and lesser reactivity as compared to DES1 (171.26 kcal/mol). The NBO and CHELPG-based CT analysis of DES7 demonstrates higher resistance to charge transfer as compared to that of DES1.

(iv) From the MD simulation study, the "relative stability factor" was introduced to successfully measure the relative stability of a DES in an aqueous medium based on the nonbonded interaction energies among the components of the deep eutectic solvents. The order of stability of DES in water based on a "relative stability factor" was found as DL-menthol: acetic acid (1:1) < DL-menthol: levulinic acid (1:1) < DL-menthol: butanoic acid (1:1) < DL-menthol: pyruvic acid (1:2) < DL-menthol: hexanoic acid (1:1) < DL-menthol: octanoic acid (1:1) < DL-menthol: decanoic acid (1:1) < DL-menthol: dodecanoic acid (2:1). The structural properties such as radial, combined and spatial distribution function (RDF, CDF and SDF) evidenced strong hydrogen bond acceptor (HBA)− hydrogen bond donor (HBD) interactions in long-chain organic acid based DESs (C8 to C12), whereas short-chain fatty acid based DESs (C1 to C6) are not stable in water media.

(v) The QTAIM analysis of the pure DESs revealed the presence of a significant closed-shell interactive network. Non-covalent interactions were revealed by multiple green and blue spikes within the range of 0 to −0.05 a.u. indicating hydrogen bonding and dispersion interactions for a stable DES formation. the DL-menthol: carboxylic acid DESs contain hydrogen bonding as well as vdW dispersion interactions for their formation. Upon mixing with water the short-chain fatty acid-based DESs get involved in enhanced non-covalent interaction (mainly H-bonding, and dispersion effects) with water molecules resulting in the disruption of the DES structures. Solvated state QTAIM analysis revealed the disappearance

of intermolecular interactions for short-chain acid-based DESs. However, long-chain fatty acid-based DESs withstand their structural integrity with a larger extent of dispersion as well as H-bonding interactions among the HBA and the HBD in the presence of external water molecules maintaining coherence with the experimental as well as MD simulation analysis. The study highlights the formation and stability mechanism of the DL-menthol: carboxylic acid-based DESs via the network of an intermolecular interactive framework.

References

(1) Hallett, J. P.; Welton, T. Room-Temperature Ionic Liquids: Solvents for Synthesis and Catalysis. 2. *Chem. Rev.* **2011**, *111* (5), 3508–3576. https://doi.org/10.1021/cr1003248.

(2) Welton, T. Ionic Liquids in Catalysis. *Coord. Chem. Rev.* **2004**, *248* (21), 2459–2477. https://doi.org/https://doi.org/10.1016/j.ccr.2004.04.015.

(3) Cassity, C. G.; Mirjafari, A.; Mobarrez, N.; Strickland, K. J.; O'Brien, R. A.; Davis, J. H. Ionic Liquids of Superior Thermal Stability. *Chem. Commun.* **2013**, *49* (69), 7590–7592. https://doi.org/10.1039/C3CC44118K.

(4) Villanueva, M.; Coronas, A.; García, J.; Salgado, J. Thermal Stability of Ionic Liquids for Their Application as New Absorbents. *Ind. Eng. Chem. Res.* **2013**, *52* (45), 15718–15727. https://doi.org/10.1021/ie401656e.

(5) Wu, B.; Liu, W.; Zhang, Y.; Wang, H. Do We Understand the Recyclability of Ionic Liquids? *Chem. – A Eur. J.* **2009**, *15* (8), 1804–1810. https://doi.org/https://doi.org/10.1002/chem.200801509.

(6) Aschenbrenner, O.; Supasitmongkol, S.; Taylor, M.; Styring, P. Measurement of Vapour Pressures of Ionic Liquids and Other Low Vapour Pressure Solvents. *Green Chem.* **2009**, *11* (8), 1217–1221. https://doi.org/10.1039/B904407H.

(7) Santos, A. G.; Ribeiro, B. D.; Alviano, D. S.; Coelho, M. A. Z. Toxicity of Ionic Liquids toward Microorganisms Interesting to the Food Industry. *RSC Adv.* **2014**, *4* (70), 37157–37163. https://doi.org/10.1039/C4RA05295A.

(8) Papu Kumar Naik, Nikhil Kumar, Nabendu Paul, T. B. *Deep Eutectic Solvents in Liquid–Liquid Extraction Correlation and Molecular Dynamics Simulation*; Taylor & Francis, 2022. https://doi.org/10.1201/9781003231158.

(9) Abbott, A. P.; Boothby, D.; Capper, G.; Davies, D. L.; Rasheed, R. K. Deep Eutectic

Solvents Formed between Choline Chloride and Carboxylic Acids: Versatile Alternatives to Ionic Liquids. *J. Am. Chem. Soc.* **2004**, *126* (29), 9142–9147. https://doi.org/10.1021/ja048266j.

(10) Abbott, A. P.; Capper, G.; Davies, D. L.; Rasheed, R. K.; Tambyrajah, V. Novel Solvent Properties of Choline Chloride/Urea Mixtures. *Chem. Commun.* **2003**, No. 1, 70–71. https://doi.org/10.1039/B210714G.

(11) Jenkin, G. R. T.; Al-Bassam, A. Z. M.; Harris, R. C.; Abbott, A. P.; Smith, D. J.; Holwell, D. A.; Chapman, R. J.; Stanley, C. J. The Application of Deep Eutectic Solvent Ionic Liquids for Environmentally-Friendly Dissolution and Recovery of Precious Metals. *Miner. Eng.* **2016**, *87*, 18–24. https://doi.org/https://doi.org/10.1016/j.mineng.2015.09.026.

(12) Abbott, A. P.; Alhaji, A. I.; Ryder, K. S.; Horne, M.; Rodopoulos, T. Electrodeposition of Copper–Tin Alloys Using Deep Eutectic Solvents. *Trans. IMF* **2016**, *94* (2), 104–113. https://doi.org/10.1080/00202967.2016.1148442.

(13) Tran, M. K.; Rodrigues, M.-T. F.; Kato, K.; Babu, G.; Ajayan, P. M. Deep Eutectic Solvents for Cathode Recycling of Li-Ion Batteries. *Nat. Energy* **2019**, *4* (4), 339–345. https://doi.org/10.1038/s41560-019-0368-4.

(14) Whitehead, A. H.; Pölzler, M.; Gollas, B. Zinc Electrodeposition from a Deep Eutectic System Containing Choline Chloride and Ethylene Glycol. *J. Electrochem. Soc.* **2010**, *157* (6), D328. https://doi.org/10.1149/1.3364930.

(15) Ruggeri, S.; Poletti, F.; Zanardi, C.; Pigani, L.; Zanfrognini, B.; Corsi, E.; Dossi, N.; Salomäki, M.; Kivelä, H.; Lukkari, J.; Terzi, F. Chemical and Electrochemical Properties of a Hydrophobic Deep Eutectic Solvent. *Electrochim. Acta* **2019**, *295*, 124–129. https://doi.org/https://doi.org/10.1016/j.electacta.2018.10.086.

(16) Söldner, A.; Zach, J.; König, B. Deep Eutectic Solvents as Extraction Media for Metal Salts and Oxides Exemplarily Shown for Phosphates from Incinerated Sewage Sludge Ash. *Green Chem.* **2019**, *21* (2), 321–328. https://doi.org/10.1039/C8GC02702A.

(17) Smith, E. L.; Abbott, A. P.; Ryder, K. S. Deep Eutectic Solvents (DESs) and Their Applications. *Chem. Rev.* **2014**, *114* (21), 11060–11082. https://doi.org/10.1021/cr300162p.

(18) Li, C.; Li, D.; Zou, S.; Li, Z.; Yin, J.; Wang, A.; Cui, Y.; Yao, Z.; Zhao, Q. Extraction Desulfurization Process of Fuels with Ammonium-Based Deep Eutectic Solvents.

Green Chem. **2013**, *15* (10), 2793–2799. https://doi.org/10.1039/C3GC41067F.

(19) Zhao, H.; Baker, G. A.; Wagle, D. V; Ravula, S.; Zhang, Q. Tuning Task-Specific Ionic Liquids for the Extractive Desulfurization of Liquid Fuel. *ACS Sustain. Chem. Eng.* **2016**, *4* (9), 4771–4780. https://doi.org/10.1021/acssuschemeng.6b00972.

(20) Hizaddin, H. F.; Ramalingam, A.; Hashim, M. A.; Hadj-Kali, M. K. O. Evaluating the Performance of Deep Eutectic Solvents for Use in Extractive Denitrification of Liquid Fuels by the Conductor-like Screening Model for Real Solvents. *J. Chem. Eng. Data* **2014**, *59* (11), 3470–3487. https://doi.org/10.1021/je5004302.

(21) Lima, F.; Dave, M.; Silvestre, A. J. D.; Branco, L. C.; Marrucho, I. M. Concurrent Desulfurization and Denitrogenation of Fuels Using Deep Eutectic Solvents. *ACS Sustain. Chem. Eng.* **2019**, *7* (13), 11341–11349. https://doi.org/10.1021/acssuschemeng.9b00877.

(22) Zhao, H.; Zhang, C.; Crittle, T. D. Choline-Based Deep Eutectic Solvents for Enzymatic Preparation of Biodiesel from Soybean Oil. *J. Mol. Catal. B Enzym.* **2013**, *85–86*, 243–247. https://doi.org/https://doi.org/10.1016/j.molcatb.2012.09.003.

(23) Gutiérrez, M. C.; Ferrer, M. L.; Mateo, C. R.; del Monte, F. Freeze-Drying of Aqueous Solutions of Deep Eutectic Solvents: A Suitable Approach to Deep Eutectic Suspensions of Self-Assembled Structures. *Langmuir* **2009**, *25* (10), 5509–5515. https://doi.org/10.1021/la900552b.

(24) van Osch, D. J. G. P.; Zubeir, L. F.; van den Bruinhorst, A.; Rocha, M. A. A.; Kroon, M. C. Hydrophobic Deep Eutectic Solvents as Water-Immiscible Extractants. *Green Chem.* **2015**, *17* (9), 4518–4521. https://doi.org/10.1039/C5GC01451D.

(25) Ribeiro, B. D.; Florindo, C.; Iff, L. C.; Coelho, M. A. Z.; Marrucho, I. M. Menthol-Based Eutectic Mixtures: Hydrophobic Low Viscosity Solvents. *ACS Sustain. Chem. Eng.* **2015**, *3* (10), 2469–2477. https://doi.org/10.1021/acssuschemeng.5b00532.

(26) Florindo, C.; Branco, L. C.; Marrucho, I. M. Development of Hydrophobic Deep Eutectic Solvents for Extraction of Pesticides from Aqueous Environments. *Fluid Phase Equilib.* **2017**, *448*, 135–142. https://doi.org/10.1016/j.fluid.2017.04.002.

(27) Ashworth, C. R.; Matthews, R. P.; Welton, T.; Hunt, P. A. Doubly Ionic Hydrogen Bond Interactions within the Choline Chloride–Urea Deep Eutectic Solvent. *Phys. Chem. Chem. Phys.* **2016**, *18* (27), 18145–18160. https://doi.org/10.1039/C6CP02815B.

(28) Zhekenov, T.; Toksanbayev, N.; Kazakbayeva, Z.; Shah, D.; Mjalli, F. S. Formation of Type III Deep Eutectic Solvents and Effect of Water on Their Intermolecular Interactions. *Fluid Phase Equilib.* **2017**, *441*, 43–48. https://doi.org/https://doi.org/10.1016/j.fluid.2017.01.022.

(29) Zahn, S.; Kirchner, B.; Mollenhauer, D. Charge Spreading in Deep Eutectic Solvents. *ChemPhysChem* **2016**, *17* (21), 3354–3358. https://doi.org/https://doi.org/10.1002/cphc.201600348.

(30) Sun, H.; Li, Y.; Wu, X.; Li, G. Theoretical Study on the Structures and Properties of Mixtures of Urea and Choline Chloride. *J. Mol. Model.* **2013**, *19* (6), 2433–2441. https://doi.org/10.1007/s00894-013-1791-2.

(31) Zhu, Z.; Lü, H.; Zhang, M.; Yang, H. Deep Eutectic Solvents as Non-Traditionally Multifunctional Media for the Desulfurization Process of Fuel Oil. *Phys. Chem. Chem. Phys.* **2021**, *23* (2), 785–805. https://doi.org/10.1039/D0CP05153E.

(32) García, G.; Atilhan, M.; Aparicio, S. An Approach for the Rationalization of Melting Temperature for Deep Eutectic Solvents from DFT. *Chem. Phys. Lett.* **2015**, *634*, 151–155. https://doi.org/https://doi.org/10.1016/j.cplett.2015.06.017.

(33) Paul, N.; Naik, P. K.; Ribeiro, B. D.; Gooh Pattader, P. S.; Marrucho, I. M.; Banerjee, T. Molecular Dynamics Insights and Water Stability of Hydrophobic Deep Eutectic Solvents Aided Extraction of Nitenpyram from an Aqueous Environment. *J. Phys. Chem. B* **2020**, *124* (34), 7405–7420. https://doi.org/10.1021/acs.jpcb.0c03647.

(34) Paul, N.; Banerjee, T. Study on the Extraction of Acetamiprid and Imidacloprid from an Aqueous Environment Using Menthol-Based Hydrophobic Eutectic Solvents: Quantum Chemical and Molecular Dynamics Insights. *ACS Sustain. Chem. Eng.* **2022**, *10* (13), 4227–4246. https://doi.org/10.1021/acssuschemeng.2c00023.

(35) Panda, D. K.; Bhargava, B. L. Intermolecular Interactions in Tetrabutylammonium Chloride Based Deep Eutectic Solvents: Classical Molecular Dynamics Studies. *J. Mol. Liq.* **2021**, *335*, 116139. https://doi.org/https://doi.org/10.1016/j.molliq.2021.116139.

(36) Kivelä, H.; Salomäki, M.; Vainikka, P.; Mäkilä, E.; Poletti, F.; Ruggeri, S.; Terzi, F.; Lukkari, J. Effect of Water on a Hydrophobic Deep Eutectic Solvent. *J. Phys. Chem. B* **2022**, *126* (2), 513–527. https://doi.org/10.1021/acs.jpcb.1c08170.

(37) Abbas, U. L.; Qiao, Q.; Nguyen, M. T.; Shi, J.; Shao, Q. Structure and Hydrogen

Bonds of Hydrophobic Deep Eutectic Solvent-Aqueous Liquid–Liquid Interfaces. *AIChE J.* **2021**, *67* (12), e17427. https://doi.org/https://doi.org/10.1002/aic.17427.

(38) Malik, A.; Kashyap, H. K. Multiple Evidences of Dynamic Heterogeneity in Hydrophobic Deep Eutectic Solvents. *J. Chem. Phys.* **2021**, *155* (4), 44502. https://doi.org/10.1063/5.0054699.

(39) Bader, R. F. W. *Atoms in Molecules: A Quantum Theory*; Clarendon Press, 1991.

(40) Frisch, M. J.; Trucks, G. W.; Schlegel, H. B.; Scuseria, G. E.; Robb, M. A.; Cheeseman, J. R.; Scalmani, G.; Barone, V.; Petersson, G. A.; Nakatsuji, H.; Li, X.; Caricato, M.; Marenich, A. V.; Bloino, J.; Janesko, B. G.; Gomperts, R.; Mennucci, B.; Hratch, D. J. Gaussian 16. Gaussian, Inc.: Wallingford CT 2016.

(41) Grimme, S.; Antony, J.; Ehrlich, S.; Krieg, H. A Consistent and Accurate Ab Initio Parametrization of Density Functional Dispersion Correction (DFT-D) for the 94 Elements H-Pu. *J. Chem. Phys.* **2010**, *132* (15), 154104. https://doi.org/10.1063/1.3382344.

(42) Grimme, S.; Ehrlich, S.; Goerigk, L. Effect of the Damping Function in Dispersion Corrected Density Functional Theory. *J. Comput. Chem.* **2011**, *32* (7), 1456–1465. https://doi.org/https://doi.org/10.1002/jcc.21759.

(43) Zhao, Y.; Truhlar, D. G. The M06 Suite of Density Functionals for Main Group Thermochemistry, Thermochemical Kinetics, Noncovalent Interactions, Excited States, and Transition Elements: Two New Functionals and Systematic Testing of Four M06-Class Functionals and 12 Other Function. *Theor. Chem. Acc.* **2008**, *120* (1), 215–241. https://doi.org/10.1007/s00214-007-0310-x.

(44) Boys, S. F.; Bernardi, F. The Calculation of Small Molecular Interactions by the Differences of Separate Total Energies. Some Procedures with Reduced Errors. *Mol. Phys.* **1970**, *19* (4), 553–566. https://doi.org/10.1080/00268977000101561.

(45) Glendening, E. D.; Landis, C. R.; Weinhold, F. NBO 6.0: Natural Bond Orbital Analysis Program. *J. Comput. Chem.* **2013**, *34* (16), 1429–1437. https://doi.org/https://doi.org/10.1002/jcc.23266.

(46) Fukui, K. Theory of Orientation and Stereoselection BT - Orientation and Stereoselection; Fukui, K., Ed.; Springer Berlin Heidelberg: Berlin, Heidelberg, 1970; pp 1–85.

(47) Marenich, A. V; Cramer, C. J.; Truhlar, D. G. Universal Solvation Model Based on Solute Electron Density and on a Continuum Model of the Solvent Defined by the Bulk Dielectric Constant and Atomic Surface Tensions. *J. Phys. Chem. B* **2009**, *113* (18), 6378–6396. https://doi.org/10.1021/jp810292n.

(48) Johnson, E. R.; Keinan, S.; Mori-Sánchez, P.; Contreras-García, J.; Cohen, A. J.; Yang, W. Revealing Noncovalent Interactions. *J. Am. Chem. Soc.* **2010**, *132* (18), 6498–6506. https://doi.org/10.1021/ja100936w.

(49) Marekha, B. A.; Kalugin, O. N.; Idrissi, A. Non-Covalent Interactions in Ionic Liquid Ion Pairs and Ion Pair Dimers: A Quantum Chemical Calculation Analysis. *Phys. Chem. Chem. Phys.* **2015**, *17* (26), 16846–16857. https://doi.org/10.1039/C5CP02197A.

(50) Lu, T.; Chen, F. Multiwfn: A Multifunctional Wavefunction Analyzer. *J. Comput. Chem.* **2012**, *33* (5), 580–592. https://doi.org/https://doi.org/10.1002/jcc.22885.

(51) Bayly, C. I.; Cieplak, P.; Cornell, W.; Kollman, P. A. A Well-Behaved Electrostatic Potential Based Method Using Charge Restraints for Deriving Atomic Charges: The RESP Model. *J. Phys. Chem.* **1993**, *97* (40), 10269–10280. https://doi.org/10.1021/j100142a004.

(52) Case, D. A.; Belfon, K.; Ben-Shalom, I. Y.; Brozell, S. R. .; Cerutti, D. S.; Cheatham, T. E.; Cruzeiro, V. W. D.; Darden, T. A. .; Duke, R. E.; Giambasu, G.; Gilson, M. K.; Gohlke, H.; Goetz, A. W. .; Harris, R.; Izadi, S.; Jhala, K. K.; Kovalenko, A.; Krasny, R. . K.; T.; Lee, T. S.; LeGrand, S.; Li, P.; Lin, C.; Liu, J.; Luchko, T.; Luo, R. .; Man, V.; Merz, K. M.; Miao, Y.; Mikhailovskii, O.; Monard, G. .; Nguyen, H.; Onufriev, A.; Pan, F.; Pantano, S.; Qi, R.; Roe, D. R. .; Roitberg, A.; Sagui, C.; Schott-Verdugo, S.; Shen, J.; Simmerling, C.; L.; Skrynnikov, N.; Smith, J.; Swails, J.; Walker, R. C.; Wang, J. .; Wilson, L.; Wolf, R. M.; Wu, X.; Yourk, D. M.; Kollman, P. A. AMBER 14. University of California: San Francisco, 2014 2014.

(53) Wang, J.; Wolf, R. M.; Caldwell, J. W.; Kollman, P. A.; Case, D. A. Development and Testing of a General Amber Force Field. *J. Comput. Chem.* **2004**, *25* (9), 1157–1174. https://doi.org/10.1002/jcc.20035.

(54) Wang, J.; Wang, W.; Kollman, P. A.; Case, D. A. Automatic Atom Type and Bond Type Perception in Molecular Mechanical Calculations. *J. Mol. Graph. Model.* **2006**, *25* (2), 247–260. https://doi.org/https://doi.org/10.1016/j.jmgm.2005.12.005.

(55) Martinez, L.; Andrade, R.; Birgin, E. G.; Martínez, J. M. PACKMOL: A Package for Building Initial Configurations for Molecular Dynamics Simulations. *J. Comput. Chem.* **2009**, *30* (13), 2157–2164. https://doi.org/10.1002/jcc.21224.

(56) Phillips, J. C.; Braun, R.; Wang, W.; Gumbart, J.; Tajkhorshid, E.; Villa, E.; Chipot, C.; Skeel, R. D.; Kalé, L.; Schulten, K. Scalable Molecular Dynamics with NAMD. *J. Comput. Chem.* **2005**, *26* (16), 1781–1802. https://doi.org/https://doi.org/10.1002/jcc.20289.

(57) Brehm, M.; Kirchner, B. TRAVIS - A Free Analyzer and Visualizer for Monte Carlo and Molecular Dynamics Trajectories. *J. Chem. Inf. Model.* **2011**, *51* (8), 2007–2023. https://doi.org/10.1021/ci200217w.

(58) Humphrey, W.; Dalke, A.; Schulten, K. VMD: Visual Molecular Dynamics. *J. Mol. Graph.* **1996**, *14* (1), 33–38. https://doi.org/https://doi.org/10.1016/0263-7855(96)00018-5.

(59) Hünenberger, P. H. Thermostat Algorithms for Molecular Dynamics Simulations. *Adv. Polym. Sci.* **2005**, *173*, 105–147.

(60) Feller, S. E.; Zhang, Y.; Pastor, R. W.; Brooks, B. R. Constant Pressure Molecular Dynamics Simulation: The Langevin Piston Method. *J. Chem. Phys.* **1995**, *103* (11), 4613–4621. https://doi.org/10.1063/1.470648.

(61) Andersen, H. C. Rattle: A "Velocity" Version of the Shake Algorithm for Molecular Dynamics Calculations. *J. Comput. Phys.* **1983**, *52* (1), 24–34. https://doi.org/https://doi.org/10.1016/0021-9991(83)90014-1.

(62) Essmann, U.; Perera, L.; Berkowitz, M. L.; Darden, T.; Lee, H.; Pedersen, L. G. A Smooth Particle Mesh Ewald Method. *J. Chem. Phys.* **1995**, *103* (19), 8577–8593. https://doi.org/10.1063/1.470117.

(63) Brooks, C. L. Computer Simulation of Liquids. *J. Solution Chem.* **1989**, *18* (1), 99. https://doi.org/10.1007/BF00646086.

(64) Kohn, W.; Becke, A. D.; Parr, R. G. Density Functional Theory of Electronic Structure. *J. Phys. Chem.* **1996**, *100* (31), 12974–12980. https://doi.org/10.1021/jp960669l.

(65) Wagle, D. V; Zhao, H.; Deakyne, C. A.; Baker, G. A. Quantum Chemical Evaluation of Deep Eutectic Solvents for the Extractive Desulfurization of Fuel. *ACS Sustain.*

Chem. Eng. **2018**, *6* (6), 7525–7531. https://doi.org/10.1021/acssuschemeng.8b00224.

(66) Fukui, K. Theory of Orientation and Stereoselection; Springer Berlin, Heidelberg, 1970; pp 1–85. https://doi.org/10.1007/978-3-642-61917-5.

(67) Zhan, C.-G.; Nichols, J. A.; Dixon, D. A. Ionization Potential, Electron Affinity, Electronegativity, Hardness, and Electron Excitation Energy: Molecular Properties from Density Functional Theory Orbital Energies. *J. Phys. Chem. A* **2003**, *107* (20), 4184–4195. https://doi.org/10.1021/jp0225774.

(68) Bankiewicz, B.; Matczak, P.; Palusiak, M. Electron Density Characteristics in Bond Critical Point (QTAIM) versus Interaction Energy Components (SAPT): The Case of Charge-Assisted Hydrogen Bonding. *J. Phys. Chem. A* **2012**, *116* (1), 452–459. https://doi.org/10.1021/jp210940b.

(69) Solimannejad, M.; Alkorta, I.; Elguero, J. Stabilities and Properties of O3–HOCl Complexes: A Computational Study. *Chem. Phys. Lett.* **2007**, *449* (1), 23–27. https://doi.org/https://doi.org/10.1016/j.cplett.2007.10.024.

(70) Paul, S.; Paul, S. The Influence of Trehalose on Hydrophobic Interactions of Small Nonpolar Solute: A Molecular Dynamics Simulation Study. *J. Chem. Phys.* **2013**, *139* (4). https://doi.org/10.1063/1.4816521.

(71) Sarangi, S. S.; Zhao, W.; Müller-Plathe, F.; Balasubramanian, S. Correlation between Dynamic Heterogeneity and Local Structure in a Room-Temperature Ionic Liquid: A Molecular Dynamics Study of [Bmim][PF6]. *ChemPhysChem* **2010**, *11* (9), 2001–2010. https://doi.org/https://doi.org/10.1002/cphc.201000111.

(72) Biswas, R.; Pasumarthi, V.; Banerjee, T.; Ghosh, P.; Musharaf Ali, S.; Joshi, J. M. Interfacial Insights on the Dibenzo-Based Crown Ether Assisted Cesium Extraction in [BMIM][Tf2N]–Water Binary System. *J. Radioanal. Nucl. Chem.* **2017**, *311* (1), 427–438. https://doi.org/10.1007/s10967-016-5050-8.

Chapter- 3

Quantum Chemical and Molecular Dynamics Study on the Extraction of Acetamiprid and Imidacloprid from Aqueous Environment using Menthol-based Hydrophobic Eutectic Solvents

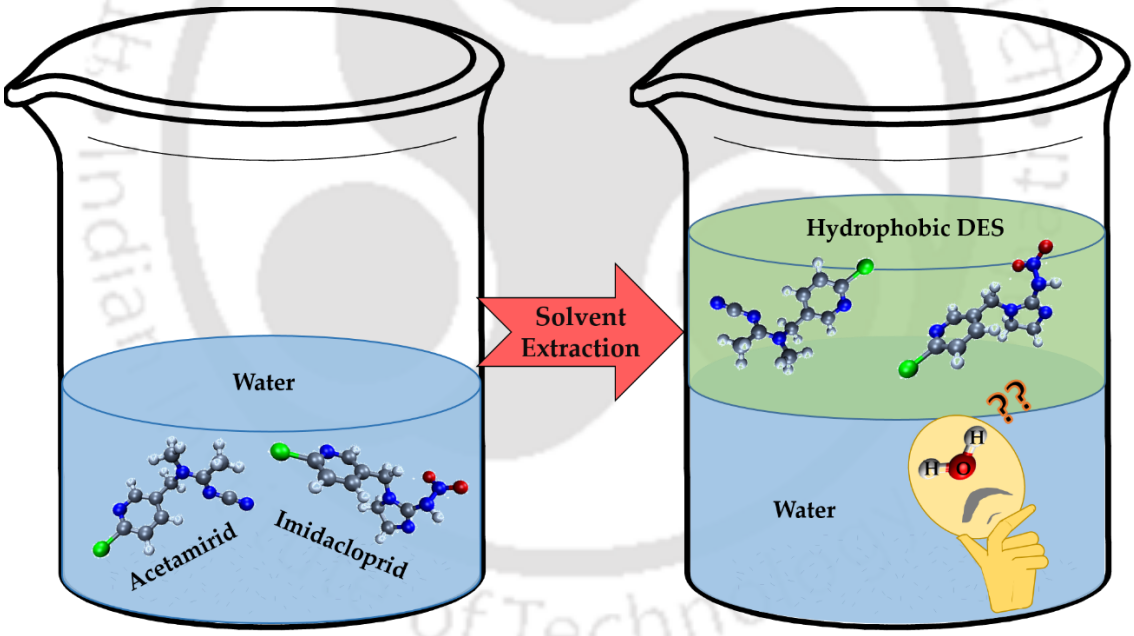

Published Article:

N. Paul, T. Banerjee, Study on the extraction of acetamiprid and imidacloprid from an aqueous environment using menthol-based hydrophobic eutectic solvents: quantum chemical and molecular dynamics insights, ACS Sustain. Chem. Eng., 10 (2022) 4227–4246.

3 Quantum Chemical and Molecular Dynamics Study on the Extraction of Acetamiprid and Imidacloprid from Aqueous Environment using Menthol-based Hydrophobic Eutectic Solvents

The current chapter reports Molecular dynamics (MD) and Quantum Chemical (QC) calculations for two pesticide systems (acetamiprid & imidacloprid) through extraction from an aqueous environment. Two separate deep eutectic solvents (DESs) consisting of DL-menthol as hydrogen bond acceptor (HBA) and two carboxylic acids (octanoic acid and dodecanoic acid) as hydrogen bond donors (HBDs) at 298.15 K temperature and atmospheric pressure have been adopted in our studies. The non-bonded interaction energy, radial, combined and spatial distribution function (RDF, CDF & SDF) and hydrogen bonding extent of the various components have been obtained via MD simulation to highlight the enhanced and favourable interactions of the DES components with the pesticides as compared to water. Further, transport properties such as mean squared displacement (MSD) and diffusivity of the compounds within the phases have been evaluated with the help of Einstein's diffusivity equation to obtain the affinity of the pesticides, namely acetamiprid and imidacloprid, towards the DES-rich phase. The extractive characteristics of pesticides, such as distribution coefficient (β), selectivity (S), and extraction efficiency (%EE) have been calculated from the simulation to be fitted with the experimental data. Within QC, the charge transfer (CT) analysis through NBO charges is carried out to obtain the extent of charge transfer among DES components and pesticides. The structural arrangements of the DES-pesticide complexes are also evaluated to confirm the increased interaction between DES and pesticide, which is validated by MD simulation. The frontier molecular orbital (FMO) study incorporating HOMO-LUMO analysis is carried out to recognise the active sites involved in charge transfer and interactive operations, also confirmed by the structural findings of the MD simulation that are initially validated by the experimental results.

3.1 Introduction

The experimental investigation on the hydrophobic nature of DL-menthol and carboxylic acid-based DESs was expended to extract four neonicotinoid pesticides from water-

based solutions using DL-menthol as HBA and long-chain fatty acids (C_8 to C_{12}) as HBD.[1] The findings related to the stability analysis of the DESs were confirmed and validated in the previous chapter (chapter 2) where an elaborate analysis of the molecular level insights into the water-stability of the hydrophobic DESs was highlighted using molecular dynamics (MD) simulation and quantum chemical (QC) calculations.[2] With respect to the activity coefficient of DES, Verevkin et al.[3] determined the activity coefficient at infinite dilution for 23 (twenty-three) solutes in choline chloride and ethylene glycol-based DESs where the PC-SAFT model was used. PC-SAFT model was effectively used by some other groups to determine the solid-liquid phase equilibrium of DESs composed of quaternary ammonium salts and carboxylic acids[4] and to determine the solubility of water and 5- hydroxymethylfurfural (HMF) in the DES phase.[5]

DESs as an alternative to ILs could be utilized in these processes to achieve higher efficiency in pesticide removal along with cost-optimization which could immensely help in developing a sustainable approach to water treatment processes. Hydrophobic DES developed between sodium salt of fatty acid and another fatty acid forms a hydrogel when mixed with water.[6] This type of DES-based gel could be used for the entrapment of pesticides from aqueous solutions. For futuristic potential, the up-gradation of the batch process to a sustainable continuous process could be significant with a regeneration and recycling approach embedded within.

From a theoretical and simulation perspective, MD simulation with a realistic approach to keeping a balance between the bulk process and the atomistic objective could be the area of focus in the future. Some membrane-based processes have been theoretically investigated by researchers,[7] However, computational frameworks are yet to be developed fully to address pesticide removal from wastewater sources. COnductor like Screening MOdel for Real Solvents (COSMO-RS) can be a valuable tool for understanding the system behaviour thermodynamically which is based on quantum chemistry. To properly investigate pesticide removal functioning, quantum chemistry (QC) should be coupled with molecular dynamics (MD) for a futuristic approach. While investigating different DES systems and their behaviour in an aqueous environment, we obtained the order of the stability of the DESs in a water medium as a function of the HBD chain length. Further, in the previous chapter (chapter 2), we explored the extraction mechanism of nitenpyram as a pesticide from water and achieved similar results as obtained in the experiments. The hydrogen bonding and the van der Waals interactions between the components of DES and the drug were found to be having a significant role in phase formation and extraction efficiency.

Therefore, the current chapter combines MD simulation and QC calculation in the extraction of two pesticides namely acetamiprid and imidacloprid from water with the help of DL-menthol and carboxylic acid-based DESs along with the validation from the experimental work performed by Florindo et al.[1] The composition of the systems for MD simulation is taken from the same experimental dataset. Initially, the non-bonded interaction energy among the different components was calculated to identify the interactions among the DES components, the pesticides and the water. Subsequently, the structural properties such as radial (RDF), combined (CDF) and spatial distribution function (SDF), hydrogen bonding properties, mean square displacement (MSD) and diffusion coefficient were evaluated for the different components present within the system. The ensuing section provides the quantum chemical calculation findings starting with the optimized structures of DES, pesticides and the complex formed between them. The CT analysis was carried out in Gaussian 09[8] with the natural bonding orbital (NBO) analysis. Further, the HOMO-LUMO energy gap, chemical hardness and stability and chemical potential were evaluated. The HOMO-LUMO results were then validated with the structural findings of the MD simulation. The individual optimized structures are provided in Figure 3.1.

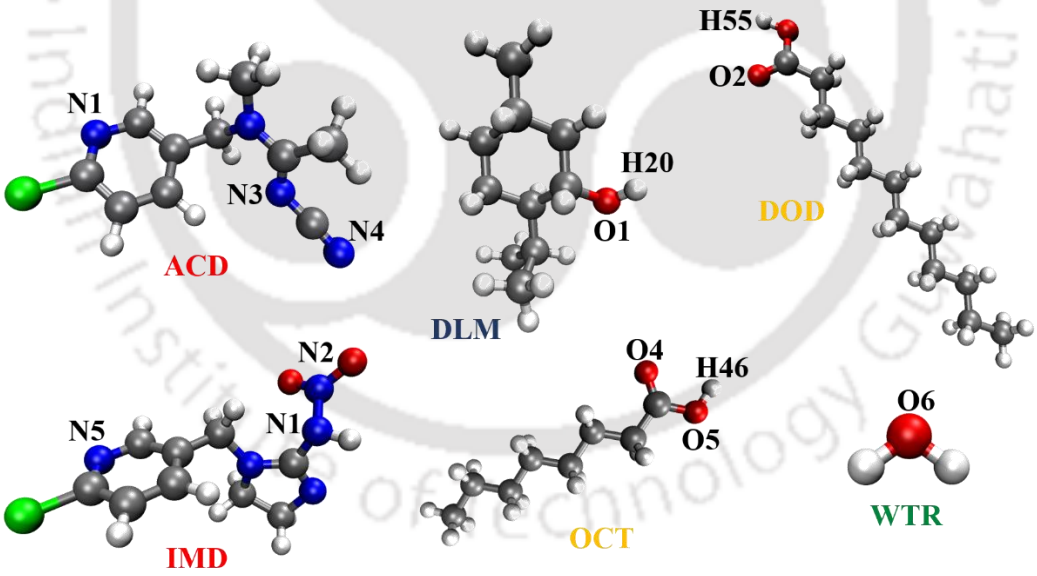

Figure 3.1: Ball and stick representation of the pesticides (ACD: acetamiprid, IMD: imidacloprid); DLM: DL-menthol; OCT: octanoic acid; DOD: dodecanoic acid; WTR: water, with useful atomic notations.

Table 3.1: Composition of different systems with simulation box size considered for MD simulation

Name of pesticide	DES		Number of molecules					Periodic Box Size
	HBA	HBD	HBA	HBD	Pesticide	Water	Total	(Å × Å × Å)
Acetamiprid	DL-menthol	Dodecanoic acid	100	50	5	475	630	51.77 × 34.513 × 34.513
Imidacloprid	DL-menthol	Octanoic acid	50	50	5	425	530	43.01 × 26.671 × 26.671

Table 3.2: MD simulated results in the calculation for distribution coefficient and selectivity at 1 atm pressure and 298.15 K temperature

System	DES-rich phase			Water-rich phase			Distribution Coefficient (β)	Selectivity (S)	Distribution ratio	
	X_{DES}	$X_{pesticide}$	X_{water}	X_{DES}	$X_{pesticide}$	X_{water}			Experimental [a]	Simulated
DES+ Acetamiprid + water	0.890	0.026	0.084	0.005	0.003	0.992	8.67 ± 0.12	102.38 ± 1.5	3.43	3.17 ± 0.23
DES+ Imidacloprid + water	0.889	0.025	0.086	0.007	0.004	0.989	6.25 ± 0.09	71.86 ± 0.75	2.67	2.48 ± 0.14

[a] The experimental value is taken from Florindo et al.[1] X_{DES}, $X_{pesticide}$ and X_{water} are the mole fraction of DES, pesticide (acetamiprid and imidacloprid) and water respectively

3.2 Computational Framework

3.2.1 Molecular Dynamics Simulation Methodology

Our earlier work provides an in-depth explanation of the molecular dynamics modelling technique. In short, the optimized structures of each HBA and HBD, as well as water and pesticides (acetamiprid and imidacloprid) were obtained using Gaussian 09[8] at the B3LYP/6-311+G(d,p) level of theory.[9] The chemical structures of all molecules are shown in Figure C.1 (see Appendix C) with their atomic notations. The partial atomic charges were determined from the optimized geometry using the restricted electrostatic potential (RESP) module[10] after fitting through in AMBER 14.[11] Subsequently, the generalized amber force field[12] functional of ANTECHAMBER,[13] a module of AMBER 14,[11] was used to generate all the force field parameters. Benchmarking study of density mapping with experimental results was carried out for validation of the force field parameters. The experimental compositions were used from an earlier work by Florindo et al.[1] The composition of the different systems has been presented in Table 3.1 and the extractive characteristics are shown in Table 3.2. The basic configuration of the simulation box of various systems composed of DES, pesticide and water molecules. This was generated using PACKMOL.[14] The MD simulations were all performed using the NAMD 2.10 software.[15] Subsequent processes of minimization run (6 ns) in the NVE ensemble and heating at 298.15 K (0.5 ns) were executed followed by an equilibration run for approximately 10 ns in the NPT ensemble. The conjugate gradient method was implemented in minimizing the systems in NAMD. The Langevin dynamics method[16] was used to maintain the appropriate temperature with a collision frequency of 1 ps^{-1}. Pressure management was accomplished using a Nosé Hoover Langevin piston with an oscillation period of 100 fs and a damping factor of 50 fs.[17] The simulation then progressed with a 100 ns production run in the NVT ensemble. Each system was subjected to a periodic boundary condition (PBC).[18] The box dimensions for each system are listed in Table 3.1. The VMD 1.9.3 programme[19] was used to observe the system configuration and analyse the simulation trajectories to obtain non-bonded, structural (RDF), distributional and transport properties (MSD) for all the systems. The combined distribution function (CDF) and spatial distribution function (SDF) were generated using the TRAVIS package[20] from the final coordinate file as the input. As per our previous work[21], each individual simulation was performed thrice to minimize inaccuracy and to achieve successful replication of the findings.

3.2.2 Quantum Chemical Methodology

Gaussview 5 visualizations and builder package was used to draw the structures of the individual DES components i.e., DL-menthol, carboxylic acids and pesticides (acetamiprid and imidacloprid) with Gaussian 09[8]. Initially, the pure-state DES components were optimized. Next, the optimization of the DES model structures was performed by positioning the components in different orientations. Similarly, the optimized pesticide molecules were introduced to the optimized DES model structures and were optimized after verifying different positions in and out of the plane around the DES components. The systems were first optimized at the B3LYP/6-311+G(d,p) level of theory, and subsequently reoptimized at the higher M06-2X/6-311+G(d,p) level of theory.[21] To verify the minimum state in potential energy surface (PES), vibrational frequency calculations at the same level of theory were undertaken using the '*freq'* keyword in Gaussian. Frontier molecular orbital (FMO)[22] and the natural bonding orbital NBO) analysis were carried out using both B3LYP/6-311+G(d,p) and M06- 2X/6-311+G(d,p) level of theories for a comparative study to explore the charge transfer process, chemical reactivity and stability of DES, pesticides and DES-pesticide complex composition.

3.3 Results and Discussion

3.3.1 MD simulation Analysis

3.3.1.1 Non-bonded Interaction Energy

Figures 3.2 (a) & (b) express the non-bonded interaction energies among various components. This is divided into electrostatic (Elec) and van der Waals (vdW) contributions, for acetamiprid and imidacloprid systems, respectively. In our present work, we have incorporated the dispersion interaction such as van der Waals forces along with other non-bonded interactions such as electrostatic and hydrogen bonding. The DES-forming precursor materials (menthol and carboxylic acids) are large molecules having a significant electron distribution. The pesticides too being large molecules and having electronegative elements polarize the electron distribution of their own forming a temporary dipole. Thus, van der Waals interaction dominates other non-bonded interactions. The interaction energy data obtained by MD simulation has been provided in Figure 3.2 incorporating the dispersion interaction. Within all the DES-pesticide component pairs, van der Waals interaction provides a greater contribution in all the nonbonded interactions.

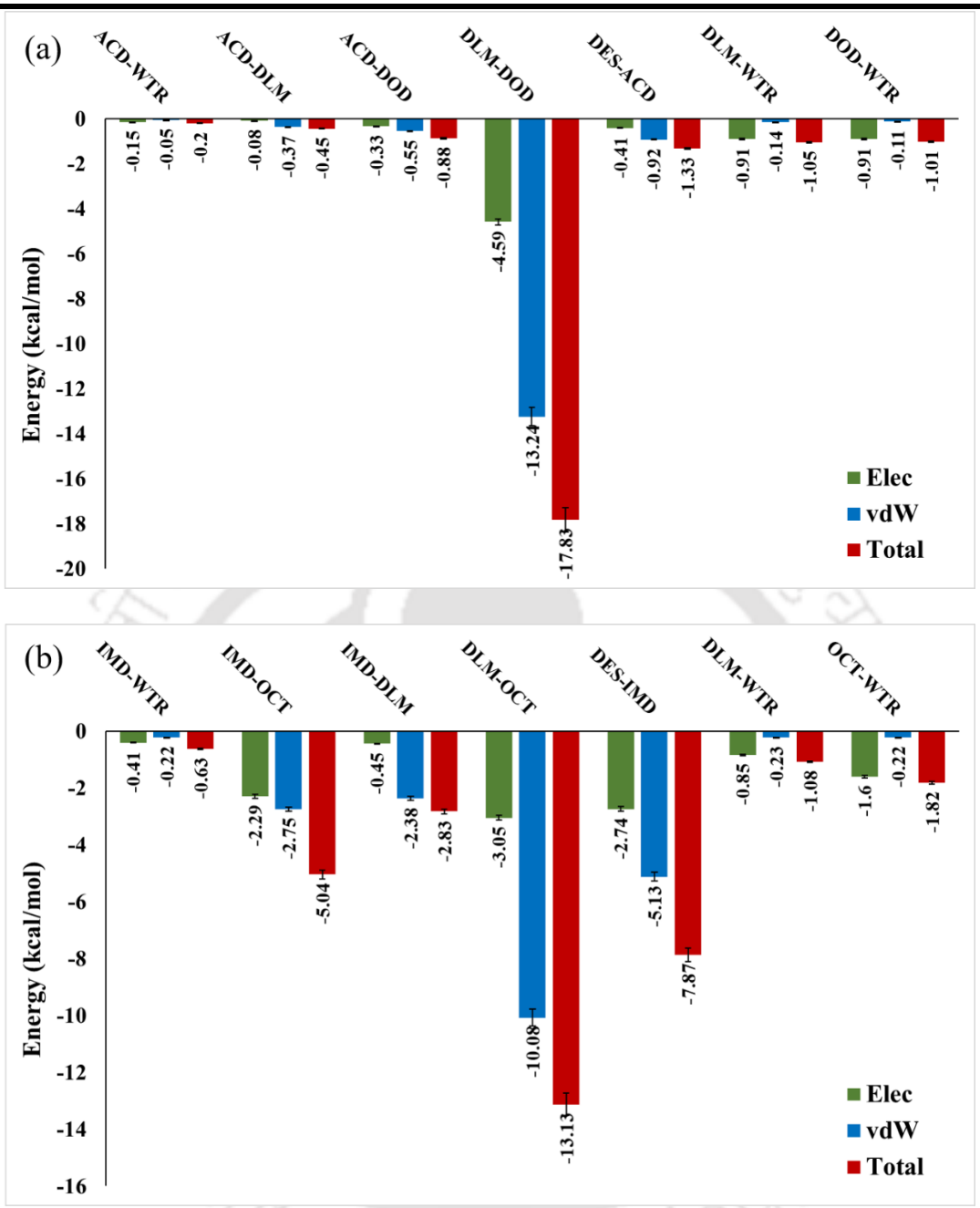

Figure 3.2: MD simulated interaction energies (kcal/mol) between the different component pairs of (a) menthol-dodecanoic acid-acetamiprid and (b) menthol-octanoic acid-imidacloprid in 298.15 K and 1 atm pressure.

DES molecules were found intact and stable for both systems, as they have shown a higher value of total interaction energy (-17.83 & -13.13 kcal/mol, respectively). HBD molecules showed higher interaction with drug molecules for both systems. The van der Waals interaction exhibited by acetamiprid-dodecanoic acid (-0.55 kcal/mol) was found to be higher than the electrostatic component (-0.33 kcal/mol). Owing to the long hydrophobic tail of

dodecanoic acid, enhanced polarizability can be witnessed leading to higher van der Waals interaction between drug-HBD as compared to the electrostatic interaction. A similar trend has been observed between imidacloprid and octanoic acid where the van der Waals component (-2.75 kcal/mol) dominated over the electrostatic part (-2.29 kcal/mol). The interaction energy between drug-water was much lower than that of drug-DES for both systems. It can be witnessed from Figure 3.2 (a), where the total ACD-water interaction (-0.2 kcal/mol) was much lower than the total DES-ACD interaction (-1.33 kcal/mol). Likewise, DES- IMD (-7.87 kcal/mol) showed an order of magnitude higher interaction as compared to IMD-water (-0.63 kcal/mol) (Figure 3.2 (b)). The higher the interaction of the pesticides with the DES molecules, the lower the ability of the water molecules to trap the same in the water phase, subsequently leading to enhanced extractive properties of the DESs. In the case of interaction with water, all the DES and the drug components displayed dominating electrostatic interaction as compared to the vdW interaction. Pesticides namely acetamiprid and imidacloprid are soluble in water and are present in the aqueous environment at a specific concentration. As the drugs are soluble in water, they exhibit significant interactions with the polar water molecules due to the presence of multiple donor and acceptor sites in the pesticides. Thus, electrostatic interaction is found to be dominating between the pesticide and water for both drugs. As evident in Figures 3.2 a & b in the manuscript, the van der Waals component is two to three-fold lesser than the electrostatic non-bonded interaction. One explanation for this could be the induced polarity of water around the pesticide entities with possible hydrogen bond formation. Both the pesticides, acetamiprid and imidacloprid, having higher dipole moments could lead to polarity-induced electrostatic interactions, however, the limited access to the active sites of the pesticides due to steric hindrance impeded the water molecules to interact favourably with the drugs. As the pesticides possess significant non-bonded interactions with DES, the pesticide-water interaction reduces considerably and as a whole, the transport of pesticides to the DES phase gets influenced by the inter-component interactions.

3.3.1.2 Radial Distribution Function (RDF)

The structural property in terms of the radial distribution function between the pesticides and the DES components along with water is demonstrated in Figure 3.3. The Menthol entity is found to have a higher probability distribution than the bulk within a distance of ~2 Å from the acetamiprid entity (Figure 3.3a). It is said to be facilitated by probable non-bonded interaction between H20 (menthol) and N4 (acetamiprid). Dodecanoic acid is also having a quite higher distribution with acetamiprid at ~3.5 Å which is superior to the

distribution with the water molecule. Overall, it can be confirmed that both DL-menthol and dodecanoic acid showed higher probability distribution as we move from 2 Å to 3.5 Å through the central molecule of acetamiprid. Whereas, compared to the DES components, water is having a relatively lower RDF peak with acetamiprid. Additionally, on close observation, a relatively sluggish trend of the water RDF plot can be observed in attaining a g(r) value of 1 (unity) that represents the bulk fluid properties. It explains that the water molecules are having higher probability distribution at a distance greater than 5 Å from the central acetamiprid molecule. As both the DES components showed higher distribution adjacent to the drug molecule, water molecules could not have enough volume available to interact with the acetamiprid molecule due to steric hindrance. However, a relatively linear g(r) curve throughout the system corresponds to a strong correlation between water and acetamiprid at a long distance.

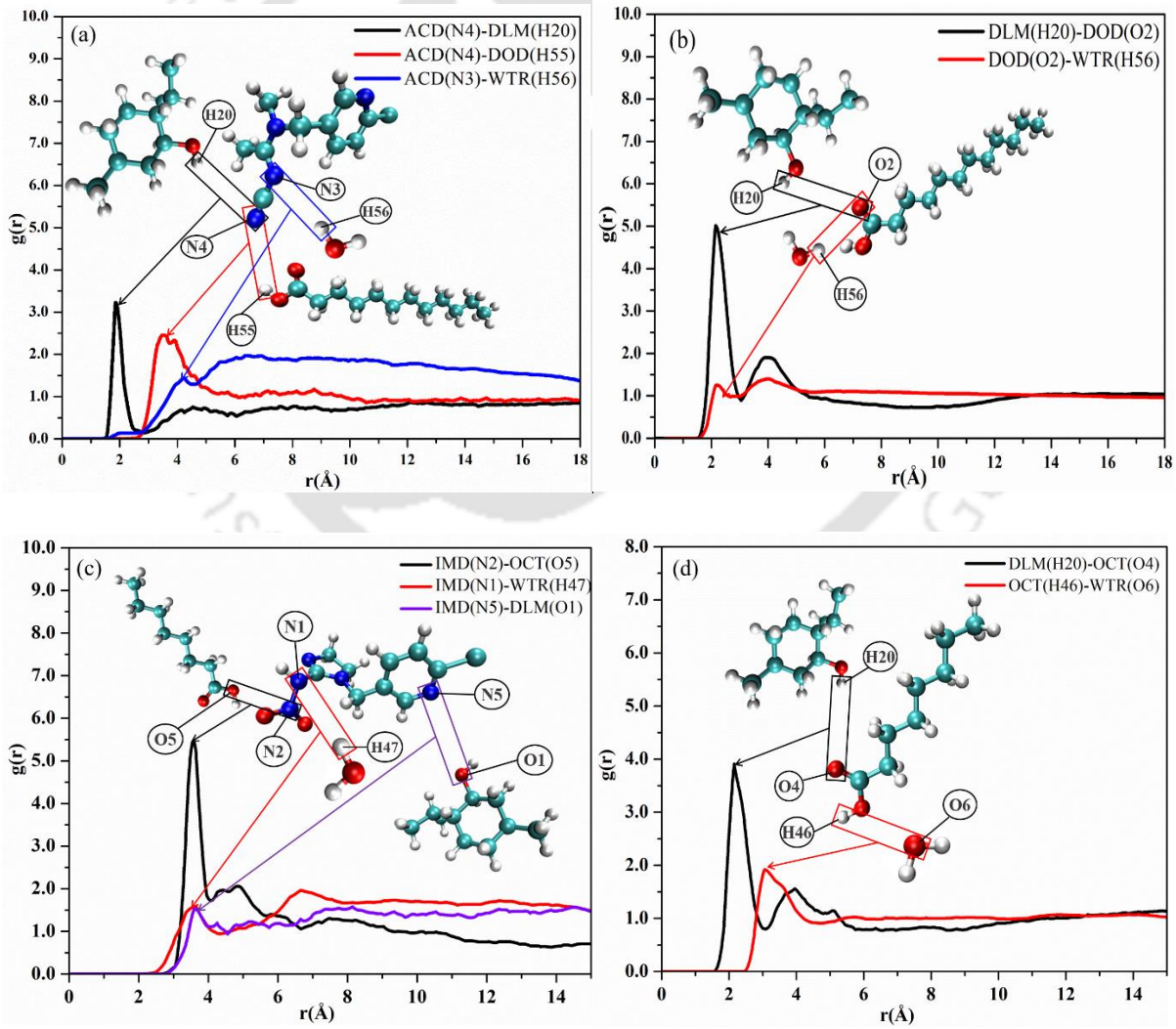

Figure 3.3: Comparison among atom-specific (site-site) radial distribution function plots between the different molecular pairs present in the system (a) Acetamiprid-dodecanoic acid, acetamiprid-DL-menthol and acetamiprid-water; (b) DL-menthol-dodecanoic acid and dodecanoic acid- water; (c) Imidacloprid-octanoic acid, imidacloprid- water and imidacloprid-DL-menthol and (d) DL-menthol- octanoic acid and octanoic acid - water at 100 ns.

In Figure 3.3c, RDF plots between imidacloprid, DES components and water have been presented. A sharp peak at a distance of ~3.5 Å can be witnessed indicating a higher coordination number between imidacloprid and octanoic acid. Comparable RDF peaks have been observed for both DL-menthol and water when calculated by keeping imidacloprid as a central molecule. The nature of the water-drug RDF curve implies a similar tendency observed earlier in the case of acetamiprid-water. A probable long-range interaction with a correlation factor may be observed in this case.

From Figures 3.3b and d, one can easily understand that the HBA and HBD components are strongly interacting with each other displaying very high probability distribution even in the presence of water molecules. Dodecanoic acid exhibited less distribution around water molecules than octanoic acid. These outcomes were discussed in detail in our previous work.[2]

3.3.1.3 Combined Distribution Function (CDF)

Combined distribution function (CDF) which can be illustrated as a combination of the radial and angular distribution function, has been obtained by the TRAVIS package[20] to observe the hydrogen bonding attributes among various components within the systems. The calculation scheme for evaluating CDF was taken from the literature.[20] Strong hydrogen bonding can be noticed between acetamiprid and DL-menthol which is evident from the higher values in the colour bar. From Figure 3.4a, it can be spotted that acetamiprid formed C−N···H bond with DL-menthol at a distance of 2 Å and an angular range of 140 to 180°. This was possible through the positively charged H atom (−OH group) of the DL-menthol molecule acting as a hydrogen bond donor atom evidently to the negatively charged N atom (−C≡N) of the acetamiprid molecule which turned out to be a hydrogen bond acceptor to form N···H hydrogen bond. Similarly, Figure 3.4b represents the CDF plot between acetamiprid and water in search of probable hydrogen bonding between the two molecular entity. The plot suggested the negligible presence of N···H hydrogen bonding within close vicinity of the molecules. A lower value in the colour bar confirmed the same. However, we have noticed some interaction

at a distance greater than 3.5 Å which implies a probable long-range interaction between acetamiprid and water as revealed previously in the RDFs.

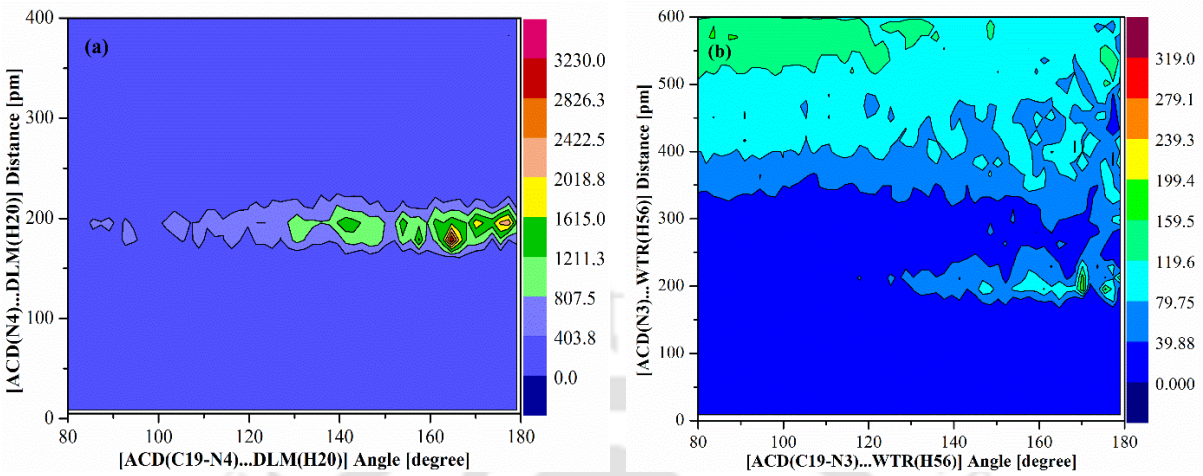

Figure 3.4: CDFs obtained by plotting the hydrogen bond distance (RDF) vs the hydrogen bond angle (ADF) for (a) C19-N4 (acetamiprid)…H20 (DL-menthol) angle against N4…H20 distance, (b) C19-N3 (acetamiprid)…H56 (water) angle against N3…H56 distance.

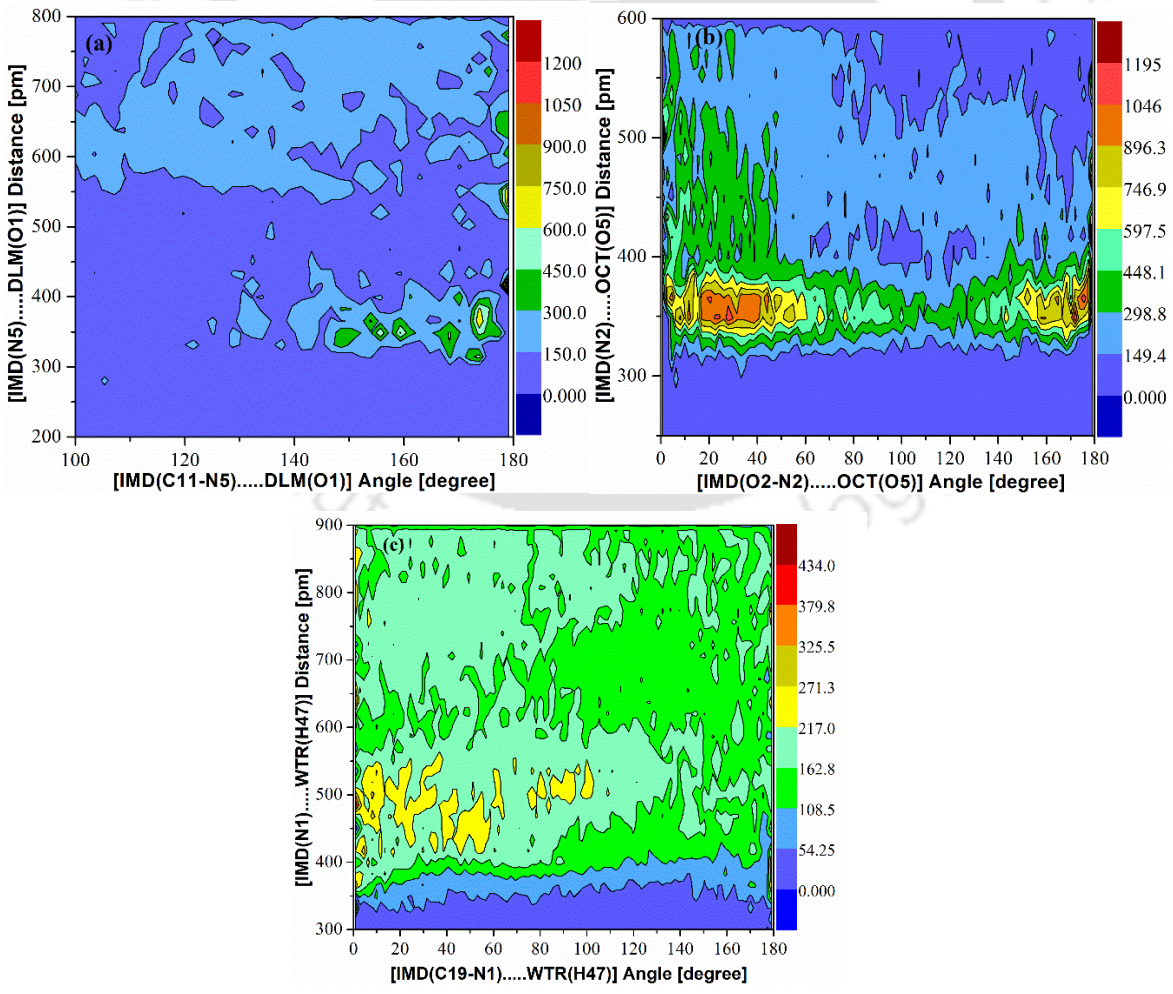

Figure 3.5: CDFs obtained by plotting the radial distribution function (RDF) vs the angular distribution function (ADF) for (a) C11-N5 (imidacloprid)…O1 (DL-menthol) angle against N5…O1 distance, (b) O2-N2 (imidacloprid)…O5 (octanoic acid) angle against N2…O5 distance, (c) C19-N1 (imidacloprid)…H47 (water) angle against N1…H47 distance.

CDFs obtained in Figure 3.5 supported the RDF plots obtained earlier for the imidacloprid system. The presence of a very low extent of hydrogen bonding is witnessed between imidacloprid with DL-menthol and water, respectively in Figures 3.5a, c. Lower interactions are observed among these molecular entities where the menthol-pesticide interaction recorded a slightly higher value than that of water-pesticide, which can be noticed from the colour bar values. The RDF plot between imidacloprid and octanoic acid presented earlier has been verified with an additional angular distribution calculation, as shown in Figure 3.5b. Interestingly, the interaction was found to be higher with angular distribution ranging from 0-60° and 140-180°. The result can be viewed in a way that the imidacloprid- octanoic acid interactions are more of a linear nature. In other words, head-to-head or head-to-tail intermolecular interaction can be witnessed between the two molecular groups. Accordingly, a branched configuration may not be observed in this type of system due to the straight-to-linear manner of interaction. The interaction can be spotted at a distance of ~3.5 Å that fittingly confirms the RDF plot.

3.3.1.4 Spatial Distribution Function (SDF)

Figure 6 describes the spatial distribution function (SDF) for the different components in the system around one central residue molecule (in this case, the pesticide molecules i.e., acetamiprid and imidacloprid, respectively). TRAVIS package[20] was used to obtain the SDFs which can reveal the average 3-dimensional density distribution of HBA, HBD and water molecules around a central pesticide molecule respective to the system. The optimum iso-values corresponding to different pairs and the percentage of maximum iso-values that were incorporated in the calculation have been presented in Table C.1 (Appendix C). For both systems, respective percentage values of I_{max} have been considered for all the components. A High iso-value usually signifies the density distribution of a moiety very close to the observed molecule, whereas a value near zero denotes the density inside the whole simulation box. From Figure 3.6a, it can be observed that water molecules (green lobe) distributed themselves around the polar acetamidine region of acetamiprid. The small size effect of the water molecules contributes to their well-enclosed distribution around acetamiprid owing to strong electrostatic

as well as hydrogen bond interactions which have been explained later in the hydrogen bonding section. Concurrent distribution of DL-menthol (blue lobe) and dodecanoic acid (red lobe) subsets in proximity to the cyclopyridine part of the drug molecule was observed which emphasized the high-density distribution of the DES components. In addition, the presence of hydrogen bonding between the (−C≡N) group of acetamiprid and the (−OH) group of DL-menthol brought about the increased presence of the latter around the drug. Correspondingly, higher sustained interaction between the HBA and HBD molecules owing to higher non-bonded interaction leads to the thick density distribution (blue and red lobes) of the DES components around acetamiprid moiety.

Figure 3.6b reveals a higher density distribution of DL-menthol and octanoic acid around the imidacloprid molecule largely in the imidazolidine segment of the drug molecule, highlighted in blue and red lobes respectively. The presence of both the acceptor and donor part of the hydrogen bond in the imidazolidine ring intensifies the distribution of HBD and HBA, respectively, around imidacloprid. Moreover, the presence of the positively charged N^+ and negative O^- atom associated with the polar imidazolidine portion enhances the non-bonded interaction with the DES components and captures a significantly higher density distribution between DES and imidacloprid. Nevertheless, the polarity of the imidacloprid molecule allured the water molecules to be distributed around it driven by relatively stronger electrostatic interaction, highlighted in green. Altogether, DES components were witnessed to have quite a higher and distinct density distribution layout around both the pesticide molecules indicating higher affinity and interaction.

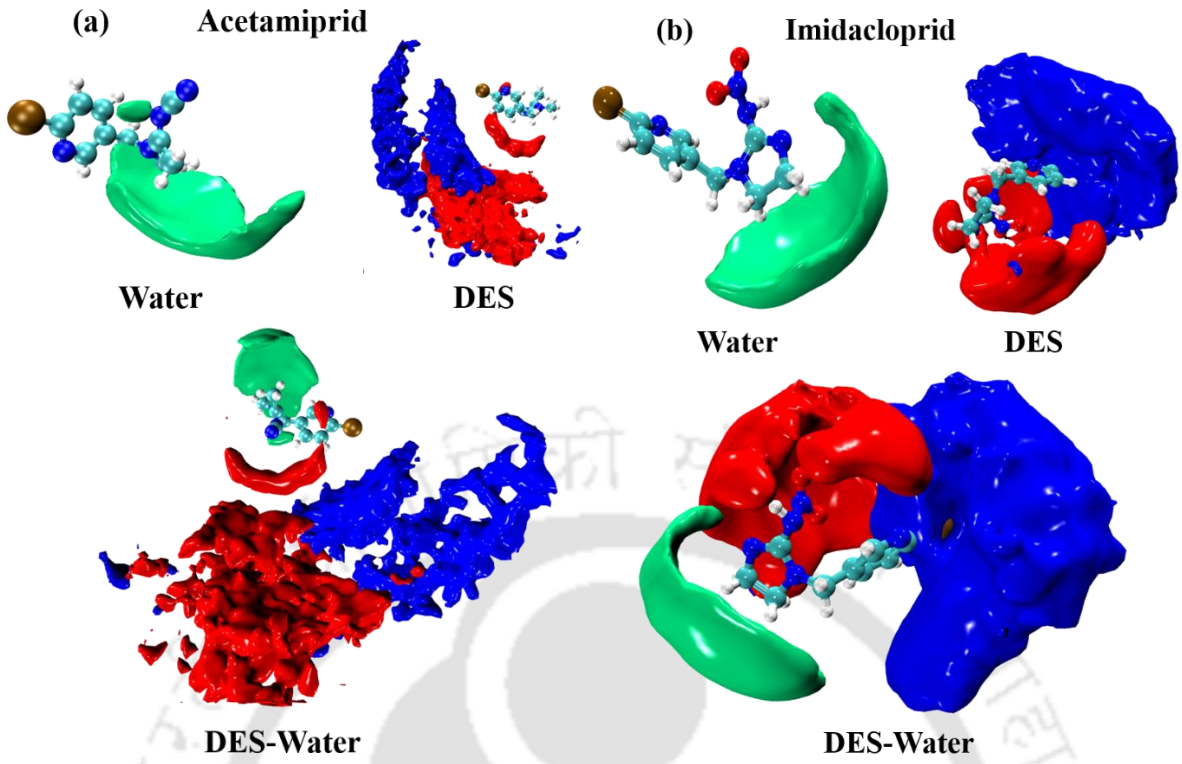

Figure 3.6: SDFs obtained for the system (a) Water around acetamiprid, DES around acetamiprid and DES-water around acetamiprid; (b) Water around imidacloprid, DES around imidacloprid and DES-water around imidacloprid; [DL-menthol- blue, dodecanoic acid/ octanoic acid- red, and water- green, respectively].

3.3.1.5 Hydrogen Bond Properties

Figure 3.7 reveals the extent of the average number of hydrogen bonds among the various constituents present in acetamiprid and imidacloprid, respectively. The plots exhibit the averaged-out values of the average number of hydrogen bonds obtained throughout 100 ns of a simulation run in the NVT ensemble at 298.15 K temperature and atmospheric pressure. Plots between different components present in each system are attained considering geometric criteria with a cut-off distance and angle between two molecular entities involved in hydrogen bonding based on the literature.[23] The range of cut-off values is subject to change, depending on several factors, including solvents and solutes, size and polarity of molecules, interactions between ions and complexes, and between the solvent and the solute. The aftermaths of all these aspects contribute to the radial distribution functions as presented in Figure 3.3. It can be deduced that the RDF peaks for all the different systems came within a range of 1.9 Å to 3.5 Å, as a result of which, a cutoff distance of 3.5 Å has been considered for our present study. From the angular distribution observed in the CDF plots presented in Figure 3.4, we have considered the cutoff angle for hydrogen bonding ranging from 140 to 180°.

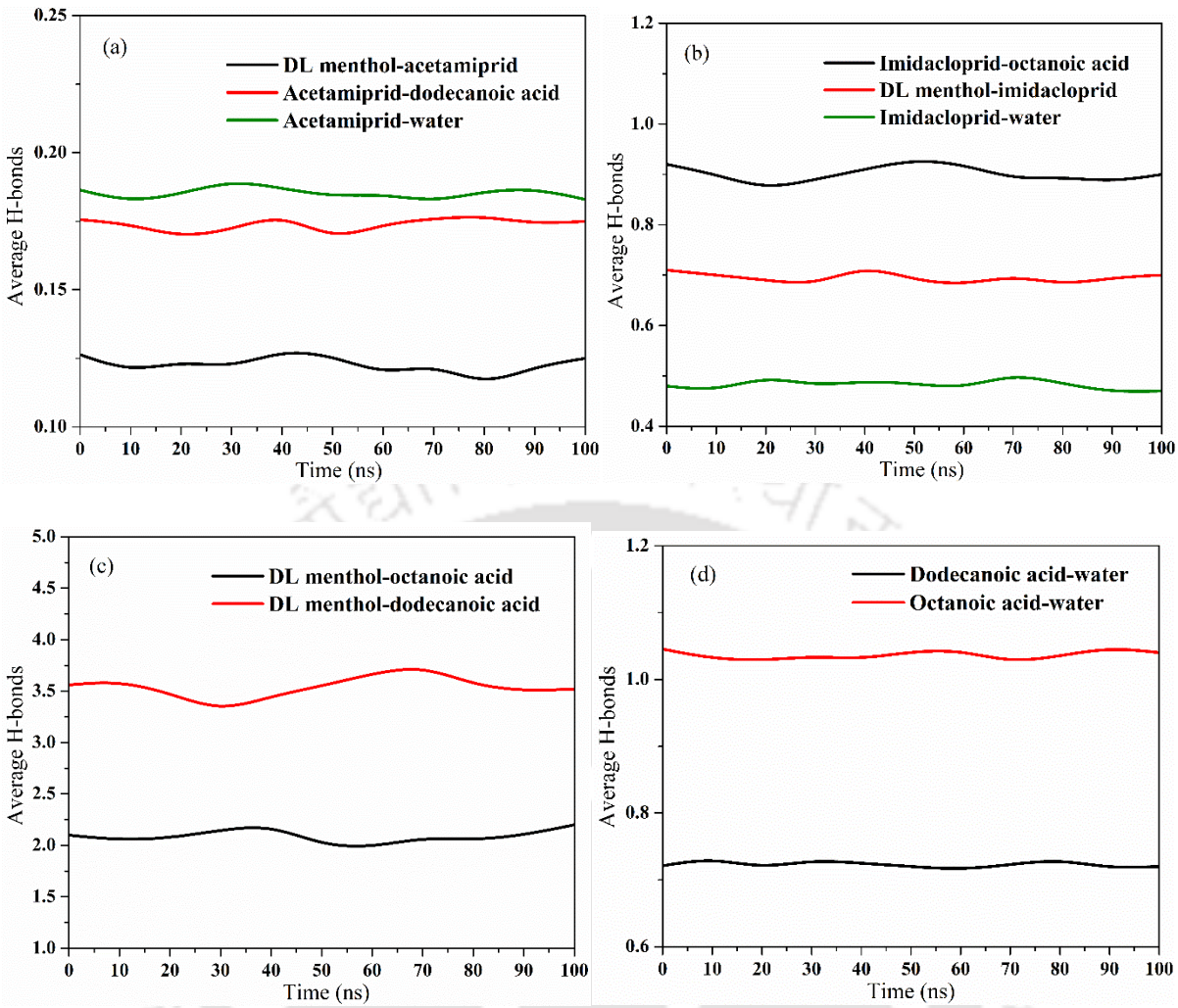

Figure 3.7: An averaged-out plot of the average number of hydrogen bonds between (a) Acetamiprid-DL menthol: dodecanoic acid-water; (b) Imidacloprid-DL menthol: octanoic acid-water; (c) HBA-HBD per DES moiety and (d) HBD-water per HBD molecule, for each system, as a function of simulation time (0-100 ns).

From Figure 3.7a, it can be concluded that the average number of hydrogen bonds per HBD molecule between acetamiprid- dodecanoic acid (~0.175) is marginally lower than the average number of hydrogen bonds per water molecule between acetamiprid-water (~0.185). The reason behind this might be the larger size of a dodecanoic acid moiety which leads to steric hindrance between HBD and the pesticide moiety (acetamiprid). Although the non-bonded interaction between HBD-acetamiprid was found to be higher than that of acetamiprid-water, a contrary was observed with hydrogen bonding. This was due to the large size steric effect provided by the HBD-acetamiprid which enabled the water molecules to come in the vicinity of the active polar part (acetamidine region) of the acetamiprid molecule. The

imidazolium cationic moiety acts as an active site for the water molecule. Thus, the gap in the extent of hydrogen bonding of acetamiprid with HBD and water, respectively, reduced drastically and the water molecules were exposed to higher H-bonding. In comparison, DL-menthol (HBA) indicated less H-bonding with acetamiprid (~0.125). However, the combined H-bonding between the DES- acetamiprid is found to be higher than that of acetamiprid- water.

The degree of average hydrogen bonding in the case of the imidacloprid system was in the order of imidacloprid- octanoic acid (0.92) > DL menthol- imidacloprid (0.71) > imidacloprid- water (0.48) [Figure 3.7b]. The average H-bonding obtained in this section is quite consistent with that of RDFs presented in Figure 3.3c. The five-membered imidazolidine ring present in imidacloprid is comprised of both hydrogen bond donor and acceptor. Consequently, HBA and HBD molecules present in the DES exhibit strong non-bonded interaction, mainly hydrogen bonding with the imidazolidine ring. $N^{+}\ldots O^{-}$ hydrogen bonding is observed between imidacloprid and both the HBA and HBD, respectively. The relatively shorter chain length of octanoic acid reduces the steric hindrance with imidacloprid and forms stronger H-bonding. Significant H-bonding between imidacloprid and water is also witnessed which supports the interaction of water with the pesticide.

Figures 3.7c and d confirmed the DES integrity in both the systems in terms of the extent of hydrogen bonding within HBA and HBD as well as comparison with HBD- water for both cases. The average H-bonding of DL-menthol is higher with dodecanoic acid than octanoic acid which supports the increased interaction between DL-menthol as HBA and long-chain fatty acids as HBDs, as shown in Figure 3.7c. The HBA-HBD interaction is higher for more hydrophobic long-chain organic acids. Figure 3.7d supports the hydrophobic characteristics of the long-chain fatty acids as HBDs. A relatively higher extent of H-bonding has been noticed for water with octanoic acid than for dodecanoic acid. Thus, it can be concluded that DL-menthol: dodecanoic acid-based DES is more stable than DL-menthol: octanoic acid-based DES, in an aqueous environment.

3.3.1.6 Mean Square Displacement (MSD) and Diffusion Coefficient

Figure 3.8 illustrates the mean square displacement (MSD) plot where three-dimensional Einstein's equation is used to calculate the self-diffusion coefficient (D). This is based on the molecule's mean square displacement (MSD). It is the estimation of the relative mobility as well as the transport behaviour of a particular species throughout the system with respect to time. It is mathematically expressed as

$$D = \frac{1}{6} \lim_{t \to \infty} \frac{d}{dt} \langle \sum_{i=1}^{N} |r_i(t) - r_i(0)|^2 \rangle \qquad (3.1)$$

The bracketed element of equation 3.1 is referred to as the MSD of the molecular species. We can compute the self-diffusion coefficient for each species based on the slope of the MSD curve acquired from the simulation. In the previous chapter (chapter 2), a comprehensive discussion of MSD and the self-diffusivity coefficient was provided.[2]

In the current chapter, we have obtained the MSD plot and diffusion coefficients for the components within the system with the help of MD simulation whereby a linear nature of the MSD curve is observed (Figure 3.8). Additionally, the volume occupied by the drug in the DES phase is very low, implying a negligible effect on the viscosity of the DES phase due to the presence of the drug. The linearity in the MSD plots by itself suggests that the Stokes-Einstein relation is valid. However, the presence of two immiscible phases (aqueous and DES) within the system influences the movement of the molecules throughout the system for which the diffusion coefficient values are different along with the simulation runtime (Table 3.3).

In the case of the DES-acetamiprid-water system, the water MSD curve's distinct behaviour throughout the simulation implies the fact that the transport properties are quite unaffected by the presence of other species, as shown in Figures 3.8a-c. The higher degree of linearity in the slope of the MSD curve indicates the relative immiscibility of water in the presence of DL menthol-dodecanoic acid-based DES, implying a strongly-formed phase separation. A hint of nonlinearity in the MSD curve of acetamiprid is witnessed in Figures 3.8a-c. The occurrence of two different phases with distinct properties and the varied molecular mobility and transport properties of acetamiprid within the phases may have contributed to the curve's minor nonlinearity. However, a similarity in their trajectories for both acetamiprid and the DES components indicates comparable transport behaviour.

On the other hand, it can be noticed from Figures 3.8d-f that initially, the curves of DES and imidacloprid were far apart but they gradually converged to the transport property equivalent of water. As the simulation progressed, the relative interactions among the molecules through the phases intensified and the mutual interaction increased at around 40-50 ns of simulation time. The separation of the drug from the water phase with the participation of DL menthol- octanoic acid-based DES can be demonstrated by the nonlinear nature of the water curve [Figure 3.8e]. The reason behind this irregular nonlinearity can be understood by the fact that the water molecule has an affinity towards the imidacloprid molecule along with

an additional truncated yet distinct interaction with the octanoic acid molecule. All these factors combined with the presence of a hydrophobic phase within the system are probably the reason behind such behaviour of water molecules in the system. As the simulation advanced towards completion, it can be witnessed that the transport behaviour of all the components was quite similar representing the bulk system behaviour after the separation as observed in Figure 3.8f.

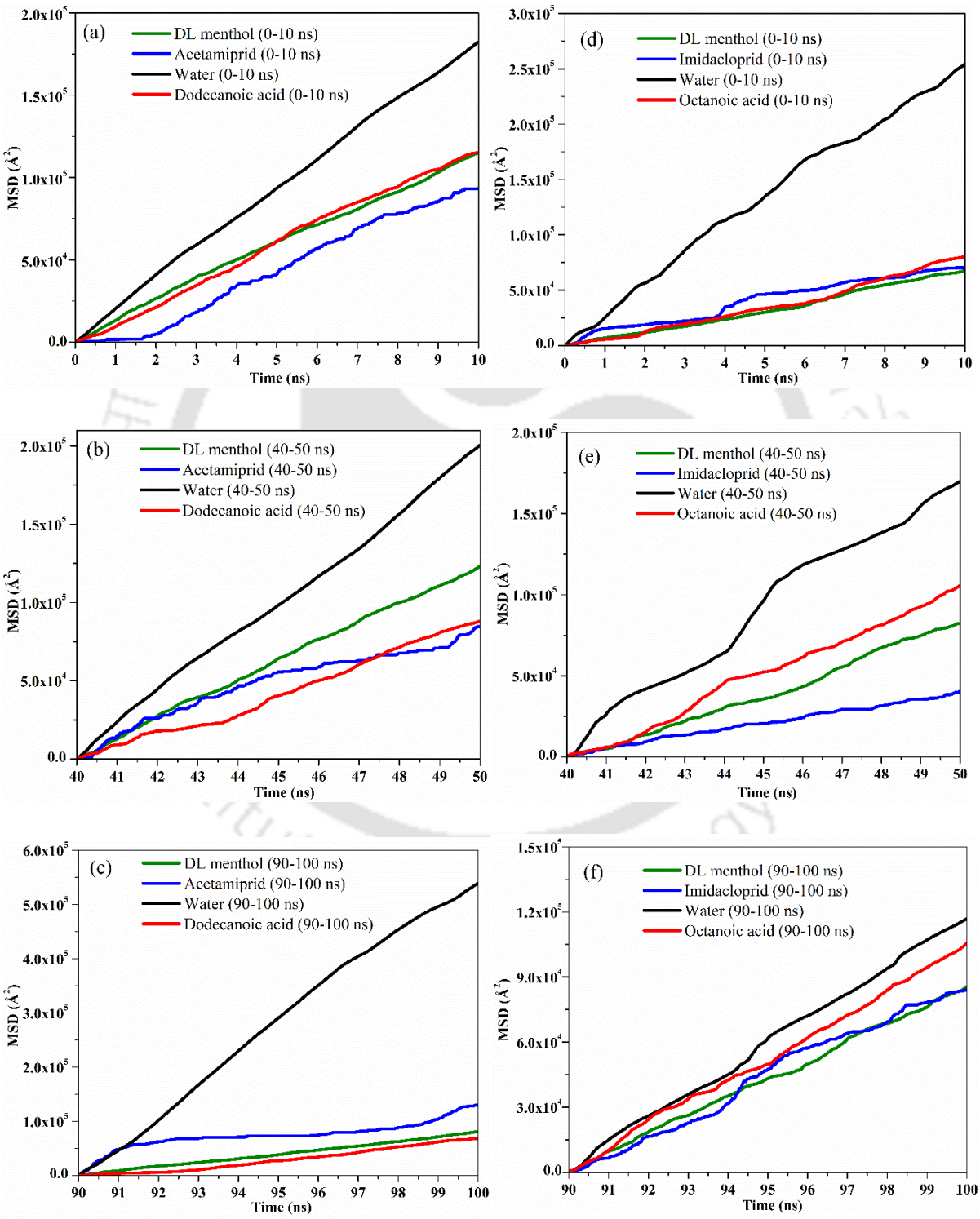

Figure 3.8: MSD plot at three different time intervals of 0-10 ns, 40-50 ns, and 90-100 ns; (a, b, c) for acetamiprid and (d, e, f) for imidacloprid system, respectively.

Diffusion coefficients for all of the species present in the system are represented in Table 3.3. In general, water molecules have a higher diffusion coefficient than other species in all systems, which is consistent with the fact that water has a lower molecular weight than other species. Water diffusion in the acetamiprid system increased gradually until the halfway point of the simulation and then increases at the end. Due to proper phase separation, the hydrophobic components present in the system (especially dodecanoic acid) push the water molecules away which in turn provides a water-rich region within the system improving the water mobility and intramolecular collisions.

Table 3.3: Self-diffusivity of different molecular species of acetamiprid and imidacloprid system, respectively at 298.15 K

System	Molecule species	Diffusion coefficient (D) × 10^{-9} (m^2/s)		
		0-10 ns	**40-50 ns**	**90-100 ns**
DES+ acetamiprid+ water	Water	1.5014	1.6005	4.7103
	Dodecanoic acid	1.0079	0.7561	0.6129
	Acetamiprid	0.9066	0.6166	0.6294
	DL-menthol	0.9283	1.0185	0.6503
DES+ imidacloprid+ water	Water	2.0927	1.4016	0.9685
	Octanoic acid	0.6710	0.8942	0.8561
	Imidacloprid	0.5864	0.3150	0.7575
	DL-menthol	0.5757	0.7120	0.7044

A part of the acetamiprid drug was also present initially to facilitate the water-drug interaction but as the simulation progressed, we noticed a decline in the diffusion coefficient till the half of the simulation, only to improve slightly at the end. One may conclude that since acetamiprid build-up occurred at the interface, (simulation time between 40-50 ns), thereafter the drug molecules were being transported from the aqueous phase to the solvent-rich phase

till the simulation was over. It can be noticed that acetamiprid and dodecanoic acid have diffusion coefficients that are comparable and similar leading to the interaction between the two components. In the case of the acetamiprid system, the diffusion coefficient of DL-menthol was almost unchanged till the half of the simulation only to decrease slightly at the end while in the case of the imidacloprid system, it increased slightly throughout the simulation. In both cases, a close resemblance in terms of the diffusion coefficients of HBA and HBD was witnessed. Imidacloprid diffusivity was found to decrease till 50 ns of simulation time after which it increased. For the initial and final part of the simulation, imidacloprid obtained a diffusion coefficient very close to that of menthol and octanoic acid. The mutual similarity in the transport behaviour and the inherent interaction among the molecules can be considered the reason behind such an outcome. The diffusion coefficient of water decreased throughout the simulation and reached a value very close to that of the other components. Overall, this validated the findings obtained by MSD calculation as shown in Figure 3.8f.

3.3.1.7 Selectivity of Solvents and Extractive Characteristics of the Pesticides

The extractive characteristics of pesticides, such as distribution coefficient (β), selectivity (S), and extraction efficiency (%EE), shown in Table 3.2, were evaluated using the following equations for both the acetamiprid and imidacloprid systems.

$$\beta = \frac{x^{E}\text{pesticide}}{x^{R}\text{pesticide}} \tag{3.2}$$

$$S = \beta\text{pesticide} / \beta\text{water} = \frac{\frac{x^{E}\text{pesticide}}{x^{R}\text{pesticide}}}{\frac{x^{E}\text{water}}{x^{R}\text{water}}} \tag{3.3}$$

$$\%EE = [(C_0 - C)/C_0] \times 100 \tag{3.4}$$

Here,

x^{E}pesticide and x^{R}pesticide = mole fractions of the pesticide (acetamiprid and imidacloprid, respectively) in DES-rich and water-rich phases, respectively.

x^{E}water and x^{R}water = mole fractions of water in DES-rich and water-rich phases, respectively.

C_o = concentration of pesticide in the aqueous phase before extraction (ppm or mg/L)

C = concentration of pesticide in the aqueous phase after extraction (ppm or mg/L)

The DES systems selected in the current chapter were obtained from the systems which gave the highest extraction efficiency.[1] The evaluation techniques of the extraction properties such as extraction efficiency and distribution ratio are similar to those presented in the previous chapter.[2] Here we obtained the extraction efficiency of nitenpyram followed by the distribution ratio with the help of MD simulation. For the benchmarking study, we have reproduced the extraction efficiency of nitenpyram in the DES (DL-Menthol: octanoic Acid). The experimental and predicted values of the distribution ratio of nitenpyram are 0.67 and 0.71, respectively indicating an excellent agreement.

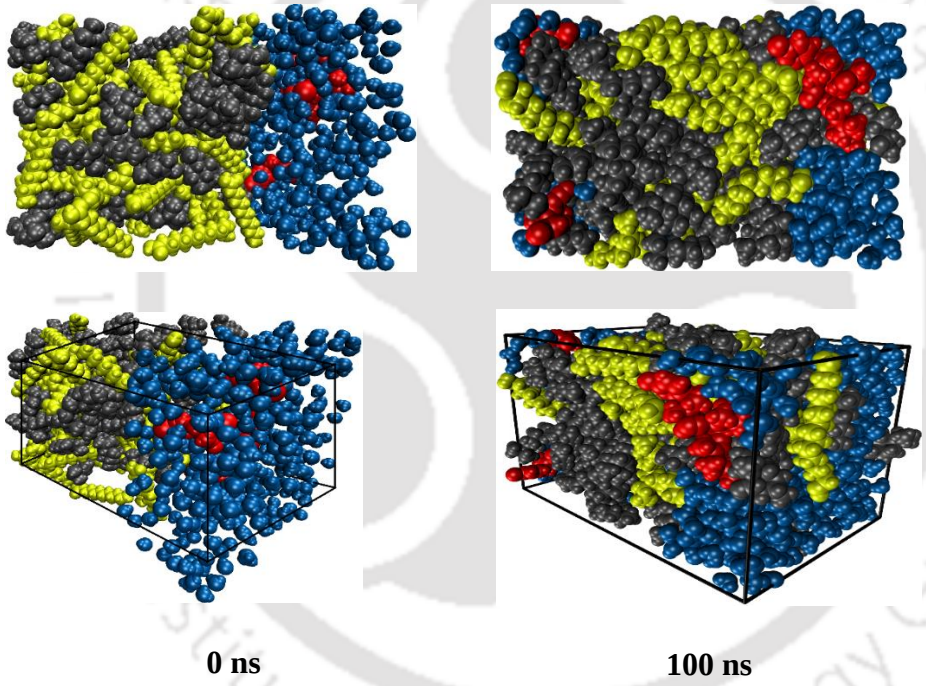

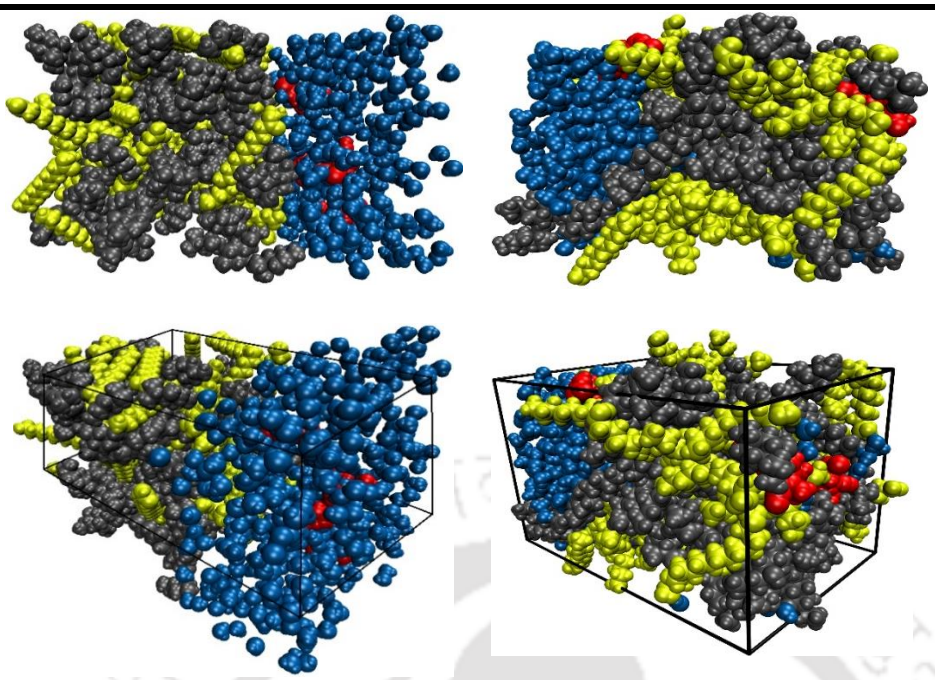

Figure 3.9: System snapshots of (a) acetamiprid and (b) imidacloprid at 0 ns and 100 ns [grey, menthol compound (HBA); yellow, dodecanoic acid and octanoic acid compound, for acetamiprid and imidacloprid system, respectively (HBD); red, acetamiprid and imidacloprid compound, respectively; blue, water compound].

As shown in Figure 3.9, it can be observed that the pesticide initially present in the aqueous phase has a greater tendency to transport to the DES phase for both drug species. The distribution snapshots are captured with the box-included and box-excluded mode at the time step of 0 ns (left part of each figure) and 100 ns (right part of each figure). The configuration of the distribution provided a general overview of each system where the hydrophobic characteristics of the DESs can easily be observed and the affinity of the pesticides towards the DES solvent-rich phase can be detected. For example, the DES molecules (in grey and yellow) as a whole maintained their integrity separate from water (in blue) even after a long simulation run. A negligible quantity of molecular leaching of the DES components towards the water phase was observed in both systems due to the hydrophobicity of the components. The pesticide entities (in red) were placed inside the water box initially, however, as the experiment progressed, their presence to a higher extent can be identified in the DES side of the box.

A higher β value signifies a higher distribution of pesticides from the water phase to the DES phase. This represents a higher selectivity enabling the higher ability of DES in

extracting pesticides from the aqueous phase. The simulated extraction efficiency of 75% and 69% were obtained for acetamiprid and imidacloprid, respectively which is within a 3-5% variation from the experimental values. The reason for the change might be explained by the fact that the simulation size used in this experiment is significantly smaller than the scale used in real-world experiments, as well as the likelihood of human error when estimating the number of molecules from the simulation. To maintain a suitable balance between the computational cost-time and the degree of accuracy of the result, we have considered a miniaturized mimic of the actual experiments in the simulation box. Additionally, there is always a possibility of improving the results by selecting a higher-order method and basis set which could reduce the discrepancies between the experimental and the simulation findings. However, it can be said unequivocally that the findings in this investigation regarding pesticide extraction are very much in agreement with the simulation. The distribution coefficient (β) obtained by simulation are 8.67 and 6.25, respectively, whereas, the attained selectivity (S) are 102.38 and 71.86, for acetamiprid and imidacloprid systems, respectively. Higher selectivity values suggest that the DESs are highly capable of extracting these pesticides from the aqueous phase. The distribution ratio can be formulated as the ratio of the concentration of the pesticide in the DES-rich phase to the concentration of the same pesticide in the water-rich phase. The distribution ratio obtained from the simulation was 3.17 and 2.48 for acetamiprid and imidacloprid, respectively, which was quite comparable to that of the experiments[1] (3.43 and 2.67, respectively).

3.3.2 Quantum Chemical Analysis

3.3.2.1 DFT Analysis

Initially, DFT calculations for optimization of the DESs and pesticides were performed at the M06-2X/6-311+G(d,p)[21] level of theory. The optimized geometries of [DL-menthol-octanoic acid] (DES2) and [DL-menthol- dodecanoic acid] (DES1) are displayed in Figures 3.10a, b. One molecule each of DL-menthol and dodecanoic acid was shown in the case of DES1 optimization in Figure 3.10b. The reason behind this was to compare HBA-HBD interactions within DES1 and DES2. From the optimized structures of the DESs, it can be concurred that strong HBA-HBD interactions lead to the formation of these DESs. In both the DESs, simultaneous O…H hydrogen bonding was witnessed between the H atom of menthol and the O atom of the carboxyl group of the acids. The distance of this interaction was determined to be 2.053 Å and 2.061 Å for DES2 and DES1, respectively which are in close agreement with the distance achieved from the RDF data obtained earlier in the ‘Radial

Distribution Functions' section. The other O (menthol)…H (acid) distance was revealed to be 1.77 Å for both DESs. Overall, it is evident that the non-bonded interaction, mainly hydrogen bonding plays a major role in the formation of these neutral DESs. Figures 3.10c and d present the DES2-imidacloprid complex where the DES components were organized in intermolecular and intramolecular arrangement, respectively, around the central imidacloprid molecule. In the former configuration (Figure 3.10c), the HBA (menthol) and the HBD (octanoic acid) of the DES2 are not a part of the individual DES but as individual moieties namely, HBA or HBD which form an intermolecular arrangement. In comparison, the intramolecular configuration (Figure 3.10d) is adapted from the combination of the pesticide molecule with a single optimized DES2 structure. Both of these configurations are adopted due to the presence of multiple donor-acceptor active sites within the components. As mentioned in the earlier sections, the imidazolidine ring largely contributed towards the active interaction site for both the inter and the intra arrangements.

(a)

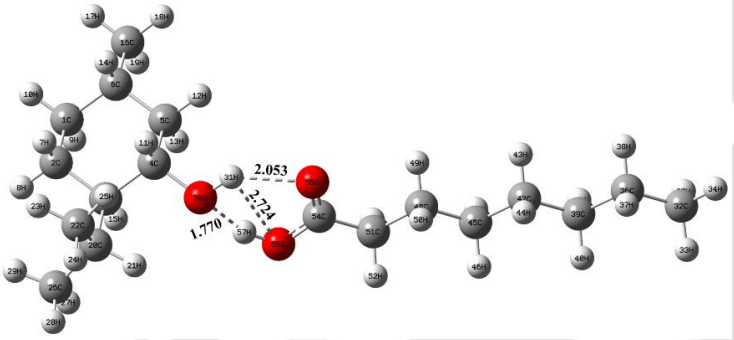

(b)

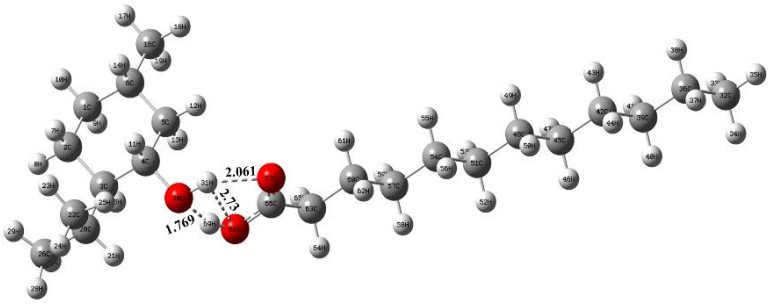

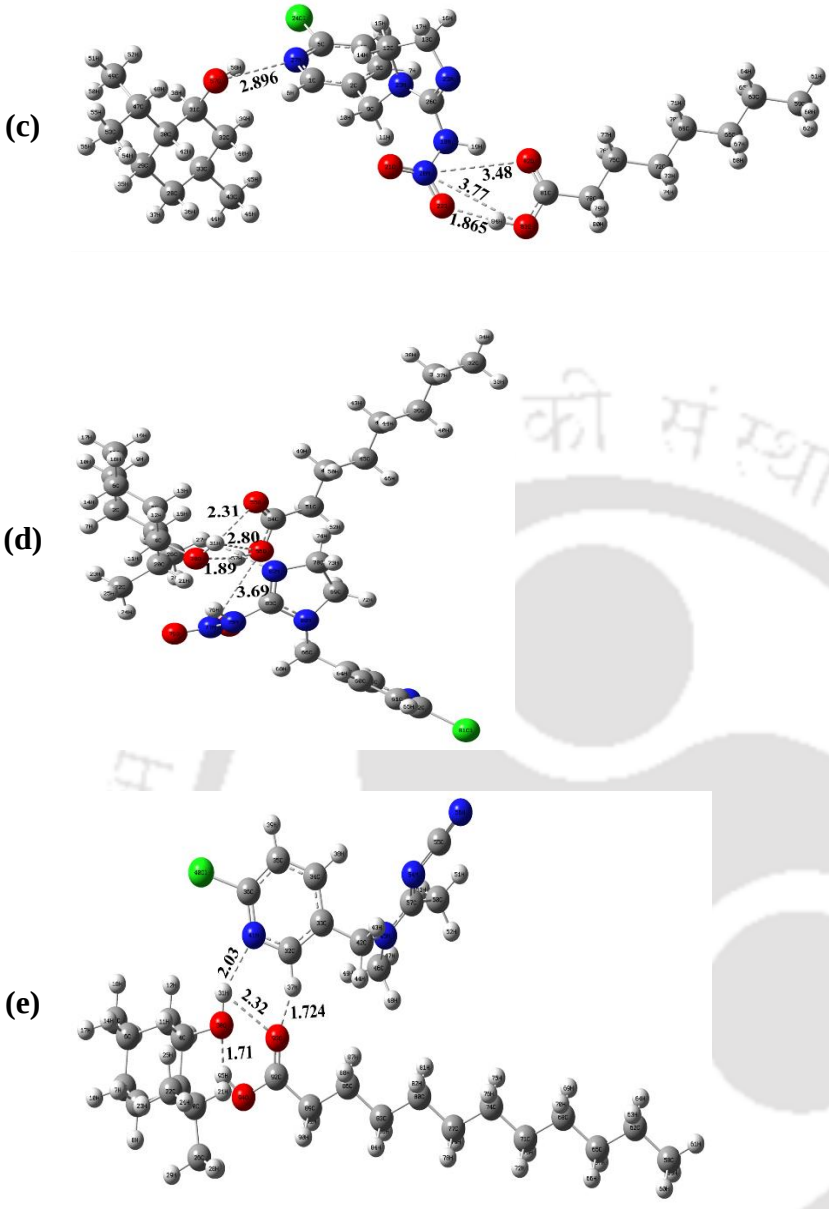

Figure 3.10: Optimized geometries at the M06-2X level of theory of (a) DL-menthol- octanoic acid (DES2), (b) DL-menthol- dodecanoic acid (DES1), (c) [DL-menthol- octanoic acid]/ [imidacloprid] (DES-intermolecular), (d) [DL-menthol- octanoic acid]/ [imidacloprid] (DES-intramolecular), and (e) [DL-menthol- dodecanoic acid]/ [acetamiprid].

In Figure 3.10c, the O (menthol)…N (cyclopyridine part of imidacloprid) distance appeared at 2.896 Å and N (imidazolidine part of imidacloprid) …O (octanoic acid) distances ranges between 3.48 to 3.77 Å which are consistent with the RDF and CDF results as shown in Figures 3.3 and 3.5, respectively. In the case of the intramolecular arrangement (Figure

3.10d), the distance between the hydroxyl H atom of menthol and the O atom of the carboxyl group of octanoic acid is increased to 2.31 Å. Similarly, the O (menthol)…H (octanoic acid) distance is seen to increase to 1.89 Å. Both these distances were lower in the optimized DES structure in Figure 3.10a, suggesting a slight relaxation of the DES-forming interaction between the HBA and the HBD components. It also put forward the enhanced interaction of imidacloprid with both the DES-forming components where the distance between the N atom attached to the imidazolidine ring and the O atom of the octanoic acid was recorded as 3.69 Å. This concurred with the finding of the RDF as presented in Figure 3.3c.

For the acetamiprid system, the optimized structure of the intramolecular configuration is presented in Figure 3.10e. Here also, the HBA-HBD interaction between the DES components reduces slightly because of the enhanced interaction of acetamiprid and DES. This is due to the presence of bulky molecular groups and a long-tailed dodecanoic acid. The distance between the N atom of the cyclopyridine group of acetamiprid and the hydroxyl H atom of DL-menthol has been obtained as 2.03 Å. The dodecanoic acid is also arranged very close to the pesticide molecule to incorporate non-bonded interaction among themselves. Overall, the DFT analysis of the DES-pesticide systems confirmed the intensive and complex mode of interaction between the pesticide and the DESs and also establishes the DES integrity when present with additional components despite having interactions with other moieties.

3.3.2.2 NBO Analysis

Two different DFT approaches, namely B3LYP and M06-2X were used in the calculation of the CT (charge transfer) process in Gaussian 09[8]. These are presented in Tables 3.4 and 3.5. DL-menthol (HBA) and the fatty acids (HBD) acquire positive and negative charges, respectively, when no other compounds are present in the system. However, the opposite behaviour is observed when the pesticide compounds interact with the DES where the HBA attains a negative charge while the HBDs develop a positive charge [Table 3.5].

The partial charges on each of the pesticide molecules in a DES-free environment are zero as the pesticides are neutral molecules. On account of this, the NBO charges associated with the neutral pesticide molecules are taken as zero. As the pesticide molecules are placed in a DES or any other solvent, the charge transfer between the pesticide and the solvent molecules takes place and non-zero partial charges develop on the individual molecules based on the electron density acquired by them.

Table 3.4: Calculated NBO charge on the pesticides in the presence and absence of the respective DES

	Acetamiprid		Imidacloprid	
	B3LYP	**M062X**	**B3LYP**	**M062X**
No DES	0	0	0	0
DES1 [DLM-DODEC]	-0.0056	-0.012	NA	NA
DES2 [DLM-OCT]	NA	NA	-0.0042	-0.0109

The presence of the pesticides initiates a complex of non-bonded interactions along with the CT (charge transfer) process between itself and the DES components, for both DES1 [DLM-DODEC] and DES2 [DLM-OCT]. After contact with the DES, both the pesticide components acquired a small negative charge, imparting a positive charge on the DES as a whole. This happens due to the rise in electron density of the pesticides upon interaction with the DESs after transporting from the aqueous phase to the DES-rich phase. As a result, charge transfer occurs in the direction of DES to the pesticide molecule in each system. Since no charged molecular entities were present in both the systems, one can witness minor charge transfer between the pesticides and the DES which ensures the nonbonded interactions such as hydrogen bonding and van der Waals interactions are dominant as compared to the electrostatic interactions.

Table 3.5: Calculated NBO Charges on the components of DESs in the presence and absence of respective pesticides

Component	Acetamiprid		Imidacloprid		Only DES	
Pairs	**B3LYP**	**M06-2X**	**B3LYP**	**M06-2X**	**B3LYP**	**M06-2X**
Charge on the hydrogen bond acceptor (HBA) of DES in DES-pesticide combination						
DES1 [DLM-DODEC]	-0.0149	-0.0078	NA	NA	0.0224	0.02593
DES2 [DLM-OCT]	NA	NA	-0.0155	-0.0083	0.0225	0.0261
Charge on the hydrogen bond donor (HBD) of DES in DES-pesticide combination						
DES1 [DLM-DODEC]	0.0205	0.0198	NA	NA	-0.0224	-0.02593
DES2 [DLM-OCT]	NA	NA	0.0197	0.0192	-0.0225	-0.0261

The HBDs lose electron density upon formation of the DES-pesticide complex whereas the electron density of the HBA rises. In the case of the imidacloprid system, the introduction of the pesticide gives rise to the formation of a complex CT process among the constituents of the DES. Multiple hydrogen bond acceptor sites present both in acetamiprid and imidacloprid due to the existence of localized electron lone pairs contribute to numerous HBA-HBD interactions within the system. Both DL-menthol and octanoic acid contain a single HBD site each, whereas the HBA count in each of them is 1 (one) and 2 (two), respectively. As a result, all of the components present in the system were able to form donor-acceptor interaction properly.

3.3.2.3 FMO Analysis

3.3.2.3.1 FMO Analysis of the Pure DESs and the Pure Pesticides

The hydrogen bonding and the electrostatic interactions were elaboratively discussed in the previous sections involving NAMD simulation. In this section, Frontier Molecular Orbital (FMO) analysis has been carried out which is considered to be an effective approach to obtain the acceptor-donor interaction along with the molecular stability and reactivity employing evaluation of the HOMO-LUMO orbital analysis.[22] The current section concentrates on the analysis of the interaction of the HOMO and LUMO species of the two DESs (DL-menthol: octanoic acid and DL-menthol: dodecanoic acid) and the pesticides (acetamiprid and imidacloprid). HOMO and LUMO are the abbreviated forms of the ‘Highest Occupied Molecular Orbital’ and the ‘Lowest Unoccupied Molecular Orbital’, respectively. The HOMO is logically viewed as a nucleophilic or electron-donating tendency, while the LUMO is an electrophilic or electron-accepting tendency of a species. The HOMO-LUMO energy gap of a molecule may be used to calculate the amount of energy required for adding or removing electrons from a molecule. The higher the HOMO-LUMO energy gap, the greater the molecular kinetic stability and the lesser the molecular reactivity.

The softness and hardness of a molecular species are also correlated with the HOMO-LUMO bandgap energy. Higher molecular hardness (η) suggests higher stability of a molecule which is associated with a larger HOMO-LUMO energy gap. The HOMO-LUMO energy gap and the global hardness (η) are higher for acetamiprid than that of imidacloprid pesticide suggesting that acetamiprid is more stable than imidacloprid and impedes the charge transfer process by resisting the change in electronic configuration and distribution. In other words, it

can be stated that acetamiprid molecules require more energy than imidacloprid to get to an excited state. This is the reason why despite being more soluble in water, the acetamiprid extraction was found to be better than that of imidacloprid. Interestingly, a lower negative value of LUMO energy (high LUMO energy) in the case of acetamiprid confirmed better hydrogen bond donor property as compared to imidacloprid. Both the pesticides have comparable hydrogen bond acceptor characteristics as can be shown by the relatively closer HOMO orbital energy values in Table C.2 (Appendix C).

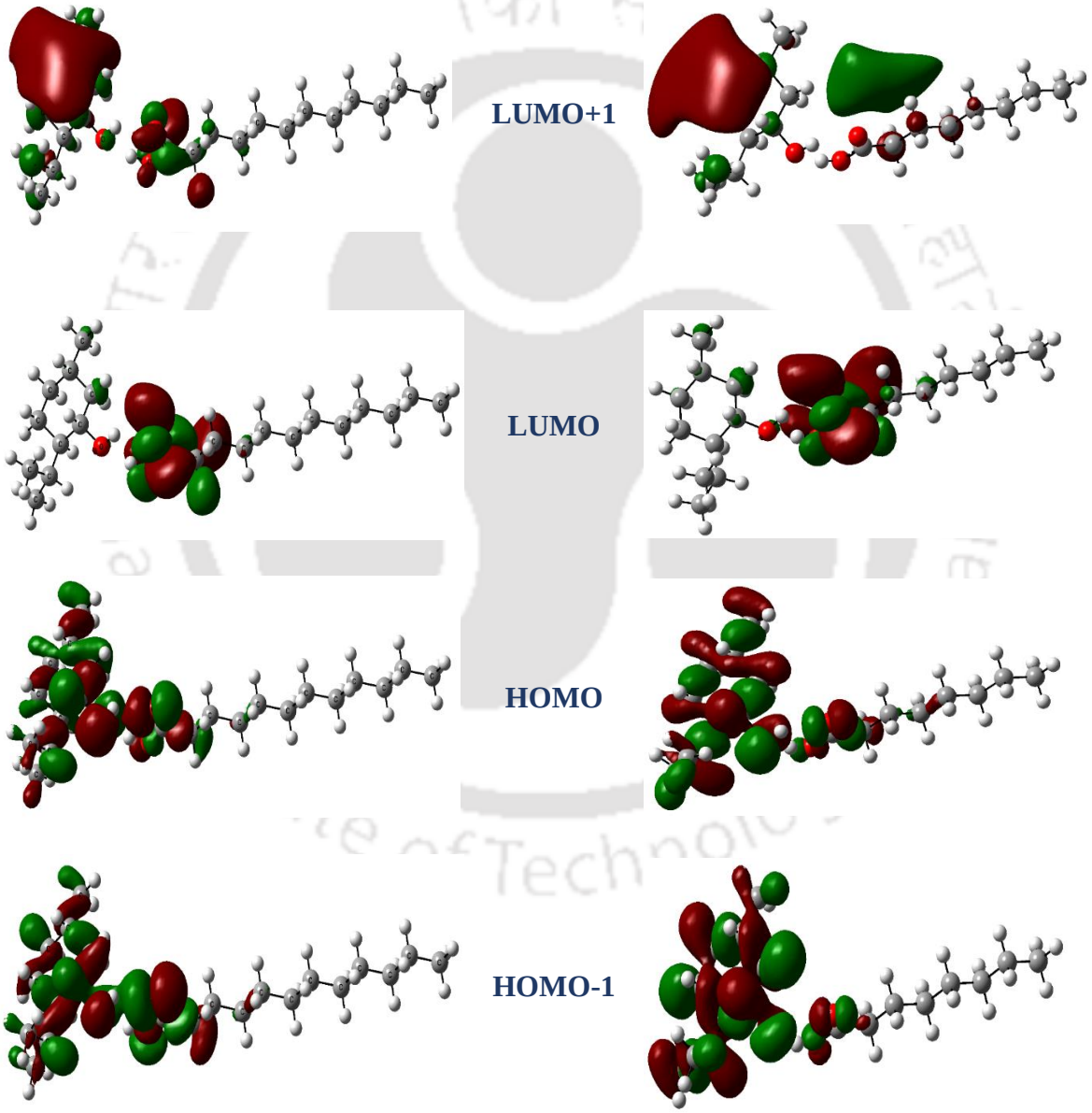

(a) DL-menthol: dodecanoic acid **(b) DL-menthol: octanoic acid**

Figure 3.11: HOMO−LUMO iso-surfaces of DESs, (a) DL-menthol: dodecanoic acid and (b) DL-menthol: octanoic acid.

The FMO diagrams of the pure pesticides and the DESs along with their ground and excited-state molecular orbitals are shown in Figure C.2 (see Appendix C) and Figure 3.11. The iso-surfaces were represented in green and red contours to highlight the positive and negative lobes of the HOMO and LUMO orbitals, respectively. From Figure B.2a, it can be noticed that the HOMO electrons were predominantly located around the imidazolidine ring, whereas the LUMO electrons were distributed around the part consisting of oxygen atoms associated with the imidazolidine ring. The occurrence of a higher HBA count than that of the HBD in the imidacloprid molecule can be validated by the dense envelope of the HOMOs. In Figure C.2b (see Appendix C), the contrast between the HOMO and LUMO species of acetamiprid can easily be spotted. The presence of localized electron lone pair in the nitrogen atoms in the acetamidine part contributed to the electron-donating tendency and hence formed the HOMOs, while the electronegative chlorine atom attracts the electron cloud of the cyclopyridine region making it a favourable electron-accepting location thus constituting the LUMO species. The orbital electronic configuration for DL menthol-dodecanoic acid and DL menthol-octanoic acid DESs were presented in Figures 3.11a and b. Interestingly, it can be observed that the HOMO comes from the HBA (DL-menthol) and the LUMO from the HBDs (octanoic and dodecanoic acid, respectively). In both cases, the HOMO electrons are predominantly clustered around the DL-menthol molecule which acted as an HBA due to the nucleophilic characteristics of the HOMO electrons. The LUMO electrons are primarily located over the carboxyl functional group present in the long-chain fatty acids (C_8 and C_{12}) acting as HBD. The presence of localized electron lone pairs in the oxygen atoms of the carboxylic acids contributed significantly towards the stronger HOMO-LUMO interaction between the DES-forming components. Keeping the non-ionic nature of the constituents of the DESs, we presented the HOMO-1 and the LUMO+1 species for both cases to ensure an accurate understanding of the electronic interaction from the ground state to an excited state. Overall, the findings are fairly in coherence with the conventional understanding of the HBA-HBD interactions in forming a DES.

Upon investigation of the HOMO- LUMO energies of the DESs, as presented in Table C.2 (Appendix C), one can observe that the band energy gap between the HOMO and the LUMO species of DL-menthol: dodecanoic acid-based DES (0.34795 Hartree) was slightly

higher than that of DL-menthol: octanoic acid-based DES (0.34772 Hartree). This confirms higher stability and lesser reactivity of the former as compared to the latter. Nevertheless, the narrow difference in the bandgap energy between the two DESs and the similarity in the global hardness (η) values established the higher chemical stability of both the hydrophobic DESs. Hence, both DESs were found to be having a strong HBA-HBD interaction that was also established by MD simulation in the earlier section. However, this chemical stability may not necessarily imply the stability of a DES in presence of water, but the inherent kinetic stability of the species to resist the transfer of the electrons from the ground state to an excited state conformation when subjected to an external energy source. In the previous chapter (chapter 2), the hydrophobic nature of these DESs was also confirmed and thoroughly elucidated.[2]

3.3.2.3.2 FMO Analysis of the DESs with Pesticides

FMO studies of DESs with pesticides were performed to determine the stability and the reactivity of the DES-pesticide clusters considering two different theories namely B3LYP and M06-2X to obtain a comparative analysis. Figure 3.12 and Figure 3.13 displayed the combined iso-surfaces of the orbitals consisting of the HOMO- LUMO for DL menthol-octanoic acid (DES2)-imidacloprid and DL menthol-dodecanoic acid (DES1)-acetamiprid systems, respectively. In the case of the imidacloprid system, the HOMO electrons are located on the HBA component of DES i.e., DL-menthol, whereas the LUMO electrons are located on the imidacloprid molecule. The presence of a hydrogen atom attached to one nitrogen atom in the imidazolidine ring of imidacloprid is attributed to the hydrogen bond donor interacting with the HOMO electrons of DL-menthol. The HOMOs, as they are occupied by electrons, generally act as favourable locations for electron transfer to another electron-deficient orbital. In this study, we have shown two different possible complex arrangements for the imidacloprid+ DES2 system where they were segregated as 'DES-intermolecular' and 'DES-intramolecular' assemblies. The orbital energy gap for imidacloprid+ DES2 (intra) complex (0.2685 Hartree) is higher than that of pure imidacloprid (0.26664 Hartree) suggesting a stable and favourable DES-pesticide interaction as presented in Table C.2 (Appendix C). On the other hand, a large deviation in the band energy gap can be noticed between DES2 (0.34772 Hartree) and the imidacloprid+ DES2 system (0.2685 Hartree). On appropriate scrutiny, one can understand that the presence of the pesticide brought about higher interaction with the individual DES-forming constituents leading to the reduction in the interaction between the HBA (DL-menthol) and the HBD (octanoic acid) itself. The 'DES-intermolecular' arrangement was considered here to illustrate the HOMO-LUMO iso-surfaces in Figure 3.12 since the arrangement can properly

emphasize the molecular orbitals from different sites of the pesticide without being sterically hindered.

In the same way, we have obtained the molecular orbitals from the optimized geometrical arrangement of acetamiprid+ DES1 as shown in Figure 3.13. However, only the DES-intramolecular arrangement was obtained in this case. No intermolecular arrangements were found to be present for these components. A probable explanation for that might be the presence of two bulky and large molecules such as menthol and dodecanoic acid along with acetamiprid in the system for which steric hindrance could play a vital role in obstructing the molecules to be placed at suitable sites. Here too, a stable and favourable DES-pesticide interaction can be witnessed as the orbital energy gap for acetamiprid+ DES1 complex (0.2801 Hartree) is higher than that of pure acetamiprid (0.27924 Hartree) [Table C.2 (Appendix C)]. The menthol-dodecanoic acid interaction was found to be quite intact in the complex system even though it had higher DES-pesticide interaction.

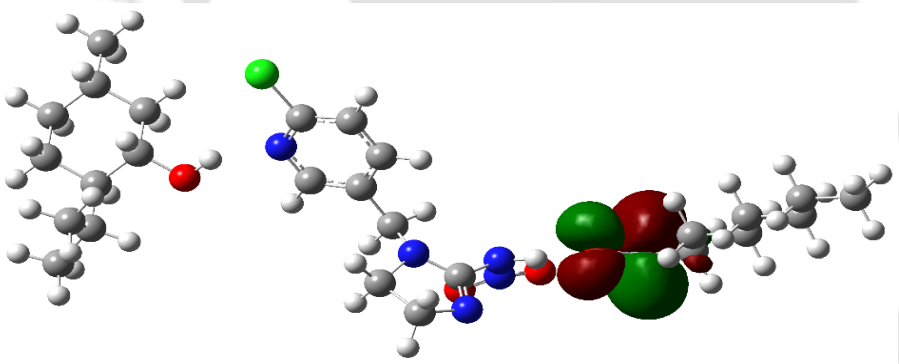

LUMO+1

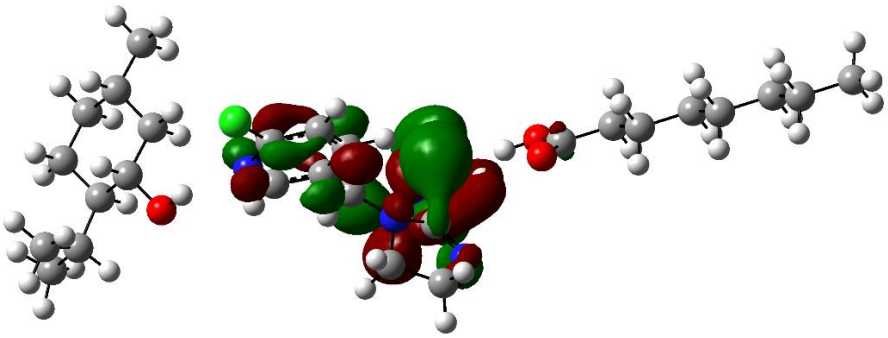

LUMO

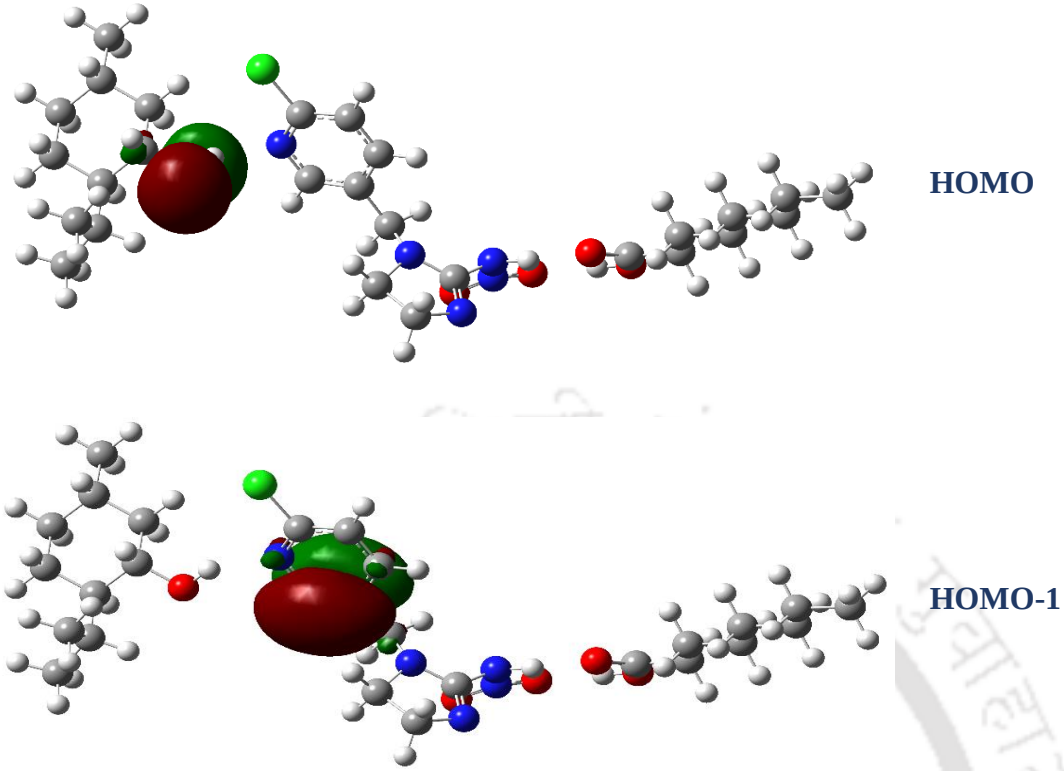

DL menthol- octanoic acid- imidacloprid

Figure 3.12: HOMO−LUMO iso-surfaces of DL menthol- octanoic acid- imidacloprid complex (DES intermolecular) moiety.

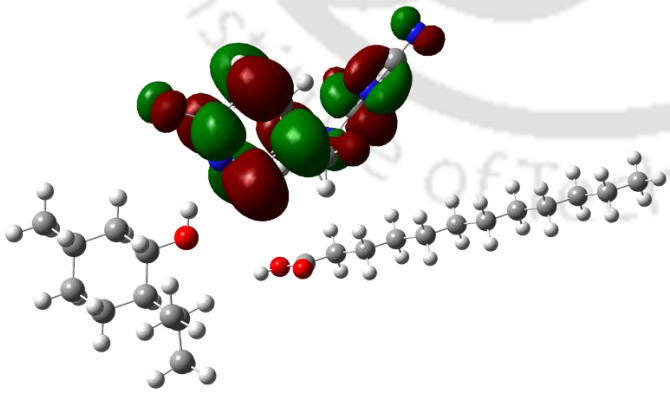

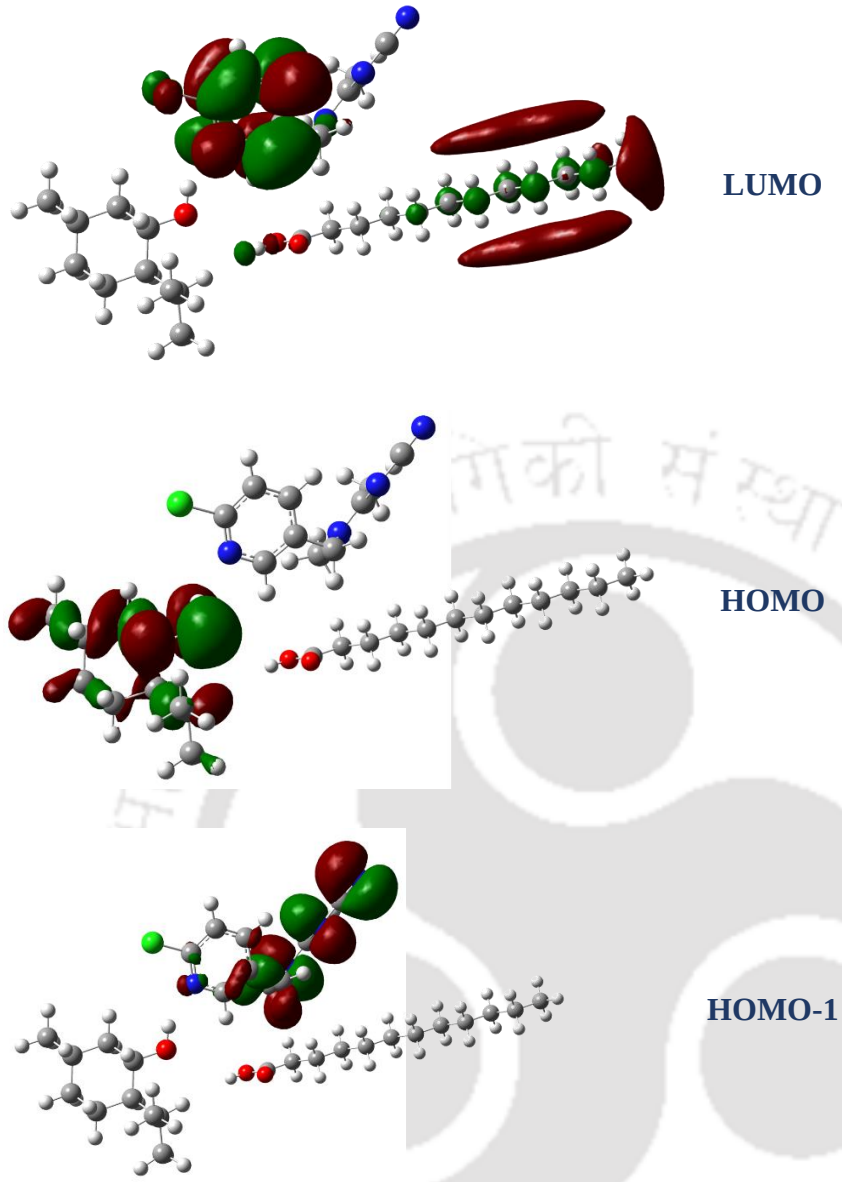

Figure 3.13: HOMO−LUMO iso-surfaces of DL menthol- dodecanoic acid- acetamiprid complex.

The HOMOs were located in DL-menthol containing a localized electron lone pair in the oxygen atom. The LUMO and LUMO+1 orbital was predominantly spread over the acetamiprid molecule mainly in the acetamidine region as can be seen in Figure 3.13. This fixture can be attributed to the available positively charged N atoms in the acetamidine part acting as a cationic moiety. A part of the dodecanoic acid was also involved in forming the LUMO orbitals that confirmed the HBA-HBD stability between the DES-forming constituents.

For both the pesticide systems, unoccupied orbitals such as second-highest (HOMO-1) and second-lowest (LUMO+1) along with the subsequent orbital gap energy were also obtained by FMO analysis. Overall, the FMO analysis of the pesticides and the DESs brought molecular-level insights into the light where the HOMOs of the menthol molecule get interacted with the LUMOs of the pesticides and the carboxylic acids. This establishes a more stable complex which turns out to be effective in the extraction of the pesticides from the aqueous phase. One noteworthy point to be mentioned here is that the DFT and the FMO study does not incorporate the presence of water molecule in the system. The primary reason behind that was to study the DES-pesticide characteristics essentially in the DES-rich phase where the negligible presence of water can be witnessed. The DFT study including water molecules in the water phase and the subsequent extraction and transportation of pesticides in the DES phase can be a potential task in the prospects to understand the systems in a better and more conclusive approach.

3.4 Extraction Mechanism for the Proposed Configurations

In this work, two different interactive assemblies for DES-pesticide complex formation, namely ‘intermolecular’ and ‘intramolecular’ arrangements have been proposed and the findings were comprehensively substantiated with the help of MD simulation and QC calculation. These arrangements are not conflicting but are complementary to each other and together they complete the whole mechanism of the extraction process for the imidacloprid system. Both the HBA and HBD play a significant role in extracting acetamiprid and imidacloprid from water. As per the observation from non-bonded interaction energy obtained by MD, the HBDs from both systems are interacting predominantly with the respective pesticides (Figure 3.2). The presence of non-ionic and large-sized compounds implies the dominating role of van der Waals interaction as compared to the electrostatic component. Initially, two immiscible phases appear in the experiments, one of which is pure DES and the other an aqueous phase containing pesticides in ppm content. During mixing, both phases mix whereby the pesticide molecules get preferentially attracted to the DES components based on their relative affinity. The interfacial tension between DES and water was measured to be less than pure water surface and the affinitive non-bonded interaction of the DES-pesticide complex enables the cross-over of the solute (pesticide) from the aqueous to DES phase. The dispersion forces are the primary force behind these interactions. After the successful attachment and the formation of the DES-pesticide complex, the inherent hydrophobic nature of the DES components inhibits further re-attachment between pesticide and water. This is further facilitated by the substantial difference in density and viscosity of the phases.

This implies that the fatty acid molecules i.e., octanoic and dodecanoic acid attract the chemically active sites of imidacloprid and acetamiprid, respectively towards them to promote higher interaction. O (octanoic acid) …N (imidacloprid) hydrogen bonding interaction occurs at ~3.69 Å agreeing both the RDF (from MD) and the optimized structures (from QC), whereas, menthol …imidacloprid interaction occurs at ~2.896 Å. It can be referred that the presence of octanoic acid molecules in the vicinity of imidacloprid is much more than menthol molecules which are also evidenced by the higher number of average hydrogen bonding (Figure 3.7b). The imidazolidine moiety within the imidacloprid molecule possesses multiple donor-acceptor sites, thereby involving multiple interactions with the HBDs. In the interaction, a small fraction (Table 3.4) of charge is transferred from DES to imidacloprid. The HBA, HBD and the pesticide form a complex structure through a hydrogen-bonding network and thus the pesticide diffuses from the water phase to the DES phase.

Similar affinitive tendency and charge transfer behaviour are observed among acetamiprid and the DES components (menthol and dodecanoic acid) (Table 3.4). The large and hydrophobic dodecanoic acid molecules due to their non-affinity with water initiate the attachment of acetamidine moiety within the acetamiprid molecule with both menthol and dodecanoic acid. This enables the formation of the DES- acetamiprid complex arrangement (Figure 3.10e). The combined average hydrogen bonding between menthol- acetamiprid and dodecanoic acid-acetamiprid is nearly double as compared to water- acetamiprid (Figure 3.7a). Thus menthol (HBA) comes closer to acetamiprid to have affinitive N (acetamiprid) …H (menthol) interaction as evidenced by RDF (Figure 3.3a) and further confirmed by the HOMO-LUMO orbital analysis (Figure 3.13). Here, as depicted, the HOMO orbital of menthol and LUMO orbital of acetamiprid are involved in the interaction. Overall, the proposed extraction mechanism has been validated and confirmed with multiscale simulation results in combination with the experiments. This provides insight with respect to acetamiprid and imidacloprid extraction with the help of menthol-fatty acid-based DESs.

3.5 Conclusion

Molecular Dynamics simulation was conducted to obtain insight into the extraction phenomena of acetamiprid and imidacloprid pesticides from an aqueous environment with DL-menthol: dodecanoic acid (2:1) and DL-menthol: octanoic acid (1:1), respectively. Furthermore, the van der Waals interaction of HBD- pesticide was higher than its electrostatic components for both pesticides. Enhanced polarizability was introduced in presence of the

hydrophobic tails of octanoic acid and dodecanoic acid which increases the vdW interaction as compared to the electrostatic one. The RDF and CDF plots suggested the formation of C−N···H bond between DL-menthol and acetamiprid at a distance of 2 Å and an angular range of 140 to 180°. Similarly, higher interaction was witnessed between imidacloprid and DL-menthol at 0-60° and from 140-180° to form hydrogen bonding between the molecules. In SDF, water molecules were having a long-range weak interaction at ~3.5 Å leading to a minimized interaction with the pesticide. The relative H-bonding number was found to be in the order of imidacloprid- octanoic acid (0.92) > DL menthol- imidacloprid (0.71) > imidacloprid- water (0.48) for imidacloprid system. In case of acetamiprid system, the order attained was acetamiprid-water (~0.185) > acetamiprid- dodecanoic acid (~0.175) > DL menthol-acetamiprid (~0.125). MSD plots supported the higher affinity of the pesticides towards the DES-rich phase for both the systems which was validated by the findings from the diffusion coefficient analysis where similar diffusive properties were observed between the pesticide and the DES components. The distribution ratios for both pesticides were obtained and closely matched with the experimental results. The extraction efficiency of 75% and 69% were achieved by the MD simulation which was in excellent agreement with that of the experiments.

The QC calculations provided the optimized geometrical arrangements of the DESs and the DES-pesticide complex forms. Interaction between the DES-forming constituents was observed with O (HBA-menthol) …H (HBD-organic acid) hydrogen bonding formation at a distance of 1.77 Å in both DESs. A slight increase in the O (HBA)…H (HBD) distance authenticated the enhanced interaction between DES and pesticide. The non-bonded interaction distances attained between the DES and pesticide in the optimized clusters were ranging from 2.896 to 3.77 Å for imidacloprid, and from 1.724 to 2.03 Å for acetamiprid, which are confirmed by MD simulation. In NBO analysis, both the pesticide components acquired a small negative charge, imparting a positive charge on the DES due to the rise in electron density of the pesticides upon interaction with the DESs in the DES-rich phase. Charge transfer occurred in the direction of DES to the pesticide molecule in each system. FMO analysis implied that the HOMO-LUMO band energy gap of DL-menthol: dodecanoic acid DES (0.34795 Hartree) was slightly higher than that of DL-menthol: octanoic acid DES (0.34772 Hartree) confirming the higher stability and lesser reactivity of the former as compared to the latter. In the DES-pesticide complex, DL-menthol provided the HOMO sites, whereas LUMOs were obtained from the pesticide molecules suggesting a relatively stronger DES-pesticide complex interaction leading to the higher extraction efficiency of the pesticides from the water

environment. Both the pesticides attained a higher HOMO-LUMO energy gap within the supermolecule approach (complex formation) as compared to its pure state bandgap energy supporting a stable formation with the DES.

References

[1] C. Florindo, L.C. Branco, I.M. Marrucho, Development of hydrophobic deep eutectic solvents for extraction of pesticides from aqueous environments, Fluid Phase Equilib. 448 (2017) 135–142. https://doi.org/10.1016/j.fluid.2017.04.002.

[2] N. Paul, T. Banerjee, P.K. Naik, B.D. Ribeiro, P.S.G. Pattader, I.M. Marrucho, Molecular dynamics insights and water stability of hydrophobic deep eutectic solvents aided extraction of nitenpyram from an aqueous environment, J. Phys. Chem. B. 124 (2020) 7405–7420. https://doi.org/10.1021/acs.jpcb.0c03647.

[3] S.P. Verevkin, A.Y. Sazonova, A.K. Frolkova, D.H. Zaitsau, I. V. Prikhodko, C. Held, Separation performance of BioRenewable deep eutectic solvents, Ind. Eng. Chem. Res. 54 (2015) 3498–3504. https://doi.org/10.1021/acs.iecr.5b00357.

[4] P.V.A. Pontes, E.A. Crespo, M.A.R. Martins, L.P. Silva, C.M.S.S. Neves, G.J. Maximo, M.D. Hubinger, E.A.C. Batista, S.P. Pinho, J.A.P. Coutinho, G. Sadowski, C. Held, Measurement and PC-SAFT modeling of solid-liquid equilibrium of deep eutectic solvents of quaternary ammonium chlorides and carboxylic acids, Fluid Phase Equilib. 448 (2017) 69–80. https://doi.org/10.1016/j.fluid.2017.04.007.

[5] C.H.J.T. Dietz, A. Erve, M.C. Kroon, M. van Sint Annaland, F. Gallucci, C. Held, Thermodynamic properties of hydrophobic deep eutectic solvents and solubility of water and HMF in them: Measurements and PC-SAFT modeling, Fluid Phase Equilib. 489 (2019) 75–82. https://doi.org/10.1016/j.fluid.2019.02.010.

[6] C. Florindo, L.G. Celia-Silva, L.F.G. Martins, L.C. Branco, I.M. Marrucho, Supramolecular hydrogel based on a sodium deep eutectic solvent, Chem. Commun. 54 (2018) 7527–7530. https://doi.org/10.1039/C8CC03266A.

[7] H. Ebro, Y.M. Kim, J.H. Kim, Molecular dynamics simulations in membrane-based water treatment processes: A systematic overview, J. Memb. Sci. 438 (2013) 112–125. https://doi.org/https://doi.org/10.1016/j.memsci.2013.03.027.

[8] M.J. Frisch, G.W. Trucks, H.B. Schlegel, G.E. Scuseria, M.A. Robb, J.R. Cheeseman,

G. Scalmani, V. Barone, B. Mennucci, G.A. Petersson, others, Gaussian 9 program, Gaussian Inc., Wallingford, CT. Gaussian 9 (2009) 2009.

[9] W. Kohn, A.D. Becke, R.G. Parr, Density functional theory of electronic structure, J. Phys. Chem. 100 (1996) 12974–12980. https://doi.org/10.1021/jp960669l.

[10] C.I. Bayly, P. Cieplak, W.D. Cornell, P.A. Kollman, A well-behaved electrostatic potential based method using charge restraints for deriving atomic charges: The RESP model, J. Phys. Chem. 97 (1993) 10269–10280. https://doi.org/10.1021/j100142a004.

[11] C.D. Case. D, Babin. V, Berryman. J, Betz. R, Cai. Q, G.H. Cheatham. T, III, Darden. T, Duke. R, AMBER 14, (2014). https://ambermd.org/doc12/Amber14.pdf.

[12] J. Wang, R.M. Wolf, J.W. Caldwell, P.A. Kollman, D.A. Case, Development and testing of a general Amber force field, J. Comput. Chem. 25 (2004) 1157–1174. https://doi.org/10.1002/jcc.20035.

[13] J. Wang, W. Wang, P.A. Kollman, D.A. Case, Automatic atom type and bond type perception in molecular mechanical calculations, J. Mol. Graph. Model. 25 (2006) 247–260. https://doi.org/10.1016/j.jmgm.2005.12.005.

[14] L. Martinez, R. Andrade, E.G. Birgin, J.M. Martínez, PACKMOL: A package for building initial configurations for molecular dynamics simulations, J. Comput. Chem. 30 (2009) 2157–2164. https://doi.org/10.1002/jcc.21224.

[15] J.C. Phillips, K. Schulten, A. Bhatele, C. Mei, Y. Sun, E.J. Bohm, L. V. Kale, Scalable molecular dynamics with NAMD, Parallel Sci. Eng. Appl. Charm++ Approach. 26 (2016) 60–76. https://doi.org/10.1201/b16251-15.

[16] P.H. Hünenberger, Thermostat algorithms for molecular dynamics simulations, Adv. Polym. Sci. 173 (2005) 105–147. https://doi.org/10.1007/b99427.

[17] S.E. Feller, Y. Zhang, R.W. Pastor, B.R. Brooks, Constant pressure molecular dynamics simulation: The Langevin piston method, J. Chem. Phys. 103 (1995) 4613–4621. https://doi.org/10.1063/1.470648.

[18] P.E. Theodorakis, H.P. Hsu, W. Paul, K. Binder, Computer simulation of bottle-brush polymers with flexible backbone: Good solvent versus theta solvent conditions, J. Chem. Phys. 135 (2011). https://doi.org/10.1063/1.3656072.

[19] W. Humphrey, A. Dalke, K. Schulten, Sartorius products, J. Mol. Graph. 14 (1996) 33–38. https://www.tapbiosystems.com/tap/products/index.htm.

[20] M. Brehm, B. Kirchner, TRAVIS - A free analyzer and visualizer for monte carlo and molecular dynamics trajectories, J. Chem. Inf. Model. 51 (2011) 2007–2023. https://doi.org/10.1021/ci200217w.

[21] Y. Zhao, D.G. Truhlar, The M06 suite of density functionals for main group thermochemistry, thermochemical kinetics, noncovalent interactions, excited states, and transition elements: Two new functionals and systematic testing of four M06-class functionals and 12 other function, Theor. Chem. Acc. 120 (2008) 215–241. https://doi.org/10.1007/s00214-007-0310-x.

[22] K. Fukui, Theory of orientation and stereoselection, Springer, 2006. https://doi.org/10.1007/bfb0051113.

[23] S. Paul, S. Paul, The influence of trehalose on hydrophobic interactions of small nonpolar solute: A molecular dynamics simulation study, J. Chem. Phys. 139 (2013). https://doi.org/10.1063/1.4816521.

Chapter- 4

Decontamination of Enoxacin containing Aqueous Phase through Hydrophobic Deep Eutectic Solvents: Solvent Regeneration and Quantum Chemical Insights

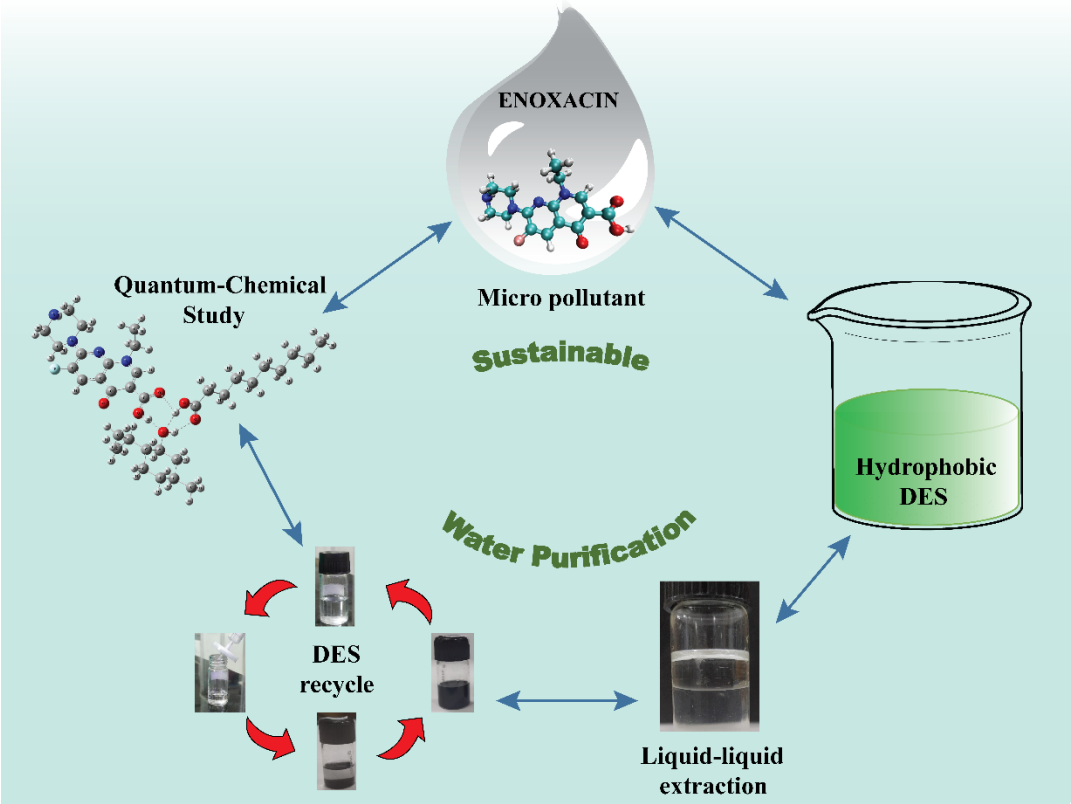

Published Article:

N. Paul, G. Harish, T. Banerjee, Decontamination of enoxacin containing aqueous phase through hydrophobic deep eutectic solvents: solvent regeneration and quantum chemical insights, J. Mol. Liq., 374 (2023) 121254.

4 Decontamination of Enoxacin containing Aqueous Phase through Hydrophobic Deep Eutectic Solvents: Solvent Regeneration and Quantum Chemical Insights

The current chapter addresses the extraction of a drug (enoxacin) from an aqueous environment by liquid-liquid extraction using three hydrophobic deep eutectic solvents (DES) namely, (a) DL-menthol: decanoic acid (1:1), (b) DL-menthol: dodecanoic acid (2:1), and (c) dodecanoic acid: decanoic acid (1:2). The experiments have been performed in a batch process with different initial drug concentrations (5 to 20 ppm) at varying mass ratios of DES/ water phase at the ambient condition to observe the extraction performance at various contamination levels followed by quantum chemical (QC) analysis. The extraction efficiency and the distribution ratio have been reported. Followed by the batch-type extraction experiments, three different recycling schemes have been implemented to assess the reuse and recovery of DESs achieved by recycling the DES phase with purification through activated carbon (AC) which allowed it to maintain its continuity of the aqueous phase. The enhanced DES-drug interaction in the form of DES-enoxacin complex has been studied by the QC analysis. The charge transfer (CT) analysis based on natural bonding orbital (NBO) and the frontier molecular orbital (FMO) analysis are performed to analyse the system. Non-bonded interactions with dispersion effect were confirmed by the structural arrangement analysis of the complex supported by. The quantum theory of atom in molecules and the non-covalent interaction (QTAIM & NCI) analysis are implemented to understand the noncovalent interactions such as hydrogen bonding and dispersion interactions (van der Waals), manifested within the system as the basis of interaction between the molecular groups.

4.1 Introduction

Previous chapter (chapter 3) discussed MD and QC studies of pesticides extraction. The most commonly employed analytical procedures are not enough in detecting the micropollutants in aquatic sources due to their lower detection limit, and only recent developments in these nonspecific approaches have allowed their discovery.[1] Micropollutants include heavy metals, medicines, personal care items, dyes, and insecticides.[2] Liquid-liquid extraction (LLE)[3,4] has recently gained the advantage over adsorption[5] as an effective wastewater treatment process, because of the availability of task-specific tunable low-volatility green solvents. LLE of pharmaceutical products along with an

additional adsorption setup can act as a successful and effective arrangement for the wastewater management process.[3] Application of suitable green and environment-friendly solvents such as ionic liquids (ILs) or deep eutectic solvents (DESs) as an LLE medium along with activated carbon (AC) as the adsorbent for cleaning of the solvent-rich phase could be effective for separation performance, cost minimization and sustainability of the overall treatment framework.[6,7] solvent extraction can increase the performance of removal of drugs; whereas, AC- assisted cleaning of the solvent phase can be advantageous in the regeneration and recycling of the solvents. In that way, one can effectively reuse and regenerate the solvents as well as the adsorbents minimizing the overall cost of the process. Florindo et al. have exercised a similar protocol.[8]

Deep Eutectic Solvents (DES) are a mixture of two or more inexpensive and environmentally benign components that can self-associate, usually through hydrogen bond and dispersion interactions, establishing a eutectic mixture having a melting point lower than that of each component individually.[9,10] At temperatures below 100 °C, DESs are usually liquid. These DESs have similar physiochemical properties to typical ionic liquids but are significantly less expensive and environmentally friendly. Because of the low lattice energy of the massive, nonsymmetric ions found in DESs, the melting point of the mixture is low as well.[11] Mostly, DESs are formed where the individual components act as hydrogen bond donors (HBD) and hydrogen bond acceptors (HBA), respectively. Eutectics exist because of the lower free energy of the liquid mixture than the average of its components facilitating non-ideal mixing of the end-members. Each eutectic forming component works as an impurity to the other component that transpires in the depression of the melting point. Charge delocalization generated by short and long-range hydrogen bonding and dispersion interactions between the components is responsible for this lower melting point of the eutectic mixture than the individual components.[11,12]

Among the DESs, hydrophobic DESs (HDESs) have emerged as a new class of DESs, which are effective in the separation of various solutes dissolved in the aqueous medium.[13,14] This involves the separation or removal of heavy metal ions, industrial paints and dyes, pesticides and other pharmaceuticals including those which have been found in aqueous environments as dissolved impurities.[13,15–17] Since their inception, a decent number of HDESs are formulated experimentally, among which a large fraction consists of naturally occurring compounds as the DES precursors. HDESs are significantly stable under an aqueous environment, which facilitates them to extract micropollutants present in water by caging them in a distinct DES-rich phase. The extent of extraction depends on the solubility and relative affinity of the specific micropollutant towards the DES phase. Thus, HDESs are

quite effective agents in extracting pharmaceuticals from wastewater streams through liquid-liquid extraction. Though HDESs have shown excellent opportunities in the field of separation and extraction, the domain of pharmaceutical removal, mainly APIs, has not been explored to that extent. One recent study revealed the batch-type extraction of ciprofloxacin from the water phase with neutral and charged DESs. This reported higher extraction efficiency with HDESs.[8] In another work, liquid-liquid microextraction was utilized to extract two antibiotics (levofloxacin and ciprofloxacin) present in water employing a hydrophobic DES based on fatty acid/alcohol to achieve maximal extraction efficiency.[18]

Enoxacin (1-ethyl-6-fluoro-1,4-dihydro-4-oxo-7-(1-piperazinyl)- 1,8-naphthyridine-3-carboxylic acid) works as an inhibiting agent to the bacterial enzyme DNA gyrase (DNA topoisomerase II). The working mechanism follows when enoxacin is attached to the enzyme DNA gyrase, which allows it to untwist one DNA double helix into two, preventing bacterial DNA replication.[19] It exhibits a resilient antibacterial effect against a diverse variety of Gram-negative bacteria, but only a modest effect on Gram-positive bacteria. The application of this drug corresponds to the treatment of uncomplicated urethral or cervical gonorrhoea due to *Neisseria gonorrhoeae* and uncomplicated urinary tract infections (cystitis). Enoxacin contamination in wastewater up to mg L^{-1} level has been confirmed by Larsson's group in a water body near a local wastewater treatment plant named Patancheru Enviro Tech Ltd. (PETL) in Hyderabad, India.[20]

In our previous chapter (chapter 3), the pesticide-DES interaction was thoroughly investigated where the occurrence of multiple interactive phenomena was witnessed.[12,21] Further, the extraction mechanism of two pesticides from an aqueous solution was explored and the frontier molecular orbital (FMO) and the CT process within the components were suggestive of a complex framework of DES-pesticide arrangement. The QC results were later validated with experimental as well as molecular dynamics (MD) simulation.[21] Another distinct application of QC-based interaction through DES was with aromatic sulfur compounds (ASCs) based on benzothiophene, dibenzothiophene, and related oxides. Here, desulfurization studies with reline and ethaline DESs were reported.[22] Furthermore, they discovered how charge transfer takes place, as well as the solvation thermodynamics. Charge transfer among ASCs and DES components were found to be dominated by several weak non-bonded contacts. AIM analysis and quantum chemical computations by Garcia et al. indicated a correlation between melting point and electronic density in ChCl-based DESs, based on their findings. García et al., using quantum chemical calculations and atom-in-molecule (AIM) analysis, predicted the relationship between melting temperatures and electron density in ChCl-based DESs.[23]

The objective of the current chapter involves the application of the hydrophobic DESs in the batch-type extraction of enoxacin, which is one of the primary drugs that was found in the surface water streams adjacent to a pharmaceutical wastewater treatment plant. Three hydrophobic DESs were selected for solvent extraction of enoxacin from an aqueous environment, among which two are consisting of DL-menthol and fatty acids such as decanoic (C_{10}) and dodecanoic acid (C_{12}). The third DES contains the above-mentioned fatty acids as HBD and HBA, respectively. The study involves the investigation of the enoxacin extraction performance of the DESs at different DES/ water mass ratios and initial concentrations of enoxacin solution for each of the three DESs. All the experiments were carried out at atmospheric pressure and 298.15 K.

Followed by the batch-type extraction experiments, three different recycling schemes have been implemented to assess the reuse and recovery of DESs to achieve higher net extraction efficiency (NEE). This ensures sustainable and a circular approach to solvent regeneration via adsorption on activated carbon (AC). The direct introduction of AC to the water phase to adsorb enoxacin was not performed to avoid carbon-particulate contamination of water. The difficulty is overcoming the high energy and cost demand for an additional filtration unit to clean the AC-contaminated water phase which can greatly affect the overall economic efficiency and viability of the extraction process. Thus, the regeneration of DES with AC can be advantageous in preventing pathogen growth in filtration media and the evolution of drug-resistive pathogens in the long run rather than the direct application of AC with water. In the later sections, quantum chemical (QC) calculations have been performed for the DES and the DES-enoxacin complex. This incorporated the optimization of the DES and its complex by Gaussian 16,[24] followed by the charge transfer (CT) process. This was executed through the natural bonding orbital (NBO) analysis. The interaction energy analysis was further adopted to assess the stability of the DES as well as the complex with frontier molecular orbital (FMO) analysis that involves the HOMO-LUMO energy gap. The QC calculation elucidates the strength of the DES-enoxacin interaction and provides insights regarding the interaction mechanism with structural arrangement combined with charge transfer behaviour. Further, AIM analysis along with NCI plots was obtained to understand the multiple interacting components in the formation of the DES-enoxacin complex with the help of electron density analysis and the progression of the non-covalent interactions.

4.2 Computational Framework

Initially, DFT calculations for DES and drug optimization were done at the B3LYP/6-311+G(d,p)[25–27] and M06-2X/6-311+G(d,p)[28] level of theory for comparative analysis.

D3BJ dispersion correction[29] was introduced for the former level of theory to incorporate the dispersion forces that might be present in the DES and DES-drug structural arrangements. The individual structures of DES (i.e., HBA and HBD) and enoxacin were built in Gaussview 5 builder package and the structures were optimized with the aforementioned levels of theory using Gaussian 16.[24] The optimization of the DES structures was accomplished by arranging the components (HBA and HBD) in different orientations to obtain the minimum energy arrangement. Figures 10a-b display the optimized geometries of DL-menthol- decanoic acid DES at different levels of theory and Figures 10c-d represent the optimized geometries of the enoxacin (drug) molecule. Likewise, the micropollutant (enoxacin) molecule was placed into the optimized DES structure and the DES-drug complex arrangement was optimized subsequently after different conformer analyses around the DES components. Vibrational frequency analysis at the very same theoretical level was carried out using the '*freq'* keyword in Gaussian to validate the minimal state of the potential energy surface (PES). Analysis of DES, enoxacin, and DES-enoxacin complex was conducted with both B3LYP/6-311+G(d,p) and M06- 2X/6-311+G(d,p)[28] levels of theories for a comparative investigation of stability, charge transfer (CT) process and interactions among the compounds through Frontier molecular orbital[30] (FMO) and the natural bonding orbital NBO) analysis. The AIM and NCI studies were carried out using the Multiwfn code.[31]

4.3 Materials and Methods

4.3.1 Materials

DL-menthol (purity ≥ 95%), decanoic acid (C_{10}) (purity ≥ 98%), and dodecanoic acid (C_{12}) (purity ≥ 98%) were purchased from Sigma-Aldrich and used as received. Enoxacin sesquihydrate micropollutant (analytical standard) was also purchased from Sigma-Aldrich and was used as supplied. All aqueous solutions and eutectic solvents were prepared by weighing the required mass using a Mettler Toledo analytic laboratory balance (Model: ME204/A04). Water used in all the experiments was obtained from an in-house high-quality Millipore water synthesis unit.

4.3.2 Experimental Protocol

4.3.2.1 Preparation of Enoxacin Stock Solution

Enoxacin aqueous stock solution with variable concentrations, mainly 5 ppm, 10 ppm and 20 ppm, were prepared by mixing the required amount of the drug in a specific amount of high-quality Millipore water. The mixtures were then subjected to vigorous stirring at 450 rpm at 25

°C for almost 24 hours to ensure complete miscibility of the micropollutant and to reach equilibrium in the water phase. A calibration curve containing the micropollutant in Millipore water (curve with $R^2 > 0.999$) was obtained for the quantification of LLE experimental findings as presented in Figure D.1 (Appendix D).

4.3.2.2 Preparation of DES

DESs were prepared by mixing both the compounds (HBA and HBD) in a reagent bottle at 50 ºC with a stirring speed of 500 rpm until a homogeneous liquid mixture was formed. The prepared DESs were then kept at room temperature for two to three days to ensure equilibrium and stability, before using them for further experiments. The Karl Fischer titration (Metrohm 870 KF Titrino Plus) was used to evaluate the water content of each pure hydrophobic DES, and the analysis indicated a water content of < 400 ppm. The composition of the three DESs used in this experiment is shown in Table 4.1.

Table 4.1: List of studied hydrophobic DESs with molar ratios

DES	Abbreviation	HBA	HBD	Molar ratio (HBA: HBD)
DES1	DLM-DEC	DL- menthol	decanoic acid	1:1
DES2	DLM-DODEC	DL- menthol	dodecanoic acid	2:1
DES3	DODEC-DEC	dodecanoic acid	decanoic acid	1:2

4.3.2.3 Solubility of Enoxacin in Different Hydrophobic DESs

Enoxacin's solubility can be evaluated by adding a small quantity of the pure pharmaceutical component (about 2 mg/ g of DES per addition) to the investigated hydrophobic DESs at room temperature. After stirring the vials for at least 12 hours, the samples were examined. To ensure a uniform mixture, a tiny amount of the solid was added after all of the solid had dissolved. To get to the stage of visual saturation (heterogeneous combination), this approach was repeated.

4.3.2.4 Hydrophobic Stability of DESs in terms of Miscibility of DESs and Water

The water content determination for each of the hydrophobic DESs was carried out by mixing the DES and water at a 1:1 molar ratio (DES: water). Thereafter, each of the mixtures was vigorously stirred for 20 minutes for imparting contact between the phases at room temperature. The mixtures were then kept idle for 12 hours to reach equilibrium to ensure complete phase separation of the DES and water phase. Using a needled syringe, the separated DES phase was injected into the Karl Fischer Coulometer Metrohm to determine the water content.

4.3.2.5 Liquid-Liquid Extraction Experiments

Three different mass ratios of DES to water phase were prepared for all three initial concentrations of 5 ppm, 10 ppm and 20 ppm respectively. The emphasis was given to minimising the amount of DES required for extraction of a unit amount of enoxacin micropollutant. Hence, the LLE experiments were carried out for three different DES phase/water phase mass ratios (1:1, 1:2 and 1:3) for each of the DESs. A temperature-controlled water bath was used to ensure uniform temperature throughout the experiments, which in the present study was kept at room temperature (25 ºC). The mixtures were allowed to stir vigorously at a stirring speed ranging from 300 to 500 rpm depending on the requirement of a full central vortex formation within the vials. Subsequently, the mixtures were allowed to settle for about 16 hours until a complete phase separation of the DES and water phase occurred. The separated DES and water phases were collected with precaution and were stored for further experiments.

4.3.2.6 Reuse and Recycling of DES

Minimizing the amount of solvent used is critical in the implementation of any separation process for an economic and long-term sustainable approach. The potential reuse and recycling of the DESs were investigated in the present study. Three different recycling schemes were implemented separately.

In the first scheme, the upper phase (DES phase) was collected after every extraction cycle and was cleaned via adsorption on activated carbon (AC), where enoxacin was removed from the extract phase. This step continued for multiple extraction cycles. The DES phase consisting of extracted enoxacin was mixed with a specific amount of AC in a glass vial followed by filtration using a hydrophobic poly (tetrafluoroethylene) syringe filter with a pore size of 0.2 μm to ensure the complete removal of the AC particles from the DES phase.

The second scheme elaborates on the reuse of the same DES that has been used and reused in each extraction cycle until a point of saturation (by enoxacin) where the extraction efficiency of the DES is reduced drastically. The nearly saturated DES phase was then recycled by removing the enoxacin through adsorption with activated carbon (AC).

The third scheme incorporates the single input of micro-polluted aqueous feed with the application of fresh DES feed in each extraction cycle to achieve a reasonably higher net extraction efficiency (%NEE) of the micropollutant.

Overall, the reuse study of the DES revealed the extraction capability of the hydrophobic DESs and the recycling emphasizes the solvent lifetime in terms of the number of extraction cycles.

4.4 Results and Discussion

4.4.1 Influence of Extraction Conditions on Experimental Extraction Efficiency

The extraction efficiency (%EE) of enoxacin from the water was evaluated using the concentration of enoxacin in the water phase before (C_0) and after extraction (C) employing the following equation:

$$\%EE = \frac{C_0 - C}{C_0} \times 100 \qquad (4.1)$$

The distribution ratio was also calculated, which is defined as the ratio of the concentration of the enoxacin in the DES phase to the concentration in the water phase. The extraction efficiency and the distribution ratio data are presented in Table D.1 and D.2, respectively (Appendix D).

The extraction efficiency of a micropollutant from an aqueous solution employing DES-based solvent extraction depends on several experimental parameters. Accordingly, to improve the extraction performance, various factors such as initial drug concentration, solvent phase-to-water phase mass ratio, choice of DES, stirring speed and stirring time were investigated. The UV-visible spectra for the extraction of 20 ppm enoxacin solution at three DESs and a varying mass ratio are presented in Figures D.2 to D.10 (Appendix D). The absorbance peak containing the highest UV-absorbance at 267.5 nm wavelength was considered for the quantification purpose.

4.4.2 Influence of Stirring Time and Stirring Speed

In our present work, the effect of stirring time and stirring speed on the extraction performance of enoxacin was investigated and is presented in Figure 4.1. The stirring time of 10, 20 and 30 minutes were selected for a wide range of studies, whereas, a stirring speed ranging from 150 to 550 rpm was chosen to observe the change in extraction efficiencies as a comparative study. We have performed the analysis with DES1 (DL-menthol: C_{10}) at a DES/water phase mass ratio of 1:1 for 20 ppm initial enoxacin concentration at 25 °C. It should be noted that the stirring speed cannot be considered a factor as it depends on the size and height of the vial used for the experiment along with the size and shape of the magnetic stirrer. In our present study, we have used magnetic stirrer beads of 6 mm × 10 mm dimension in a glass vial of 10 ml volume. All the experiments were carried out using the same type of glass

wares and external components. No significant impact of the stirring time was witnessed on the extraction efficiency of enoxacin, however 20 minutes of stirring produced the best result as can be observed in Figure 4.1a. From the stirring speed analysis, it can be observed that at 150 rpm, the %EE was drastically low as compared to other speeds. Although, the extraction efficiency did not change much from 300 to 550 rpm, with 450 rpm we obtained the most promising result. Accordingly, 20 minutes of stirring at 450 rpm were selected for the ensuing extraction study.

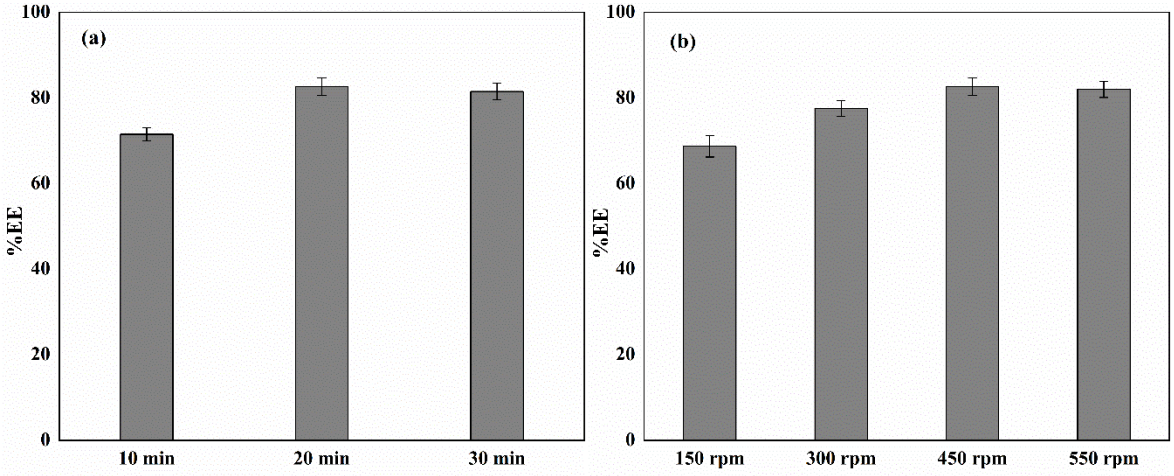

Figure 4.1: Effect of (a) stirring time, and (b) stirring speed, in the extraction of enoxacin from 20 ppm enoxacin aqueous solution using DES1 (DL- menthol: C_{10}) at a DES/water mass ratio of 1:1 at 25 °C.

4.4.3 Influence of Initial Concentration of Enoxacin and DES/water Phase Mass Ratios for Different DESs

The existence of micropollutants in a wide variety of water bodies, from surface to groundwater is already well documented. Subsequently, the initial concentration of the drug is an essential factor for the process of extraction of enoxacin using DES. Apart from this, the mass ratio of DES to enoxacin solution is needed to be considered for the effective use of DES and to keep the extraction process economical and viable leading to a sustainable approach for application in an industrial plant setting.

Considering both the parameters mentioned, three different initial concentrations of enoxacin in water (20, 10, and 5 ppm) were prepared. The solvent extraction was performed with three different DES to water phase mass ratios (1:1, 1:2, and 1:3) with each of the three hydrophobic DESs namely, DL-menthol-decanoic acid (1:1), DL-menthol- dodecanoic acid (2:1) and decanoic acid- dodecanoic acid (2:1). Table 4.1 displays the molar ratios and abbreviations related to each DESs.

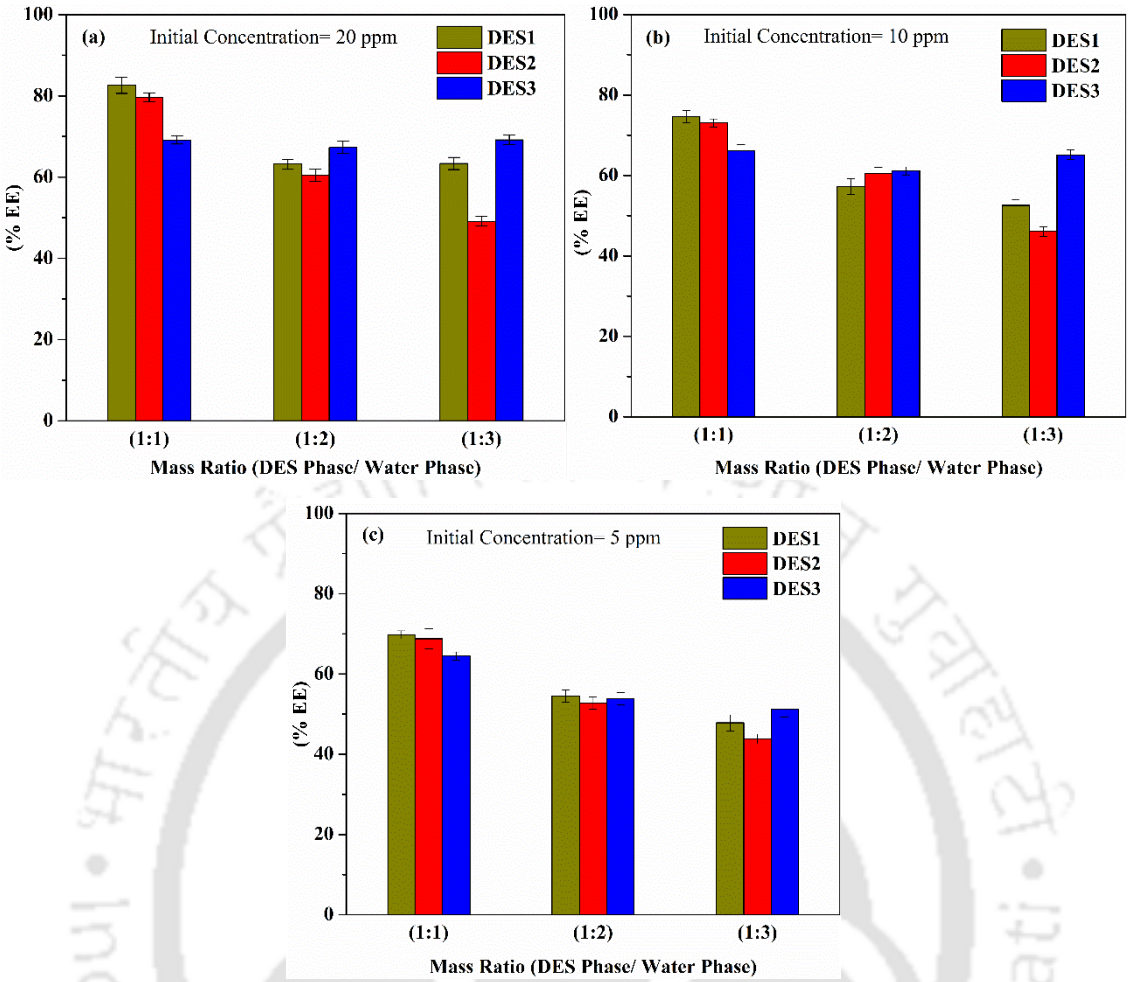

Figure 4.2: Effect of the DES phase/ water phase mass ratio at different initial concentrations (a. 20 ppm; b. 10 ppm; c. 5 ppm) on the extraction efficiency of enoxacin using different hydrophobic DESs (dark yellow- DES1; red- DES2; blue- DES3) [stirring time = 20 minutes, stirring speed = 450 rpm, and temperature = 25 °C].

Figure 4.2 presents the extraction efficiencies of enoxacin at three different mass ratios and three initial concentrations for a given DES. A general decreasing trend of extraction efficiency can be observed as we move from a higher to a lower DES/water phase mass ratio (1:1 to 1:3) in each of the solutions containing a different initial concentration of enoxacin. DES3 showed some varied results as no significant change in the extraction efficiencies was observed with the change in the mass ratios at 20 and 10 ppm initial concentrations. However, in the case of a higher concentration of enoxacin (20 ppm), the extraction efficiencies were almost similar for mass ratios of 1:2 and 1:3 for DES1.

At an intermediate as well as a lower concentration (10 and 5 ppm, respectively), similar development was observed as the extraction efficiency decreased significantly with the change in DES/water mass ratios (from 1:1 to 1:3) as presented in Figures 4.2b and c. The

change in extraction efficiencies for the different mass ratios ranged from 5 -27 % for 10 ppm solution, and 13-25 % for 5 ppm initial concentration for different DESs. Therefore, it can be concluded that the presence of a higher amount of DES can trigger higher enoxacin removal from water as there is a possibility of an enhanced interaction between the molecules of enoxacin and the DES. Furthermore, the higher concentration of enoxacin in the aqueous solution provides a greater driving force for the distinct DES phase to interact with enoxacin molecules and hence increase the extraction efficiency.

4.4.4 Influence of the Different Hydrophobic DESs in Enoxacin Extraction

Figure 4.3 demonstrates the water solubility and the solubility of enoxacin in all three hydrophobic DESs. Our previous study[12] elaborately explained the higher hydrophobicity of DL-menthol and the long-chain fatty acid-based DESs. Accordingly, in the present analysis, the order of water solubility of different DESs follows the trend of DL-menthol: decanoic acid > DL-menthol: dodecanoic acid > dodecanoic acid: decanoic acid. However, the water contents present in each of the DESs used in this study were very much close to each other. The water phase calculation revealed an almost negligible amount of DES contamination as no extra peaks were obtained in the spectroscopic studies. Because of the hydrophobic nature of each of the DES-forming components, the DESs as a whole are almost insoluble in water. However, one can associate the water content in the DES with the mass loss of that said solvent towards the water phase during vigorous stirring and mixing operations. For that, Figure 4.3 data can be useful in obtaining the DES mass loss in the water phase. As a whole, the water content of the DESs lies within 0.5 to 1.7% (in wt%).

Because of the higher hydrophobicity (low level of water present), these DESs have been effective in extracting enoxacin from water as the micropollutant has low water solubility (1 g/3330 ml). The solubility of enoxacin in the respective DESs as presented in Figure 4.3 is higher as compared to enoxacin's water solubility. This favours the enoxacin molecules to transport towards the DES phase. These findings are consistent with the higher extraction efficiency as well as higher distribution ratio of enoxacin in the DES phase as presented in Tables D.1 and D.2 (Appendix D).

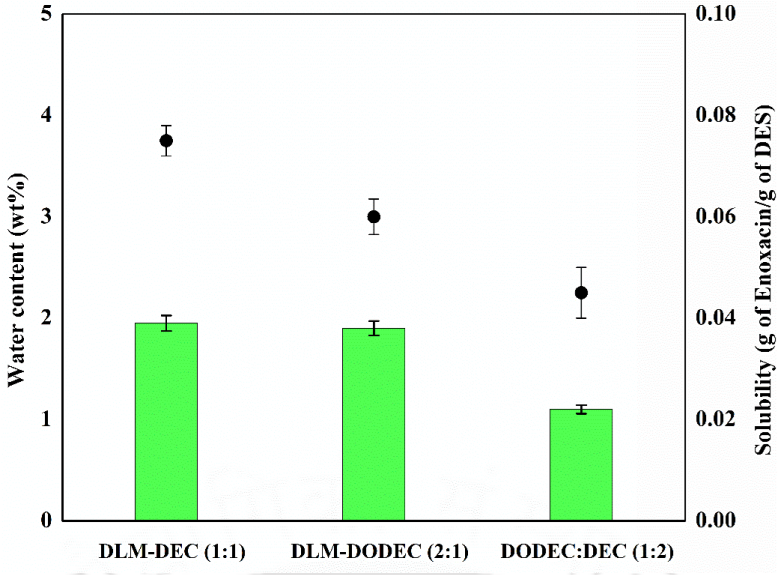

Figure 4.3: Water content in wt% (bars) and the solubility of enoxacin (symbols) in the hydrophobic DESs studied in this work at 25°C.

From Figure 4.2a, it is quite evident that DES1 displayed higher extraction efficiency at a mass ratio of 1:1 for all the initial concentrations of 20 ppm (EE ≅ 82%), 10 ppm (EE ≅ 74%) and 5 ppm (EE ≅ 70%). The %EE for 20 ppm initial concentration suffered a significant change (from 82 to 63%) for both the mass ratios of 1:2 and 1:3 in the case of DES1 (Figures 4.2b and c). For the 1:2 mass ratio, DES1 maintained almost similar extraction efficiencies of 57% and 53% for 10 ppm and 5 ppm initial concentrations, respectively. Overall, it can be concluded that DES1 is suitable for applications at a higher DES/ water mass ratio such as 1:1 for all initial concentrations, where higher extraction efficiency can be achieved due to the presence of the excess amount of solvent. The reason behind the better performance of DES1 can be concurred by the higher solubility of enoxacin in the DES as shown earlier in Figure 4.3.

DES2 presented in Figure 4.2, exhibited extraction efficiency results similar to that of DES1 for all the initial concentrations for mass ratio 1:1 accounting for extraction efficiency of ~80% for 20 ppm, ~73% for 10 ppm and ~69% for 5 ppm of initial concentration, respectively. The solubility of enoxacin is quite comparable in both DESs, thus explaining the similar nature of extraction. The extraction appeared to be slightly lower in the case of mass ratio 1:2 (EE ≅ 60%) and a further decrease is observed in the case of mass ratio 1:3 (EE ≅ 49%), for 20 ppm initial concentration. This may be attributed to the increase in carboxylic acid chain length of the HBD (C_{12}) in DES2 as compared to C_{10} in DES1. The high EE% obtained in the case of mass ratio 1:1 is due to the increase in the amount of DES per unit

amount of enoxacin as compared to the other mass ratios, indicating a favourable interaction between DES and enoxacin.

DES3 displayed an extraction efficiency of ~69% in 20 ppm concentration for a mass ratio of 1:1, which slightly declined to ~66% for 10 ppm and ~64 for 5 ppm concentrations, respectively, as presented in Figure 4.2. These slight variations can be attributed to the decrease in %EE with a decrease in concentration due to the decrease in driving force for enoxacin to penetrate through the DES-enoxacin interface from the enoxacin solution phase to the DES phase. The elevated hydrophobicity of DES3 played a significant role in enhancing the extraction efficiency at lower concentrations of enoxacin solution (such as 10 and 5 ppm). The highest extraction obtained by DES3 (EE ≅ 69%) is quite lower than the higher margins acquired by both DES1 (EE ≅ 82%) and DES2 (EE ≅ 79%). The outcome can simply be explained by the fact that enoxacin showed less solubility in DES3 as compared to the other two DESs. The higher viscosity of DES3 might be another reason why the enoxacin molecules could have encountered a challenging task to mobilize through the aqueous phase to the DES phase. This reduced mobility impacted the overall extraction efficiency of enoxacin in DES3 despite having higher hydrophobicity as compared to DES1 and DES2. Another point to be noted is that the extraction with DES3 required a higher operating temperature as compared to the other two DESs (because of the higher melting point of DES3), otherwise, there lies a possibility of solidification of the DES and thus its operation is rather complex as compared to DES1 and DES2.

Although the extraction efficiency is found to be slightly lower in the case of the 1:1 mass ratio for DES3, the extraction performance for the mass ratios of 1:2 and 1:3 are quite promising even at lower concentrations. In both cases, DES3 fairly outperformed the other two DESs, thus proving to be best suited if the operation requires to be performed at a mass ratio of 1:3 or 1:2 where the priority is somewhat inclined towards reducing the use of DES or extraction with minimal requirement of DES. At a higher DES phase/water phase mass ratio (1:1), DES1 and DES2 achieve higher separation than DES3 because of the higher degree of enoxacin-DES interaction as more enoxacin molecules are available to interact with the DES molecules. In addition, due to the higher solubility of enoxacin, the extraction efficiency is higher in DES1 and 2 as compared to DES3 at a higher DES phase/water phase mass ratio. However, at lower mass ratios (1:2, 1:3), a higher number of water molecules are present in the system that reduces the DES-enoxacin contacts for DES1 and DES2 and increases the DES-water contacts. Whereas, DES3 having much lower water-solubility, can reduce the DES-water interaction and in turn increase DES-enoxacin contacts which is the primary reason for the better performance of DES3 as compared to DES1 and DES2 at lower DES phase/water

phase mass ratios. This, in turn, boosted the efficacy and sustainability of solvent conservation, which was further supplemented by the recycling process where the extraction efficiency might show a net increase, thus ensuring minimal use of DES and higher output.

4.4.5 Recycling and Reuse of DESs

4.4.5.1 Recycling Process 1

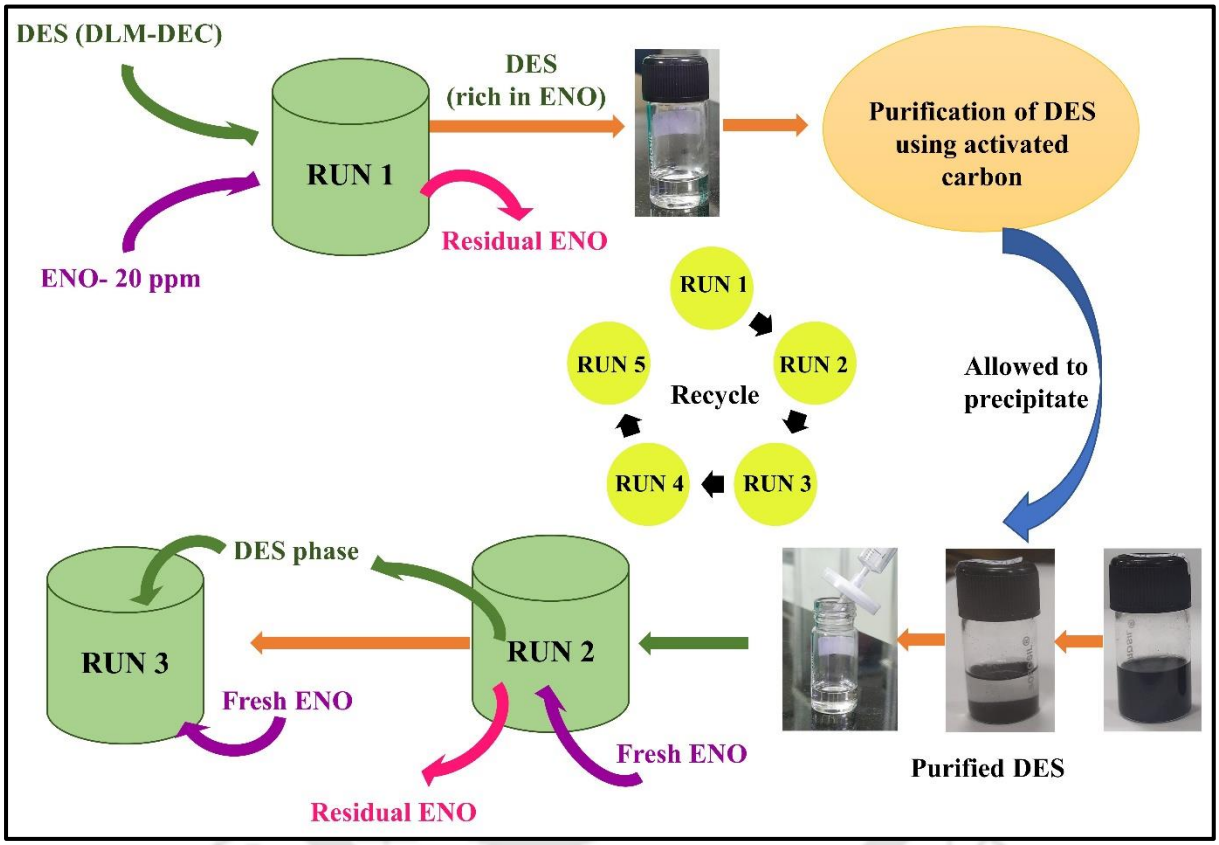

Figure 4.4: Schematic representation of recycling process 1 (RP1): Reuse and recycling of enoxacin extraction using DL-menthol: decanoic acid (1:1) DES at a DES/water mass ratio of 1:1 and 20 and 10 ppm initial enoxacin concentrations, cleaning the extract DES phase continuously using activated carbon for five consecutive cycles at 25 °C.

The first recycling scheme is presented in Figure 4.4. In this recycling process (RP1), DES1 (DL-menthol- C_{10}) was used to extract 20 ppm and 10 ppm enoxacin solutions at a DES/water mass ratio of 1:1 in a batch process. The system was subjected to vigorous stirring at 450 rpm for 20 minutes using a magnetic stirrer, and the system was then allowed to settle for 16 hours till the formation of clear distinct phases of DES and enoxacin aqueous solution. The DES1 extracted ~ 79% (15.76 ppm) of the enoxacin from a 20 ppm solution in RUN 1 of the recycling process followed by careful separation of both phases by a needled syringe. The

enoxacin-rich DES phase was purified by adsorbing the micropollutant through activated carbon (AC) to recover the maximum amount of DES to carry out the next extraction cycle. The purified DES was used again in RUN 2 to extract enoxacin from a fresh 20 ppm enoxacin solution at the DES/water mass ratio of 1:1 identical to RUN 1. The DES and water phases were separated carefully and UV analysis of the water sample was performed to assess the extraction efficiency. The extraction efficiency marginally improved to ~ 81% (16.16 ppm) as compared to the previous run. This slight improvement is accounted for by the adsorption of impurities by activated carbon present in the DES sample taken from RUN1 effectively enhancing the capability of the DESs to extract the micropollutant. This reuse and recycling scheme was extended to three more cycles to be continued to RUN 5 and similar extraction efficiencies were obtained (around 81%) for each of the individual cycles. The extraction efficiencies obtained in each cycle (from RUN 1 to RUN 5) are presented in Figure 4.5. Thus, the entire recycling process 1 (RP1) delivered promising results to assess the reusability of the DES and it emphasizes that DES1 (DLM-DEC) can be used to perform at least five runs of enoxacin solution extraction under the above-mentioned working conditions. Similar results were obtained for DES1 for the initial enoxacin concentration of 10 ppm as presented in Figure D.11 (Appendix D) and for the initial enoxacin concentration of 20 ppm at a DES/water mass ratio of 1:2 in Figure D.12 (Appendix D).

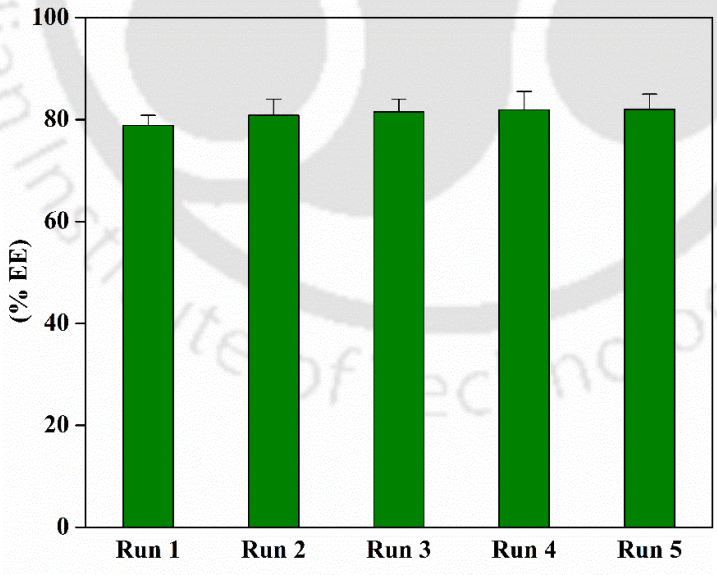

Figure 4.5: Extraction and recycling performances of DL-menthol: decanoic acid (1:1) DES at a DES/water mass ratio of 1:1 and 20 ppm initial enoxacin concentration for various extraction cycles using AC as an adsorbent in DES phase at 25 °C for recycling process 1.

4.4.5.2 Recycling Process 2

In the second recycling scheme (RP2) as presented in Figure 4.6, DES1 (DL-menthol-C_{10}) was used to extract 20 ppm enoxacin solution at a mass ratio of 1:2 between DES and water phase in a batch process where the system is stirred vigorously for 20 min at 450 rpm using a magnetic stirrer (RUN 1). The system was allowed to settle for 16 hours until clear and distinct phase separation occurred between the DES phase and the enoxacin aqueous phase. The phases were carefully separated by a needled syringe and the aqueous phase was analyzed by UV spectroscopy. The DES1 extracted 60.57% (12.11 ppm) of the enoxacin present in the initial 20 ppm enoxacin sample.

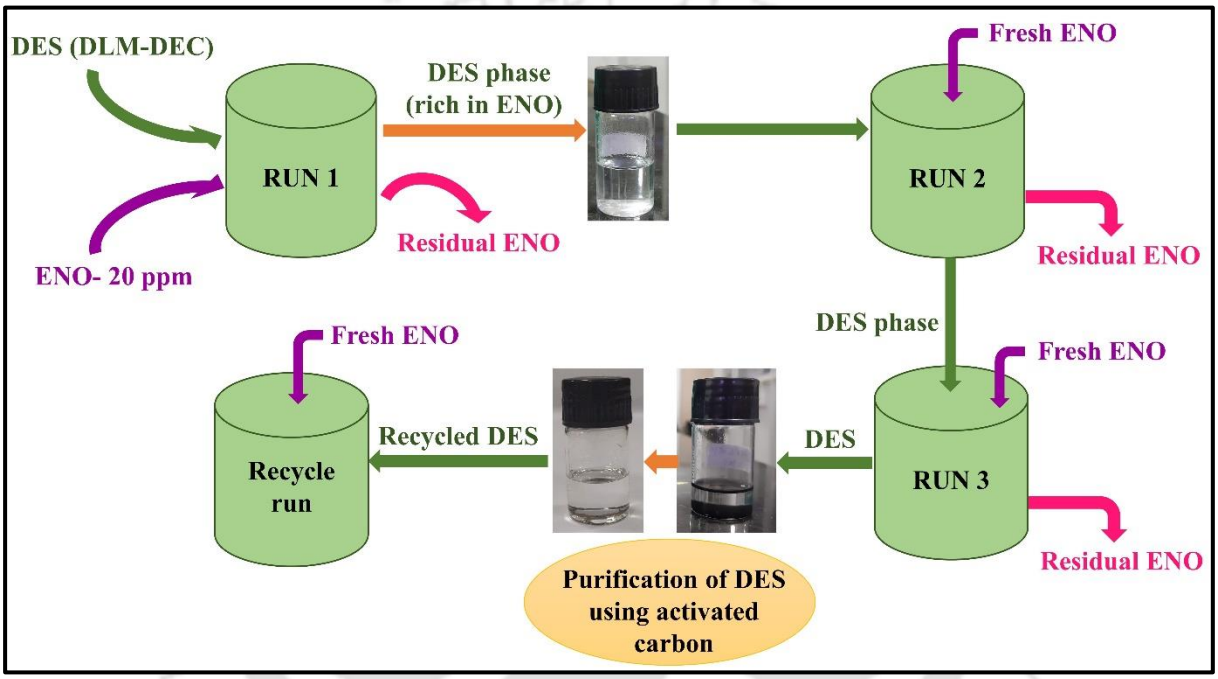

Figure 4.6: Schematic representation of recycling process 2 (RP2): Reuse and recycling of enoxacin extraction using DL-menthol: decanoic acid (1:1) DES at a DES/water mass ratio of 1:2 and 20 ppm initial enoxacin concentrations; the DES phase is reused in consecutive cycles at 25 °C.

The enoxacin-rich DES sample was once again reused in RUN 2 where a fresh 20 ppm enoxacin aqueous solution at a DES/water mass ratio of 1:2 was again introduced in a batch process similar to that of RUN 1. The water phase was carefully collected and the enoxacin concentration was quantified through UV spectroscopy. The enoxacin extraction efficiency obtained in RUN 2 was around 51% (10.2 ppm) and a reduction of around 9.5% (1.9 ppm) in extraction efficiency were observed compared to RUN 1. A similar protocol was followed for RUN 3 and the obtained extraction efficiency was around 33 % (6.54 ppm) and a decrease of 18.3% (3.66 ppm) extraction efficiency was witnessed as compared to RUN 2. Thus, the initial sample of DES1 extracted a total amount of 29.74 ppm of enoxacin in the three runs combined.

The enoxacin-rich DES phase being saturated with the micropollutant resulted in a significant decrease in extractability. To investigate the reuse and recyclability of the DES, the saturated DES phase was then subjected to purification via the removal of enoxacin through the application of activated carbon as an adsorbent for the micropollutant. The procedure was mentioned in the earlier section of the recycling process 1. After cleaning of the DES phase, it was applied for another extraction run with the introduction of 20 ppm fresh enoxacin solution and the resultant extraction efficiency (62.5%) was higher than that of RUN 1. Figure 4.7 displayed the extraction efficiencies obtained in this recycling scheme. Thus, from this type of recycling scheme, one can conclude that the hydrophobic DESs used in this work could very well be reused for several recycling steps without compromising their extraction capability.

Figure 4.7: Extraction efficiency (%EE) at each cycle of extraction using DL-menthol: decanoic acid (1:1) DES at a DES/water mass ratio of 1:2 and 20 ppm initial enoxacin concentration at 25 °C following recycling process 2.

4.4.5.3 Recycling Process 3

In the third recycle process (RP3) as demonstrated in Figure 4.8, DES1 (DL-menthol-C_{10}) was used to extract enoxacin from a 20 ppm aqueous solution of enoxacin at a DES/water phase mass ratio of 1:2 through multiple extraction runs by using fresh DES sample at each intermittent stage. The residual enoxacin aqueous phase sample from the previous run was used as feed for the subsequent RUN. This was performed to accomplish a higher net extraction efficiency (%NEE) that could be obtained by reducing the initial 20 ppm enoxacin concentration to a significantly lower possible residual concentration. In RUN 1, when DES1

was used to extract the 20 ppm enoxacin solution, an extraction efficiency of 60.56 % (12.11 ppm) was obtained and about 7.88 ppm of enoxacin remained in the water phase. This residual water phase consisting of 7.88 ppm of enoxacin was further inserted as RUN 2 of extraction using fresh DES maintaining the same experimental conditions as in the previous run. The fresh DES extracted about 4.454 ppm of enoxacin micropollutant, accounting for a NEE of 82.84%. Thereafter, a 3.43 ppm of residual enoxacin was carried forward to further extraction in RUN 3 using fresh DES. In RUN3, the residual enoxacin aqueous phase solution obtained from RUN 2 was used to perform the extraction similar to that of the earlier cycles using fresh DES. A NEE of about 90.63% was obtained as the DES extracted about 1.56 ppm of enoxacin from the feed containing 3.43 ppm of enoxacin with a residual enoxacin aqueous phase containing 1.87 ppm of the micropollutant. All the extraction performances are quantified and are depicted in Figure 4.9. Thus, DES1 (DLM-DEC) at the DES/water phase mass ratio of 1:2 truncated the initial 20 ppm enoxacin concentration to a very low concentration (< 2 ppm) after three successive cycles of the residual enoxacin solution using fresh DES at each intermittent stage to promisingly achieve more than 90% of net extraction efficiency.

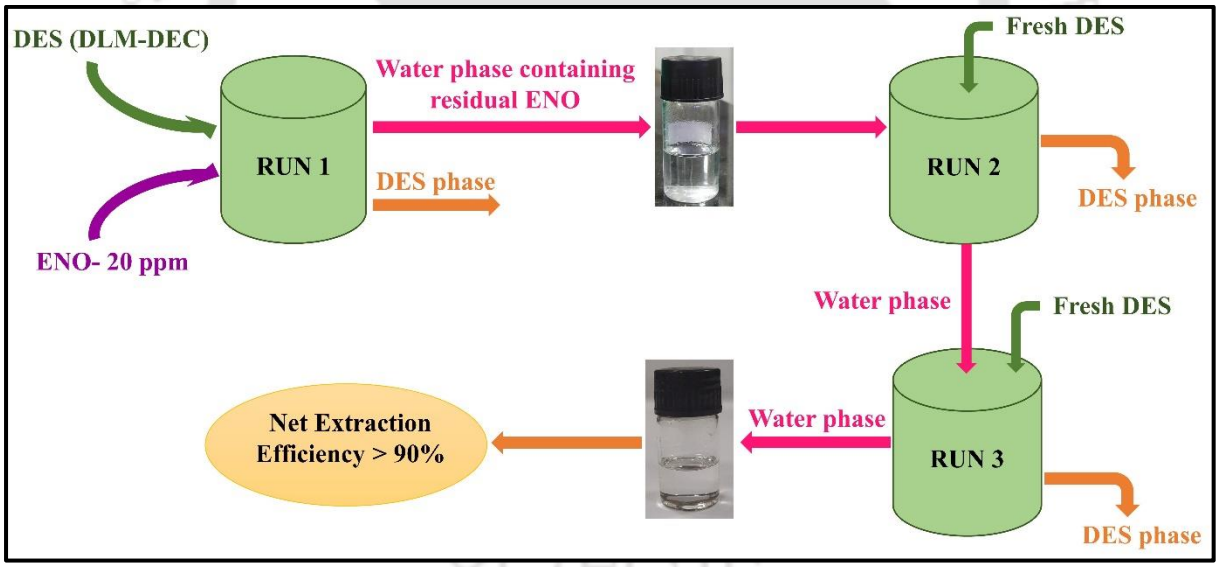

Figure 4.8: Schematic representation of recycling process 3 (RP3): Reuse and recycling of enoxacin extraction using DL-menthol: decanoic acid (1:1) DES at a DES/water mass ratio of 1:2 and 20 ppm initial enoxacin concentrations; the enoxacin aqueous phase is reused in consecutive cycles at 25 °C.

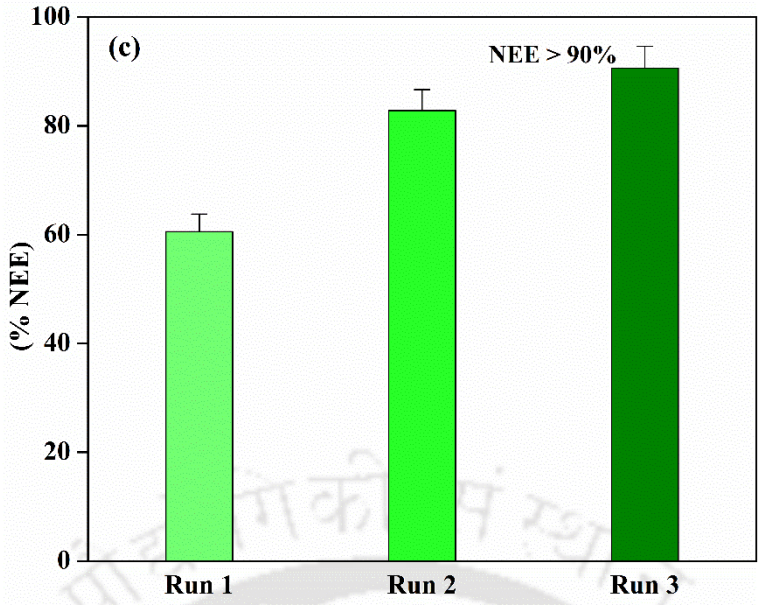

Figure 4.9: Net extraction efficiency (%NEE) at each cycle of extraction using DL-menthol: decanoic acid (1:1) DES at a DES/water mass ratio of 1:2 and 20 ppm initial enoxacin concentration at 25 °C following recycling process 3.

Figure D.12 (Appendix D), Figures 4.7 and 4.9 can be interpreted for the comparison of three types of recycling processes. RP1 is the continuation of recycle process with the introduction of fresh DES in each step. RP2 is carried out to obtain the saturation limit of the DES. RP3 is performed to achieve higher net extraction efficiency (NEE). In RP3, the same water phase is continued for several recycling runs introducing fresh DES in each step, but without the fresh introduction of enoxacin solution. Thus, to achieve a higher cumulative extraction efficiency or net extraction efficiency (NEE), RP3 can be implemented.

4.4.6 Quantum Chemical Insights

To understand the extraction mechanism of enoxacin at an atomic-molecular level, a quantum chemical (QC) analysis was performed. All three DES systems were evaluated for the extraction study of enoxacin. The investigation was intended to find the interactive properties of the HBA and the HBD with the drug molecule (enoxacin), for a possible formation of a DES-enoxacin complex. Understanding the structural properties, charge transfer behaviour, molecular level energies, thermochemistry, and molecular orbitals can be of immense value in highlighting the inherent molecular as well as atomic interactions as can be approached by our previous study.[21] The interactions between the HBA, HBD and the drug molecule (enoxacin) could elucidate the enhanced molecular rearrangement that might help understand the promising extraction results obtained in the experimental section as presented earlier. QC study drives at an atomistic level where each molecular entity can be expressed individually and the

resultant interactions can be analyzed without the expense of the experiments, thus making it a viable and effective tool for the validation of the experimental findings.

4.4.6.1 Geometry Analysis

Figures 4.10a-b revealed the HBA-HBD interactions in DES1 for both methods. Strong HBA-HBD interactions led to the formation of this DES, according to the optimal structures of the DES. The H atom of menthol and the O atom of the carboxyl group of the acid formed O...H hydrogen bond in the DES. The hydrogen bond distance in the DES was found to be 2.018Å in B3LYP optimization and 2.061 Å in the case of M06-2X optimization. The O (menthol)…H (carboxylic acid) distance was found to be 1.731 Å in B3LYP optimization while in M062X, it was 1.768 Å. Overall, non-bonded interactions, particularly hydrogen bonding and dispersion interactions such as the van der Waals interaction appeared to play a significant role in the creation of these neutral DESs.

(a)

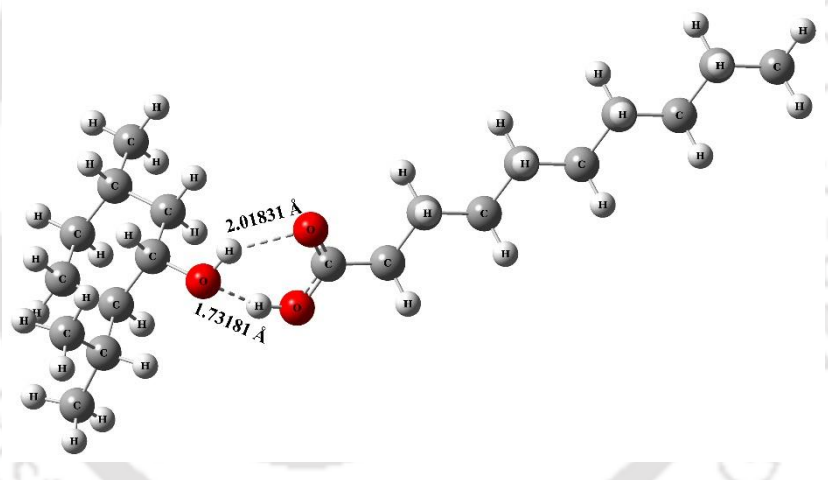

(b)

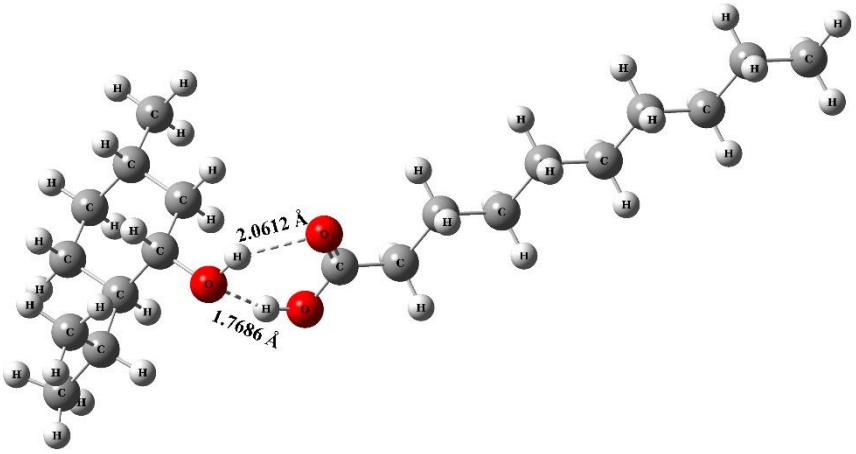

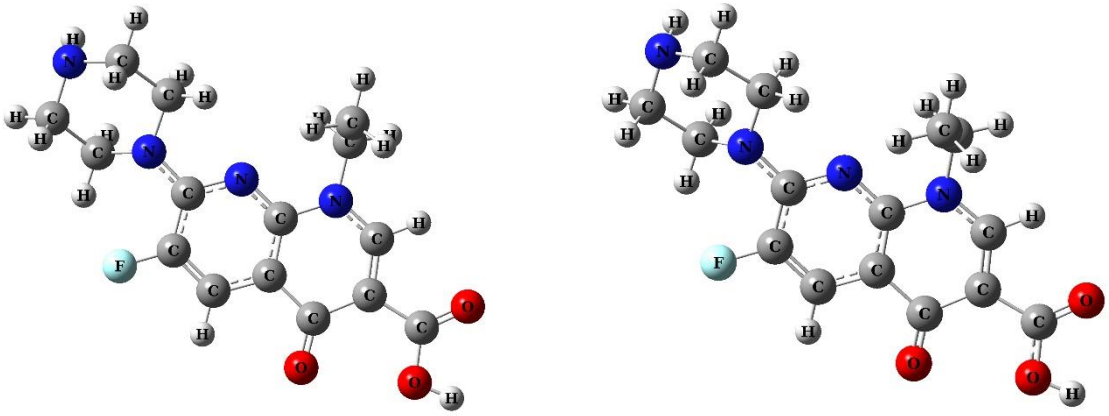

(c) **(d)**

Figure 4.10: Optimized structures of pure DL-menthol: decanoic acid (1:1) DES at (a) DFT-B3LYP/6-311+G(d,p) with D3BJ dispersion correction, (b) M06-2X/6-311+G(d,p); and of enoxacin molecule at (c) DFT-B3LYP/6-311+G(d,p) with D3BJ dispersion correction, (d) M06-2X/6-311+G(d,p) level of theory.

In B3LYP optimization, the O (menthol)…H (acid) bond distance increased to 1.922 Å in the DES1-enoxacin complex compared to the earlier 1.731 Å of the pure DES1 structure. Similarly, in M06-2X optimization, the O (menthol)…H (carboxylic acid) bond distance increased to 1.956 Å in the DES-enoxacin complex as compared to the earlier 1.768 Å in the DES structure. This indicated a slight relaxation of the intermolecular non-bonded interaction between the HBA and HBD components of the DES. Another point to be noted is that this relaxation happened on the side of the DES where the enoxacin molecule interacted with the DES components to get accommodated signifying its penetration and interaction. A similar arrangement was also observed in the case of the M06-2X optimized complex. The other O (carboxylic acid) …H (menthol) bond distance was reduced from 2.018 to 1.881 Å in B3LYP optimization and from 2.061 to 1.888 Å for M06-2X optimization in the DES1- enoxacin complex. This is attributed to a slight bending of the DES structure to accommodate the enoxacin on the opposite side. Figures 4.10 and 4.11 can be referred to authenticate the above findings.

(a)

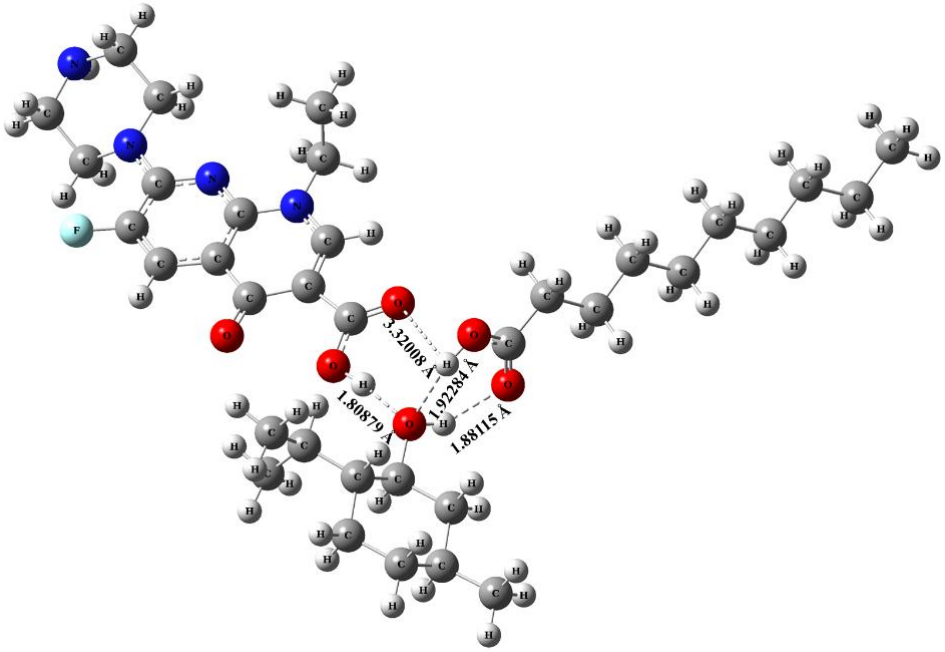
3.32008 Å
1.92284 Å
1.80879 Å
1.88115 Å

(b)

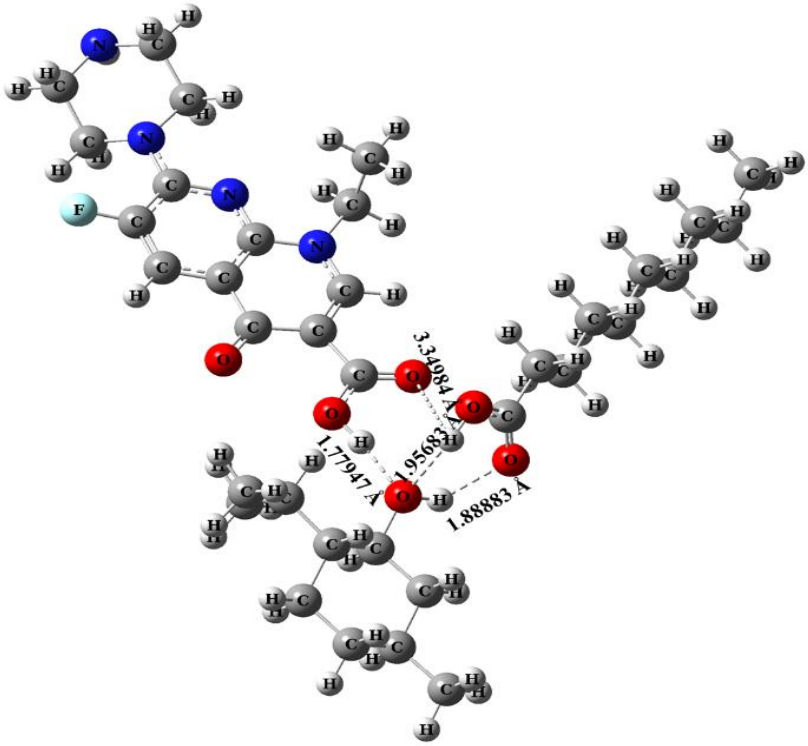
3.34984 Å
1.95683 Å
1.77947 Å
1.88883 Å

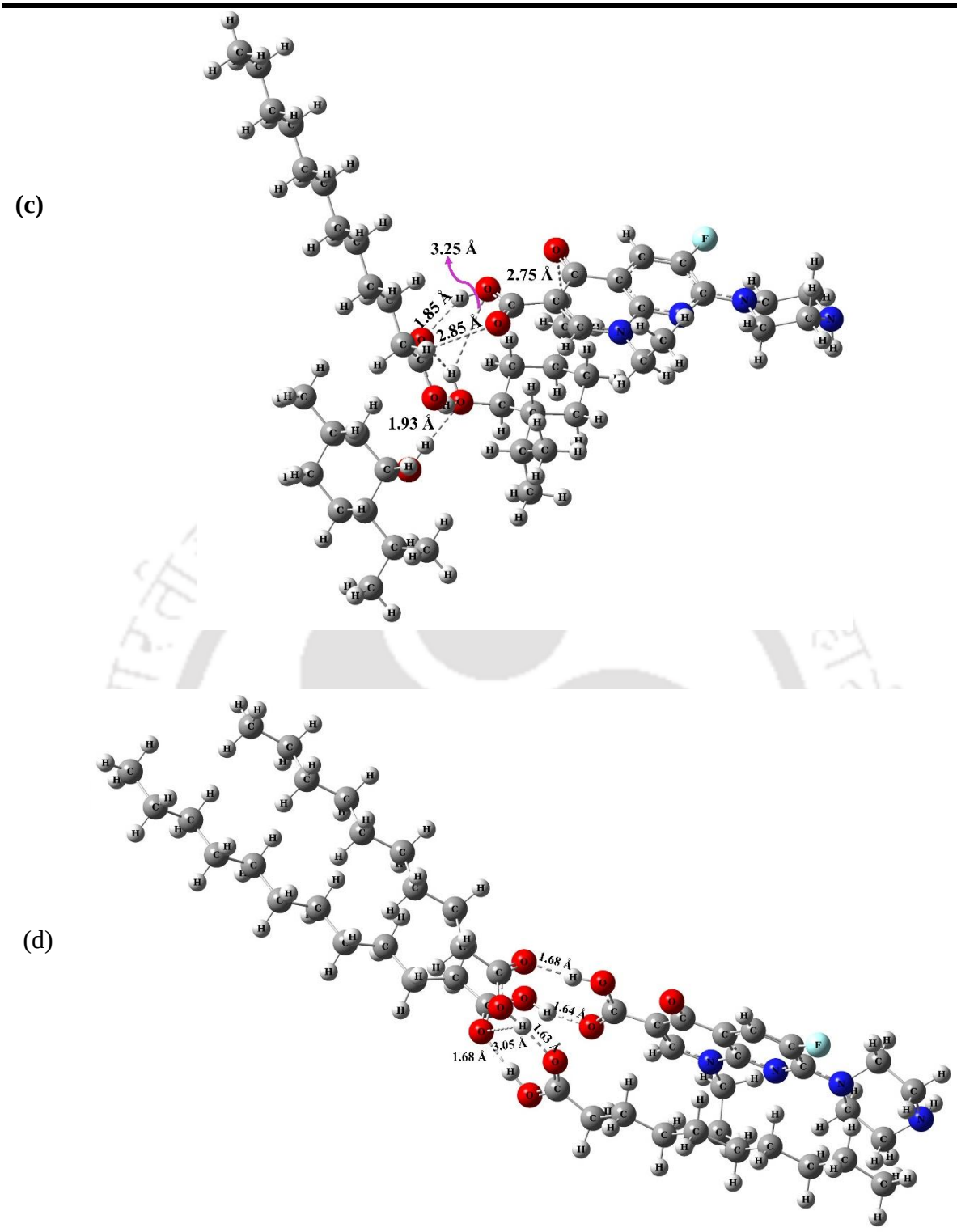

Figure 4.11: Optimized structures of DES-enoxacin complex at different levels of theory (a) [DL-menthol- decanoic acid]/ [enoxacin] complex at DFT-B3LYP/6-311+G(d,p) with D3BJ dispersion correction, (b) [DL-menthol- decanoic acid]/ [enoxacin] complex at M06-2X/6-311+G(d,p), (c) [DL-menthol- dodecanoic acid]/ [enoxacin] complex at DFT-B3LYP/6-311+G(d,p) with D3BJ dispersion correction and (d) [decanoic acid- dodecanoic acid]/ [enoxacin] complex at DFT-B3LYP/6-311+G(d,p) with D3BJ dispersion correction.

The Carboxyl group attached to the 1, 8-naphthyridine part of the enoxacin molecule appeared to be the active site to interact with the DES components. Enoxacin molecule contained multiple hydrogen bond donor and acceptor sites that facilitated the non-bonded interaction whether be a hydrogen bonding or polarity-induced van der Waals dispersion interaction. As identified in Figure 4.11, it can be confirmed that long-range dispersion interaction might play a dominating role in the non-bonded interactions among the components considering the weak interactions.

As presented in Figure 4.11a, in the B3LYP optimization of the DES1-enoxacin complex, the O (menthol)…H (enoxacin) interaction distance can be recorded as 1.808 Å indicating short-range non-bonded interaction. Analogously, the M06-2X optimization suggested the same interaction to be at a distance of 1.779 Å. The O (enoxacin)…H (carboxylic acid) interaction distance is found to be 3.32 Å in the B3LYP optimization and 3.349 Å M06-2X optimization which indicated a long-range ordering. Both of these O…H hydrogen bonds demonstrate the nonbonded interactions between HBA-enoxacin and HBD-enoxacin separately once enoxacin molecules are present in the DES phase after diffusing through the DES-water interphase. The development of these non-bonded interactions appeared to be following the increase in the bending angle between the HBA and the HBD with the introduction of enoxacin to form a stable complex arrangement of DES-enoxacin. For the DES1-enoxacin complex, when the individual HBA-enoxacin and HBD-enoxacin non-bonded interactions were compared, it was found that the interaction of HBA with the enoxacin seems too stronger as compared to the HBD interactions with the enoxacin. This can be validated by the shorter distance for the non-bonded interactions that occurred between O (menthol) and H (enoxacin) as can be observed in Figure 4.11a-b.

Figures 4.11c-d represents the DES2-enoxacin and DES3-enoxacin complex structures, respectively. DES2 contains DL-menthol and dodecanoic acid at a molar ratio of 2:1, whereas, DES3 consists of decanoic acid and dodecanoic acid at a molar ratio of 2:1. As the number of the molecules present within both these systems is higher, these two DESs display greater complexity in the DES-enoxacin arrangement. In the DES2-enoxacin complex (Figure 4.11c), multiple HBD-enoxacin distances range from 1.85 to 3.25 Å and HBA-enoxacin distance ranges from around 2.75 Å. The intermolecular interactions between the HBA and the HBD support a stable DES formation. In the case of the DES3-enoxacin complex (Figure 4.11d), the carboxyl part of enoxacin exhibits multiple closed-shell non-bonded interactive positions ranging from 1.64 to 1.68 Å resulting in a stable DES-enoxacin complex.

4.4.6.2 Interaction Energy Analysis

Interaction energy refers to the reduction in energy of the system due to the interaction between two or more molecules. The calculation of interaction energy corresponds to computing the difference between the energy of the system or complex formed and the sum of the energies of the individual molecules which are involved in the interaction[32]. This calculation shall consider basis set superposition error (BSSE) corrected by using the counterpoise method.[33] In the current discussion, the interaction energy of the HBA-HBD pair in the DES is calculated by finding the difference between the total energy of the DES formed and the total energy of HBA and HBD as shown below:

$$\Delta E_{DES} = E_{DES} - (E_{HBA} + E_{HBD}) + E_{BSSE} \quad (4.2)$$

Where, E_{DES} is the total energy of the DES and E_{HBA} and E_{HBD} are the total energies of the HBA and HBD, respectively, and E_{BSSE} is the basis set superposition error (BSSE) corrected by using the counterpoise method.[33] All the energies can be expressed in kcal/mol.

Accordingly, the interaction energy between the DES and enoxacin is calculated as follows:

$$\Delta E_{COMPLEX} = E_{COMPLEX} - (E_{DES} + E_{ENO}) + E_{BSSE} \quad (4.3)$$

Where $E_{COMPLEX}$ is the total energy of the complex and E_{DES} and E_{ENO} are the energies of the DES and enoxacin molecules, respectively. All the calculated values of the interaction energies are presented in Figure 4.12.

Interaction energy provides insights into the compactness of the molecules involved in the interaction and the distance between the interacting atoms in the molecules. The negative values of the interaction energies indicate the decrease in the overall energies of the final entities formed from the initial components in both DES as well as DES-enoxacin complex formation. This decrease in energy is justified by the development of non-bonded interactions such as hydrogen bonding and van der Waals interaction between the oxygen and hydrogen atoms of the interacting components. In the case of DES1 formation, the decrease in interaction energy (−9.14 kcal/mol, for B3LYP and −11.68 kcal/mol, for M062X) is due to the O (DL-menthol) …H (decanoic acid) hydrogen bond formation with a bond distance of 1.768 Å as shown in Figure 4.10. This concurred with the higher stability of the DES.

In the case of the enoxacin complexes, the negative value of the interaction energy can be explained by the multiple weak interactions such as hydrogen bonding formed as shown in Figure 4.12. As the compactness is increased i.e., the distance between interacting atoms decreases, the strength of the hydrogen bond increases and as a result the total energy of the system gets lowered. The negative interaction energy suggests a much more stable DES-drug complex. The shorter O (DES) …H (enoxacin) hydrogen bonding distance of 1.779, 1.85 and 1.68 Å, for DES1, DES2 and DES3, respectively, as displayed in Figure 4.11b further confirms

the fact that favourable interaction between interaction components leads to better compactness of the DES-enoxacin complexes.

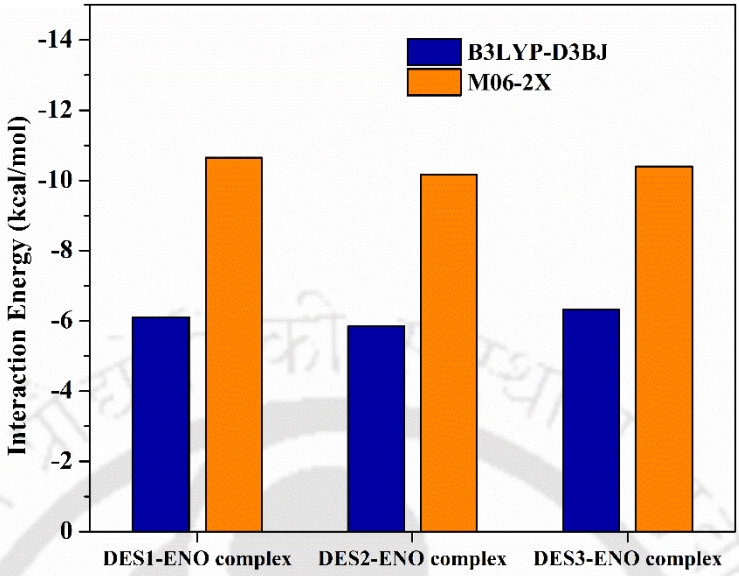

Figure 4.12: Interaction energies for the DES-enoxacin complexes (DL-menthol- decanoic acid/ enoxacin; DL-menthol- dodecanoic acid/ enoxacin; and decanoic acid- dodecanoic acid/ enoxacin) at different levels of theory.

4.4.6.3 Natural Bonding Orbital (NBO) Analysis

The CT (charge transfer) process in Gaussian 16 was calculated using two separate DFT techniques, B3LYP and M06-2X. Tables 4.2 and 4.3 outlines this information. When no other compounds are present in the system, DL-menthol (HBA) and decanoic acid (HBD) acquire positive and negative charges, respectively. Similar distribution happens in DES2 where dodecanoic acid acquires a negative charge. The values are presented in Table 4.3. However, upon interaction with enoxacin, the HBA undergoes a slight decrease in positive charge while the HBD loses a considerable amount of negative charge in both the optimization methods for DES1 and DES2.

In a DES-free environment, the partial charges on the enoxacin molecule are zero since enoxacin is neutral. The NBO charges associated with the neutral enoxacin molecule are therefore assumed to be zero. The charge transfer between the enoxacin molecule and the solvent molecules takes place when the enoxacin molecule is placed in a DES or any other solvent. A non-zero partial charge arises on the individual molecules based on the electron density gained or lost by them through the solvent environment.

For DES1, the HBA slightly gains a negative charge whereas the HBD undergoes a significant loss of negative charge. Overall, the DES now entirely behaves as an electrophilic

entity with a net positive charge. Thus, enoxacin gains a net amount of negative charge and thus behaves as a nucleophilic entity. In M06-2X optimization, similar behaviour is observed except for the fact that the net charge on the DES and enoxacin is 0.0184 with respect to a positive and negative value, respectively. This is lower than that observed in B3LYP optimization.

Table 4.2: Calculated NBO charge on the enoxacin in the presence and absence of the respective DESs

	Enoxacin (a.u.)	
	B3LYP	**M062X**
Without DES	0	0
DES1 [DLM-DEC]	−0.03081	−0.01836
DES2 [DLM-DODEC]	0.00148	0.00313
DES3 [DODEC-DEC]	0.0018	0.00379

The presence of enoxacin initiates a complex of non-bonded interactions as well as a charge transfer mechanism between itself and the DES1 components, i.e., DL-menthol and decanoic acid. The enoxacin gains a negative charge after interaction with the DES, while on the contrary, a positive charge develops on the DES as a whole. This occurs due to the rise in enoxacin's electron density upon interacting with the DES, after being diffused from the aqueous to the DES-rich phase. As a result, charge transfer takes place in the system in the direction of the DES molecule to the enoxacin molecule. Due to the absence of charged molecular entities in systems, charge transfer at a lower magnitude between enoxacin and the DES may be observed, indicating that the nonbonded interactions such as hydrogen bonding and van der Waals contacts are dominating as compared to electrostatic interactions.

The HBDs are seen to lose electron density as the DES-enoxacin complex forms, whereas the HBA's electron density increases. The introduction of enoxacin in this context results in the formation of a complex CT process among the DES ingredients. Due to the presence of localized electron lone pairs, enoxacin has several hydrogen bond acceptor sites, resulting in various HBA-HBD interactions within the system. Both DL-menthol and decanoic acid have a single HBD site, whereas enoxacin has a high HBA count. As a result, all of the components in the system were able to form a donor-acceptor connection.

In the presence of DES2 and DES3, the enoxacin moiety acts as an electrophile by obtaining a positive charge of 0.00313 and 0.00379, respectively. DES2 and DES3 act as nucleophilic entities in the presence of enoxacin. The direction of CT for DES2-enoxacin and

DES3-enoxacin complexes is from enoxacin to the DESs, which is opposite as compared to the DES1-enoxacin complex.

Table 4.3: NBO charges attained by the components of DESs with and without enoxacin

DES	Only DES		With enoxacin	
	B3LYP	**M062X**	**B3LYP**	**M062X**
	Charge on the hydrogen bond acceptor (HBA) of DES in DES-enoxacin combination (a.u.)			
DES1 (DL-menthol)	0.02236	0.02593	0.02152	0.0206
DES2 (DL-menthol)	0.02214	0.02447	0.0117	0.0135
DES3 (dodecanoic acid)	−0.00686	−0.0104	−0.0015	−0.0034
	Charge on the hydrogen bond donor (HBD) of DES in DES-enoxacin combination (a.u.)			
DES1 (decanoic acid)	−0.02236	−0.02593	0.00937	−0.00224
DES2 (dodecanoic acid)	−0.02214	−0.02447	−0.01318	−0.01558
DES3 (decanoic acid)	0.00686	0.0104	−0.0003	−0.0004

4.4.6.4 Frontier Molecular Orbital Analysis

Frontier Molecular Orbital (FMO) study is recognized to be an efficient method for determining the acceptor-donor interaction, as well as the molecular stability and reactivity, using HOMO-LUMO orbital analysis.[30] The current section emphasizes the interaction between the HOMO and LUMO species of DES and enoxacin. The abbreviated forms of 'Highest Occupied Molecular Orbital' and 'Lowest Unoccupied Molecular Orbital', respectively, are HOMO and LUMO. The HOMOs possess a nucleophilic or electron-donating tendency, whereas the LUMOs act as electrophilic or electron-accepting species. A molecule's HOMO-LUMO energy gap can be implemented to calculate the energy required to add or remove electrons from that molecule. The larger the HOMO-LUMO energy gap, the more the molecular kinetic stability and the lower the molecular reactivity.

The HOMO-LUMO energy values for enoxacin, DES1 as well as the DES-enoxacin complexes are presented in Table 4.4. The HOMO-LUMO energy gap of an individual molecule is indicative of the molecular reactivity through the lowest electronic excitation energy, whereas, for complexes formed via the interaction between two or more components, the HOMO-LUMO gap represents thermochemical electronic hopping energy among

themselves.[32] The HOMO-LUMO energy gap of the DES-enoxacin complex is fairly close to that of the pure enoxacin molecule showing considerable stability despite the presence of bulky DES forming groups (DL-menthol, decanoic acid and dodecanoic acid).

The above-mentioned findings are quite evident that can be observed from the values as presented in Table 4.4. The HOMO-LUMO energy gap for the enoxacin molecule is 0.23927 Hartree for M06-2X optimization which confirms that the individual enoxacin molecule obtains a stable form in itself. The HOMO-LUMO energy gaps of the DES-enoxacin complexes are 0.23909, 0.23813 and 0.23401 Hartree, for DES1, DES2 and DES3 respectively, quite close to that of the individual enoxacin molecule. This comparable HOMO-LUMO energy gap for enoxacin and the DES-enoxacin complexes further confirms the stability of the complex as discussed above.

Table 4.4: Theoretically obtained HOMO, LUMO (Ground and Excited State), Energy Gap, Chemical Hardness (η), and Chemical Potential (μ) computed in DFT-B3LYP and M06-2X method (All the units are in Hartree)

Systems	Method	HOMO energy	LUMO energy	Energy gap	η	μ
Enoxacin	B3LYP	−0.2281	−0.07131	0.15679	0.078395	−0.149705
	M06-2X	−0.27628	−0.03701	0.23927	0.119635	−0.156645
DES1 [DLM-DEC]	B3LYP	−0.27845	−0.00351	0.27494	0.13747	−0.14098
	M06-2X	−0.33896	0.00852	0.34748	0.17374	−0.16522
DES1-enoxacin complex	B3LYP	−0.22328	−0.06531	0.15797	0.078985	−0.14429
	M06-2X	−0.27384	−0.03475	0.23909	0.119545	−0.15429
DES2-enoxacin complex	B3LYP	−0.23138	−0.07521	0.15617	0.07809	−0.15329
	M06-2X	−0.28205	−0.04392	0.23813	0.11906	−0.16298
DES3-enoxacin complex	B3LYP	−0.22964	−0.07388	0.15576	0.07788	−0.15176
	M06-2X	−0.27913	−0.04512	0.23401	0.11701	−0.16212

The energy gap between the HOMO and the LUMO is directly related to a molecule's global hardness and softness. The charge transfer and stability of a certain molecule or complex can be recognized by the global hardness, where a higher η value suggests greater stability and resistance charge transfer, and vice versa.

$$\text{Global Hardness } (\eta) = (E_{LUMO} - E_{HOMO})/2 \qquad (4.4)$$

The high hardness value 0.078395 Hartree (B3LYP) and 0.119635 Hartree (M06-2X) in the case of enoxacin in Table 4.4 suggests its high resistance to charge transfer which further shows its tendency to react less and thus exist as a stable molecule. However, in the NBO analysis as mentioned earlier in Table 4.2, a small but specific amount of charge transfer was observed for the DES-enoxacin complexes. The relatively lower value of η for DES-enoxacin complexes in M06-2X optimization concurred with the findings of the NBO analysis suggesting a lower extent of charge transfer. Although, the value suggests a stable complex formation. The chemical potential (μ) as presented in Table 4.4 also suggests a similar understanding. Overall, it can be concluded that all the DES-enoxacin complexes are quite stable in their formation.

4.4.6.5 Investigation of Weak Interactions using Quantum Theory of "Atoms in Molecules" Analysis

The Quantum Theory of "Atoms in Molecules" or the QTAIM analysis was incorporated as a powerful technique to understand the different intermolecular interactions among the components present in the DES-enoxacin system where multiple donor and acceptor pairs are involved. Based on Bader's QTAIM scheme,[34] one can interpret the various non-covalent interactions between molecules or atoms by analyzing the electron density distribution at the so-called bond critical points or BCPs (3,−1). A BCPs is the critical point between two neighbouring atoms that exists as a saddle point with maximum electron density in two directions and minimum in one direction perpendicular to the others defining a bonded interaction. The electron density at BCP (ρ_{BCP}) and its Laplacian ($\nabla\rho_{BCP}^2$) provide valuable information regarding the nature, mechanism and strength of the interaction.[35] The ρ_{BCP} corresponds to the strength of the interaction and the sign of $\nabla\rho_{BCP}^2$ specifies the character of the interaction. A higher value of the electron density in the BCP suggests a stronger bonding interaction whereas, a smaller value indicates lower bond strength and larger interatomic distance. A negative Laplacian of electron density ($\nabla\rho_{BCP}^2$) designates a covalent bond, whereas a positive value suggests closed-shell interactive properties such as ionic, van der Waals, or hydrogen bonds.[36] Along with these two properties, energetic property such as the electron energy density at BCP (H_{BCP}), which is a combination of kinetic (G_{BCP}) and potential (V_{BCP}) energy density components, is useful in determining the type of interaction. The value of ($-G_c/V_c$) attains a value greater than 1 when noncovalent interaction is present, and it indicates a partly covalent nature of the interaction as the value ranges between 0.5 and 1. All these calculated values for the DES-enoxacin complex molecular system are presented in Table

4.5. The analysis supports the proposed criteria of weak interactions as all the electron densities (ρ_{BCP}) lie within the range of 0.002-0.034 a.u. and the Laplacian of electron densities ($\nabla\rho_{BCP}^2$) varying between 0.024-0.139 a.u.

Table 4.5: Electron Density (ρ_{BCP}), the Laplacian of Electron Density ($\nabla\rho_{BCP}^2$) and the energetic components at the Relevant BCPs in the [DES-enoxacin] complexes

Component pair	BCP interaction	Distance (Å)	ρ_{BCP} (a.u.)	$\nabla\rho_{BCP}^2$ (a.u.)	G_c (a.u.)	V_c (a.u.)	$-G_c/V_c$
DES1-ENO	BCP1: H_{31}-O_{51}	1.888	0.0286	0.1102	0.0259	−0.0243	1.066
	BCP2: O_{30}-H_{53}	1.956	0.0238	0.0959	0.0219	−0.0198	1.106
	BCP3: O_{30}-H_{77}	1.780	0.0340	0.1275	0.032	−0.0321	0.997
	BCP4: H_{25}-O_{76}	2.680	0.0076	0.0308	0.0065	−0.0052	1.250
	BCP5: H_{21}-O_{76}	2.465	0.0096	0.0370	0.0078	−0.0064	1.218
	BCP6: C_{50}-O_{75}	2.767	0.0118	0.0473	0.0103	−0.0088	1.170
	BCP7: H_{46}-O_{75}	2.649	0.0066	0.0254	0.0054	−0.0044	1.227
DES2-ENO	BCP1: H_{31}-O_{54}	2.069	0.0212	0.0731	0.0168	−0.0153	1.098
	BCP2: O_{30}-H_{56}	1.775	0.0382	0.1204	0.0318	−0.0335	0.949
	BCP3: O_{55}-H_{83}	2.809	0.0056	0.0183	0.004	−0.0034	1.176
	BCP4: O_{55}-H_{81}	2.871	0.0054	0.0202	0.0043	−0.0035	1.228
	BCP5: O_{55}-H_{80}	2.653	0.0071	0.0249	0.0053	−0.0044	1.204
	BCP6: O_{30}-H_{100}	1.928	0.0263	0.0972	0.0226	−0.0209	1.081
	BCP7: O_{99}-H_{25}	3.540	0.0014	0.0052	0.0009	−0.0006	1.500
	BCP8: O_{54}-H_{81}	2.813	0.0053	0.0174	0.0037	−0.0031	1.194
	BCP9: O_{54}-H_{114}	1.854	0.0292	0.1083	0.0256	−0.0241	1.062
	BCP10: C_{53}-O_{112}	2.876	0.0105	0.0379	0.0083	−0.0071	1.169
	BCP11: H_{13}-O_{113}	2.631	0.0071	0.0206	0.0046	−0.004	1.150
	BCP12: H_{19}-O_{115}	2.752	0.0054	0.0158	0.0035	−0.003	1.167
DES3-ENO	BCP1: H_{60}-O_{20}	1.681	0.0443	0.1652	0.0449	−0.0485	0.926
	BCP2: O_{58}-H_{92}	1.635	0.048	0.1797	0.0497	−0.0545	0.912
	BCP3: C_{57}-O_{114}	2.920	0.0093	0.0372	0.0081	−0.0069	1.174
	BCP4: O_{90}-H_{116}	1.684	0.0435	0.1627	0.0441	−0.0475	0.928
	BCP5: H_{50}-N_{120}	2.835	0.006	0.0199	0.0045	−0.0039	1.154
	BCP6: H_{44}-N_{119}	2.788	0.0066	0.0203	0.0045	−0.0039	1.154
	BCP7: H_{62}-N_{142}	2.795	0.0069	0.0209	0.0048	−0.0043	1.116
	BCP8: H_{65}-F_{118}	3.090	0.0019	0.0101	0.0019	−0.0012	1.583
	BCP9: H_{22}-O_{114}	1.645	0.0476	0.1762	0.0489	−0.0537	0.911

The molecular graphs of [DL-menthol- decanoic acid]/ [enoxacin] complex, [DL-menthol- dodecanoic acid]/ [enoxacin] complex and [decanoic acid- dodecanoic acid]/ [enoxacin] complex is presented in Figure 4.13. Positive values attained for all the BCPs confirm closed-shell noncovalent interactions among the different components present in the molecular space. Higher electron density and Laplacian of electron density at BCP1 (H_{31}-O_{51}) and BCP2 (O_{30}-H_{53}) indicate stronger intermolecular closed-shell interaction (primarily hydrogen bond and van der Waals interaction) between the HBA and the HBD components of the DES1. This can be corroborated by the shorter distance between the atoms (1.888 to 1.956 Å) thus forming a stronger interaction. The non-covalent interactions in the DES1-enoxacin complex can be further established by the values of ($-G_c/V_c$) as a value greater than 1 is obtained in all the BCPs except for BCP3, where it attains a value of 0.997, slightly less than 1. As the interaction between O_{30} (DL menthol) and H_{77} (enoxacin) is significantly short (1.78 Å), a partly covalent nature of interaction can be witnessed along with the non-covalent interaction between the HBA and the drug molecule. This interaction is substantially stronger as can be revealed by the higher values of ρ_{BCP} and $\nabla\rho_{BCP}^2$. The rest of the BCPs, i.e., BCP4, BCP5, BCP6 and BCP7, have comparatively lower values of electron density as well as the Laplacian of electron density. This implies that the H_{25}-O_{76} and H_{21}-O_{76} pairs between menthol and enoxacin, and the C_{50}-O_{75} and H_{46}-O_{75} pairs between decanoic acid and enoxacin correspond to weaker nonbonded interactions.

The BCPs associated with DES2-enoxacin and DES3-enoxacin complexes reveal a quantum of non-covalent interactions as described by the relevant electron densities obtained by the components in the complex. A large number of possible dispersion interactions and hydrogen bonding connections are observed supporting a stable complex formation between DES and enoxacin molecule supported by closed-shell con-covalent interactions as most of the BCPs obtained the ($-G_c/V_c$) value of greater than 1.

The QTAIM analysis indicates the coherent existence of multiple weak interactions in the form of noncovalent interactions such as hydrogen bonds and van der Waals interaction.

(a)

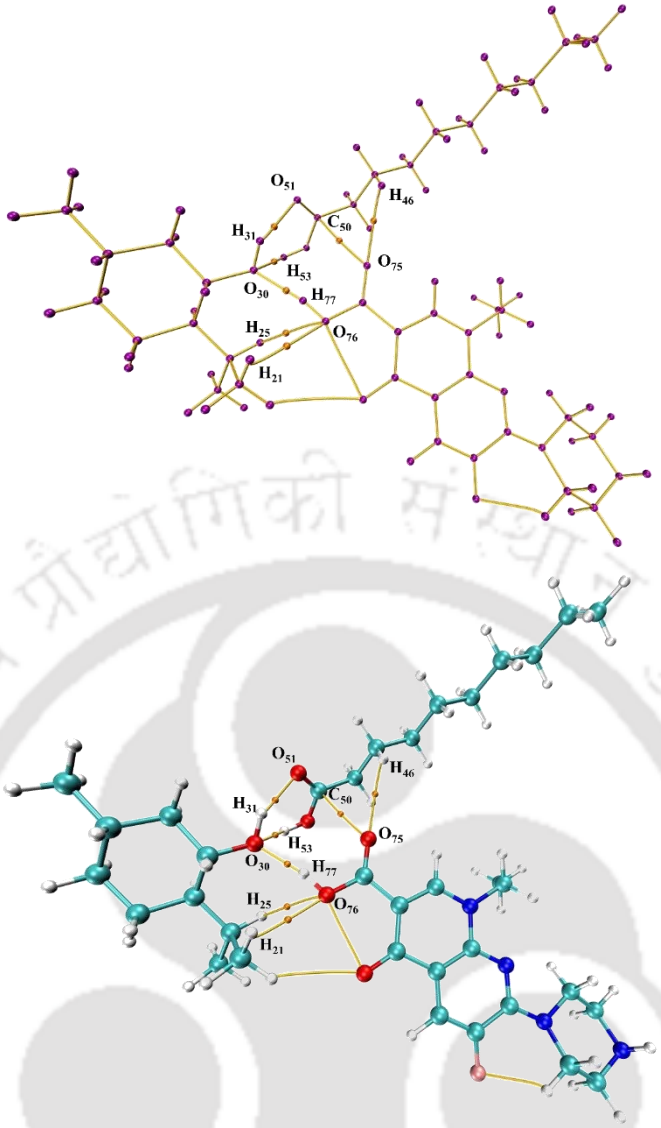
O51
H46
C50
H31
O75
H53
O30
H77
H25
O76
H21
O51
H46
C50
H31
O75
H53
O30
H77
H25
O76
H21

(b)

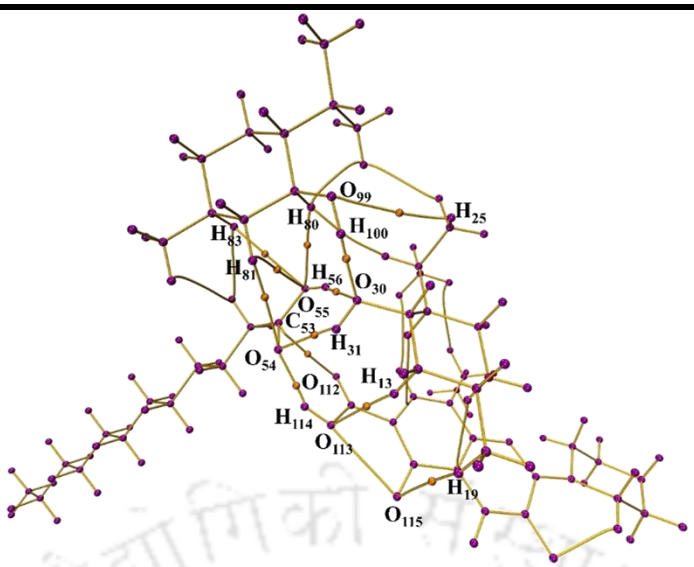
O99
H25
H80
H100
H83
H81
H56
O30
O55
C53
H31
O54
H13
O112
H114
O113
H19
O115

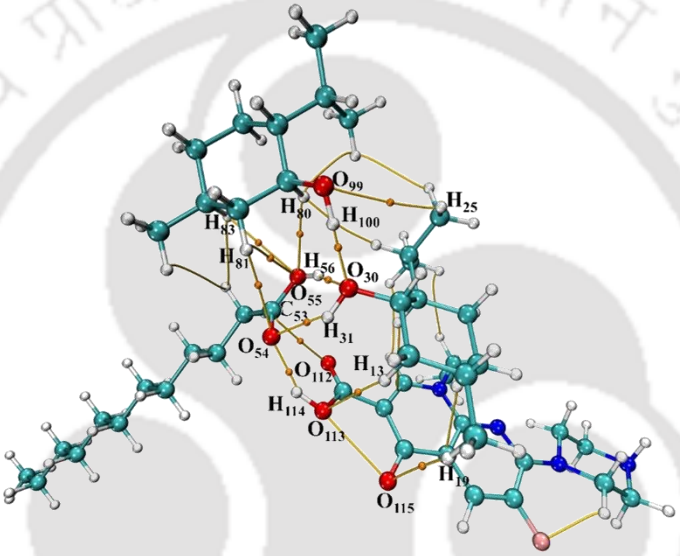
O99
H25
H80
H100
H83
H81
H56
O30
O55
C53
H31
O54
H13
O112
H114
O113
H19
O115

(c)

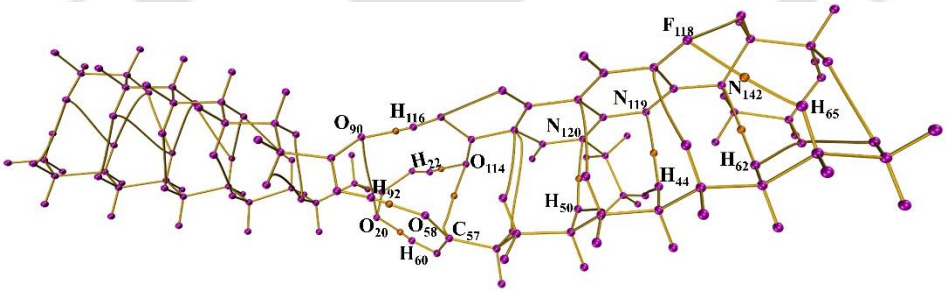
F118
N142
N119
H65
O90
H116
N120
H22
O114
H62
H92
H44
H50
O20
O58
C57
H60

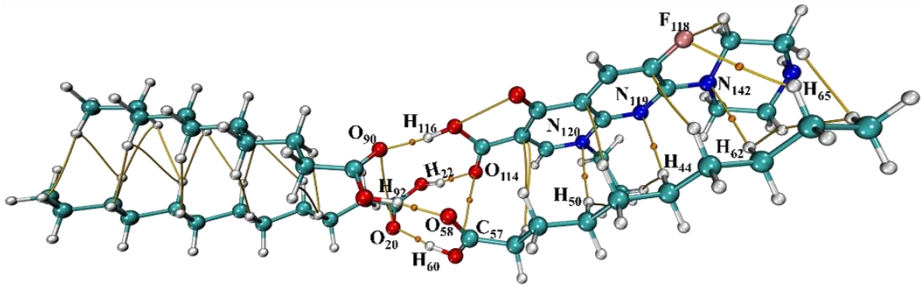
F118
N142
N119
H65
O90
H116
N120
H22
O114
H62
H92
H44
H50
O20
O58
C57
H60

Figure 4.13: Molecular graphs of (a) [DL-menthol- decanoic acid]/ [enoxacin] complex, (b) [DL-menthol- dodecanoic acid]/ [enoxacin] complex, (c) [decanoic acid- dodecanoic acid]/ [enoxacin] complex at the M06-2X/6-311+G(d,p) level revealing bond critical points (BCPs) and their corresponding paths.

4.4.6.6 Noncovalent Interactions

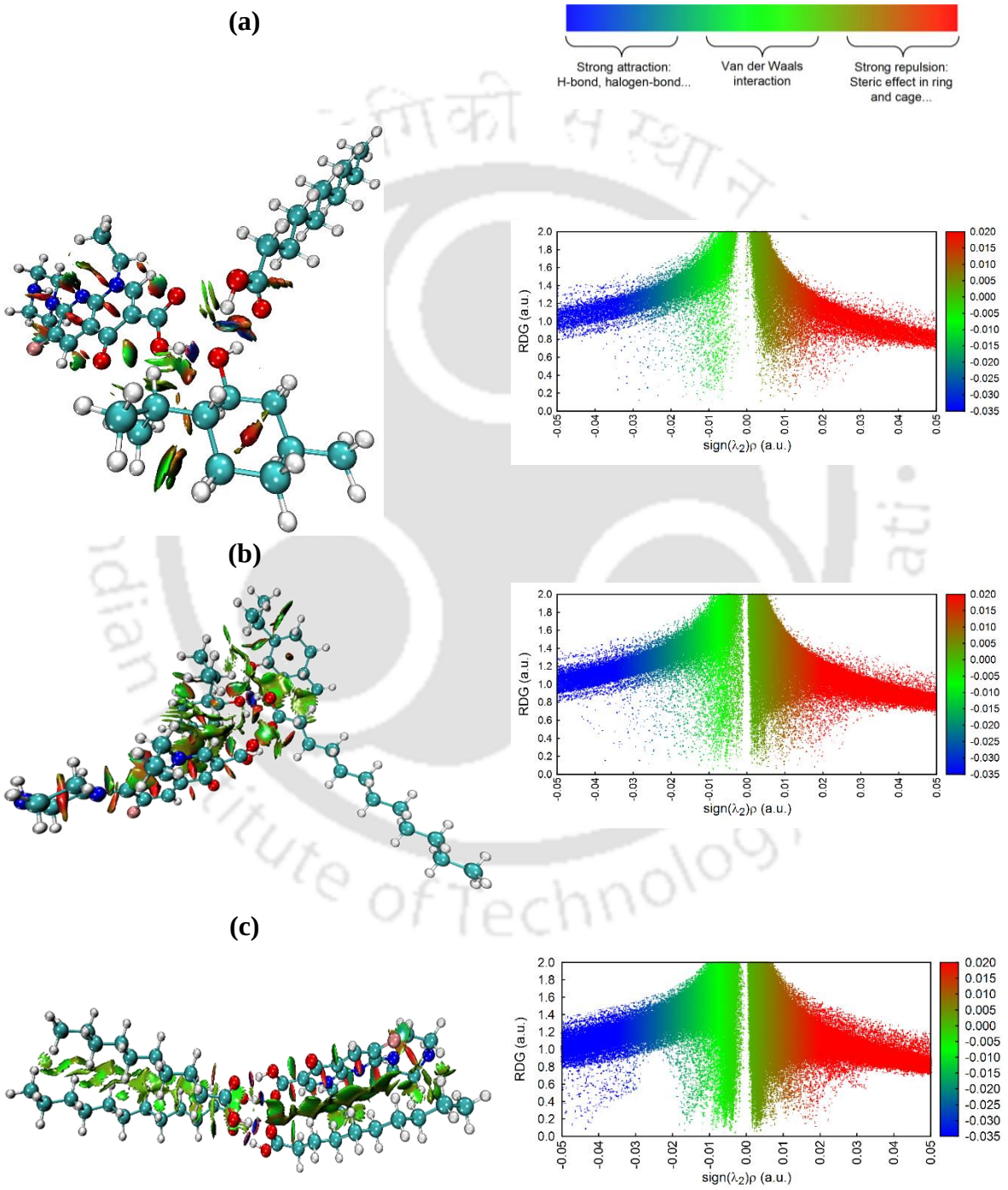

Figure 4.14: RDG isosurfaces and scatter graphs of RDG for (a) [DL-menthol- decanoic acid]/ [enoxacin] complex, (b) [DL-menthol- dodecanoic acid]/ [enoxacin] complex, and (c) [decanoic acid- dodecanoic acid]/ [enoxacin] at the M06-2X/6-311+G(d,p) level.

The study of noncovalent interactions, or NCI, developed by Contreras-Garcı́a and Johnson[37–39] is implemented to overcome the numerical accuracy of the AIM analysis.[40] The approach is termed a 'reduced density gradient' or, 'RDG' analysis which is based on analysing the electron density distribution where low electron density and low gradient value regions are present and are expressed by the following equation.

$$\mathrm{RDG} = \frac{1}{2(3\pi^2)^{1/3}} \frac{|\nabla\rho|}{\rho^{4/3}} \qquad (4.5)$$

The interpretation of the RDG spikes provides valuable NCI analysis.[41] Different kinds of weak interactions such as hydrogen bonding, van der Waals and dispersion interactions, can be revealed and quantified by the NCI analysis using the RDG method. The RDG scatter graph is plotted as a function of electron density multiplied by the sign of the electron density Hessian second eigenvalue, $[\mathrm{sign}(\lambda_2)\rho]$. Figure 4.14 shows the RDG isosurfaces and the RDG scatter plot revealing various weak interactions ranging from positive to negative $[\mathrm{sign}(\lambda_2)\rho]$ values for the [DL-menthol- decanoic acid]/ [enoxacin] complex, [DL-menthol- dodecanoic acid]/ [enoxacin] complex and [decanoic acid- dodecanoic acid]/ [enoxacin] complex at the M06-2X/6-311+G(d,p) level of theory. Spikes present in the different coloured regions suggest specific interaction types (blue: H-bonds; green: van der Waals or dispersion interaction; and red: steric effect). The attractive interactions occur in the regions where $\lambda_2 < 0$ and for the vdW interactions, the λ_2 value approaches 0. Repulsive interaction can be identified as regions where $\lambda_2 > 0$. Bonded interactions ($\lambda_2 < 0$) can be distinguished from nonbonded interactions ($\lambda_2 > 0$).[37] The present RDG study denotes the presence of the combination of hydrogen bonding and dispersion interactions (vdW) as multiple low-density RDG peaks are witnessed between 0 to −0.02 a.u. The density of the RDG peaks in this region is higher in the case of DES3 as compared to DES1 and DES2 due to the closely packed arrangement of DES3 and enoxacin. The presence of this vdW interaction along with hydrogen bonding at a lower order can be witnessed by the iso-surfaces of the RDG analysis. These interactions are confirmed and presented earlier in DFT analysis section of the quantum chemical analysis. The dispersion interactions between the DES and enoxacin moiety are responsible for a more stable structural arrangement of the DES-enoxacin complex leading to higher non-covalent intermolecular interactions. The existence of attractive interactions such as hydrogen bonding can be confirmed by the lowly dense RDG peaks between −0.05 to −0.02 a.u. Thus, it is certain that dispersion along with hydrogen bonding interactions are dominantly responsible in developing non-covalent interactions. The presence of bulky groups in the molecular systems gives rise to steric hindrance which can be witnessed by the RDG peaks

obtained in the range > 0.005 a.u. The spike present in the range > 0.02 a.u. can be attributed to the long-chain hydrophobic part of fatty acids (decanoic and dodecanoic acid) and the intermittent ring structures present within the DES constituents. The dominant presence of dispersion interactions within the molecular system supports the fact that DES components interact with the enoxacin molecules via non-covalent interactions devoid of any significant electrostatic interaction.

4.5 Conclusion

The experimental extraction of enoxacin from the aqueous environment with three hydrophobic DESs was performed. An 82.6% extraction efficiency for DL-menthol: decanoic acid-based DES (DES1) was obtained followed by 79.6% and 69.1% for DL-menthol: dodecanoic acid and decanoic acid: dodecanoic acid-based DESs, respectively. The results were obtained for a DES/water mass ratio of 1:1 at 20 ppm of initial concentration of enoxacin in water. A higher distribution ratio of 4.75 has been obtained for DES1 signifying an effective extraction performance with higher selectivity. Decanoic acid: dodecanoic acid-based DES (DES3) works better in lower initial drug concentrations of 5 ppm as compared to the other two DESs. Three different recycling frameworks were then implemented. Around 90% net extraction efficiency was achieved in the third run in the 3rd recycle process where fresh DES (DL-menthol: decanoic acid) was introduced in every run and the reduced enoxacin solution was used as a continuous feed. Overall, the reuse and recyclability of the DES were demonstrated which implies its effectiveness in maintaining a sustainable approach.

Finally, the quantum chemical study on the DES-enoxacin complexes suggests a stable formation of the DES-enoxacin complex in the DES phase. In general, all the DESs are relatively stable in terms of their respective HOMO-LUMO energy gap and interaction energy. The DES-enoxacin complexes possess a stable structural arrangement with multiple interactions with the menthol as well as the decanoic acid molecule. Non-bonded interactions such as hydrogen bonding and dispersion interactions were present in the formation of the DES and the DES-enoxacin complexes. The distance of interaction ranges from 1.731 to 2.061 Å for DL-menthol: C_{10} DES, whereas for the DES-enoxacin complex, long-range interactions at 1.779 to 3.349 Å distance were observed. In the DES2-enoxacin complex, the interaction distance ranges from 1.85 to 3.25 Å and for the DES3-enoxacin complex, it is from 1.64 to 1.68 Å. Higher compactness can be witnessed in terms of a significant lowering of the interaction energy for the DES as well as the DES-enoxacin formation. The NBO study suggests the direction of charge transfer is from DES to enoxacin for DES1 and from enoxacin to DES, in the case of DES2 and DES3. Overall, the three DESs are quite effective in the

removal of enoxacin from an aqueous environment to impart a green and sustainable approach to water purification. The QTAIM analysis suggests the formation of the DES-enoxacin complex via a combined effect of hydrogen bonding linkage with van der Waals dispersion interaction as supported by the electron density at BCP (ρ_{BCP}) and the Laplacian of electron density ($\nabla\rho_{BCP}^2$). The NCI plot with RDG analysis was performed to highlight the regions of weak interaction. Hydrogen bonding and dispersion interactions (vdW) were witnessed between 0 to −0.02 a.u. confirming the presence of weak nonbonded interactions in the formation of DES as well as the DES-enoxacin complex.

References

[1] Y. Luo, W. Guo, H.H. Ngo, L.D. Nghiem, F.I. Hai, J. Zhang, S. Liang, X.C. Wang, A review on the occurrence of micropollutants in the aquatic environment and their fate and removal during wastewater treatment., Sci. Total Environ. 473–474 (2014) 619–641. https://doi.org/10.1016/j.scitotenv.2013.12.065.

[2] M.T. Amin, A.A. Alazba, U. Manzoor, A Review of Removal of Pollutants from Water/Wastewater Using Different Types of Nanomaterials, Adv. Mater. Sci. Eng. 2014 (2014) 825910. https://doi.org/10.1155/2014/825910.

[3] J.C. López-Montilla, S. Pandey, D.O. Shah, O.D. Crisalle, Removal of non-ionic organic pollutants from water via liquid-liquid extraction., Water Res. 39 (2005) 1907–1913. https://doi.org/10.1016/j.watres.2005.02.018.

[4] A.P. de los Ríos, F.J. Hernández-Fernández, L.J. Lozano, S. Sánchez, J.I. Moreno, C. Godínez, Removal of Metal Ions from Aqueous Solutions by Extraction with Ionic Liquids, J. Chem. Eng. Data. 55 (2010) 605–608. https://doi.org/10.1021/je9005008.

[5] I. Ali, V.K. Gupta, Advances in water treatment by adsorption technology, Nat. Protoc. 1 (2006) 2661–2667. https://doi.org/10.1038/nprot.2006.370.

[6] V.K. Gupta, B. Gupta, A. Rastogi, S. Agarwal, A. Nayak, Pesticides removal from waste water by activated carbon prepared from waste rubber tire., Water Res. 45 (2011) 4047–4055. https://doi.org/10.1016/j.watres.2011.05.016.

[7] M. Carballa, F. Omil, J.M. Lema, Issn : 1579-4377 Removal of Pharmaceuticals and Personal Care Products (Ppcps) From Municipal Wastewaters By Physico-Chemical Processes, (1999) 309–313.

[8] C. Florindo, F. Lima, L.C. Branco, I.M. Marrucho, Hydrophobic Deep Eutectic Solvents: A Circular Approach to Purify Water Contaminated with Ciprofloxacin,

ACS Sustain. Chem. Eng. 7 (2019) 14739–14746. https://doi.org/10.1021/acssuschemeng.9b02658.

[9] A.P. Abbott, D. Boothby, G. Capper, D.L. Davies, R.K. Rasheed, Deep Eutectic Solvents Formed between Choline Chloride and Carboxylic Acids: Versatile Alternatives to Ionic Liquids, J. Am. Chem. Soc. 126 (2004) 9142–9147. https://doi.org/10.1021/ja048266j.

[10] E.L. Smith, A.P. Abbott, K.S. Ryder, Deep Eutectic Solvents (DESs) and Their Applications, Chem. Rev. 114 (2014) 11060–11082. https://doi.org/10.1021/cr300162p.

[11] W. Tang, Y. An, K.H. Row, Emerging applications of (micro) extraction phase from hydrophilic to hydrophobic deep eutectic solvents: opportunities and trends, TrAC Trends Anal. Chem. 136 (2021) 116187. https://doi.org/https://doi.org/10.1016/j.trac.2021.116187.

[12] N. Paul, P.K. Naik, B.D. Ribeiro, P.S. Gooh Pattader, I.M. Marrucho, T. Banerjee, Molecular Dynamics Insights and Water Stability of Hydrophobic Deep Eutectic Solvents Aided Extraction of Nitenpyram from an Aqueous Environment, J. Phys. Chem. B. 124 (2020) 7405–7420. https://doi.org/10.1021/acs.jpcb.0c03647.

[13] D.J.G.P. van Osch, L.F. Zubeir, A. van den Bruinhorst, M.A.A. Rocha, M.C. Kroon, Hydrophobic deep eutectic solvents as water-immiscible extractants, Green Chem. 17 (2015) 4518–4521. https://doi.org/10.1039/C5GC01451D.

[14] B.D. Ribeiro, C. Florindo, L.C. Iff, M.A.Z. Coelho, I.M. Marrucho, Menthol-based Eutectic Mixtures: Hydrophobic Low Viscosity Solvents, ACS Sustain. Chem. Eng. 3 (2015) 2469–2477. https://doi.org/10.1021/acssuschemeng.5b00532.

[15] C. Florindo, L.C. Branco, I.M. Marrucho, Development of hydrophobic deep eutectic solvents for extraction of pesticides from aqueous environments, Fluid Phase Equilib. 448 (2017) 135–142. https://doi.org/https://doi.org/10.1016/j.fluid.2017.04.002.

[16] E.E. Tereshatov, M.Y. Boltoeva, C.M. Folden, First evidence of metal transfer into hydrophobic deep eutectic and low-transition-temperature mixtures: indium extraction from hydrochloric and oxalic acids, Green Chem. 18 (2016) 4616–4622. https://doi.org/10.1039/C5GC03080C.

[17] C. Florindo, L. Romero, I. Rintoul, L.C. Branco, I.M. Marrucho, From Phase Change Materials to Green Solvents: Hydrophobic Low Viscous Fatty Acid–Based Deep

Eutectic Solvents, ACS Sustain. Chem. Eng. 6 (2018) 3888–3895. https://doi.org/10.1021/acssuschemeng.7b04235.

[18] W. Tang, Y. Dai, K.H. Row, Evaluation of fatty acid/alcohol-based hydrophobic deep eutectic solvents as media for extracting antibiotics from environmental water., Anal. Bioanal. Chem. 410 (2018) 7325–7336. https://doi.org/10.1007/s00216-018-1346-6.

[19] S. Arayne, N. Sultana, U. Haroon, M.A. Mesaik, Synthesis, Characterization, Antibacterial and Anti-Inflammatory Activities of Enoxacin Metal Complexes, Bioinorg. Chem. Appl. 2009 (2009) 914105. https://doi.org/10.1155/2009/914105.

[20] J. Fick, H. Söderström, R.H. Lindberg, C. Phan, M. Tysklind, D.G.J. Larsson, Contamination of surface, ground, and drinking water from pharmaceutical production., Environ. Toxicol. Chem. 28 (2009) 2522–2527. https://doi.org/10.1897/09-073.1.

[21] N. Paul, T. Banerjee, Study on the Extraction of Acetamiprid and Imidacloprid from an Aqueous Environment Using Menthol-Based Hydrophobic Eutectic Solvents: Quantum Chemical and Molecular Dynamics Insights, ACS Sustain. Chem. Eng. 10 (2022) 4227–4246. https://doi.org/10.1021/acssuschemeng.2c00023.

[22] D. V Wagle, H. Zhao, C.A. Deakyne, G.A. Baker, Quantum Chemical Evaluation of Deep Eutectic Solvents for the Extractive Desulfurization of Fuel, ACS Sustain. Chem. Eng. 6 (2018) 7525–7531. https://doi.org/10.1021/acssuschemeng.8b00224.

[23] G. García, M. Atilhan, S. Aparicio, An approach for the rationalization of melting temperature for deep eutectic solvents from DFT, Chem. Phys. Lett. 634 (2015) 151–155. https://doi.org/https://doi.org/10.1016/j.cplett.2015.06.017.

[24] M.J. Frisch, G.W. Trucks, H.B. Schlegel, G.E. Scuseria, M.A. Robb, J.R. Cheeseman, G. Scalmani, V. Barone, B. Mennucci, G.A. Petersson, others, Gaussian 16, Gaussian Inc., Wallingford, CT. Gaussian 1 (2016).

[25] C. Lee, W. Yang, R.G. Parr, Development of the Colle-Salvetti correlation-energy formula into a functional of the electron density., Phys. Rev. B. Condens. Matter. 37 (1988) 785–789. https://doi.org/10.1103/physrevb.37.785.

[26] A.D. Becke, Density-functional exchange-energy approximation with correct asymptotic behavior, Phys. Rev. A. 38 (1988) 3098–3100. https://doi.org/10.1103/PhysRevA.38.3098.

[27] A.D. Becke, Density-functional thermochemistry. III. The role of exact exchange, J. Chem. Phys. 98 (1993) 5648–5652. https://doi.org/10.1063/1.464913.

[28] Y. Zhao, D.G. Truhlar, The M06 suite of density functionals for main group thermochemistry, thermochemical kinetics, noncovalent interactions, excited states, and transition elements: two new functionals and systematic testing of four M06-class functionals and 12 other function, Theor. Chem. Acc. 120 (2008) 215–241. https://doi.org/10.1007/s00214-007-0310-x.

[29] S. Grimme, S. Ehrlich, L. Goerigk, Effect of the damping function in dispersion corrected density functional theory, J. Comput. Chem. 32 (2011) 1456–1465. https://doi.org/https://doi.org/10.1002/jcc.21759.

[30] K. Fukui, Theory of orientation and stereoselection BT - Orientation and Stereoselection, in: K. Fukui (Ed.), Springer Berlin Heidelberg, Berlin, Heidelberg, 1970: pp. 1–85.

[31] T. Lu, F. Chen, Multiwfn: A multifunctional wavefunction analyzer, J. Comput. Chem. 33 (2012) 580–592. https://doi.org/https://doi.org/10.1002/jcc.22885.

[32] H.F. Hizaddin, M.A. Hashim, R. Anantharaj, Evaluation of Molecular Interaction in Binary Mixture of Ionic Liquids + Heterocyclic Nitrogen Compounds: Ab Initio Method and COSMO-RS Model, Ind. Eng. Chem. Res. 52 (2013) 18043–18058. https://doi.org/10.1021/ie403032t.

[33] S. Simon, M. Duran, J.J. Dannenberg, How does basis set superposition error change the potential surfaces for hydrogen-bonded dimers?, J. Chem. Phys. 105 (1996) 11024–11031. https://doi.org/10.1063/1.472902.

[34] R.F.W. Bader, A quantum theory of molecular structure and its applications, Chem. Rev. 91 (1991) 893–928. https://doi.org/10.1021/cr00005a013.

[35] B. Bankiewicz, P. Matczak, M. Palusiak, Electron Density Characteristics in Bond Critical Point (QTAIM) versus Interaction Energy Components (SAPT): The Case of Charge-Assisted Hydrogen Bonding, J. Phys. Chem. A. 116 (2012) 452–459. https://doi.org/10.1021/jp210940b.

[36] M. Solimannejad, I. Alkorta, J. Elguero, Stabilities and properties of O3–HOCl complexes: A computational study, Chem. Phys. Lett. 449 (2007) 23–27. https://doi.org/https://doi.org/10.1016/j.cplett.2007.10.024.

[37] E.R. Johnson, S. Keinan, P. Mori-Sánchez, J. Contreras-García, A.J. Cohen, W. Yang, Revealing Noncovalent Interactions, J. Am. Chem. Soc. 132 (2010) 6498–6506. https://doi.org/10.1021/ja100936w.

[38] J. Contreras-García, E.R. Johnson, S. Keinan, R. Chaudret, J.-P. Piquemal, D.N. Beratan, W. Yang, NCIPLOT: a program for plotting non-covalent interaction regions., J. Chem. Theory Comput. 7 (2011) 625–632. https://doi.org/10.1021/ct100641a.

[39] J. Contreras-García, M. Calatayud, J.-P. Piquemal, J.M. Recio, Ionic interactions: Comparative topological approach, Comput. Theor. Chem. 998 (2012) 193–201. https://doi.org/https://doi.org/10.1016/j.comptc.2012.07.043.

[40] J.R. Lane, J. Contreras-García, J.-P. Piquemal, B.J. Miller, H.G. Kjaergaard, Are Bond Critical Points Really Critical for Hydrogen Bonding?, J. Chem. Theory Comput. 9 (2013) 3263–3266. https://doi.org/10.1021/ct400420r.

[41] B.A. Marekha, O.N. Kalugin, A. Idrissi, Non-covalent interactions in ionic liquid ion pairs and ion pair dimers: a quantum chemical calculation analysis, Phys. Chem. Chem. Phys. 17 (2015) 16846–16857. https://doi.org/10.1039/C5CP02197A.

Chapter- 5

Experimental and Computational Studies on Removal of Ciprofloxacin and Fluconazole from Water with Microfluidic Device-based Extraction by Hydrophobic Deep Eutectic Solvents

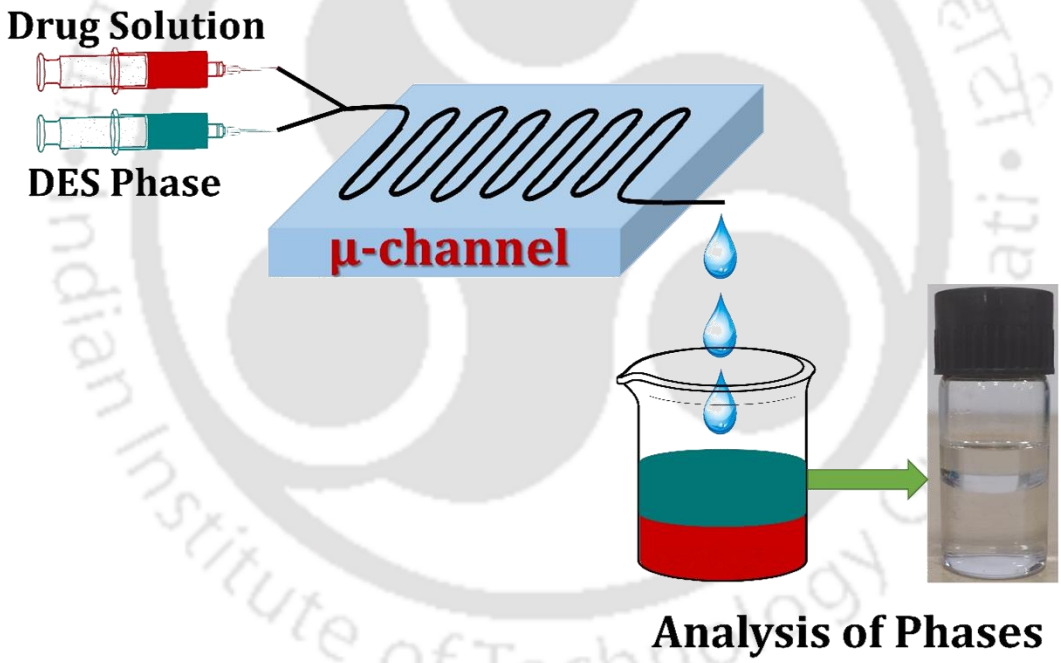

Manuscript in line:

N. Paul, S. K. Singh, P.S. Gooh Pattader, T. Banerjee, Enhancement of the Extraction Performance of Ciprofloxacin and Fluconazole via Microchannel-based Solvent Extraction with Hydrophobic Deep Eutectic Solvent- a Combined Experimental and MD Simulation Study. (ready for submission)

5 Experimental and Computational Studies on Removal of Ciprofloxacin and Fluconazole from Water with Microfluidic Device-based Extraction by Hydrophobic Deep Eutectic Solvents

The current chapter addresses the PDMS (Polydimethylsiloxane) microchannel-based continuous extraction of ciprofloxacin (antibiotic) and fluconazole (antifungal) from an aqueous environment by liquid-liquid extraction using two hydrophobic deep eutectic solvents (DES) namely, (a) DL-menthol: decanoic acid (1:1), (b) DL-menthol: dodecanoic acid (2:1). The influence of flow rate, residence time and DES/water mass ratio on extraction efficiency (%EE) have been evaluated through experiments. Later, QC calculation and molecular dynamics (MD) simulation have been implemented to obtain atomistic and molecular-level insights into the drug-DES complexes. Charge transfer (CT), frontier molecular orbital (FMO), non-bonded interaction energy, and hydrogen bonding analysis are performed to explain the stability and interactive nature of the components. Non-covalent interaction (NCI) associated with reduced density gradient (RDG) analysis was incorporated to understand the noncovalent interactions such as hydrogen bonding and dispersion interactions (van der Waals) that prevailed within the drug-DES complexes.

5.1 Introduction

In the previous chapter (chapter 4), we discussed the extraction of enoxacin from an aqueous stream using hydrophobic deep eutectic solvents with effective solvent regeneration with quantum chemical (QC) validations. The threat from drug-resistant microbes in aquatic sources is immense. It has been demonstrated that certain bulk medicine manufacturing plants in Hyderabad, South India, either dump trash into their surrounding environment or fail to treat factory outputs adequately, which results in the contamination of rivers and lakes [1–5]. Sewers in the Patancheru-Bollaram industrial area in Hyderabad, India included high quantities of moxifloxacin, voriconazole, and fluconazole (up to 694.1, 2500, and 236,950 µg/L, respectively), in addition to elevated concentrations of eight additional antibiotics.[6] Ciprofloxacin is also another antibiotic that was detected by research groups in surface water bodies well above its permissible limit. As a direct result of this, India has developed into a hotspot of drug resistance, which has had severe repercussions for therapeutic practice.

Thousands of newborn babies in India pass away every year as a result of diseases caused by bacteria that are resistant to the first line of antibiotic treatment. [7]

The majority of the studies related to pharmaceutical removal with the help of green solvents follow batch-type one-time solvent extraction processes using ionic liquids (ILs) and deep eutectic solvents (DESs). While these are effective in their easy-to-handle mechanism, they adhere to some drawbacks such as lower extraction efficiency, difficulty in handling a large volume of wastewater feed, high manufacturing and processing cost, and inability to operate as a continuous process. These problems hinder the evolution of a large-scale industrial waste-water treatment plant with a continuous circuit of removal with high efficiency and lesser wastage of green solvents. Thus, a continuous or semi-continuous process of pharmaceutical waste treatment can prove to be highly effective in terms of energy and solvent requirements along with economic advantage in developing a sustainable treatment approach. To attain the continuous circular approach of treatment, researchers have come up with a semi-batch approach to cleaning pharmaceutical wastewater.[8] However, the application of microfluidic platforms for the treatment of pharmaceutical wastewater through green solvents is very rare. The advantages of microfluidics are diverse and include a high surface-to-volume ratio, a very steady laminar flow, a diffusion-dominated mass transfer effect, the ability to handle a small sample size, parallel processes, a short reaction time, a low operational cost, etc.[9–12]

The objective of the current chapter involves the application of the hydrophobic DESs in the microfluidic device as a robust, efficient, sensitive, and cost-effective extraction process of ciprofloxacin and fluconazole, heavily polluting the surface water streams adjacent to a pharmaceutical wastewater treatment plant. DL-menthol: decanoic acid (1:1) and DL-menthol: dodecanoic acid (2:1) DESs were the most suitable hydrophobic DESs for solvent extraction of these drugs from an aqueous environment. The study involves the fabrication of a Polydimethylsiloxane (PDMS) microchannel and the investigation of the ciprofloxacin and fluconazole extraction performance at variable inlet flowrates with an increase in the residence time at different DES/water phase mass ratios. All the experiments were carried out at atmospheric pressure and 298.15 K.

In the later sections, quantum chemical (QC) calculations have been performed for the DES-drug complexes. This incorporated the optimization of the DES-complex by Gaussian 16,[13] followed by the charge transfer (CT) process. the stability of the complex was analyzed with frontier molecular orbital (FMO) analysis that involves the frontier orbital energy gap. The QC calculation elucidates the strength of the DES-drug interaction and provides insights regarding the interaction mechanism with structural arrangement combined with charge transfer behaviour. Further, non-covalent interaction (NCI) plots were obtained to understand

the multiple closed-shell non-covalent interacting components in the formation of the DES-drug complex along with molecular dynamics (MD) simulation analysis to boost the overall interactive insights.

5.2 Materials and Methods

5.2.1 Materials

DL-menthol (purity ≥ 95%), decanoic acid (C_{10}) (purity ≥ 98%), and dodecanoic acid (C_{12}) (purity ≥ 98%) were purchased from Sigma-Aldrich and used as received. Ciprofloxacin (purity ≥ 98%) and fluconazole (purity ≥ 98%) in powder form were also purchased from Sigma-Aldrich and were used as supplied. All aqueous solutions and eutectic solvents were prepared by weighing the required mass using a Mettler Toledo analytic laboratory balance (Model: ME204/A04). Water used in all the experiments was obtained from an in-house high-quality Millipore water synthesis unit. Sylgard^{TM}184 Silicone Elastomer Kit was purchased from Dow Chemical International PVT. LTD. USA, for the preparation of polydimethylsiloxane (PDMS). Acrylonitrile Butadiene Styrene (ABS) filament was obtained from Ultimaker, Netherlands. Filter paper (100R) was purchased from Axiva, India. Silicone rubber tubes and non-toxic polyethylene tubing were purchased from Sigma-Aldrich USA and Pro Lab Marketing PVT. LTD. India, respectively. 10 mL Dispo Van disposable syringes were purchased from 1 mg, India.

5.2.1.1 Apparatus

The fluids inside the μ-mixture reactor were infused at a steady rate using a syringe pump (Harvard Apparatus, PHD 2000). Silicone rubber tubing (Sigma-Aldrich, I.D. × O.D. 1/16 in. × 1/8 in.) and micropipette tips (Tarsons, 0.2 μL - 10 μL) were used to connect the syringe to the μ-reactor and the μ-reactor outlet to the sample collection.

The round serpentine shape of the Acrylonitrile Butadiene Styrene (ABS) wire was produced using a 3D printer (Ultimaker 3, Netherlands). As a sacrificial mould, this 3D-printed ABS wire was utilized to fabricate a PDMS microfluidic channel with an internal diameter of d ~ 500 μm.

5.2.2 Methods

5.2.2.1 Preparation of Aqueous Stock Solutions of Ciprofloxacin and Fluconazole

Ciprofloxacin and fluconazole aqueous stock solution with a concentration of 10 ppm and 236 ppm, respectively, were prepared by mixing the required amount of the drug in a specific amount of high-quality Millipore water. The mixtures were then subjected to vigorous stirring at 450 rpm at 25 °C for almost 24 hours to ensure complete miscibility of the micropollutant and to reach equilibrium in the water phase. A calibration curve containing the micropollutant in Millipore water (curve with $R^2 > 0.999$) was obtained for the quantification of LLE experimental findings and presented in Figure E.1 (see Appendix E). The absorbance peak containing the highest UV-absorbance at 275 nm for ciprofloxacin, and 261 nm wavelength for fluconazole was considered for the quantification purpose.

5.2.2.2 Fabrication of μ-mixture Reactor

The 3D printer was used to extrude ABS into a serpentine microfilament (d ~ 500 μm) (Ultimaker 3). The PDMS microchannel was fabricated by molding technique. Sylgard™ 184 elastomer kit components A (oligomer) and B (crosslinker) were combined in a 10:1 ratio first. After that, the mixture underwent 40 minutes of degassing in a vacuum desiccator to get rid of any remaining air bubbles. Rectangular molds were made using double-sided tape and a cleaned glass slide. The glass slide was coated with a thin layer of oligomer by pouring a little amount of the oligomer-crosslinker mixture into it and shaking it. After 30 minutes in a hot air oven set to 85 °C, the film was only partially cured before being allowed to cool to room temperature. The thin partially cured PDMS layer was placed on top of the prefabricated 3D-printed serpentine ABS microfilament, which was then washed with DI water and dried with nitrogen flow. It was then poured with more of the degassed oligomer-crosslinker (10:1) solution. After pouring the oligomers-crosslinker mixture, it was checked to make sure no air bubbles had become trapped within the liquid. Finally, the setup spent six hours in an 85 °C hot air oven to crosslink the PDMS. The ABS filament was cut with care to ensure that its ends were outside of the PDMS block. The PDMS block with the embedded ABS microfilament was allowed to cure before being submerged for 12 hours in an acetone bath. Acetone was used to dissolve the ABS microfilament, which resulted in the fabrication of a microchannel within the PDMS block. Afterwards, the PDMS block containing the microchannel was ultra-sonicated in an acetone bath for 5 hours to ensure that all traces of ABS had been removed. The microchannel was then cleaned for a total of 10–15 minutes with DI water and acetone. After washing, the micro-channel was dried by blowing nitrogen gas and kept in a 75 °C hot air oven for 30 minutes.

5.2.2.3 Preparation of DES

DESs were prepared by mixing both the compounds (HBA and HBD) in a reagent bottle at 50 ºC with a stirring speed of 450 rpm until a homogeneous liquid mixture was formed. The prepared DESs were then kept at room temperature for two to three days to ensure equilibrium and stability, before using them for further experiments. The Karl Fischer titration (Metrohm 870 KF Titrino Plus) was used to evaluate the water content of each pure hydrophobic DES, and the analysis indicated a water content of < 400 ppm.

5.2.2.4 Computational Framework

Initially, DFT calculations for DES and drug optimization were done at the B3LYP/6-311+G(d,p)[14–16] level of theory. D3BJ dispersion correction[17] was introduced for the former level of theory to incorporate the dispersion forces that might be present in the DES and DES-drug structural arrangements. The individual structures of DES (i.e., HBA and HBD) and drug (ciprofloxacin and fluconazole) were built in Gaussview 6 builder package and the structures were optimized using Gaussian 16.[13] The optimization of the DES structures was accomplished by arranging the components (HBA and HBD) in different orientations to obtain the minimum energy arrangement. Likewise, the micropollutant (ciprofloxacin, fluconazole) molecule was placed into the optimized DES structure and the DES-drug complex arrangement was optimized subsequently after different conformer analyses around the DES components. Vibrational frequency analysis at the very same theoretical level was carried out using the '*freq'* keyword in Gaussian to validate the minimal state of the potential energy surface (PES). Analysis of DES, drug, and DES-drug complex was conducted with B3LYP/6-311+G(d,p) functional to understand the stability, charge transfer (CT) process and interactions among the compounds through Frontier molecular orbital[18] (FMO) analysis. The non-covalent interaction (NCI) studies were carried out using Multiwfn code.[19]

The molecular dynamics (MD) simulation scheme is similar as mentioned in the earlier chapters (chapters 2 and 3). Non-bonded interaction energy and H-bonding analysis were carried out to investigate the DES-drug interaction and the relative affinity of the drugs towards the DES phase.

5.3 Results and Discussion

5.3.1 Screening of Different Hydrophobic DESs with Potential to Extract Drugs

To accomplish the microchannel-based enhancement of the extraction performance of the DESs to extract the drugs (ciprofloxacin and fluconazole) from the aqueous phase, the best-

performing DESs need to be identified considering various factors such as low melting point, higher solubility of drugs, better hydrophobicity and easy application at room temperature. To achieve that, a screening analysis of various hydrophobic DESs was carried out to extract ciprofloxacin and fluconazole, respectively and separately in a one-step batch solvent extraction process and the extraction efficiency (%EE) results have been presented in Figure 5.1.

The screening experiments were carried out for a single DES phase/water phase mass ratio (1:1) for each of the DESs as mentioned in Figure 5.1. A temperature-controlled water bath was used to ensure uniform temperature throughout the experiments, which in the present study was kept at room temperature (25 ºC). The mixtures were allowed to stir vigorously at a stirring speed of 450 rpm achieving a full central vortex formation within the vials. Subsequently, the mixtures were allowed to settle for about 16 hours until a complete phase separation of the DES and water phase occurred. The separated DES and water phases were collected with precaution and the concentration of the drugs was quantified with UV-vis spectroscopy analysis.

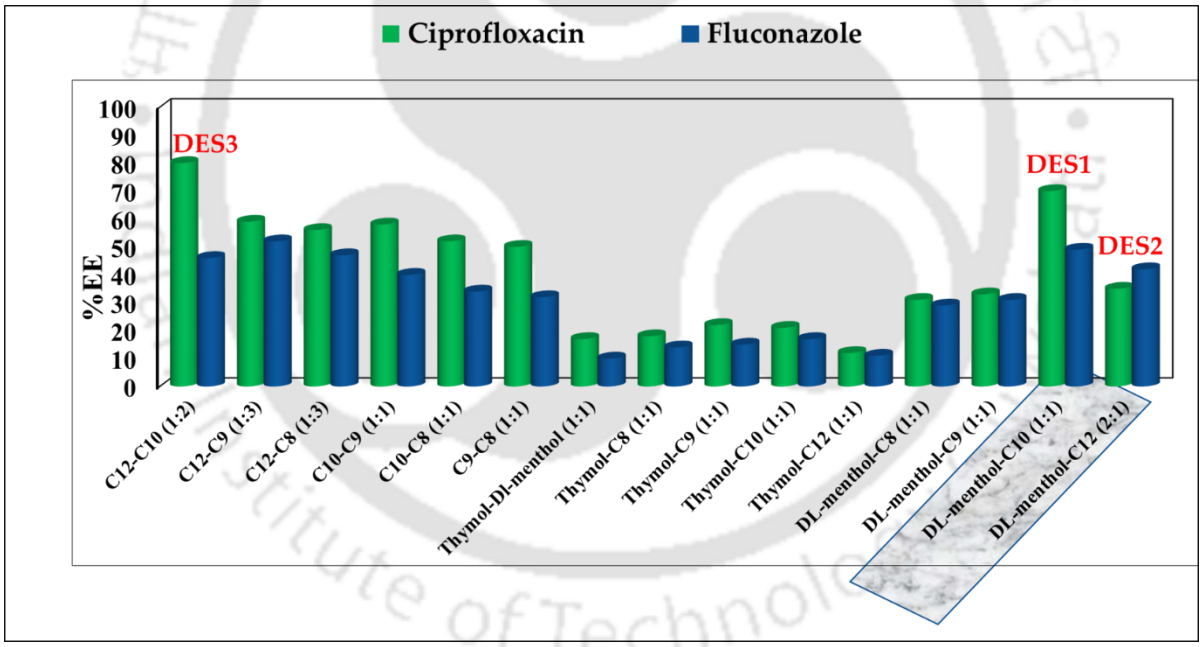

Figure 5.1: Screening of different hydrophobic DESs as per one-step batch-type extraction of ciprofloxacin and fluconazole at a DES/water mass ratio of 1:1 and 298.15 K temperature. [C12: dodecanoic acid; C10: decanoic acid; C9: nonanoic acid; C8: octanoic acid]

For ciprofloxacin extraction, DES3 [dodecanoic acid: decanoic acid (1:2)] exhibited the highest %EE. However, DES3 possess a freezing point (~ 21 °C) relatively closer to that of the operating room temperature (25 °C). During the flow of DES3 through the microchannel, solidification of the DES components was noticed in quite some parts of the channel leading

to blockage of the channel cross-sectional area that hindered the flow pattern as well as the extraction process. Thus, DES3 has been discarded from further microchannel-based extraction. DES1 [DL-menthol: decanoic acid (1:1)] and DES2 [DL-menthol: dodecanoic acid (2:1)] have been selected based on their suitable working condition properties and superior extractability of both drugs. The composition of the DESs used in this experiment is shown in Table 5.1.

Table 5.1: List of studied hydrophobic DESs with molar ratios

DES	Abbreviation	HBA	HBD	Molar ratio (HBA: HBD)
DES1	DLM-DEC	DL- menthol	decanoic acid	1:1
DES2	DLM-DODEC	DL- menthol	dodecanoic acid	2:1

5.3.2 Extraction of Ciprofloxacin and Fluconazole using Microchannel

Figure 5.2 illustrates the experimental setup of a microchannel-based extraction unit with an optical image of a serpentine-shaped circular microchannel with an inner diameter of d ~ 500 μm and a total path length of l ~ 80 cm. The DES phase and the aqueous stock solution of the drugs were injected through the two inlet openings at the left-hand side of the microchannel unit. The injection of the phases at a desired inlet flow rate was implemented through a syringe pump so that the inlet flow rate and desired DES/water phase mass ratio can be maintained. The two phases get attached within the single path of the microchannel and transport of the drug molecules from the water phase to the DES phase occurs due to a higher contact time. The phases then are collected in the outlet of the channel and after successful phase separation, the quantification of the phases is carried out. The temperature of the room while experimenting is maintained around 25 °C.

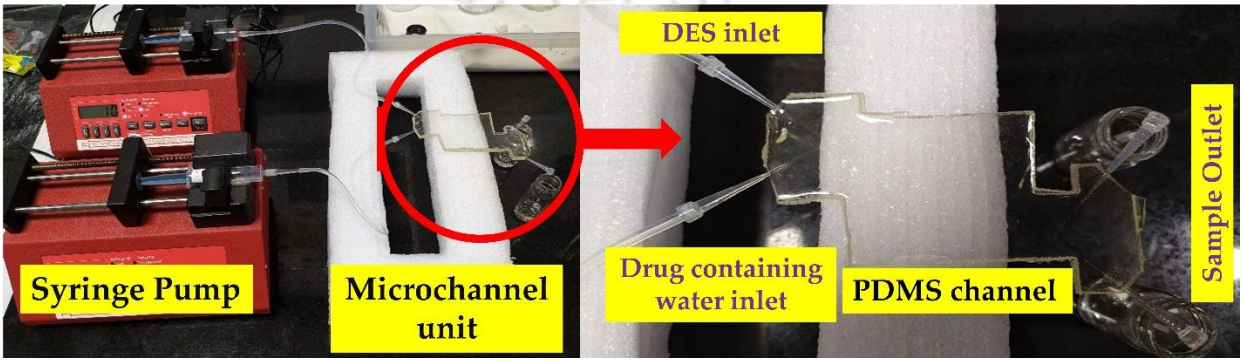

Figure 5.2: Microchannel setup used for extraction of ciprofloxacin and fluconazole.

5.3.2.1 Influence of Different Factors Affecting the Experimental Extraction Efficiency

The extraction efficiency (%EE) of the drugs (ciprofloxacin and fluconazole) from the aqueous phase was evaluated using the concentration of the drugs in the water phase before (C_0) and after extraction (C) employing the following equation:

$$\%EE = \frac{C_0 - C}{C_0} \times 100 \qquad (5.1)$$

The extraction efficiency of a micropollutant from an aqueous solution employing DES-based solvent extraction through a microchannel depends on several factors. Accordingly, to improve the extraction performance, various factors such as type of DES, the flow rate of phases within the microchannel, contact time or residence time within the channel, and solvent phase to water phase mass ratio, were investigated. Each of these is discussed below.

5.3.2.1.1 Influence of the Flow Rate in Microchannel

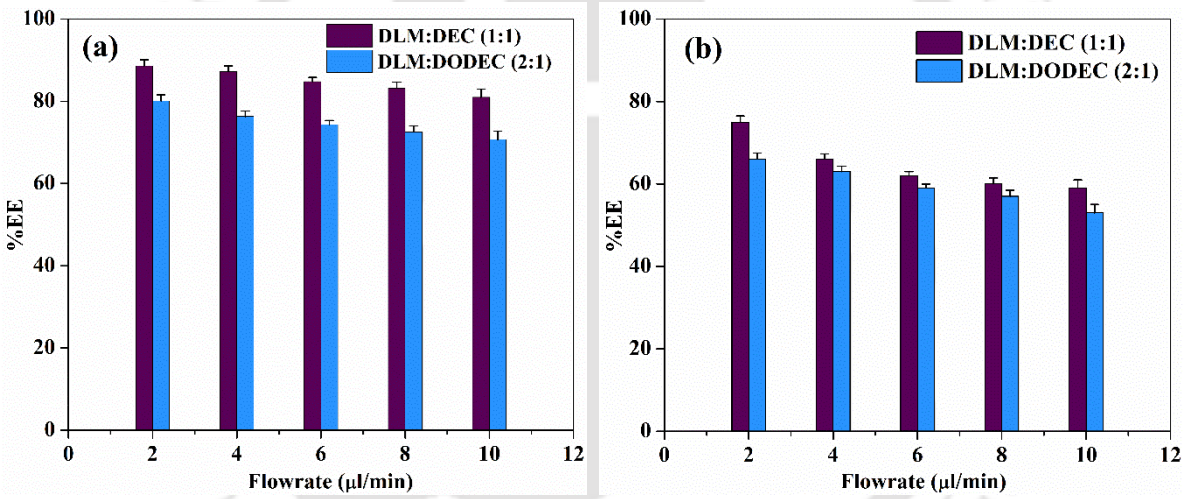

Figure 5.3: Effect of the flowrate of DES and aqueous phase within the microchannel on the extraction efficiencies (%EE) of (a) ciprofloxacin and (b) fluconazole using two different DESs.

The influence of the flow rate of both the phases (DES and aqueous) within the microchannel on the extraction efficiency of ciprofloxacin and fluconazole is presented in Figure 5.3. Variable flow rates ranging from 2 to 10 µl/min were incorporated to observe its influence on the %EE of the drugs. From Figure 5.3a, it is evident that DL menthol: decanoic acid (1:1) DES (~89%) has shown almost 12% higher extraction efficiency than DL menthol: dodecanoic acid (2:1) DES (~77%) at the lowest flowrate (2 µl/min). Upon increasing the flow rate, the %EE decreases simultaneously because of the lesser available time of contact among the phases. Thus, by modulating the flow rate, a higher %EE can be achieved as compared to

that of one-step batch-type LLE experiments. At 10 µl/min flow rate, DES1 and DES2 achieved %EE of 82% and 73%, respectively.

In the case of fluconazole microextraction in Figure 5.3b, 75% and 65% of extraction efficiency were achieved at a flowrate of 2 µl/min for DES1 and DES2, respectively which decreased to 59% and 53%, respectively for DES1 and DES2 at 10 µl/min flowrate. Thus, a reduced flow rate promotes higher extraction efficiency of the drugs.

5.3.2.1.2 Influence of the Contact Time and DES/water Mass Ratio within the Channel

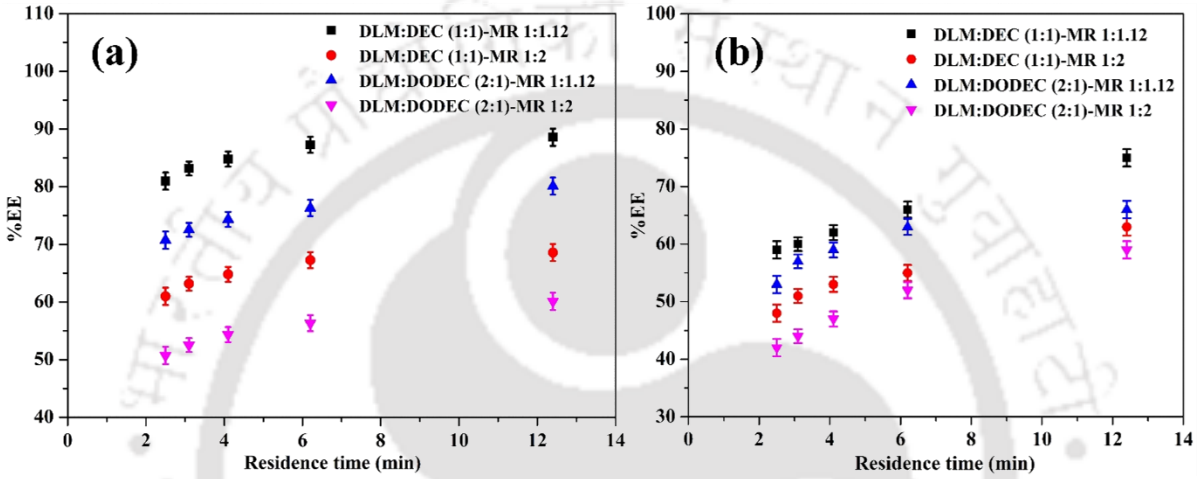

Figure 5.4: Effect of the contact time/ residence time of DES and aqueous phase within the microchannel on the extraction efficiencies (%EE) of (a) ciprofloxacin and (b) fluconazole using two different DESs at different DES/water mass ratios at 298.15 K.

Figure 5.4 is the illustration of the influence of the contact time of mixing between DES and aqueous phase within the microchannel along with DES phase/ water phase mass ratio on the extraction performance of ciprofloxacin and fluconazole for both the DESs. The contact time within the microchannel can be construed as the time spent by both the inlet phases within the channel, equivalent to the residence time. In our experiment, a range of different residence times (from 2.5 to 12.4 min) have been achieved by precisely regulating the inlet flow rates of the phases, the residence time ranges from 2.5 to 12.4 min. Higher inlet flow rate results in reduced contact time within the channel because the properties are inversely proportional to each other. To achieve better removal efficiency, higher residence time needs to be provided. Two different DES/water mass ratios of 1:1.12 and 1:2 have been applied to assess the impact on the removal efficiency. From Figure 5.4, for both drugs, the extraction efficiency increased significantly with an increase in the residence time of inlet streams within the channel. However, a substantial drop in the %EE for ciprofloxacin extraction at a residence time of 2.5 min can be detected, where almost 20% reduction in the efficiency (Figure 5.4a) has been

witnessed between the mass ratios of 1:1.12 and 1:2. Similar reduction in %EE has been observed in other residence time experiments also.

In the case of the fluconazole system, as given in Figure 5.4b, the values of reduction are much less (around 12%) as compared to that of the ciprofloxacin system. Higher residence time with a higher DES/water mass ratio (1:1.12, in this case) can be implemented to obtain significantly superior extraction properties.

Overall, it can be observed that the flow rate of the inlet phases and the residence time inside the microchannel play a major role in improving the extraction performance of the hydrophobic DESs. Perhaps, the closer attachment of the DES-drug molecules leads to having closed-shell non-covalent interaction among the DES components and the drugs. These interactions can be visualized and spotted at a molecular level through quantum chemical (QC) studies along with non-covalent interactions (NCI) and molecular dynamics (MD) simulation studies. The ensuing part contributes towards the molecular-level understanding of these DES-drug systems through extensive computational analysis.

5.3.3 Quantum Chemical Insights

5.3.3.1 Geometry Analysis

Figure 5.5 revealed the optimized structures of the DES-drug complex. A single orientation of ciprofloxacin-DES1 was obtained whereas three different fluconazole-DES1 complexes were found in the potential energy surface with a stable ground state geometry. In Figure 5.5a, the O atom of DL-menthol showed close-range interaction with the H atom of the piperazine group of ciprofloxacin at 1.72 Å. Decanoic acid, on the other hand, is positioned near the carboxyl group of ciprofloxacin to obtain O…H interaction at distances of 1.31 Å and 2.3 Å. Both of the sites having hydrogen bond donor capacity in the ciprofloxacin molecule have been able to have interactions with the hydrogen bond acceptor part of the HBA and HBD of DES1. Based on the distances of these interactions, it can be termed quite evidently that hydrogen bonding and dispersion interactions can play a major role in establishing the ciprofloxacin-DES1 complex.

(a)

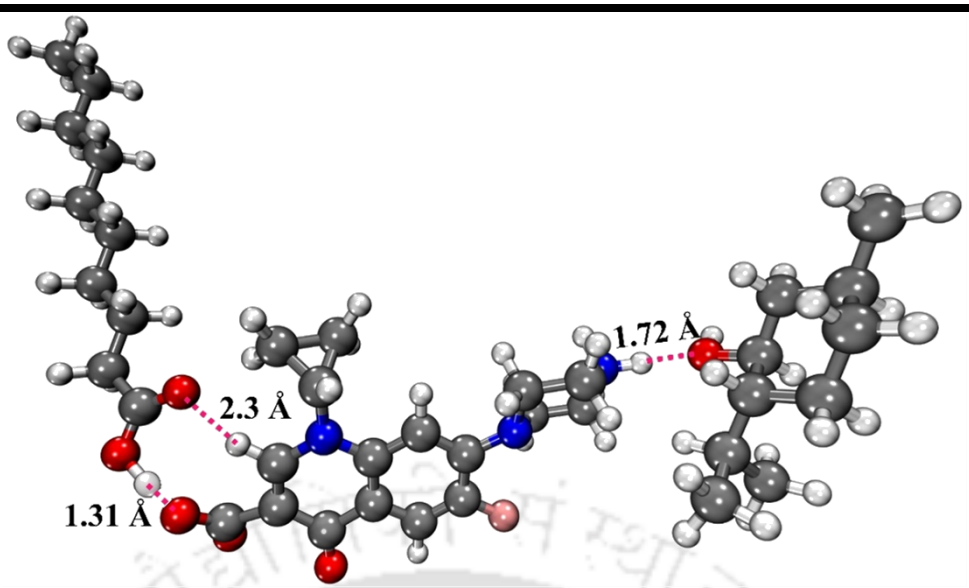

(b)

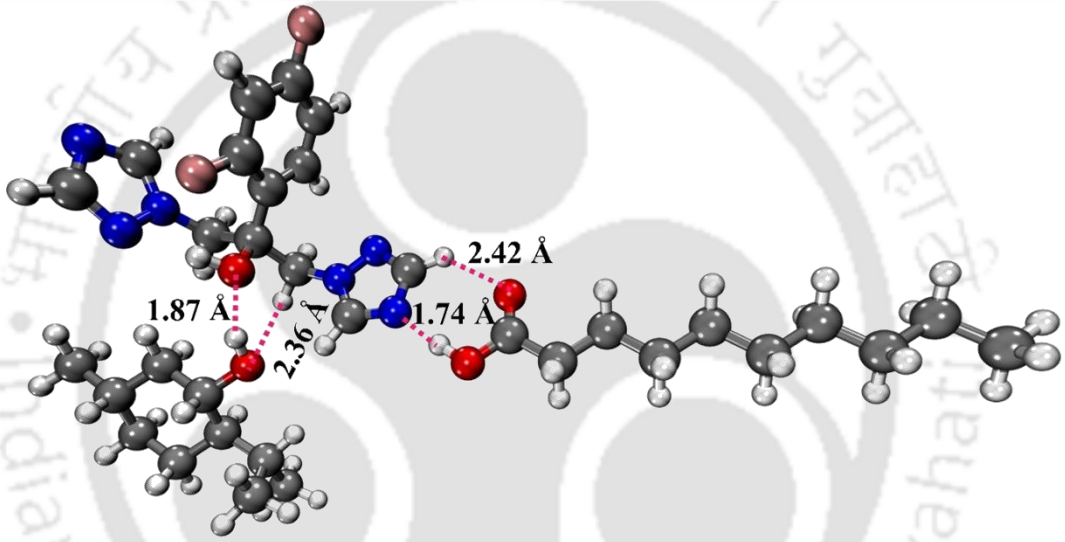

Energy = −2118.741 Hartree

(c)

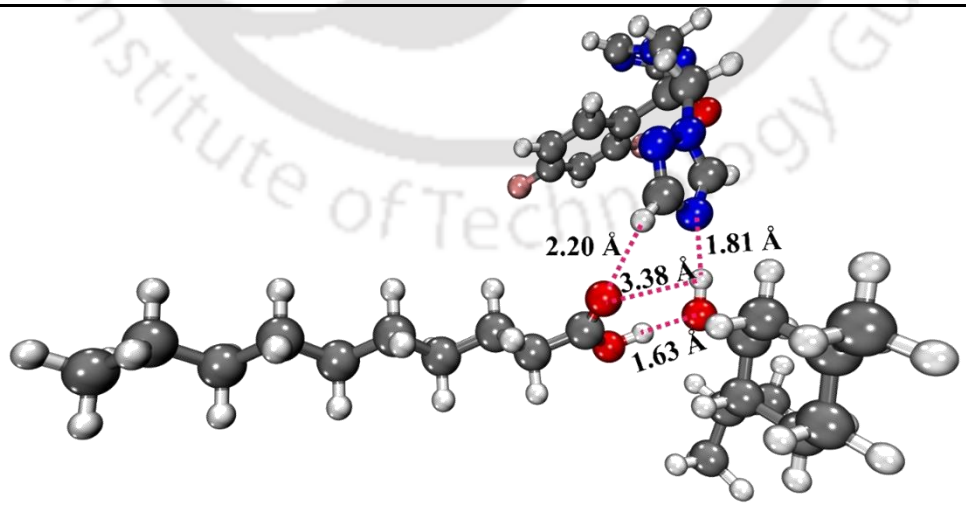

Energy = −2118.744 Hartree

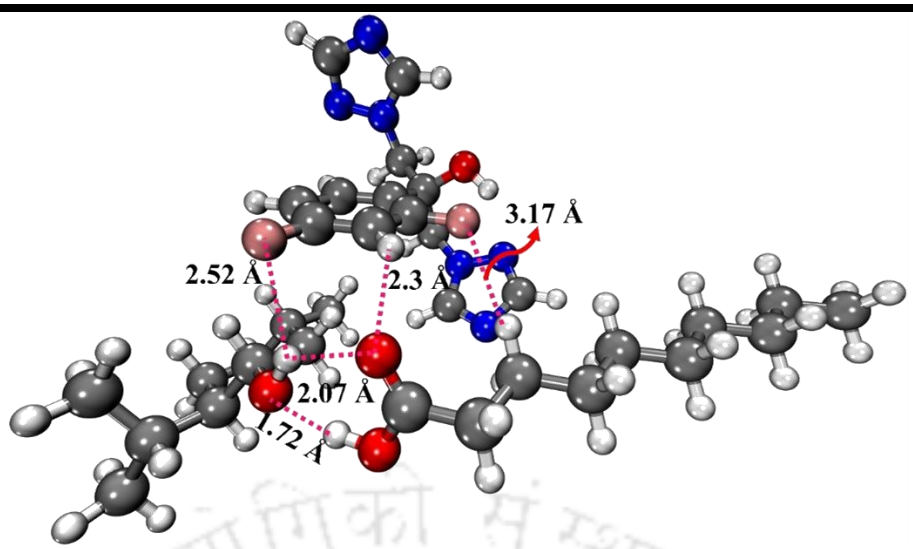

Figure 5.5: Optimized structures of drug-DES complexes at DFT-B3LYP/6-311+G (d,p) with D3BJ dispersion correction: (a) ciprofloxacin-DES1, (b) fluconazole-DES1-O1, (c) fluconazole-DES1-O2, and (d) fluconazole-DES1-O3 [O1, O2, and O3 are three different types of drug- DES orientation].

The three orientations of fluconazole-DES1 complexes are based on the affinity of the DES components towards the different active sites of fluconazole moiety. Fluconazole-DES1-O1 is the orientation where Dl-menthol attacks the hydroxyl group (−OH) of fluconazole with a distance of 1.87 Å and 2.36 Å, and decanoic acid finds a way to interact with the N and H atom the (1,2,4-triazole) group with possible interaction range of 1.74 Å (N…H) and 2.42 Å (O…H) as depicted in Figure 5.5b. Another orientation confirmed the intactness of the DES1 structure with considerable relaxation of O (carboxylic acid) …H (menthol) interaction as the distance increased to 3.38 Å (Figure 5.5c). This fluconazole-DES1-O2 complex established N (fluconazole) …H (menthol) interaction and O (carboxylic acid) …H (fluconazole) with distances of 1.81 Å and 2.20 Å, respectively with the (1,2,4-triazole) group being the active site of fluconazole, as shown in Figure 5.5c. In the fluconazole-DES1-O3 complex, the (2,4-difluorophenyl) part of fluconazole acted as the active group contributing to the fluconazole-DES1 interaction. The higher electronegative property of the fluorine atom in the fluorophenyl group provided the necessary initiation for fluconazole-DES1 complex formation as displayed in Figure 5.5d. Quite an interesting occurrence can be noticed in this type of orientation as the disruption or relaxation of the DES components was negligible. Thus, a highly stable DES structure has been involved in forming this orientation of the fluconazole-DES1-O3 complex.

The interatomic distances of 1.72 Å and 2.07 Å between O and H atoms of both DL-menthol and decanoic acid supported this fact. In this orientation, the F (fluorine) atom of the 2,4-difluoro phenyl group of fluconazole moiety involves in a closer interaction of 2.52 Å with DL-menthol and relatively long-range interaction with decanoic acid at a distance of 3.17 Å. The involvement of both HBA (DL-menthol) and HBD (decanoic acid) individually in interacting with fluconazole implied the relative affinity and strength of both the interactions (HBA-fluconazole and HBD-fluconazole). All of these three orientations of fluconazole-DES1 could be possible at different surrounding effects, however, the single point energy analysis indicated the feasibility of the formation of fluconazole-DES1-O2 and fluconazole-DES1-O3 complexes as compared to fluconazole-DES1-O3 since the difference in their ground state energies for both the prior complexes were 2.05 and 2.21 kcal/mol, respectively with respect to that of the O3 orientation. The frontier molecular orbital (FMO) study could further expand the understanding with additional information regarding the chemical stability of the complexes.

5.3.3.2 Frontier Molecular Orbital Analysis

Acceptor-donor interaction, molecular stability, and reactivity may all be calculated with HOMO-LUMO orbital analysis, and the Frontier Molecular Orbital (FMO) study is widely acknowledged as an effective method.[18] In this subsection, we focus on how the HOMO (Highest Occupied Molecular Orbital) and LUMO (Lowest Unoccupied Molecular Orbital) species of DES1 and drugs (ciprofloxacin and fluconazole) interact with one another. Whereas the HOMOs are more nucleophilic, or electron-donating, the LUMOs are more electrophilic, or electron-accepting. The energy needed to add or remove an electron from a molecule can be calculated using its HOMO-LUMO energy gap. The kinetic stability of molecules improves with increasing HOMO-LUMO energy gap and the reactivity decreases. The global hardness or softness of a molecule is correlated with the energy difference between its HOMO and LUMO. A higher global hardness (η) value indicates better stability and resistance to charge transfer, and vice versa, so that the global hardness can be used to identify the charge transfer and stability of a certain molecule or complex. η can be mathematically written as:

$$\text{Global Hardness } (\eta) = (E_{LUMO} - E_{HOMO})/2 \qquad (5.2)$$

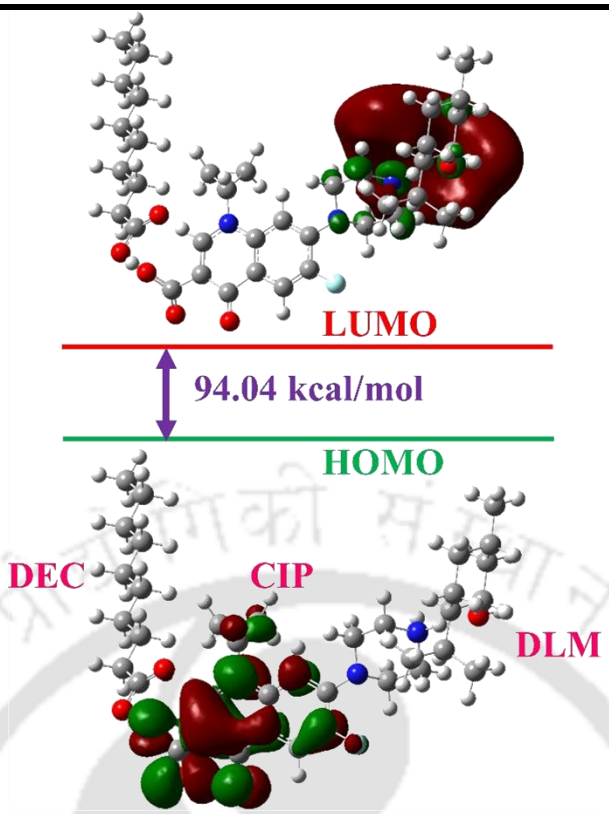

Figure 5.6: HOMO−LUMO iso-surfaces of the ciprofloxacin-DES1 complex at DFT-B3LYP/6-311+G (d,p) with D3BJ dispersion correction.

The HOMO-LUMO energy values for the complexes of ciprofloxacin and fluconazole individually with DES1 are presented in Table 4. Figure 5.6 and Figure 5.7 display the HOMO-LUMO iso-surfaces of ciprofloxacin-DES1 complex and fluconazole-DES1 complexes, respectively illustrated by green and red contours, respectively, to highlight the HOMO's positive and negative lobes of HOMOs and LUMOs. The HOMO species are primarily localized around the ciprofloxacin moiety suggesting the presence of electron-donating entities in ciprofloxacin (Figure 5.6), whereas LUMOs are predominantly restricted in the DL-menthol molecule revealing hydrogen bond-donating tendency towards ciprofloxacin. One thing that needs to be noticed here is that while interacting with a third incoming moiety, the HBA as well as the HBD of the DES can participate in a different role as compared to their usual interactive frameworks. It is already established computationally in chapter 2 of this thesis that while the formation of DL-menthol: decanoic acid DES, DL-menthol plays the role of an HBA. However, in the present scenario, it might act as an HBD upon interacting with ciprofloxacin to form a stable DES-drug complex. The HOMO-LUMO energy gap of 94.04 kcal/mol is an exhibition of the chemical stability of this ciprofloxacin-DES1 complex.

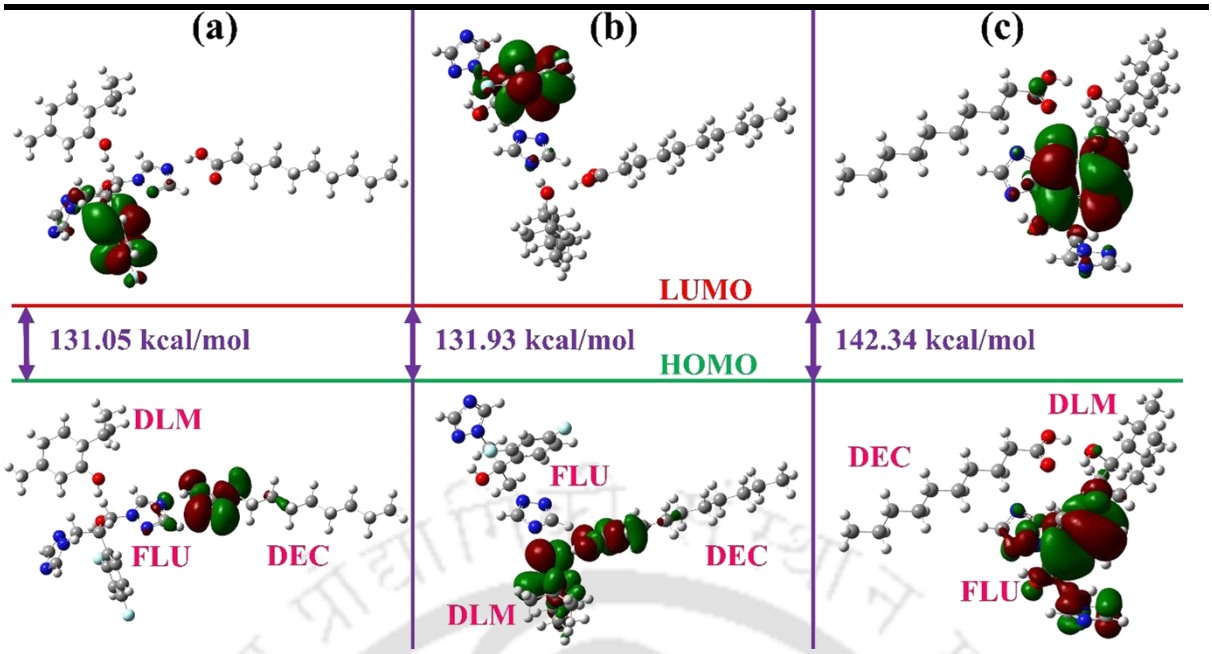

Figure 5.7: HOMO-LUMO isosurfaces of (a) fluconazole-DES1-O1, (b) fluconazole-DES1-O2, (c) fluconazole-DES1-O3 at DFT-B3LYP/6-311+G (d,p) with D3BJ dispersion correction. [O1, O2, and O3 are three different types of drug- DES orientation]

Figure 5.7 demonstrates the HOMO-LUMO iso-surfaces for three different fluconazole-DES1 complexes. In Figure 5.7a, the HOMO species are located in the carboxyl (−COOH) group of decanoic acid, whereas the (2,4-difluorophenyl) group contributes to the LUMO species. Decanoic acid here exhibits nucleophilic properties to form the fluconazole-DES1-O1 complex. On the other hand, both the DES-forming components (DL-menthol and decanoic acid) contributed to the HOMO species of fluconazole-DES1-O2 complex supporting a stable DES as well as DES-drug structure in Figure 5.7b. The Hydroxyl (−OH) group in combination with the difluorophenyl group of fluconazole contribute to the LUMOs. A strong menthol-fluconazole stable interaction can be observed in Figure 5.7c as the fluconazole-DES1-O3 complex revealed the highest HOMO-LUMO energy gap (142.34 kcal/mol) among all three orientations of the fluconazole-DES1 complexes. A higher global hardness (η) value supports the findings from the HOMO-LUMO analysis as presented in Table 5.2. The multiple contributing functional groups present within the system formulated a stronger interconnective donor-acceptor framework to achieve a stable DES-drug complex sustained by numerous closed-shell non-bonded interactions.

Table 5.2: Theoretically obtained HOMO, LUMO (ground and excited state), energy gap, and chemical hardness (η) computed in the DFT-B3LYP method (All the units are in Hartree)

Systems	HOMO energy	LUMO energy	Energy gap	η
Ciprofloxacin-DES1	−0.22479	−0.075	0.14979	0.074895
Fluconazole-DES1-O1	−0.26042	−0.05157	0.20885	0.104425
Fluconazole-DES1-O2	−0.26179	−0.05155	0.21024	0.10512
Fluconazole-DES1-O3	−0.27251	−0.04566	0.22685	0.113425

5.3.3.3 Charge Transfer (CT) Analysis

The CT (charge transfer) process was calculated in Gaussian 16 using APT (atomic polar tensor) charges at B3LYP functional.[21,22] The calculated APT charges on ciprofloxacin, fluconazole and DES components (HBA and HBD) in different DES-drug complexes have been recorded and presented in Tables 5.3 and 5.4. Although APT (atomic polar tensor) charge is the most expensive CT analysis of the common atomic charges, it has been considered due to its higher accuracy and stronger correlations with the spectra properties corresponding to a suitable DFT functional.

Table 5.3: Calculated APT charges (in a.u.) on fluconazole and ciprofloxacin in the different DES-drug complexes

	Fluconazole	Ciprofloxacin
Without DES	0	0
in Ciprofloxacin-DES1	NA	0.047
in Fluconazole-DES1-O1	−0.071	
in Fluconazole-DES1-O2	−0.013	NA
in Fluconazole-DES1-O3	0.011	

Due to the neutrality of the isolated ciprofloxacin and fluconazole, their partial charges are zero in a DES-free environment. As the drugs are neutral entities, zero APT charges in each can be assumed. When the drug molecules are dissolved in a DES or other solvent, a charge transfer occurs between the drug and the solvent molecules. Due to changes in electron density as a result of interaction with the solvent, individual drug molecules acquire or lose charge, leading to a non-zero partial charge. Ciprofloxacin acts as an electrophile attaining a positive charge of 0.047 a.u. in the ciprofloxacin-DES1 complex, thus making DES1 a nucleophilic entity with a net negative charge. In the case of fluconazole-DES1-O1 and

fluconazole-DES1-O2 complexes, as presented in Table 5.3, the fluconazole molecule obtains −0.071 a.u. and −0.013 a.u., respectively to become nucleophiles by gaining electron density from DES1. In this case, DES1 possess electrophilic property. However, the fluconazole-DES1-O3 complex exhibits different charge characteristics as compared to the other two complexes. A positive charge of 0.011 a.u. develops electrophilic attributes in fluconazole molecules. From the pieces of evidence mentioned above it can be inferred that the charge-related characteristics of a molecule depend on the structural orientation of that molecule in a multi-component system which alters the electron density upon modification of the electron cloud.

When no other compounds are present in the system, DL-menthol (HBA) and decanoic acid (HBD) acquire positive and negative charges, respectively. The values are presented in Table 5.4. However, upon interaction with the drugs, the HBA undergoes a decrease in positive charge. The reduction is maximum in ciprofloxacin, where DL-menthol obtains −0.05 a.u. due to a rise in electron density to be modified as a nucleophilic entity. The negative charge in the HBD (decanoic acid) decreased due to a reduction in electron density. While decanoic acid attains positive charge in ciprofloxacin-DES1 (0.003 a.u.) and fluconazole-DES1-O1 complexes (0.053 a.u.), it attains positive charge in fluconazole-DES1-O2 (−0.006 a.u.) and fluconazole-DES1-O3 (−0.012 a.u.). Overall, the CT analysis suggests a significant involvement of HBA-HBD interactions for a stable DES-drug structure.

Table 5.4: Calculated APT charges (in a.u.) on the components of DESs in the different DES-drug complexes

System	With Drugs	Only DES
Charge on the hydrogen bond acceptor (HBA) of DES in DES-pesticide combination		
in Ciprofloxacin-DES1	−0.05	0.0224
in Fluconazole-DES1-O1	0.018	
in Fluconazole-DES1-O2	0.02	
in Fluconazole-DES1-O3	0.001	
Charge on the hydrogen bond donor (HBD) of DES in DES-pesticide combination		
in Ciprofloxacin-DES1	0.003	−0.0224
in Fluconazole-DES1-O1	0.053	
in Fluconazole-DES1-O2	−0.006	
in Fluconazole-DES1-O3	−0.012	

5.3.4 MD Simulation Analysis

5.3.4.1 Non-bonded Interaction Energy

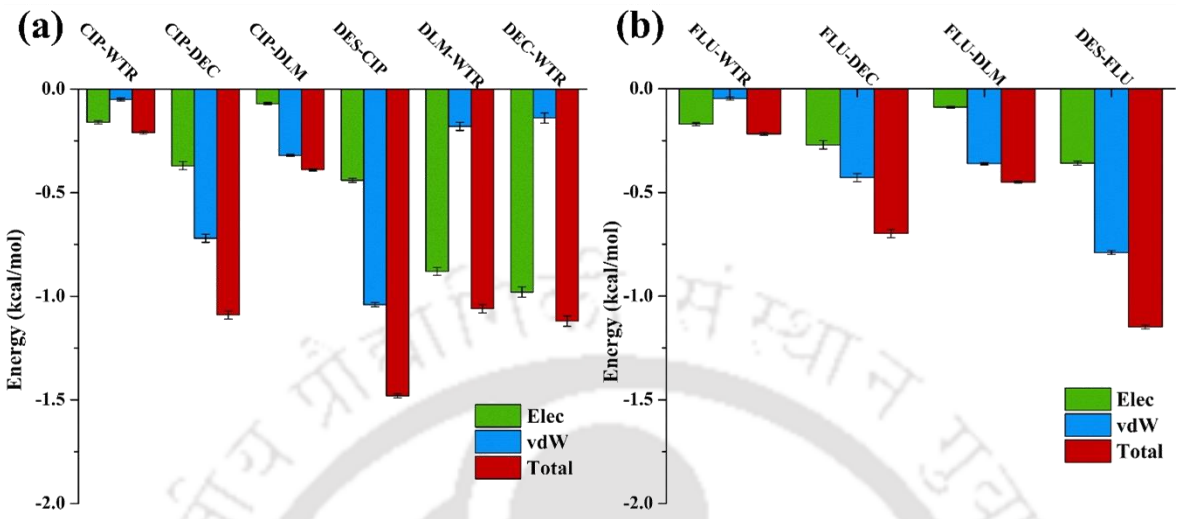

Figure 5.8: MD simulated interaction energies (kcal/mol) between the different component pairs of (a) DL-menthol−decanoic acid−ciprofloxacin and (b) DL-menthol−decanoic acid−fluconazole in 298.15 K and 1 atm pressure.

The nonbonded interaction energy between the different components is depicted in Figure 5.8 a,b. This is subdivided into electrostatic (Elec) and van der Waals (vdW) contributions for ciprofloxacin and fluconazole systems. The DES-drug interaction energy is higher than that of the respective water-drug interactions. Ciprofloxacin-water interaction energy (−0.21 kcal/mol) was affected due to the enhanced ciprofloxacin-DES1 interaction (−1.48 kcal/mol) as shown in Figure 5.8a. The van der Waals component (−1.04 kcal/mol) dominates over the electrostatic counterpart (−0.44 kcal/mol) because of the presence of large molecular groups with relatively higher neutral behaviour. A similar outcome can be observed for fluconazole-DES1 interaction (−1.15 kcal/mol) with the electrostatic interaction (−0.36 kcal/mol) is less as compared to the vdW energy (−0.79 kcal/mol), as presented in Figure 5.8b. However, the electrostatic component dominates over the dispersion-based van der Waals component for drug-water pairs in both systems. Water is having electrostatic interactions with the drugs due to its polar nature and involvement in forming H-bonding. However, the lower interaction energy leads to lesser interactions among the drug and the water molecules leading to higher extraction of the drugs from the aqueous phase to the DES phase. The DES molecules are intact within the aqueous surroundings making it feasible for drug extraction and maintaining a DES-rich phase with higher drug concentration.

Table 5.5: Composition of the system considering the 1:1 mass ratio of DES and the aqueous solution of the drug (ciprofloxacin and fluconazole) and the number of molecules considered for MD simulation)

Name of pesticide	DES		Number of molecules				
	HBA	HBD	HBA	HBD	Pesticide	Water	Total
Ciprofloxacin	DL-menthol	Decanoic acid	100	100	5	912	1117
Fluconazole	DL-menthol	Decanoic acid	100	100	5	912	1117

5.3.4.2 Hydrogen Bond Properties

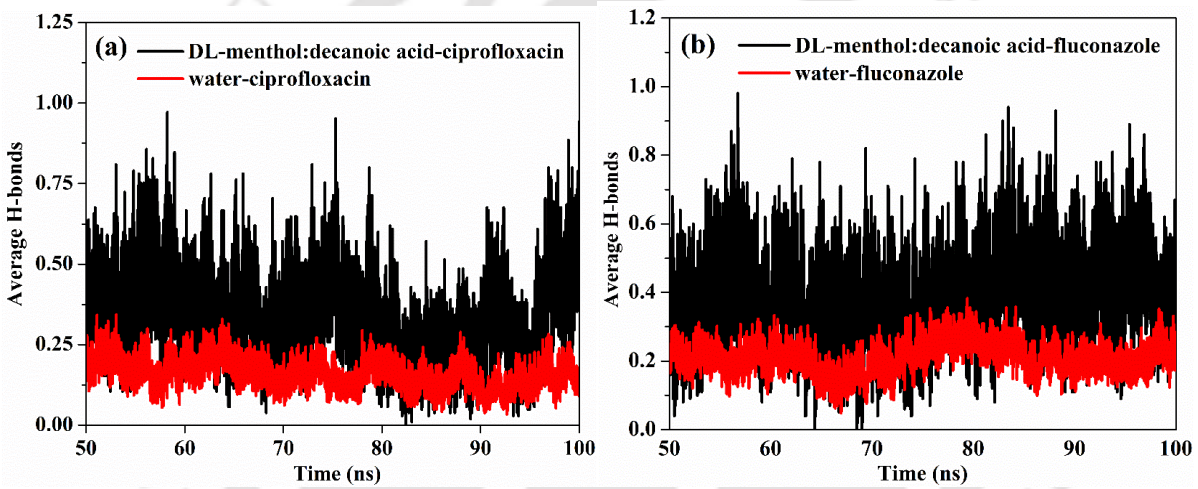

Figure 5.9: Average number of hydrogen bonds for (a) ciprofloxacin-DES1 (DL-menthol-decanoic acid)-water system; and (b) fluconazole-DES1 (DL-menthol-decanoic acid)-water system; as a function of simulation time.

Figure 5.9 presents the average number of hydrogen bonding between the DES and the drugs within each system as a function of simulation time (50 to 100 ns). The first 50 ns simulation time was not considered for H-bonding calculation to avoid any kind of non-equilibrium nature of the production run. The criteria for hydrogen bonding were taken from the work as presented in earlier chapters containing MD simulation i.e., 3.5 Å distance between donor-acceptor and angular cut-off of 135 to 180°. From Figure 5.9a, it can be noticed that the average H-bonding between DES1-ciprofloxacin is higher than that of water-ciprofloxacin. The possible reason could be the presence of a higher number of acceptor-donor groups in the drug-DES complex as presented by the optimized geometries of the drug-DES complexes, where multiple closed-shell interactions have been observed. The presence of electronegative elements within the system allowed partially positively charged elements to involve in

hydrogen bonding with another electron-rich atom. The averaged-out values of the average H-bonding follow the order: DES1-ciprofloxacin (0.33) > water-ciprofloxacin (0.16). Figure 5.9b presents the average H-bonding formed between different components within the fluconazole-DES1-water system. Fluconazole confirmed higher H-bonding interactions with DES1 as compared to water. The average DES1-fluconazole H-bonding (0.38) exceeded that of water-fluconazole (0.21). In both systems, the presence of hydrophobic DES deterred the water molecules to come to the close vicinity of both drugs which affected the water-drug H-bonding. Strong HBA-HBD interaction among the DES components and drug molecules constructed a well-formed stable DES-drug complex assisted by closed-shell H-bonding as well as dispersion interactions.

5.3.5 Non-covalent Interactions (NCI) Analysis

The study of noncovalent interactions, or NCI, developed by Contreras-Garci´a and Johnson[23–25] is implemented to overcome the numerical accuracy of the AIM analysis.[26] The approach is termed a 'reduced density gradient' or, 'RDG' analysis which is based on analysing the electron density distribution where low electron density and low gradient value regions are present and are expressed by the following equation.

To achieve the atom-in-molecules (AIM) analysis's numerical precision, we employ the study of noncovalent interactions, or NCI, pioneered by Contreras-Garci´a and Johnson.[26] The method is referred to as "reduced density gradient" (RDG) analysis, and it involves solving an equation that describes the distribution of electron density in areas of low electron density and low gradient value.

$$\mathrm{RDG} = \frac{1}{2(3\pi^2)^{1/3}} \frac{|\nabla\rho|}{\rho^{4/3}} \qquad (5)$$

The insightful NCI analysis is based on the interpretation of RDG spikes.[27] The NCI analysis with the RDG approach can identify and characterize several types of weak interactions, including hydrogen bonding, van der Waals, and dispersion interactions. Specifically, the scatter graph of the RDG is represented as a function of the electron density multiplied by the sign of the second eigenvalue of the Hessian of the electron density. Here, in this chapter, we refrain from a detailed description of the mechanism and theoretical background of RDG analysis as this has already been covered thoroughly in the previous chapters (mainly, chapter 3 and chapter 4). Figure 5.10 shows the RDG isosurfaces and the RDG scatter plot revealing various weak interactions ranging from positive to negative [sign (λ_2)ρ] values for the ciprofloxacin/[DL-menthol- decanoic acid] complex, fluconazole/[DL-

menthol- decanoic acid]-O1 complex, fluconazole/[DL-menthol- decanoic acid]-O2 complex, and fluconazole/[DL-menthol- decanoic acid]-O3 complex at the B3LYP/6-311+G(d,p) level of theory. Spikes present in the different coloured regions suggest specific interaction types (blue: H-bonds; green: van der Waals or dispersion interaction; and red: steric effect). To figure out what each colour means in the NCI plots, you could think of strong, attractive interactions like hydrogen bonds, halogen bonds, and electrostatic interactions as being in the blue areas. The red regions show strong repulsion caused by non-bonded overlap or steric effect, while the transitions region contains information on vdW interactions like dispersion interaction, dipole-dipole interaction, and so on.[23]

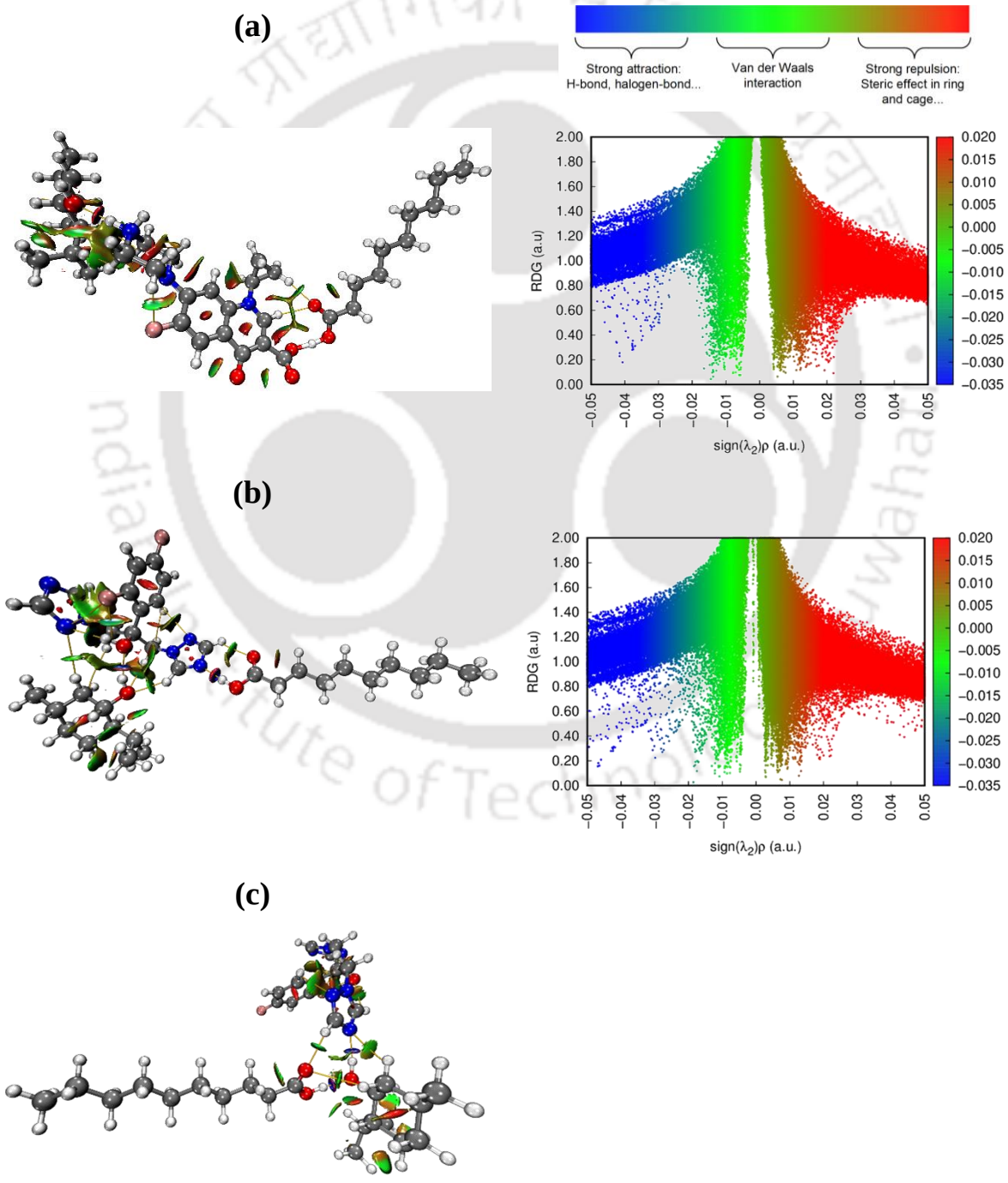

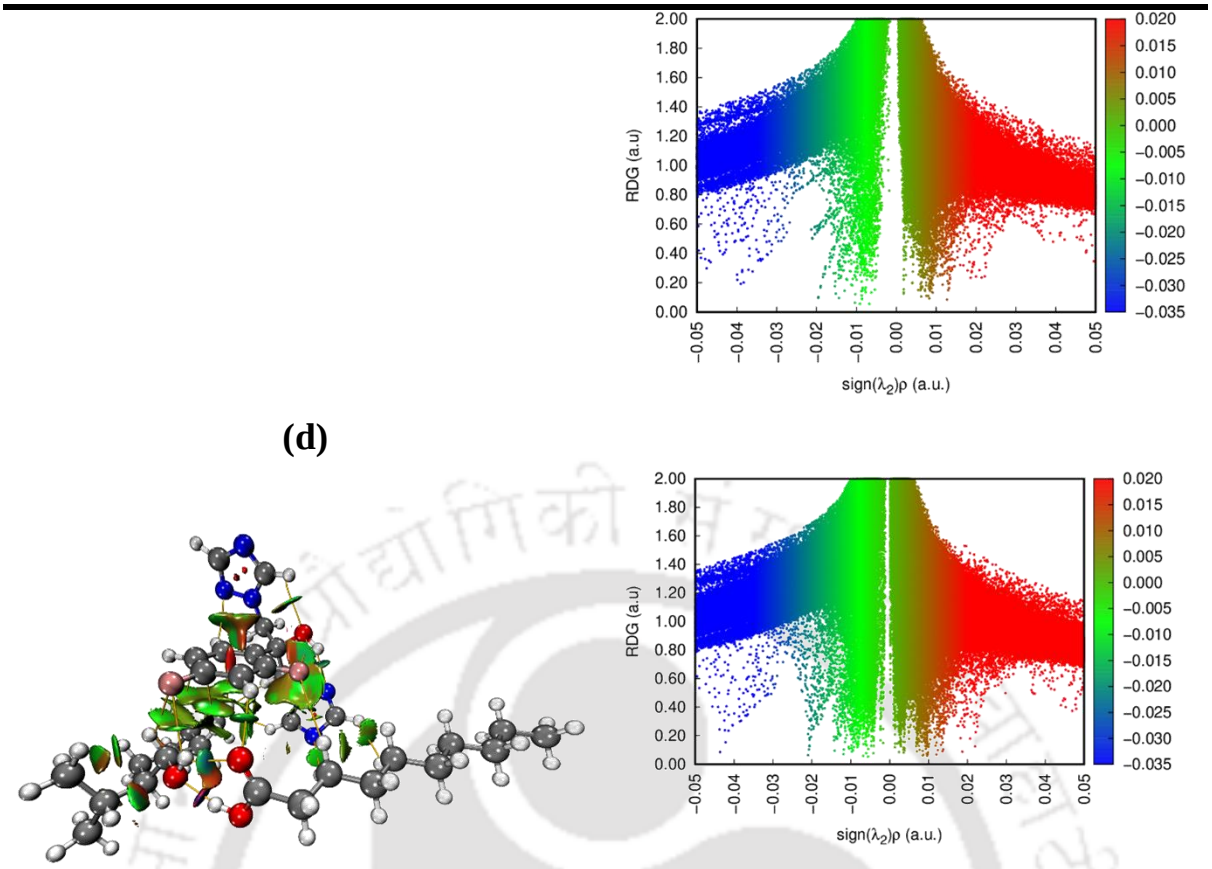

Figure 5.10: RDG isosurfaces and scatter graphs of RDG for (a) ciprofloxacin-DES1, (b) fluconazole-DES1-O1, (c) fluconazole-DES1-O2, and (d) fluconazole-DES1-O3 complex at the B3LYP/6-311+G(d,p) level. [O1, O2, and O3 are three different types of drug- DES orientation]

The study suggests the presence of dispersion interactions (vdW) witnessed by high-density RDG peaks between 0 to −0.015 a.u. between ciprofloxacin and DES1 as displayed in Figure 5.10a. A very low-density RDG peak can be witnessed between −0.04 to −0.05 a.u. suggesting the possible existence of hydrogen bonding. The left-sided NCI plot in Figure 5.10a revealed the occurrence of closed-shell dispersion interactions associated with the green flakes present among the DES components and ciprofloxacin. A significantly higher extent of dispersion as well as hydrogen bonding can be witnessed in the fluconazole-DES complexes as multiple dense RDG spikes can be spotted between −0.005 to −0.04 a.u. in Figures 5.10b-c. The interactive network between DES1 and fluconazole with three different orientations revealed multiple donor-acceptor sites for hydrogen bonding with closed-shell dispersion effects. The presence of green flakes along with the blue-coloured region in the NCI plots confirmed the site-specific closed-shell non-covalent interactions. Upon visual exploration, fluconazole-DES1-O3 orientation in Figure 5.10c revealed a much higher number of dense RDG peaks in the closed-shell region which is evident from the presence of a higher number

of green and blue flake regions in the NCI plot of the same complex. The closely packed structure of fluconazole-DES1 complexes induced a higher degree of non-covalent attractive interactions. The presence of red spikes in the range > 0.02 a.u. can be attributed to the long-chain carboxylic acid (decanoic acid) and the ring formations present within the drug molecules. As a whole, the presence of non-covalent interactions in the form of closed-shell hydrogen bonds and dispersion interactions are very much responsible for a stable DES-drug structure and can prove to be the driving force in extracting the drugs (ciprofloxacin and fluconazole) from an aqueous phase.

5.4 Conclusion

This chapter deals with microfluidic device-based extraction of ciprofloxacin and fluconazole with hydrophobic DESs [DL-menthol: decanoic acid (1:1) {DES1}, and DL-menthol: dodecanoic acid (2:1) {DES2}] as an enhancement operation in the extraction efficiency (%EE) as compared to the batch-type extraction. The extraction performance was evaluated at variable inlet flow rates (2 to 10 µl/min) with residence time ranging from 2.5 to 12.4 min at two different DES/water phase mass ratios (1:1.12 and 1:2). 89% and 75% of ciprofloxacin extraction were achieved by DES1 and DES2, respectively at a flow rate of 2 µl/min. At the same flow rate, 75% and 65% of fluconazole extraction were achieved for DES1 and DES2, respectively. Quantum chemical (QC) and non-covalent interaction (NCI) analysis suggest a strong ciprofloxacin-DES1 complex along with three different orientations of fluconazole-DES1 with non-bonded interactions such as hydrogen bonding and dispersion interactions responsible for the stability of the complexes. A larger HOMO-LUMO gap (94.04 kcal/mol, for DES1-CIP and 131.05 to142.34 kcal/mol, for DES1-FLU) supports the higher stability of the complexes. The NCI plot with RDG analysis was performed to highlight the regions of weak interaction. Hydrogen bonding and dispersion interactions (vdW) were witnessed between 0 to −0.04 a.u. confirming the presence of weak nonbonded interactions in the formation of DES-drug complexes.

References

[1] D.G.J. Larsson, C. de Pedro, N. Paxeus, Effluent from drug manufactures contains extremely high levels of pharmaceuticals, J. Hazard. Mater. 148 (2007) 751–755. https://doi.org/https://doi.org/10.1016/j.jhazmat.2007.07.008.

[2] J. Fick, H. Söderström, R.H. Lindberg, C. Phan, M. Tysklind, D.G.J. Larsson, Contamination of surface, ground, and drinking water from pharmaceutical production., Environ. Toxicol. Chem. 28 (2009) 2522–2527.

https://doi.org/10.1897/09-073.1.

[3] C. Rutgersson, J. Fick, N. Marathe, E. Kristiansson, A. Janzon, M. Angelin, A. Johansson, Y. Shouche, C.-F. Flach, D.G.J. Larsson, Fluoroquinolones and qnr Genes in Sediment, Water, Soil, and Human Fecal Flora in an Environment Polluted by Manufacturing Discharges, Environ. Sci. Technol. 48 (2014) 7825–7832. https://doi.org/10.1021/es501452a.

[4] J. Bengtsson-Palme, F. Boulund, J. Fick, E. Kristiansson, D.G.J. Larsson, Shotgun metagenomics reveals a wide array of antibiotic resistance genes and mobile elements in a polluted lake in India., Front. Microbiol. 5 (2014) 648. https://doi.org/10.3389/fmicb.2014.00648.

[5] N.P. Marathe, V.R. Regina, S.A. Walujkar, S.S. Charan, E.R.B. Moore, D.G.J. Larsson, Y.S. Shouche, A treatment plant receiving waste water from multiple bulk drug manufacturers is a reservoir for highly multi-drug resistant integron-bearing bacteria., PLoS One. 8 (2013) e77310. https://doi.org/10.1371/journal.pone.0077310.

[6] C. Lübbert, C. Baars, A. Dayakar, N. Lippmann, A.C. Rodloff, M. Kinzig, F. Sörgel, Environmental pollution with antimicrobial agents from bulk drug manufacturing industries in Hyderabad, South India, is associated with dissemination of extended-spectrum beta-lactamase and carbapenemase-producing pathogens, Infection. 45 (2017) 479–491. https://doi.org/10.1007/s15010-017-1007-2.

[7] Characterisation and antimicrobial resistance of sepsis pathogens in neonates born in tertiary care centres in Delhi, India: a cohort study, Lancet Glob. Heal. 4 (2016) e752–e760. https://doi.org/https://doi.org/10.1016/S2214-109X(16)30148-6.

[8] C. Florindo, F. Lima, L.C. Branco, I.M. Marrucho, Hydrophobic Deep Eutectic Solvents: A Circular Approach to Purify Water Contaminated with Ciprofloxacin, ACS Sustain. Chem. Eng. 7 (2019) 14739–14746. https://doi.org/10.1021/acssuschemeng.9b02658.

[9] D.J. Beebe, G.A. Mensing, G.M. Walker, Physics and applications of microfluidics in biology., Annu. Rev. Biomed. Eng. 4 (2002) 261–286. https://doi.org/10.1146/annurev.bioeng.4.112601.125916.

[10] S.K. Sia, G.M. Whitesides, Microfluidic devices fabricated in Poly(dimethylsiloxane) for biological studies, Electrophoresis. 24 (2003) 3563–3576. https://doi.org/https://doi.org/10.1002/elps.200305584.

[11] H.A. Stone, A.D. Stroock, A. Ajdari, Engineering Flows in Small Devices: Microfluidics Toward a Lab-on-a-Chip, Annu. Rev. Fluid Mech. 36 (2004) 381–411. https://doi.org/10.1146/annurev.fluid.36.050802.122124.

[12] S.K. Singh, P. Gogoi, A. Deb, P.S. Gooh Pattader, Chiral resolution of racemic amines in µ-reactor-crystallizer, Chem. Eng. Sci. 256 (2022) 117686. https://doi.org/https://doi.org/10.1016/j.ces.2022.117686.

[13] M.J. Frisch, G.W. Trucks, H.B. Schlegel, G.E. Scuseria, M.A. Robb, J.R. Cheeseman, G. Scalmani, V. Barone, B. Mennucci, G.A. Petersson, others, Gaussian 16, Gaussian Inc., Wallingford, CT. Gaussian 1 (2016).

[14] C. Lee, W. Yang, R.G. Parr, Development of the Colle-Salvetti correlation-energy formula into a functional of the electron density., Phys. Rev. B. Condens. Matter. 37 (1988) 785–789. https://doi.org/10.1103/physrevb.37.785.

[15] A.D. Becke, Density-functional exchange-energy approximation with correct asymptotic behavior, Phys. Rev. A. 38 (1988) 3098–3100. https://doi.org/10.1103/PhysRevA.38.3098.

[16] A.D. Becke, Density-functional thermochemistry. III. The role of exact exchange, J. Chem. Phys. 98 (1993) 5648–5652. https://doi.org/10.1063/1.464913.

[17] S. Grimme, S. Ehrlich, L. Goerigk, Effect of the damping function in dispersion corrected density functional theory, J. Comput. Chem. 32 (2011) 1456–1465. https://doi.org/https://doi.org/10.1002/jcc.21759.

[18] K. Fukui, Theory of orientation and stereoselection BT - Orientation and Stereoselection, in: K. Fukui (Ed.), Springer Berlin Heidelberg, Berlin, Heidelberg, 1970: pp. 1–85.

[19] T. Lu, F. Chen, Multiwfn: A multifunctional wavefunction analyzer, J. Comput. Chem. 33 (2012) 580–592. https://doi.org/https://doi.org/10.1002/jcc.22885.

[20] N. Paul, T. Banerjee, Study on the Extraction of Acetamiprid and Imidacloprid from an Aqueous Environment Using Menthol-Based Hydrophobic Eutectic Solvents: Quantum Chemical and Molecular Dynamics Insights, ACS Sustain. Chem. Eng. 10 (2022) 4227–4246. https://doi.org/10.1021/acssuschemeng.2c00023.

[21] J. Cioslowski, A new population analysis based on atomic polar tensors, J. Am. Chem. Soc. 111 (1989) 8333–8336. https://doi.org/10.1021/ja00204a001.

[22] W.E. Richter, L.J. Duarte, R.E. Bruns, Are "GAPT Charges" Really Just Charges?, J. Chem. Inf. Model. 61 (2021) 3881–3890. https://doi.org/10.1021/acs.jcim.1c00165.

[23] E.R. Johnson, S. Keinan, P. Mori-Sánchez, J. Contreras-García, A.J. Cohen, W. Yang, Revealing Noncovalent Interactions, J. Am. Chem. Soc. 132 (2010) 6498–6506. https://doi.org/10.1021/ja100936w.

[24] J. Contreras-García, E.R. Johnson, S. Keinan, R. Chaudret, J.-P. Piquemal, D.N. Beratan, W. Yang, NCIPLOT: a program for plotting non-covalent interaction regions., J. Chem. Theory Comput. 7 (2011) 625–632. https://doi.org/10.1021/ct100641a.

[25] J. Contreras-García, M. Calatayud, J.-P. Piquemal, J.M. Recio, Ionic interactions: Comparative topological approach, Comput. Theor. Chem. 998 (2012) 193–201. https://doi.org/https://doi.org/10.1016/j.comptc.2012.07.043.

[26] J.R. Lane, J. Contreras-García, J.-P. Piquemal, B.J. Miller, H.G. Kjaergaard, Are Bond Critical Points Really Critical for Hydrogen Bonding?, J. Chem. Theory Comput. 9 (2013) 3263–3266. https://doi.org/10.1021/ct400420r.

[27] B.A. Marekha, O.N. Kalugin, A. Idrissi, Non-covalent interactions in ionic liquid ion pairs and ion pair dimers: a quantum chemical calculation analysis, Phys. Chem. Chem. Phys. 17 (2015) 16846–16857. https://doi.org/10.1039/C5CP02197A.

Chapter- 6

Research Conclusions and Future Work

6 Research Conclusions and Future Work

6.1 Research Conclusions

The major conclusions of this thesis are discussed below:

In the initial part of the thesis i.e., chapter 2, density functional theory (DFT) calculations and molecular dynamics (MD) simulation were applied to investigate the mechanism of formation, stability, compactness in an aqueous medium, structural integrity, the charge transfer (CT) analysis and structural stability of DL-menthol: carboxylic acid, and tetrabutylammonium chloride ($N_{4444}Cl$): carboxylic acid deep eutectic solvents (DESs) in an aqueous environment. From the MD simulation study the "relative stability factor" was introduced to successfully measure the relative stability of a DES in an aqueous medium based on the nonbonded interaction energies among the components of the deep eutectic solvents. The order of stability of DES in water based on a "relative stability factor" was found as DL-menthol: acetic acid (1:1) < DL-menthol: levulinic acid (1:1) < DL-menthol: butanoic acid (1:1) < DL-menthol: pyruvic acid (1:2) < DL-menthol: hexanoic acid (1:1) < DL-menthol: octanoic acid (1:1) < DL-menthol: decanoic acid (1:1) < DL-menthol: dodecanoic acid (2:1). The structural properties such as radial, combined and spatial distribution function (RDF, CDF and SDF) and quantum chemical solvation study evidenced strong hydrogen bond acceptor (HBA)− hydrogen bond donor (HBD) interactions in long-chain organic acid based DESs (C_8 to C_{12}), whereas short-chain fatty acid based DESs (C_1 to C_6) are not stable in water media. This was supported by the higher HOMO-LUMO energy gap of DL-menthol: dodecanoic acid DES (173.80 kcal/mol) as compared to DL-menthol: acetic acid (171.26 kcal/mol). Short to medium-range interactions ranging from 1.730 to 2.07 Å were observed between the −OH (DL-menthol) and −COOH (organic acid) group indicating the occurrence of a network of non-bonded interactions such as hydrogen bonds and van der Waals or dispersion interactions between the HBA and the HBD to achieve stable DES formation. Solvated state quantum theory of atoms in molecules (QTAIM) analysis revealed the disappearance of intermolecular interactions for short-chain acid-based DESs. However, long-chain fatty acid-based DESs withstand their structural integrity with a larger extent of dispersion as well as H-bonding interactions among the HBA and the HBD in the presence of external water molecules. Non-covalent interaction (NCI) plots revealed hydrogen bonding and dispersion interactions for a stable DES formation. Later, nitenpyram extraction was carried out to validate the MD simulation results with greater accuracy than that of the experimental extraction efficiency (%EE).

After the stability analysis of the DESs, acetamiprid and imidacloprid (pesticides) extraction using DL-menthol: dodecanoic acid (2:1) and DL-menthol: octanoic acid (1:1) DES, respectively was studied with MD and QC calculations. The relative H-bonding number was found to be in the order of imidacloprid- octanoic acid (0.92) > DL menthol- imidacloprid (0.71) > imidacloprid- water (0.48) for imidacloprid system. In case of acetamiprid system, the order attained was acetamiprid-water (~0.185) > acetamiprid- dodecanoic acid (~0.175) > DL menthol- acetamiprid (~0.125). The extraction efficiency of 75% and 69% were achieved by the MD simulation which was in excellent agreement with that of the experiments. QC calculation suggested interaction between the DES-forming constituents with O (HBA-menthol) …H (HBD-organic acid) hydrogen bonding formation at a distance of 1.77 Å in both DESs. DES-pesticide optimized clusters were ranging from 2.896 to 3.77 Å for imidacloprid, and from 1.724 to 2.03 Å for acetamiprid, which were confirmed by MD simulation. NBO-based charge transfer study indicated the direction of charge transfer from DES to the pesticide molecule in each system.

The experimental investigation was carried out to extract enoxacin from the aqueous phase using hydrophobic DES. 82.6% extraction efficiency for DL-menthol: decanoic acid-based DES was obtained followed by 79.6% and 69.1% for DL-menthol: dodecanoic acid and decanoic acid: dodecanoic acid-based DESs, respectively. Three different recycling frameworks were then implemented for effective solvent regeneration. Around 90% net extraction efficiency was achieved in the third run in the 3rd recycle process where fresh DES (DL-menthol: decanoic acid) was introduced in every run and the reduced enoxacin solution was used as a continuous feed. The reuse and recyclability of the DES demonstrated an effective sustainable approach. QC and AIM/NCI analysis suggested stable DES-enoxacin formation with all three DESs. The three DES-enoxacin complexes obtained short to long-range interactions at 1.779 to 3.349 Å, 1.85 to 3.25 Å and from 1.64 to 1.68 Å. The QTAIM analysis suggested the formation of the DES-enoxacin complex via a combined effect of hydrogen bonding linkage with van der Waals dispersion interaction. The NCI plot with RDG analysis highlighted hydrogen bonding and dispersion interactions (vdW) confirming the presence of weak nonbonded interactions in the formation of DES as well as the DES-enoxacin complex.

In the final part of the thesis work (chapter 5), microfluidic device-based extraction of ciprofloxacin and fluconazole with hydrophobic DESs [DL-menthol: decanoic acid (1:1), and DL-menthol: dodecanoic acid (2:1)] was carried out to obtain a continuous, sustainable, robust and efficient approach. The extraction performance was evaluated at variable inlet flow rates (2 to 10 µl/min) with residence time ranging from 2.5 to 12.4 min at two different DES/water

phase mass ratios (1:1.12 and 1:2). 89% and 75% of ciprofloxacin extraction were achieved DL-menthol: decanoic acid (1:1), and DL-menthol: dodecanoic acid (2:1), respectively at a flowrate of 2 µl/min. At the same flow rate, 75% and 65% of fluconazole extraction were achieved, respectively. QC and non-covalent interaction NCI analysis suggest a strong ciprofloxacin-DES1 complex along with three different orientations of fluconazole-DES1 with non-bonded interactions such as hydrogen bonding and dispersion interactions responsible for the stability of the complexes. A larger HOMO-LUMO gap (94.04 kcal/mol, for DES1-CIP and 131.05 to142.34 kcal/mol, for DES1-FLU) supports the higher stability of the complexes. The NCI plot with RDG analysis was performed to highlight the regions of weak interaction and supported by MD simulation findings.

6.2 Scope of the Future Work

1. Biocompatible DESs can effectively be applied in the biological fields. Application of DESs in modulating the rheology and transport properties of the mucus layer can be a significant task. Choline-based DESs have shown effective mucus modulation properties by reducing the viscosity of the mucus layer. However, computational studies can impart significant insights into the charge transfer, intermolecular interactions and involvement of mucus-forming components with DES components. This study needs extensive research.
2. Development and application of therapeutic DESs (THEDES) for the application in the field of drug delivery is another significant area where a lot of interest has been developed. Experimental studies with computational approaches can lead to finding new classes of compounds that can be utilized to develop new THEDESs for specific and targeted therapeutic applications.
3. Currently, there are no sustainable and effective DES-regeneration pathways available in this regard. It is essential to make DES-based applications an economically reachable zone by reducing solvent requirements and wastage of solvents to utilize DESs in various global industrial applications at a large scale.

APPENDIX

A Appendix

Materials and Methods

A.1 Computational Details

A.1.1 Molecular Dynamics Simulation

The MD simulation scheme starts with firstly drawing the structures of the individual HBA, HBD, and water molecules in GaussView 6 with geometry optimization using Gaussian 16 at the B3LYP/6-31G* level of theory. The partial atomic charges of the molecules were obtained by the restricted electrostatic potential (RESP) module of AMBER 14 and the partial charges were fitted. The generalized amber force field functional of the ANTECHAMBER module of AMBER 14, was applied to generate all force field parameters.

Initially, a specific number of the DES components (HBA, HBD) and water molecules were packed in a simulation box using PACKMOL. Following that, the MD simulation for each system was carried out in NAMD 2.10 package at 298.15 K and atmospheric pressure. NAMD simulation was carried out with a 6 ns minimization run, followed by heating at 298.15 K for 0.5 ns and an equilibration run for 10 ns. NPT ensemble was employed to equilibrate the system where the simulation box size was equilibrated. A uniform system energy has been obtained to confirm the successful completion of the equilibration step and to continue the production run. Lastly, a 100 ns production run employing the NVT ensemble at 298.15 K and 1 atm pressure was carried out. The periodic boundary condition (PBC) was applied for maintaining the system continuum. To obtain the spatial density function (SDF) data, TRAVIS package was used, where the parameter file and the final trajectory file were utilized. VMD 1.9.3 trajectory analyzer visualization tool was used to obtain the SDF iso-surfaces and MD simulation-driven angular distribution findings. Specific reference and observed molecules were selected to obtain the SDF coordinate file.

The Langevin dynamics method with a collision frequency of 1 ps^{-1} was used for maintaining the desired temperature. The Nosé−Hoover Langevin piston was used for pressure-control with an oscillation period of 100 fs and a damping factor of 50 fs. Subsequently, the production runs were carried out for 100 ns for each of the systems with the NVT ensemble. The trajectory data were saved at every 5ps. The SHAKE algorithm was considered to restrain the bonds involving hydrogen atoms. VMD 1.9.3 package was used for visualizing the trajectory of the molecules within the systems. The particle mesh Ewald method was used for the calculation of the long-

range intermolecular electrostatic interactions. A cutoff distance of 12 Å was considered for short-range interactions. Periodic boundary condition (PBC) was applied in each system. Each system was initiated with three different starting configurations to ensure successful completion and reproducibility of the simulation that can provide a realistic estimate of the trajectory and the thermodynamic properties. This was performed to remove any numerical or modelling bias in the simulation procedure.

A.1.2 Quantum Chemical Calculation

Initially, the DES-optimized structures were generated by inserting the individual carboxylic fatty acids (acetic acid, butanoic acid, hexanoic acid, octanoic acid, decanoic acid and dodecanoic acid) around multiple possible orientations around the DL-menthol moiety using GaussView 6. Geometry optimization was carried out primarily employing B3LYP density functional in combination with 6-311+G(d,p) basis set, for the DES components using Gaussian 16. Grimme and coworkers' atom-pair-wise correction techniques with Becke-Johnson damping (D3BJ) were used to accounting for the long-range dispersion effects between the HBA and the HBD. The BJ-damping requires one fit parameter more for each functional (three instead of two) but has the advantage of avoiding repulsive interatomic forces at shorter distances. With BJ-damping better results for non-bonded distances and clear effects of intramolecular dispersion in the molecular systems can be obtained with higher precision in calculating the non-bonded interaction. Energy minima were identified as the consequent stationary points on the hypersurface of potential energy by vibrational frequency analysis as triggered by the ‘freq’ keyword in Gaussian at the same level of theory. Subsequently, the geometries are re-optimized again at the M06-2X functional with the same basis set, i.e., 6-311+G(d,p) for a comparative study considering the suitability of this functional in analyzing similar systems. The counterpoise approach in eliminating the basis set superposition error is exercised for the interaction energy and other subsequent quantum chemical calculations. Natural bond orbital (NBO) analysis and CHELPG partial charge analysis designed for the charge distribution and transfer in eutectic systems, and frontier molecular orbital (FMO) analysis, for the molecular electronic structure based on the frontier orbital overlap and the electronic transition were carried out. NBO study elucidated the charge transfer (CT) profile of the DES systems based on the distribution of charges over the components. The implicit solvation study was performed by employing the SMD solvation model developed by the Truhler group on the optimized DES structures to calculate the Gibbs free energy of solvation (ΔG_{solv}), selecting water as the solvent medium and the explicit solvation was performed with

two water molecules explicitly positioned around each of the DESs and optimizing those structures. All the calculations were performed using the Gaussian 16 package.

A.1.3 QTAIM Calculation

To comprehensively investigate the intermolecular interactions between the HBA and the HBD, Bader's QTAIM approach supported by non-covalent interaction (NCI) and RDG (Reduced Density Gradient) analysis were implemented using the MultiWFN code. The electron density at the bond critical points (BCP), (ρ_{BCP}) and its Laplacian ($\nabla\rho_{BCP}^2$) were obtained which provided valuable insights regarding the strength and the character of the interactions. The NCI analysis can be exercised in identifying different interaction regions within the DES and the electron density distribution of DESs containing low density and gradient of density.

A.2 Experimental Details

A.2.1 Preparation of DES

DESs were prepared by mixing both the compounds (HBA and HBD) in a reagent bottle at 50 ºC with a stirring speed of 500 rpm until a homogeneous liquid mixture was formed. The prepared DESs were then kept at room temperature for two to three days to ensure equilibrium and stability, before using them for further experiments. The Karl Fischer titration (Metrohm 870 KF Titrino Plus) was used to evaluate the water content of each pure hydrophobic DES, and the analysis indicated a water content of < 400 ppm.

A.2.2 Solubility of Drugs in Different Hydrophobic DESs

Drug solubility can be evaluated by adding a small quantity of the pure pharmaceutical component (about 2 mg/ g of DES per addition) to the investigated hydrophobic DESs at room temperature. After stirring the vials for at least 12 hours, the samples were examined. To ensure a uniform mixture, a tiny amount of the solid was added after all of the solid had dissolved. To get to the stage of visual saturation (heterogeneous combination), this approach was repeated.

A.2.3 Batch-type Liquid-Liquid Extraction Experiments

Three different mass ratios of DES to water phase were prepared for all various initial concentrations of drug (e.g., 5 ppm, 10 ppm and 20 ppm respectively). To minimize the amount of DES required for extraction of a unit amount of enoxacin micropollutant, the LLE experiments were carried out for different DES phase/water phase mass ratios (e.g., 1:1, 1:2

and 1:3) for each of the DESs. A temperature-controlled water bath was used to ensure uniform temperature throughout the experiments, which in the present study was kept at room temperature (25 ºC). The mixtures were allowed to stir vigorously at a stirring speed ranging from 300 to 500 rpm depending on the requirement of a full central vortex formation within the vials. Subsequently, the mixtures were allowed to settle for about 16 hours until a complete phase separation of the DES and water phase occurred. The separated DES and water phases were collected with precaution and were stored for further experiments.

A.2.4 Extraction of Ciprofloxacin and Fluconazole using Microchannel

A serpentine-shaped circular microchannel extraction unit was setup with an inner diameter of d ~ 500 μm and a total path length of l ~ 80 cm. The DES phase and the aqueous stock solution of the drugs were injected through the two inlet openings at the left-hand side of the microchannel unit. The injection of the phases at a desired inlet flow rate was implemented through a syringe pump so that the inlet flow rate and desired DES/water phase mass ratio can be maintained. The two phases get attached within the single path of the microchannel and transport of the drug molecules from the water phase to the DES phase occurs due to a higher contact time. The phases then are collected in the outlet of the channel and after successful phase separation, the quantification of the phases is carried out. The temperature of the room while experimenting is maintained around 25 °C.

B Appendix (Chapter-2)

Table B.1: Partial charges of all the atoms of different molecular species

DL-menthol		Acetic acid		Water		Octanoic acid	
Atom type	**Partial charge**	**Atom type**	**Partial charge**	**Atom type**	**Partial charge**	**Atom type**	**Partial charge**
C1	-0.189206	C11	-0.457106	O6	-0.810208	C20	-0.308932
H3	0.058027	H21	0.142750	H56	0.405104	H31	0.069673
H4	0.058027	H22	0.142750	H57	0.405104	H32	0.069673
C2	-0.162554	H23	0.142750	**Dodecanoic acid**		H33	0.069673
H1	0.052018	C12	0.856071	**Atom type**	**Partial charge**	C21	0.191054
H2	0.052018	O3	-0.665878			H34	-0.029995
C3	0.084112	H24	0.445797	C21	-0.304857	H35	-0.029995
H9	0.040931	O2	-0.607133	H32	0.067749	C22	-0.00381
C8	0.294800	**Decanoic acid**		H33	0.067749	H36	-0.002271
H13	0.023503	**Atom type**	**Partial charge**	H34	0.067749	H37	-0.002271
C9	-0.432540			C22	0.196597	C23	-0.034935
H14	0.097230	C11	-0.305472	H35	-0.032847	H38	0.000397
H15	0.097230	H21	0.068137	H36	-0.032847	H39	0.000397
H16	0.097230	H22	0.068137	C23	-0.003457	C24	0.052343
C10	-0.432540	H23	0.068137	H37	-0.004852	H40	-0.012444
H17	0.097230	C12	0.192863	H38	-0.004852	H41	-0.012444
H18	0.097230	H24	-0.031335	C24	-0.022894	C25	0.016689
H19	0.097230	H25	-0.031335	H39	-0.009184	H42	0.01712
C4	0.254862	C13	0.001227	H40	-0.009184	H43	0.01712
H5	0.025419	H26	-0.005469	C25	0.089169	C26	-0.187542
O1	-0.748355	H27	-0.005469	H41	-0.027108	H44	0.081235
H20	0.444137	C14	-0.032050	H42	-0.027108	H45	0.081235
C5	-0.475968	H28	-0.007085	C26	0.032018	C27	0.807784
H6	0.133764	H29	-0.007085	H43	-0.014595	O5	-0.702213
H7	0.133764	C15	0.097558	H44	-0.014595	**Hexanoic acid**	

C6	0.386348	H30	-0.027229	C27	0.004193	**Atom type**	**Atom type**
H8	-0.027666	H31	-0.027229	H45	-0.010482		
C7	-0.519159	C16	0.015573	H46	-0.010482	C11	-0.307235
H10	0.120959	H32	-0.005266	C28	0.044887	H21	0.070054
H11	0.120959	H33	-0.005266	H47	-0.011808	H22	0.070054
H12	0.120959	C17	-0.015341	H48	-0.011808	H23	0.070054
Butanoic acid		H34	-0.000687	C29	0.001536	C12	0.188949
Atom type	**Partial charge**	H35	-0.000687	H49	-0.002977	H24	-0.024322
		C18	0.018757	H50	-0.002977	H25	-0.024322
C11	-0.312851	H36	0.013892	C30	0.00517	C13	-0.033224
H21	0.075734	H37	0.013892	H51	0.016467	H26	0.008148
H22	0.075734	C19	-0.151317	H52	0.016467	H27	0.008148
H23	0.075734	H38	0.070239	C31	-0.154553	C14	-0.050744
C12	0.165466	H39	0.070239	H53	0.070812	H28	0.024236
H24	-0.000841	C20	0.809922	H54	0.070812	H29	0.024236
H25	-0.000841	O3	-0.700955	C32	0.812934	C15	-0.096241
C13	-0.199222	H40	0.465064	O3	-0.700429	H30	0.059993
H26	0.083053	O2	-0.614364	H55	0.464201	H31	0.059993
H27	0.083053			O2	-0.614613	C16	0.802087
C14	0.797752					O3	-0.704599
O3	-0.696720					H32	0.466153
H28	0.466979					O2	-0.611419
O2	-0.613031						

TBAC		**Pyruvic acid**		**Levulinic acid**		**Hexanoic acid**	
Atom type	**Partial charge**	**Atom type**	**Partial charge**	**Atom type**	**Partial charge**	**Atom type**	**Partial charge**
N1	0.876948	C11	-0.483844	C11	-0.481950	C11	-0.307235
C1	-0.271987	H21	0.142335	H21	0.129201	H21	0.070054
H1	0.078874	H22	0.142335	H22	0.129201	H22	0.070054
H2	0.078874	H23	0.142335	H23	0.129201	H23	0.070054
C2	-0.068684	C12	0.597649	C12	0.749864	C12	0.188949
H3	0.044135	O2	-0.473862	O2	-0.573793	H24	-0.024322

H4	0.044135	C13	0.680126	C13	-0.298802	H25	-0.024322
C3	0.290840	O4	-0.659898	H24	0.083993	C13	-0.033224
H5	0.002368	H24	0.482012	H25	0.083993	H26	0.008148
H6	0.002368	O3	-0.569188	C14	-0.034778	H27	0.008148
C4	-0.625112	**Butanoic acid**		H26	0.066274	C14	-0.050744
H7	0.227476	**Atom type**	**Partial charge**	H27	0.066274	H28	0.024236
H8	0.227476			C15	0.780110	H29	0.024236
C5	-0.271987	C11	-0.312851	O4	-0.692491	C15	-0.096241
H9	0.078874	H21	0.075734	H28	0.466644	H30	0.059993
H10	0.078874	H22	0.075734	O3	-0.602940	H31	0.059993
C6	-0.068684	H23	0.075734			C16	0.802087
H11	0.044135	C12	0.165466			O3	-0.704599
H12	0.044135	H24	-0.000841			H32	0.466153
C7	0.290840	H25	-0.000841			O2	-0.611419
H13	0.002368	C13	-0.199222				
H14	0.002368	H26	0.083053				
C8	-0.625112	H27	0.083053				
H15	0.227476	C14	0.797752				
H16	0.227476	O3	-0.696720				
C9	-0.271987	H28	0.466979				
H17	0.078874	O2	-0.613031				
H18	0.078874						
C10	-0.068684						
H19	0.044135						
H20	0.044135						
C11	0.290840						
H21	0.002368						
H22	0.002368						
C12	-0.625112						
H23	0.227476						
H24	0.227476						

C13	-0.271987
H25	0.078874
H26	0.078874
C14	-0.068684
H27	0.044135
H28	0.044135
C15	0.290840
H29	0.002368
H30	0.002368
C16	-0.625112
H31	0.227476
H32	0.227476
Cl1	-1.000000

Table B.2: Calculated CHELPG charges (in a.u.) on the different components before and after the formation of the DESs [DLM (HBA): DL-menthol, acid (HBD): different fatty acids corresponding to the respective DESs, $-OH_{HBA}$: −OH group of DL-menthol and $-COOH_{HBD}$: −COOH group of different HBDs] ($CD_{-OH/-COOH}$: charge difference between $-OH_{HBA}$ and $-COOH_{HBD}$)

DES systems	B3LYP					M06-2X				
	DLM (HBA)	Acid (HBD)	$-OH_{HBA}$	$-COOH_{HBD}$	$CD_{-OH/-COOH}$	DLM (HBA)	Acid (HBD)	$-OH_{HBA}$	$-COOH_{HBD}$	$CD_{-OH/-COOH}$
DES1	0.0201	−0.0201	−0.29061	−0.0305	0.26011	0.0243	−0.0243	−0.28881	−0.03534	0.25347
DES2	0.0195	−0.0195	−0.2898	−0.0237	0.26610	0.0227	−0.0227	−0.28675	−0.02641	0.26034
DES3	0.0187	−0.0187	−0.29001	−0.0228	0.26721	0.0221	−0.0221	−0.28699	−0.02547	0.26152
DES4	0.0179	−0.0179	−0.29004	−0.02254	0.2675	0.0213	−0.0213	−0.28735	−0.02554	0.26181
DES5	0.0177	−0.0177	−0.29018	−0.02249	0.26769	0.0210	−0.0210	−0.2876	−0.02551	0.26209
DES6	0.0175	−0.0175	−0.29023	−0.02245	0.26778	0.0208	−0.0208	−0.28766	−0.02545	0.26221
DES7	0.0174	−0.0174	−0.29021	−0.02241	0.26780	0.0207	−0.0207	−0.28757	−0.02532	0.26225
pure component	0.00	0.00	-	-	-	0.00	0.00	-	-	-

Table B.3: Theoretically Obtained HOMO, LUMO Energies (Ground and Excited State), HOMO-LUMO Energy Gap, Ionization Potential (I), Electron affinity (A), Chemical Hardness (η), and Chemical Potential (μ) Computed in the DFT-B3LYP Method with D3BJ Dispersion Correction for DESs (All the units are in Hartree)

System	E_{HOMO}	E_{LUMO}	energy gap	E_{HOMO-1}	E_{LUMO+1}	energy gap	η
DES1	−0.27822	−0.00528	0.27294	−0.28869	−0.00139	0.2873	0.1365
DES2	−0.27842	−0.00444	0.27398	−0.28768	−0.00129	0.28639	0.1369
DES3	−0.27856	−0.00392	0.27464	−0.28749	−0.00106	0.28643	0.1373
DES4	−0.27859	−0.00365	0.27494	−0.28728	−0.00101	0.28627	0.1375
DES5	−0.27869	−0.00358	0.27511	−0.28721	−0.001	0.28621	0.1376
DES6	−0.27898	−0.00351	0.27547	−0.28716	−0.00101	0.28615	0.1377
DES7	−0.28041	−0.00344	0.27697	−0.28704	−0.00103	0.28601	0.1384

Table B.4: Electron Density (ρ_{BCP}), the Laplacian of electron density ($\nabla\rho_{BCP}^2$) and the energetic components at the relevant BCPs for DL-menthol- acetic acid, DL-menthol- butanoic acid, DL-menthol- octanoic acid, and DL-menthol- dodecanoic acid DESs in the explicitly solvated state. [DLM: DL menthol, ACE: acetic acid, BUT: butanoic acid, OCT: octanoic acid, DODEC: dodecanoic acid]

Component pair	BCP interaction	ρ_{BCP} (a.u.)	$\nabla\rho_{BCP}^2$ (a.u.)	G_{BCP} (a.u.)	V_{BCP} (a.u.)	$-G_{BCP}/V_{BCP}$
DLM-ACE Solvated	BCP1a: H_{15}-O_{34}	0.0071	0.0249	0.0054	−0.0047	1.17
	BCP1b: O_{30}-H_{35}	0.0678	0.1518	0.056	−0.074	0.76
	BCP1c: O_{33}-H_{13}	0.004	0.0124	0.0026	−0.0022	1.18
	BCP1d: O_{34}-H_{40}	0.025	0.105	0.0234	−0.021	1.11
	BCP1e: O_{39}-H_{44}	0.007	0.026	0.0055	−0.0045	1.22
	BCP1f: O_{33}-H_{38}	0.029	0.118	0.027	−0.025	1.08
	BCP1g: O_{36}-H_{31}	0.0329	0.127	0.031	−0.03	1.03
	BCP1h: O_{39}-H_{15}	0.0054	0.0173	0.0037	−0.0031	1.19
	BCP1i: O_{39}-H_{27}	0.007	0.021	0.0047	−0.0041	1.14
DLM-BUT Solvated	BCP2a: O_{40}-H_{51}	0.024	0.101	0.0223	−0.0194	1.14
	BCP2b: O_{30}-H_{41}	0.0567	0.1495	0.048	−0.059	0.81
	BCP2c: O_{39}-H_{48}	0.0234	0.103	0.0224	−0.019	1.18
	BCP2d: O_{49}-H_{27}	0.0054	0.0154	0.0035	−0.0031	1.13
	BCP2e: O_{46}-H_{12}	0.007	0.026	0.0055	−0.0045	1.22
	BCP2f: H_{37}-O_{49}	0.0068	0.0232	0.005	−0.0041	1.21
	BCP2g: O_{39}-H_{13}	0.0073	0.0224	0.0051	−0.0045	1.13
DLM-OCT Solvated	BCP4a: O_{51}-H_{31}	0.017	0.061	0.014	−0.013	1.07
	BCP4b: H_{53}-O_{30}	0.0489	0.1402	0.042	−0.048	0.87
	BCP4c: O_{51}-C_5	0.006	0.0213	0.0046	−0.0038	1.21
	BCP4d: O_{58}-H_{18}	0.0026	0.0104	0.0021	−0.0015	1.4
	BCP4e: O_{61}-C_{47}	0.0075	0.0323	0.0067	−0.0051	1.31
	BCP4f: O_{52}-H_{63}	0.018	0.07	0.0198	−0.0167	1.18
	BCP4g: O_{51}-H_{60}	0.014	0.058	0.023	−0.019	1.21
DLM-DODEC Solvated	BCP7a: H_{31}-O_{54}	0.022	0.091	0.012	−0.011	1.09
	BCP7b: O_{30}-H_{56}	0.049	0.142	0.043	−0.05	0.86
	BCP7c: O_{55}-H_{13}	0.074	0.023	0.0053	−0.0047	1.13
	BCP7d: O_{73}-H_{15}	0.0062	0.018	0.0041	−0.0036	1.14
	BCP7e: O_{73}-H_9	0.0067	0.02	0.0045	−0.004	1.12
	BCP7f: O_{54}-H_{71}	0.013	0.057	0.0215	−0.0185	1.16
	BCP7g: O_{55}-H_{74}	0.012	0.05	0.02	−0.0175	1.14
	BCP7h: O_{73}-H_{52}	0.006	0.02	0.0043	−0.0036	1.19

Table B.5: Coordination number obtained from the radial distribution function for different DES systems

System	Component pairs	Coordination number (Z)
S1	Menthol- water	0.70
	Menthol- acetic acid	1.50
	Acetic acid- water	2.60
S2	Menthol- water	0.55
	Menthol- butanoic acid	2.60
	Butanoic acid-water	2.30
S3	Menthol- water	0.60
	Menthol- hexanoic acid	3.40
	Hexanoic acid-water	2.15
S4	Menthol- water	0.45
	Menthol- octanoic acid	3.60
	Octanoic acid-water	2.05
S5	Menthol- water	0.40
	Menthol- decanoic acid	3.8
	Decanoic acid-water	1.97
S6	Menthol- water	0.50
	Menthol- dodecanoic acid	4.0
	Dodecanoic acid-water	1.77
S7	Menthol- water	0.85
	Menthol- pyruvic acid	2.4
	Pyruvic acid-water	2.2
S8	Menthol- water	0.75
	Menthol- levulinic acid	1.3
	Levulinic acid-water	2.37
S9	$N_{4444}Cl$- water	1.65
	$N_{4444}Cl$- acetic acid	1.70
	Acetic acid- water	1.45
S10	$N_{4444}Cl$- water	2.40
	$N_{4444}Cl$- octanoic acid	1.75

	Octanoic acid- water	1.25
DES+ nitenpyram+ water	Nitenpyram- octanoic acid	2.00
	Nitenpyram- DL menthol	1.90
	Nitenpyram- water	1.50
	Octanoic acid- DL menthol	5.50
	Octanoic acid- water	0.75

Table B.6: Self-Diffusivity for different molecular species of DL-menthol- based and tetrabutylammonium- based DES systems with water at 298.15 K at different time intervals

System Number	Molecule species	Diffusion coefficient (D) X 10^{-9} (m^2/s)		
		0-10 ns	40-50 ns	90-100 ns
S1	Acetic acid	1.150	0.884	0.665
	DL-menthol	0.564	0.705	0.905
	Water	1.484	1.162	0.844
S2	Butanoic acid	1.003	0.918	0.601
	DL-menthol	0.656	0.495	0.960
	Water	1.239	1.765	0.828
S3	Hexanoic acid	0.834	0.818	0.728
	DL-menthol	0.775	0.975	0.450
	Water	1.506	0.841	2.438
S4	Octanoic acid	0.722	0.840	0.734
	DL-menthol	0.560	0.793	0.793
	Water	2.145	1.463	1.557
S5	Decanoic acid	0.944	0.632	0.916
	DL-menthol	1.002	0.627	0.592
	Water	1.078	2.633	2.385
S6	Dodecanoic acid	0.908	0.980	0.774
	DL-menthol	0.808	0.806	0.852
	Water	1.091	1.182	1.365
S7	Pyruvic acid	0.804	0.944	0.608
	DL-menthol	0.613	0.433	0.912

	Water	1.301	1.848	0.846
S8	Levulinic acid	0.904	0.566	0.887
	DL-menthol	0.729	1.042	0.700
	Water	1.291	0.950	1.309
S9	Acetic acid	0.745	0.658	0.890
	TBA cation	0.633	0.661	0.597
	Chloride ion	0.740	0.822	0.835
	Water	0.912	0.964	0.963
S10	Octanoic acid	0.813	1.068	0.994
	TBA cation	0.657	0.546	0.551
	Chloride ion	0.851	0.702	0.908
	Water	0.925	0.803	0.941

Table B.7: Self-diffusivity of different molecular species of DL-menthol- octanoic acid-nitenpyram-water system at 298.15 K

System	**Molecule species**	**Diffusion coefficient (D) X 10^{-9} (m^2/s)**		
		0-10 ns	**40-50 ns**	**90-100 ns**
DES+ nitenpyram+ water	Water	0.914	1.001	1.088
	Octanoic acid	0.709	0.578	0.646
	Nitenpyram	0.732	0.776	0.568
	DL-menthol	0.684	0.672	0.729

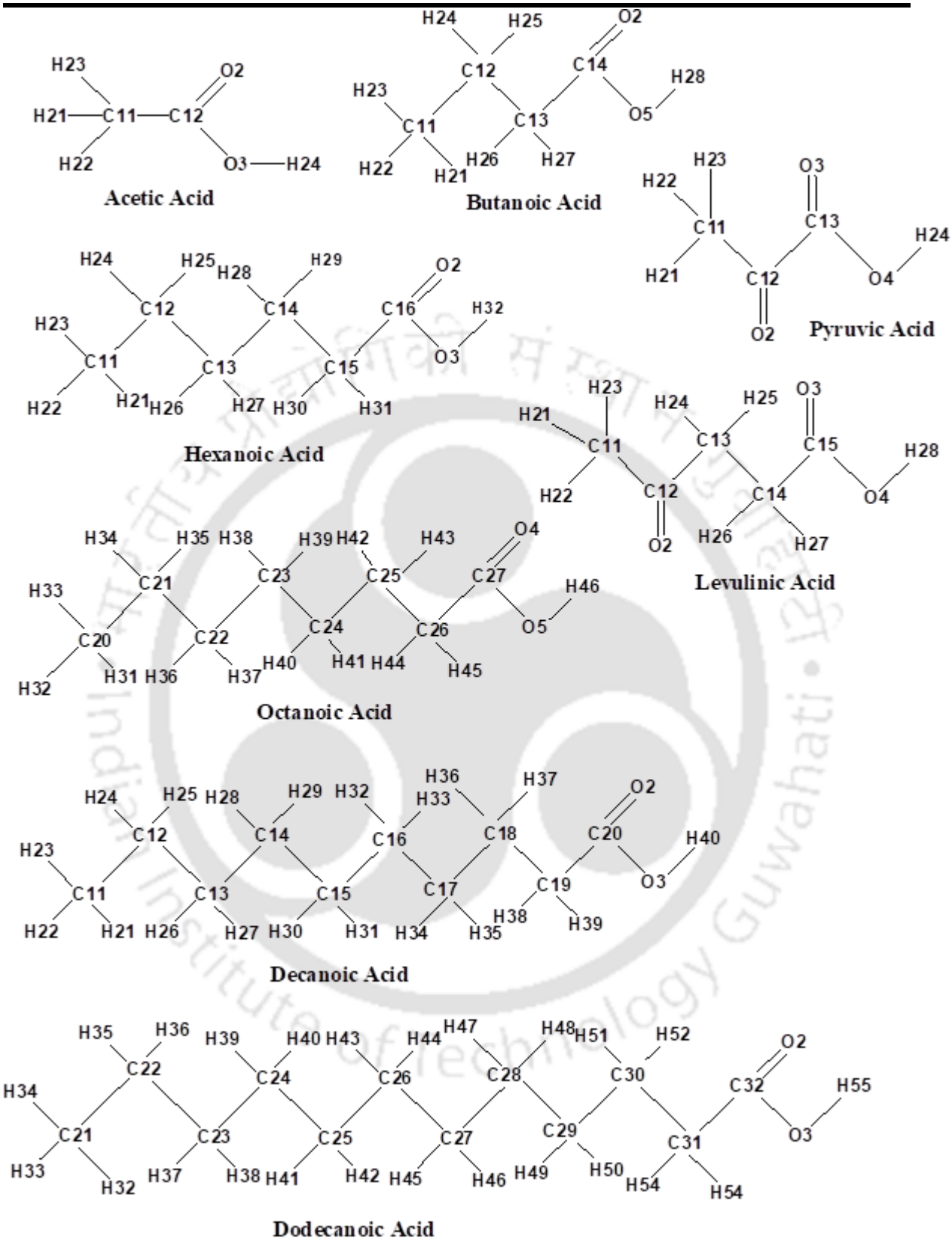

Figure B.1. Structures of all the HBD molecules with atom notations

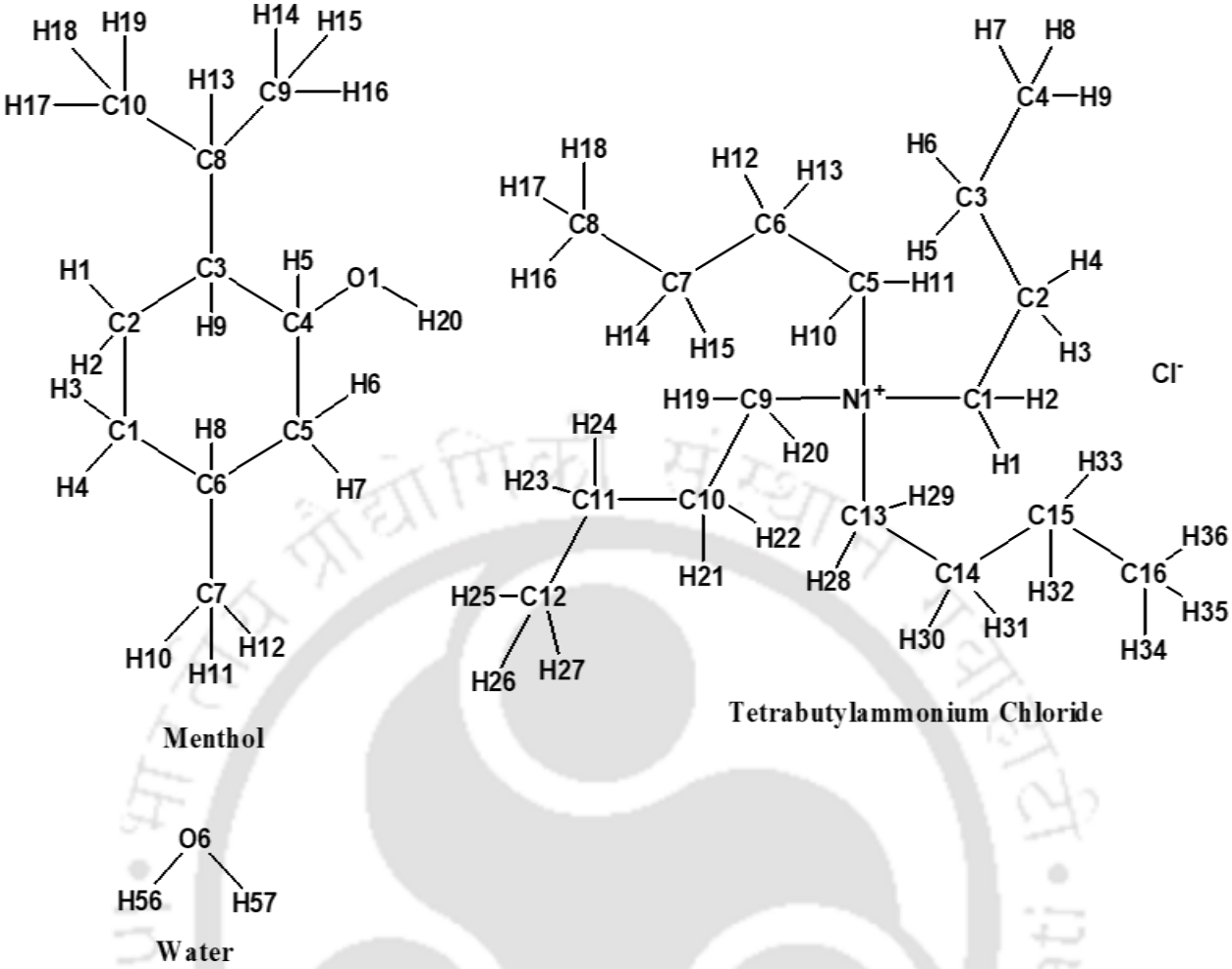

Figure B.2: Structures of HBA molecules and water with atom notations

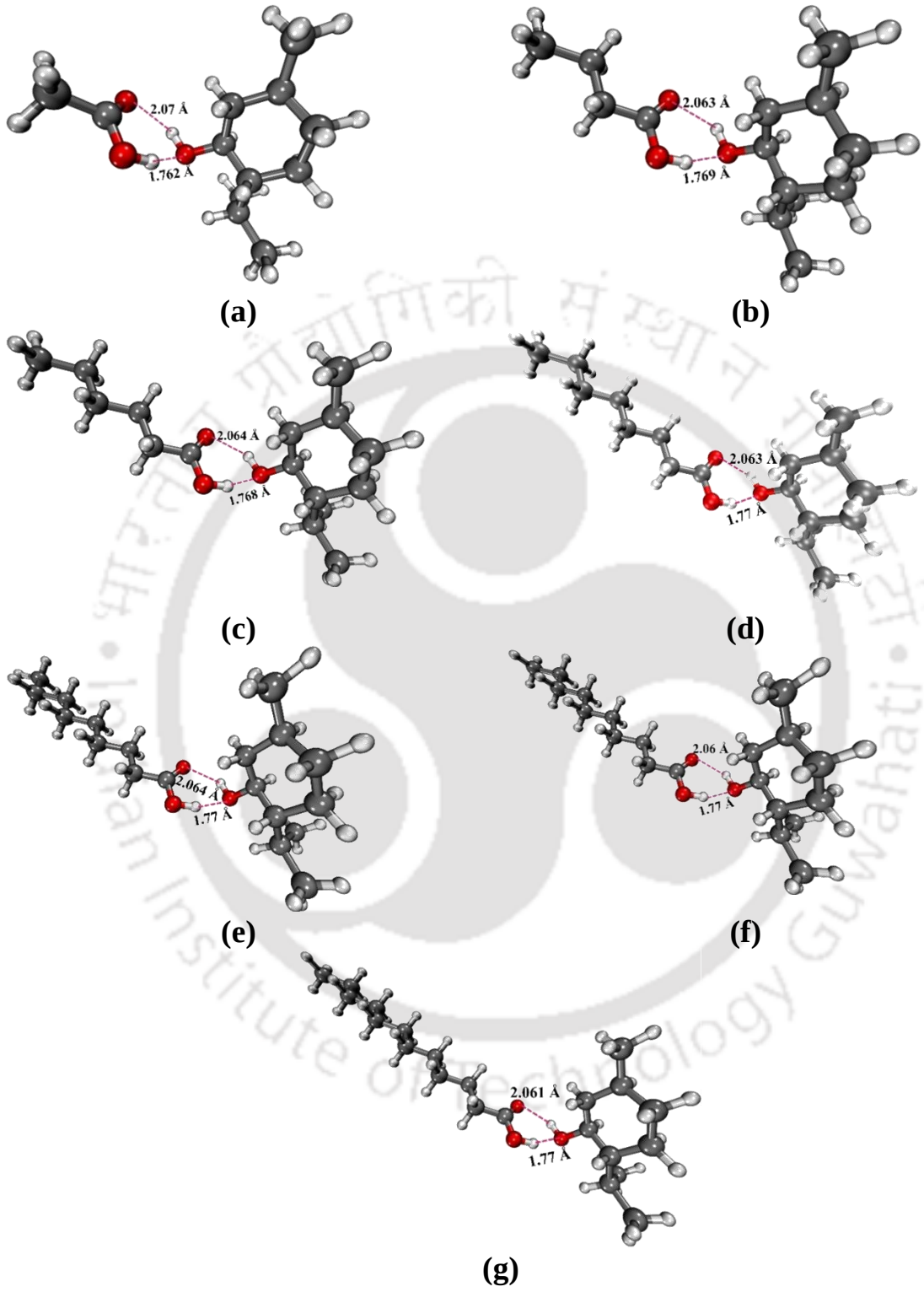

Figure B.3: Optimized Structures of (a) DL-menthol/ acetic acid, (b) DL-menthol/ butanoic acid, (c) DL-menthol/ hexanoic acid, (d) DL-menthol/ octanoic acid, (e) DL-menthol/ nonanoic

acid, (f) DL-menthol/decanoic acid and (g) DL-menthol/ dodecanoic acid DESs (pure DESs) at the M06-2X/6-311+G (d,p) level of theory.

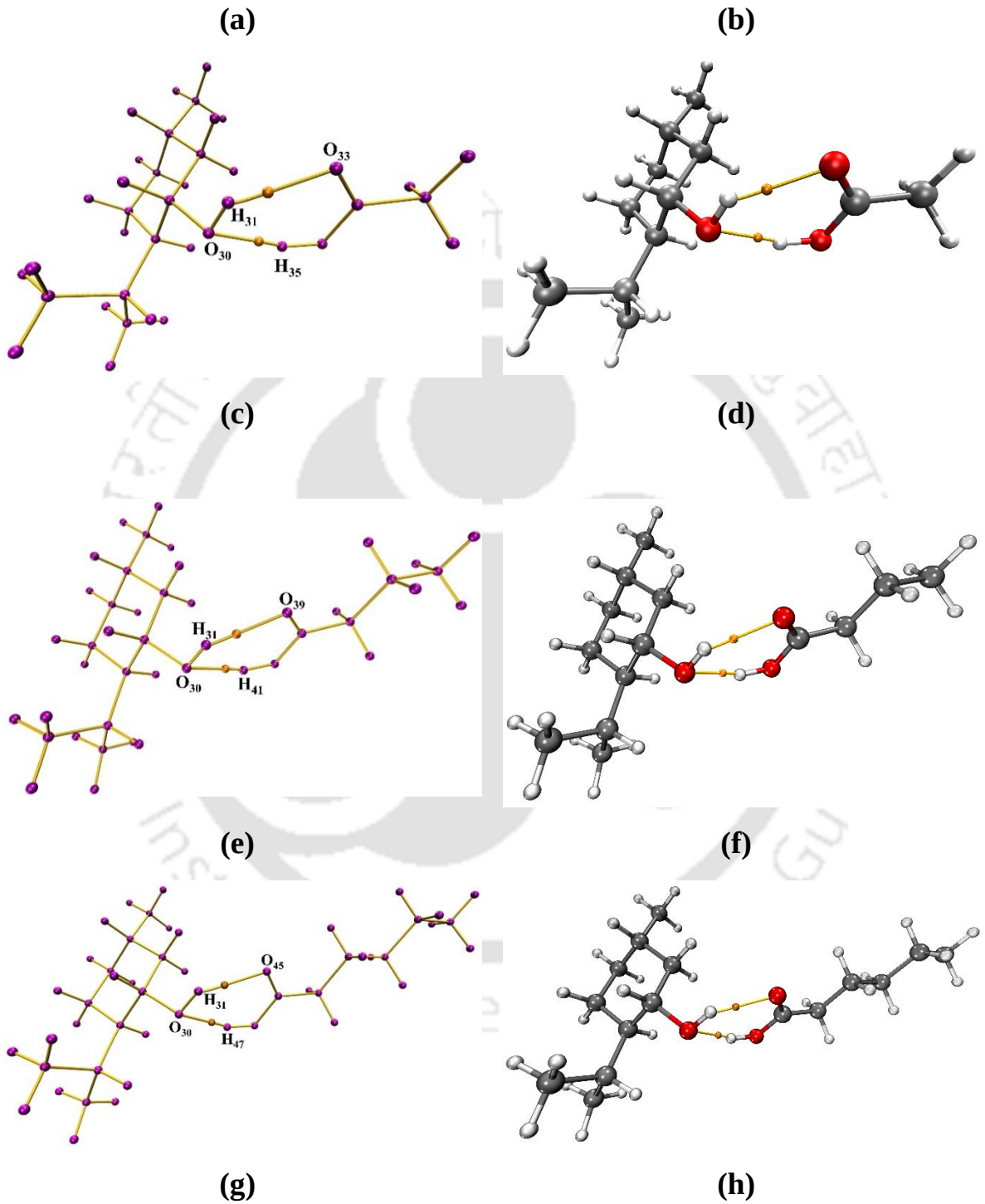

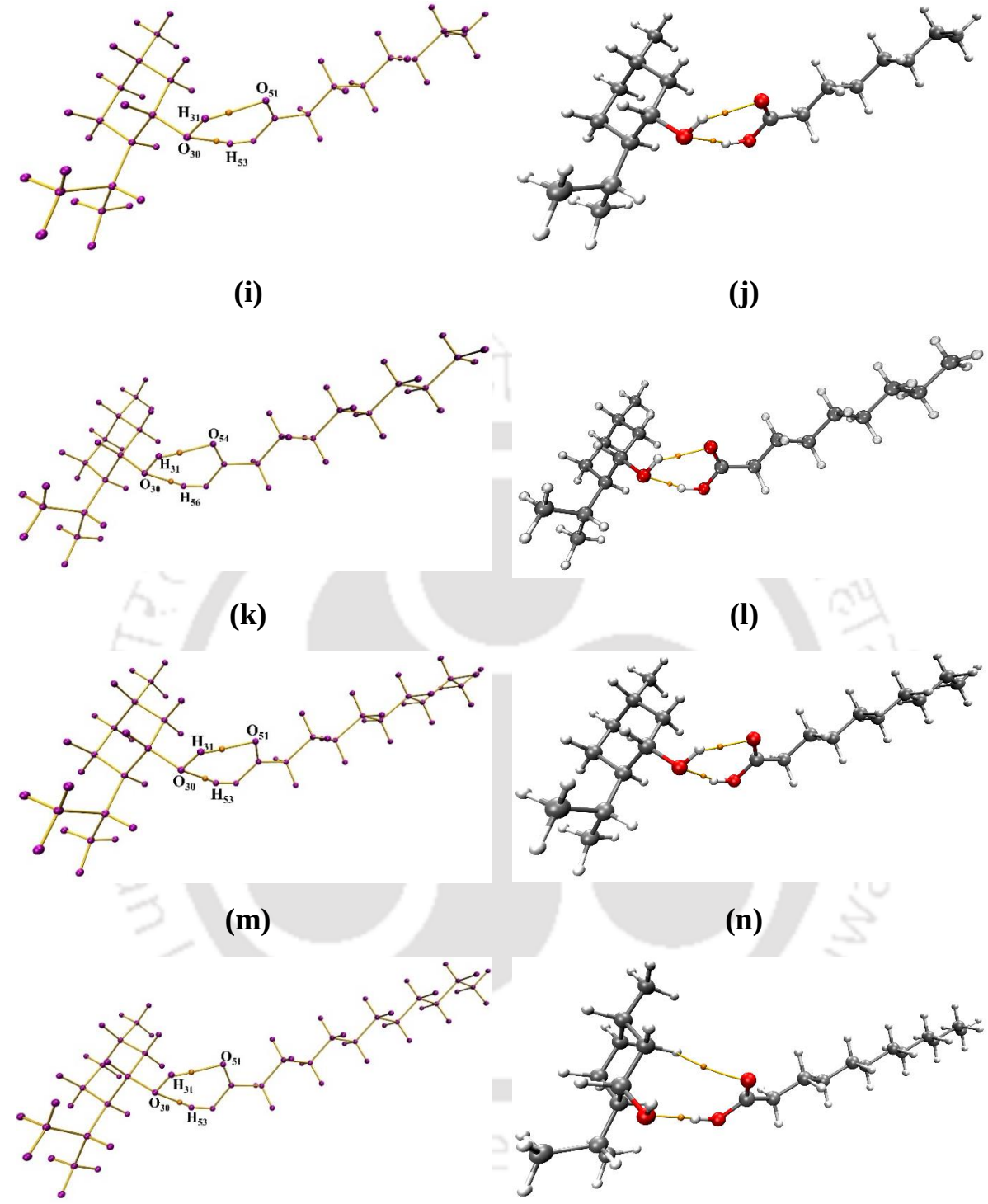

Figure B.4: Molecular graphs of optimized structure of pure DES: (a,b) DES1, (c,d) DES2, (e,f) DES3, (g,h) DES4, (i,j) DES5, (k,l) DES6, and (m,n) DES7, at the B3LYP/6-311+G(d,p) level with D3BJ dispersion correction revealing bond critical points (BCPs) and their corresponding paths

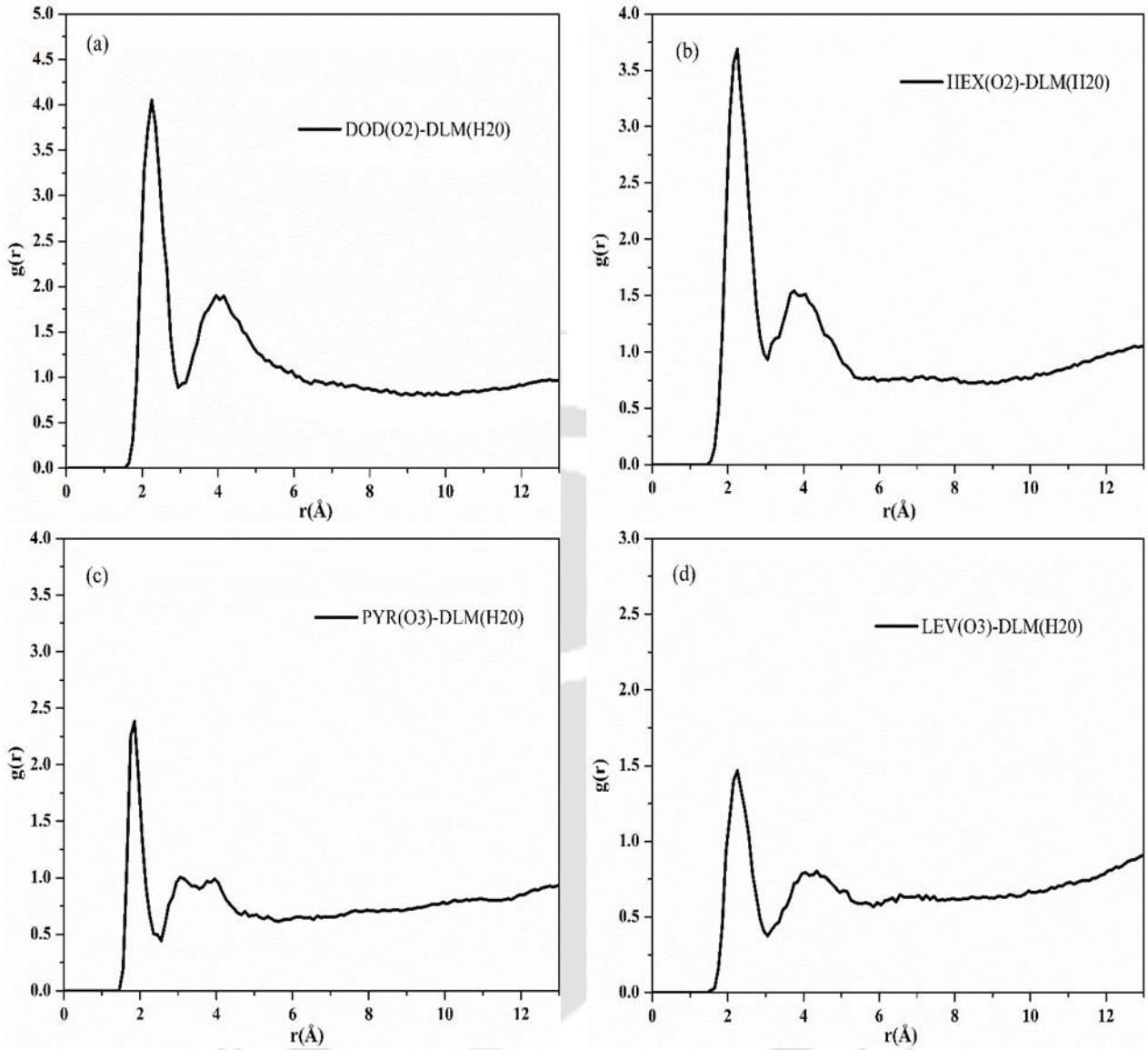

Figure B.5: Atom-atom RDF plots between DL-menthol and (a) dodecanoic acid (S6), (b) hexanoic acid (S3), (c) pyruvic acid (S7), and (d) levulinic acid (S8), at 100 ns

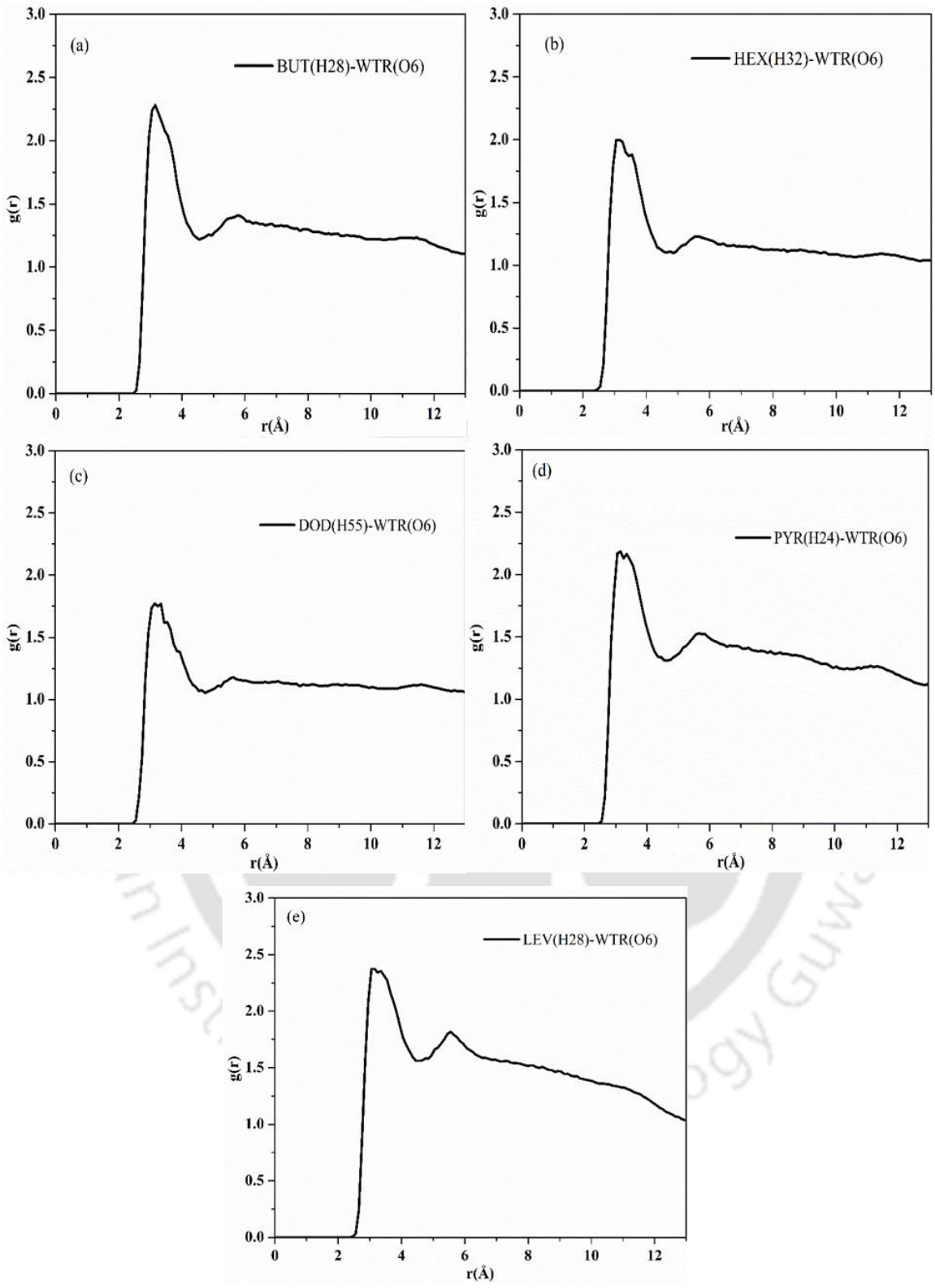

Figure B.6: Atom-atom RDF plots for individual systems of DL-menthol-based DESs between (a) butanoic acid-water (S2), (b) hexanoic acid-water (S3), (c) dodecanoic acid-water (S6), (d) pyruvic acid-water (S7), and (e) levulinic acid-water (S8), at 100 ns

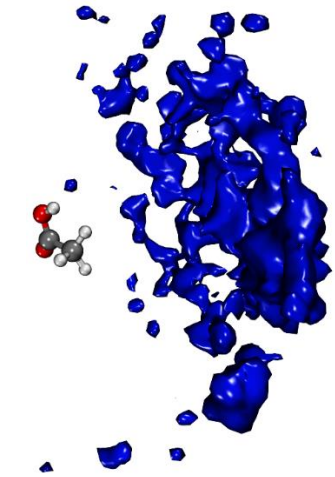

(a)

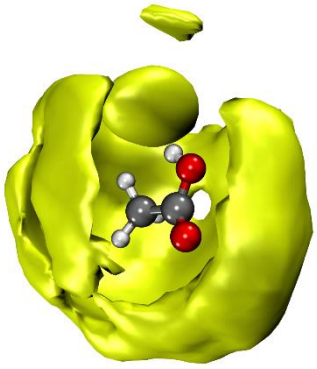

(b)

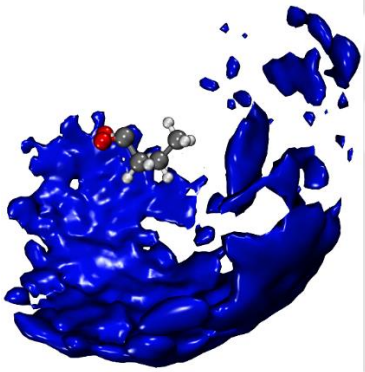

(c)

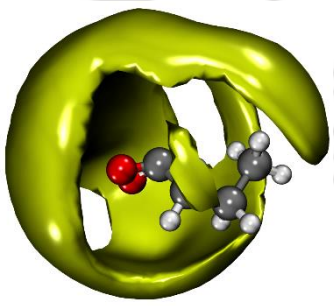

(d)

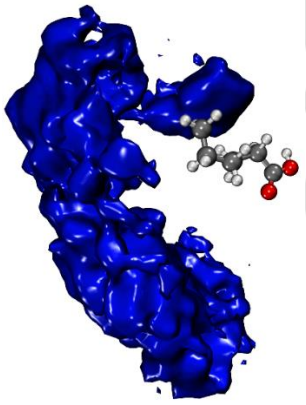

(e)

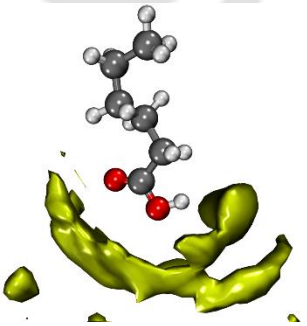

(f)

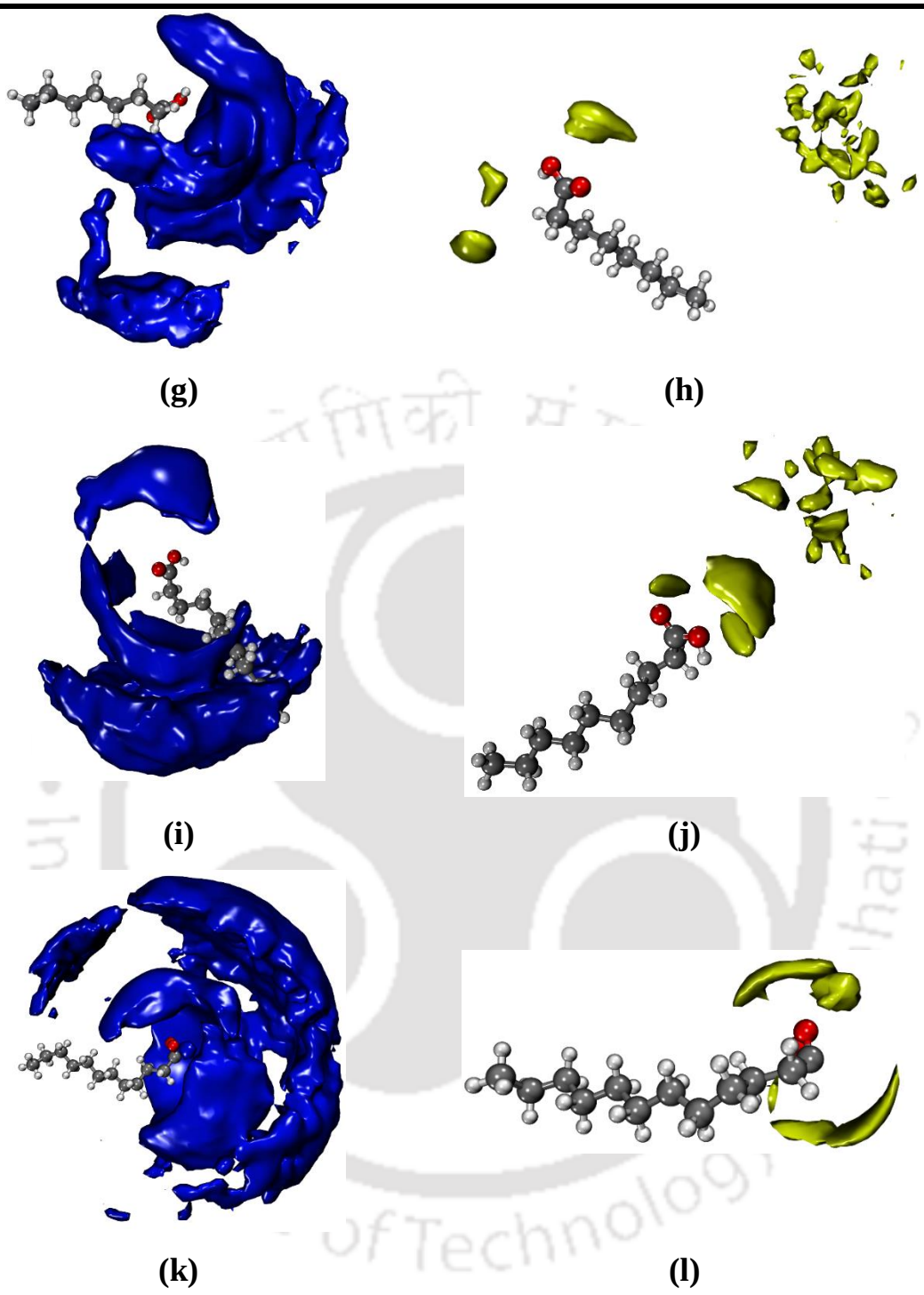

Figure B.7: Spatial distribution functions (SDFs) of DL-menthol (HBA) (left side) and water molecules (right side) around respective carboxylic acids (HBDs) of different DESs calculated from the MD simulations of the DL menthol- carboxylic acid (DES)-water system. Menthol (in blue) and water (in yellow) around (a,b) acetic acid, (c,d) butanoic acid, (e,f) hexanoic acid, (g,h) octanoic acid, (i,j) decanoic acid, and (k,l) dodecanoic acid. [menthol around carboxylic acid: isovalue of 2.1 particle nm^{-3}; water around carboxylic acid: isovalue of 20 particle nm^{-3}]

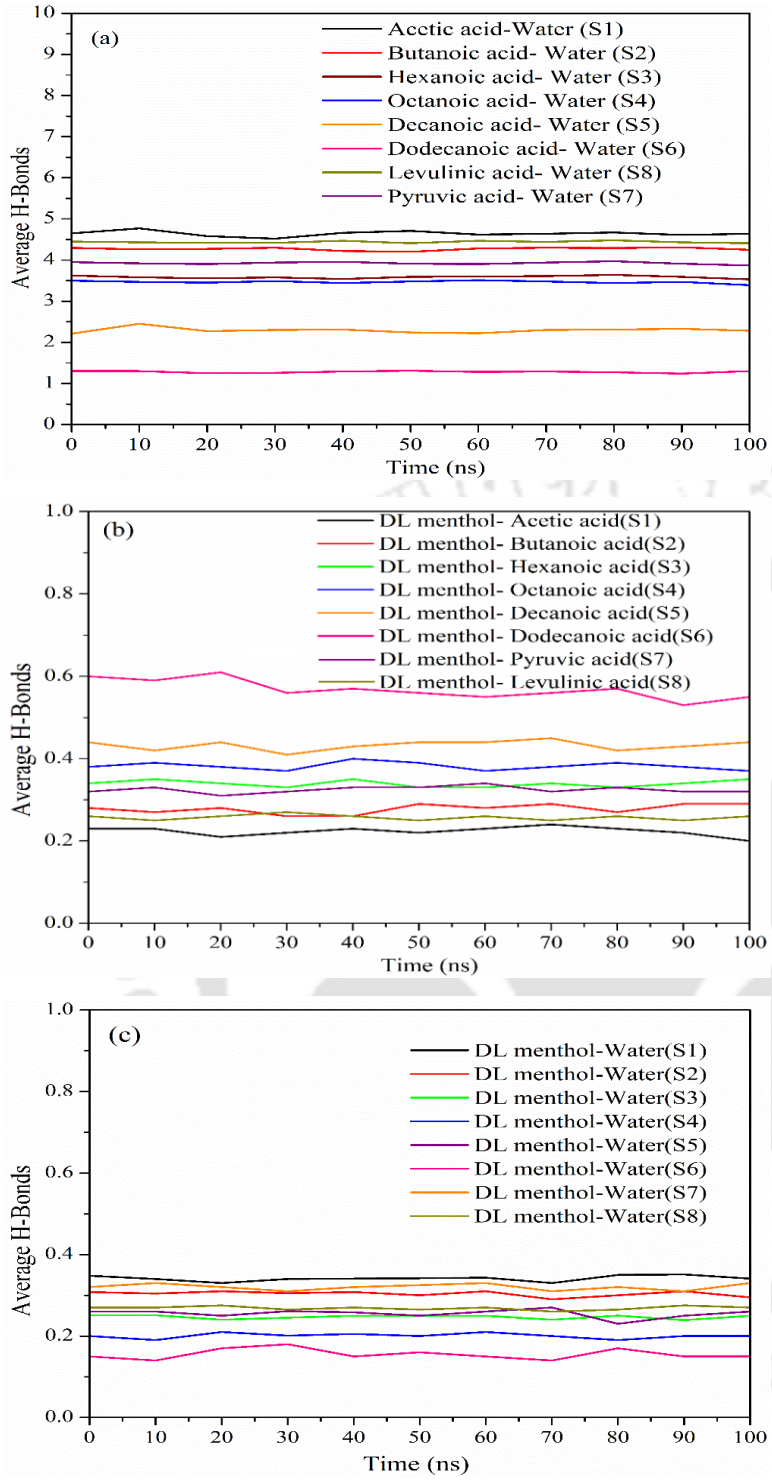

Figure B.8: Averaged out plot of the average number of hydrogen bonds between (a) HBD-water per HBD molecule; (b) HBA-HBD per DES molecule; and (c) HBA- water per HBA molecule, for the DL-menthol based systems (S1 to S8), as a function of simulation time

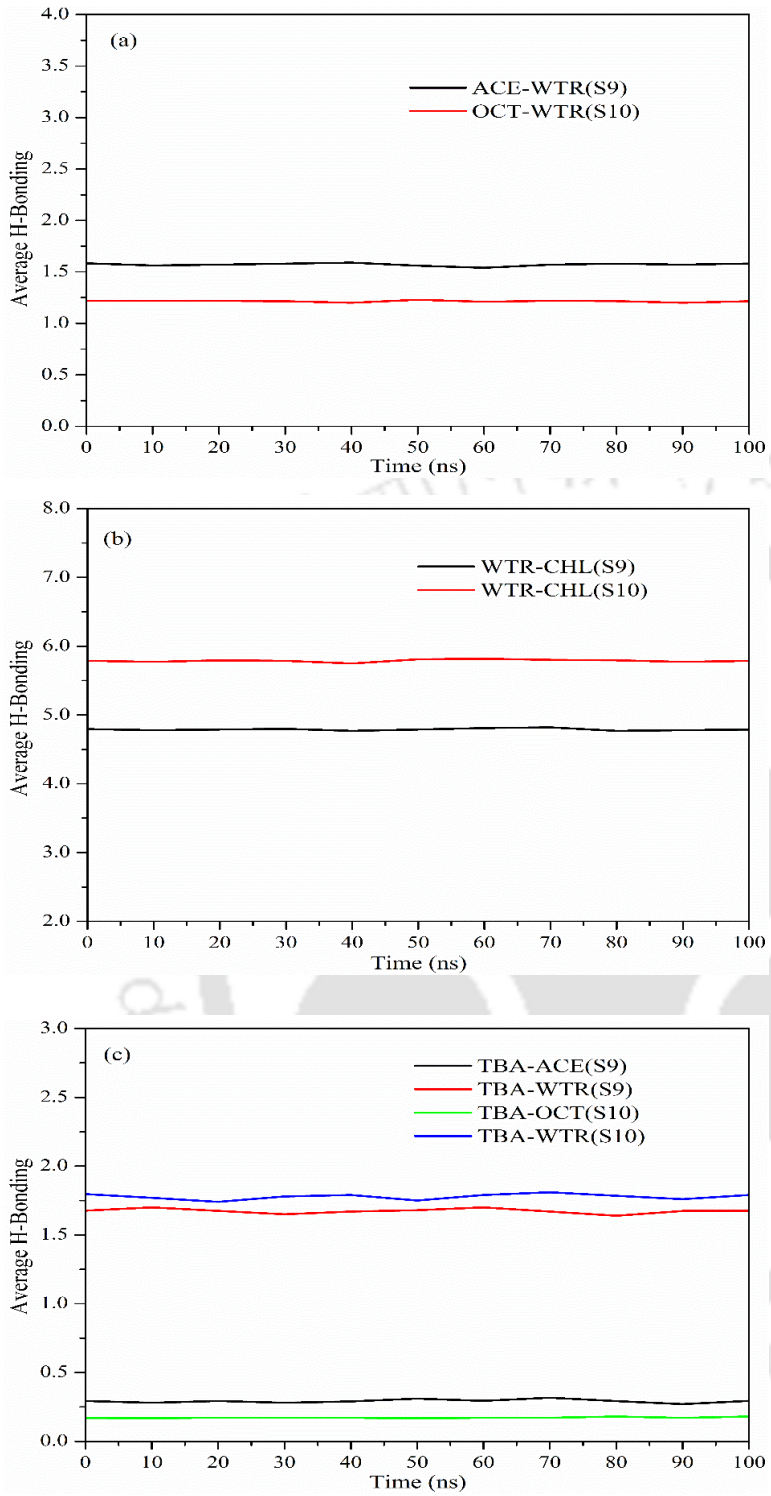

Figure B.9: Averaged out plot of the average number of hydrogen bonds between (a) HBD-water per HBD molecule; (b) chloride anion- water per chloride ion; (c) tetrabutylammonium cation - HBD and tetrabutylammonium cation - water for system S9 and S10; as a function of simulation time

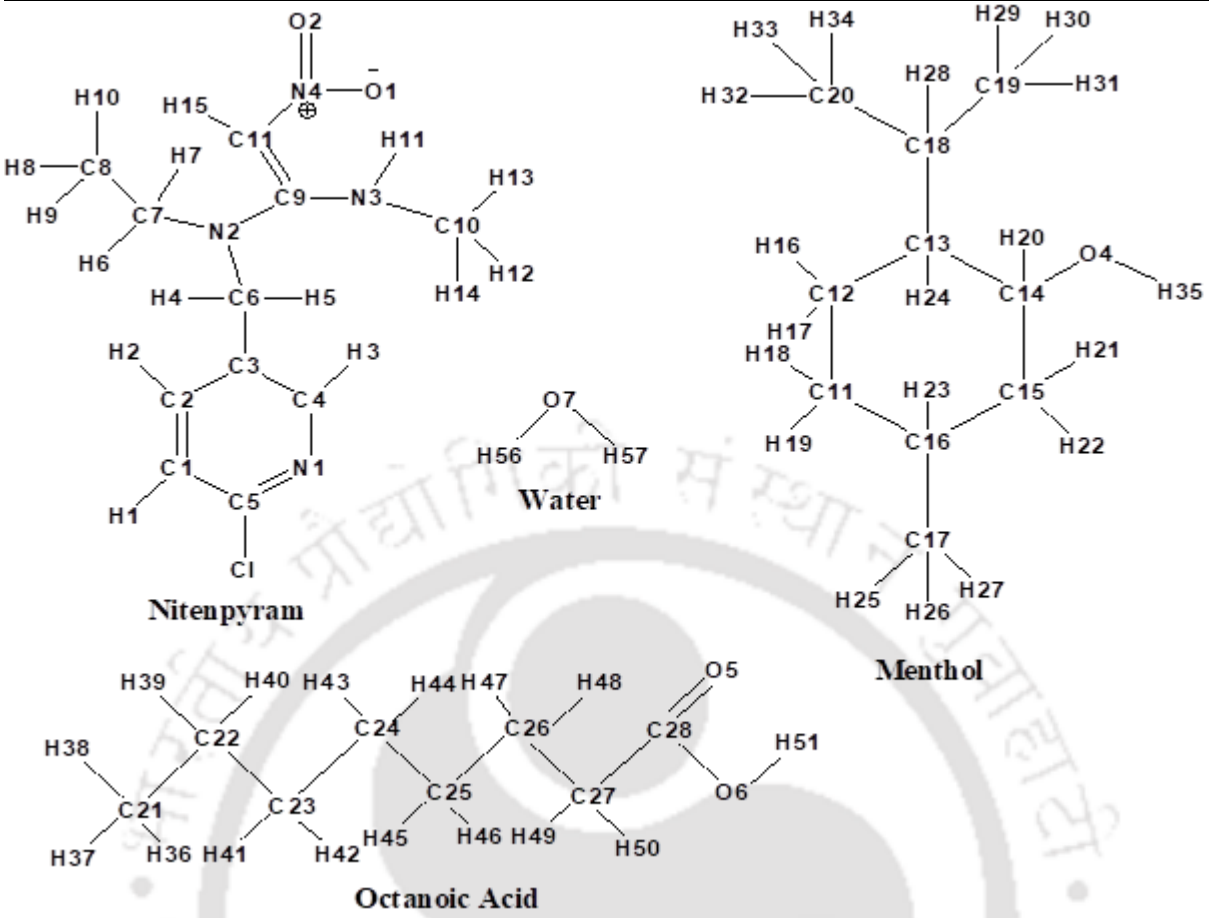

Figure B.10: Structures of different components with atom notation used in the extraction of pesticide

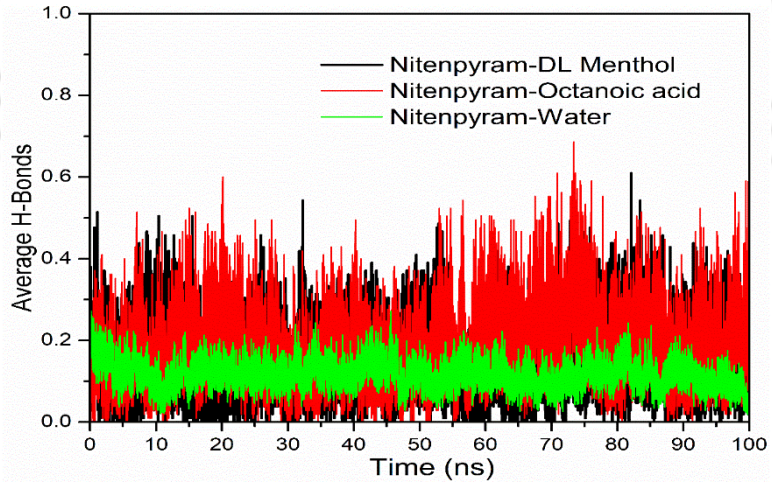

Figure B.11: Average number of NIT-DLM, NIT-OCT and NIT-water hydrogen bonds as a function of simulation time

C Appendix (Chapter-3)

Table C.1: Maximal iso-values (I_{max}), chosen optimum iso-values (I_{opt}) and resulting percentages (P in %) from the upper limit of SDFs iso-surface intensities with color arrangements are presented for the acetamiprid and imidacloprid systems.

Color	Acetamiprid- DL menthol- Dodecanoic acid- Water			Imidacloprid- DL menthol- Dodecanoic acid- Water		
	I_{max}	I_{opt}	P (%)	I_{max}	I_{opt}	P (%)
Blue	1.90	1.40	73.57	1.42	2.03	70.10
Red	1.04	0.76	73.57	3.27	4.66	70.10
Green	38.90	28.62	73.57	38.06	26.64	70.10

Appendix - C

Table C.2: Theoretically obtained HOMO, LUMO (Ground and Excited State), Energy Gap, Chemical Hardness (η), and Chemical Potential (μ) computed in DFT-B3LYP and M06-2X method (All the units are in Hartree)

Systems	Method	HOMO energy	LUMO energy	Energy gap	HOMO-1 energy	LUMO+1 energy	Energy gap	η	μ
Acetamiprid	B3LYP	-0.25397	-0.0634	0.19057	-0.27364	-0.05359	0.22005	0.095285	-0.15869
	M06-2X	-0.30505	-0.02581	0.27924	-0.32493	-0.01708	0.30785	0.13962	-0.16543
Imidacloprid	B3LYP	-0.24891	-0.09144	0.15747	-0.27658	-0.06413	0.21245	0.078735	-0.17018
	M06-2X	-0.30401	-0.03737	0.26664	-0.32433	-0.02659	0.29774	0.13332	-0.17069
DES1 [DLM-DODEC]	B3LYP	-0.27852	-0.00304	0.27548	-0.28776	-0.00091	0.28685	0.13774	-0.14078
	M06-2X	-0.33939	0.00856	0.34795	-0.35079	0.01394	0.36473	0.173975	-0.16542
DES2 [DLM-OCT]	B3LYP	-0.27868	-0.00366	0.27502	-0.28741	-0.0005	0.28691	0.13751	-0.14117
	M06-2X	-0.33917	0.00855	0.34772	-0.34884	0.01398	0.36282	0.17386	-0.16531
Acetamiprid+ DES1	B3LYP	-0.24513	-0.0447	0.20043	-0.2705	-0.04874	0.22176	0.100215	-0.14492
	M06-2X	-0.29885	-0.01875	0.2801	-0.32234	-0.01419	0.30815	0.14005	-0.1588
Imidacloprid+ DES2	B3LYP	-0.24007	-0.07574	0.16433	-0.27174	-0.05928	0.21246	0.082165	-0.15791
(DES intramolecular)	M06-2X	-0.29881	-0.03031	0.2685	-0.32197	-0.02427	0.2977	0.13425	-0.16456
Imidacloprid+ DES2	B3LYP	-0.24643	-0.09065	0.15578	-0.25291	-0.06961	0.1833	0.07789	-0.16854
(DES intermolecular)	M06-2X	-0.30064	-0.03861	0.26203	-0.32097	-0.03099	0.28998	0.131015	-0.16963

Table C.3: Partial Charges of all the atoms of different molecular species

DL-menthol		Imidacloprid		Octanoic acid		Acetamiprid		Dodecanoic acid	
Atom type	**Partial charge**	**Atom type**	**Partial charge**	**Atom type**	**Partial charge**	**Atom type**	**Partial charge**	**Atom type**	**Partial charge**
C1	-0.189206	C11	0.409681	C20	-0.308932	C11	0.414298	C21	-0.304857
H3	0.058027	H21	0.055126	H31	0.069673	H21	0.049969	H32	0.067749
H4	0.058027	N5	-0.606175	H32	0.069673	N1	-0.629697	H33	0.067749
C2	-0.162554	C12	-0.088662	H33	0.069673	C12	-0.142103	H34	0.067749
H1	0.052018	C16	-0.614811	C21	0.191054	C16	-0.332518	C22	0.196597
H2	0.052018	H24	0.255348	H34	-0.029995	H24	0.169132	H35	-0.032847
C3	0.084112	H25	0.255348	H35	-0.029995	H25	0.169132	H36	-0.032847
H9	0.040931	N3	-0.055303	C22	-0.003810	N2	-0.083840	C23	-0.003457
C8	0.294800	C17	-0.362324	H36	-0.002271	C17	-0.279545	H37	-0.004852
H13	0.023503	C18	0.265375	H37	-0.002271	H26	0.120306	H38	-0.004852
C9	-0.432540	H28	0.038759	C23	-0.034935	H27	0.120306	C24	-0.022894
H14	0.097230	H29	0.038759	H38	0.000397	H28	0.120306	H39	-0.009184
H15	0.097230	N4	-0.715811	H39	0.000397	C20	0.572025	H40	-0.009184
H16	0.097230	C19	0.804777	C24	0.052343	C18	-0.308781	C25	0.089169
C10	-0.432540	N1	-0.699928	H40	-0.012444	H29	0.109989	H41	-0.027108
H17	0.097230	H30	0.422880	H41	-0.012444	H30	0.109989	H42	-0.027108
H18	0.097230	N2	0.803594	C25	0.016689	H31	0.109989	C26	0.032018
H19	0.097230	O2	-0.417302	H42	0.017120	N3	-0.660631	H43	-0.014595
C4	0.254862	O3	-0.417302	H43	0.017120	C19	0.615960	H44	-0.014595
H5	0.025419	H26	0.155748	C26	-0.187542	N4	-0.611736	C27	0.004193
O1	-0.748355	H27	0.155748	H44	0.081235	C13	0.083262	H45	-0.010482
H20	0.444137	C13	0.103952	H45	0.081235	H22	0.152022	H46	-0.010482
C5	-0.475968	H22	0.111768	C27	0.807784	C14	-0.396752	C28	0.044887
H6	0.133764	C14	-0.379591	O5	-0.702213	H23	0.183203	H47	-0.011808
H7	0.133764	H23	0.184777	H46	0.464571	C15	0.487519	H48	-0.011808
C6	0.386348	C15	0.449338	O4	-0.612112	Cl	-0.141803	C29	0.001536
H8	-0.027666	Cl	-0.153770					H49	-0.002977
C7	-0.519159	**Water (IMD system)**				**Water (ACD system)**		H50	-0.002977
H10	0.120959	**Atom type**	**Partial charge**			**Atom type**	**Partial charge**	C30	0.005170
H11	0.120959							H51	0.016467
H12	0.120959	O6	-0.810208			O6	-0.810208	H52	0.016467
		H47	0.405104			H56	0.405104	C31	-0.154553
		H48	0.405104			H57	0.405104	H53	0.070812
								H54	0.070812

Appendix - C

								C32	0.812934
								O3	-0.700429
								H55	0.464201
								O2	-0.614613

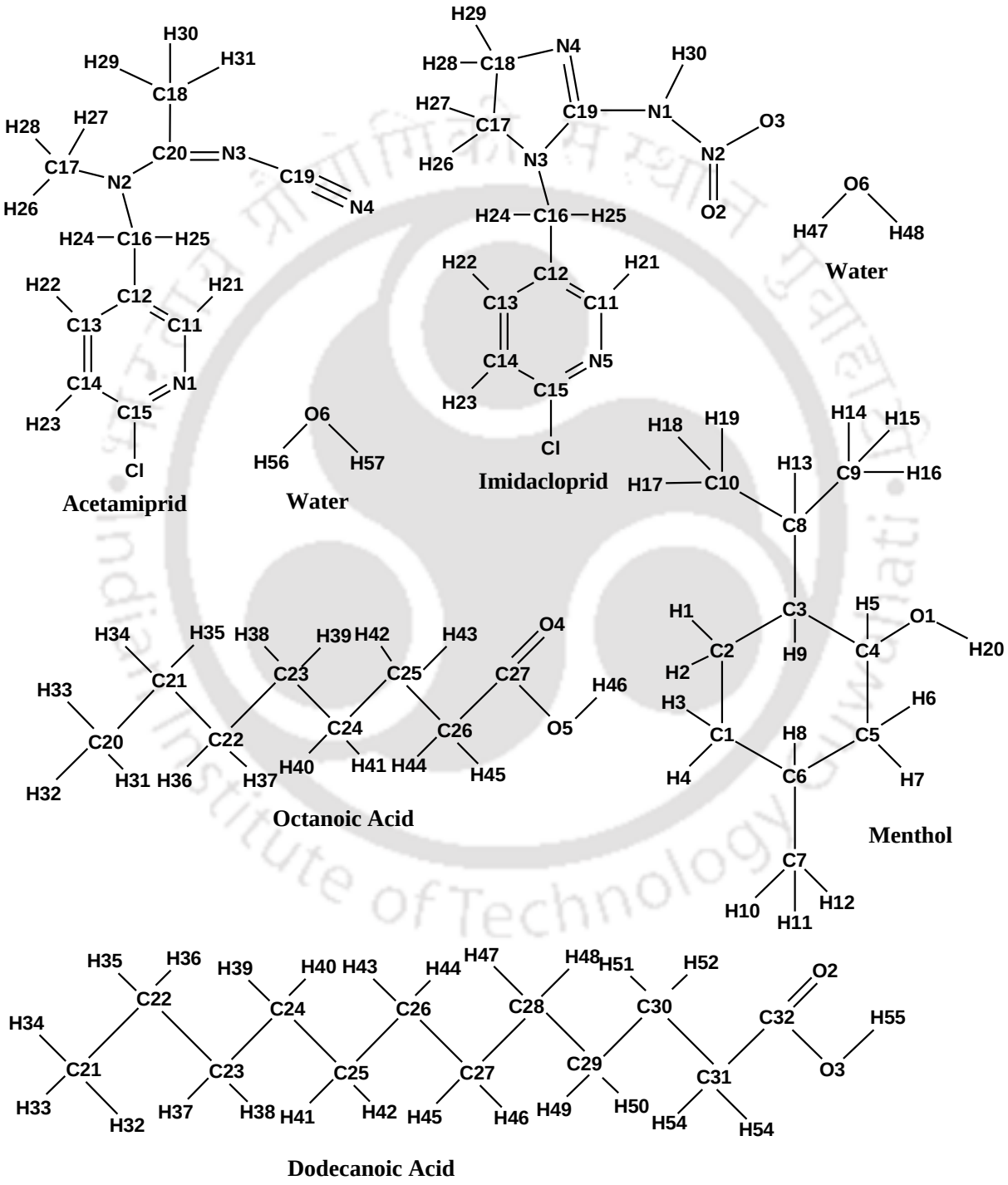

Figure C.1: Structures of the molecules with atom notations

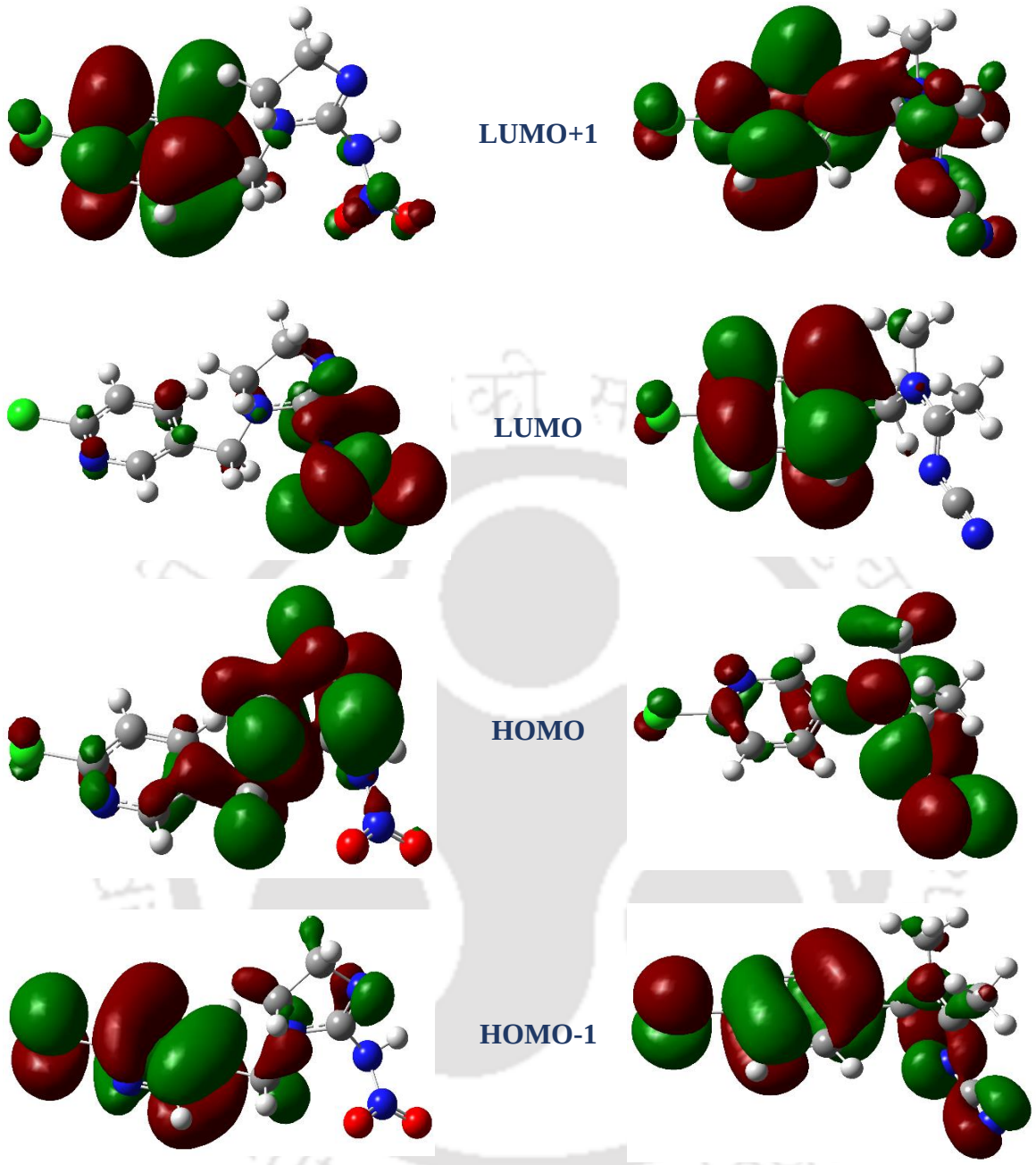

Figure C.2: HOMO−LUMO iso-surfaces of (a) imidacloprid and (b) acetamiprid

D Appendix (Chapter-4)

Table D.1: Extraction efficiencies (% EE) of enoxacin using hydrophobic DESs at different DES/water mass ratio and initial concentration

Mass ratio (DES/ water) / DESs	Extraction Efficiencies (% EE)								
	Initial Concentration: 20 ppm			Initial Concentration: 10 ppm			Initial Concentration: 5 ppm		
	1:1	1:2	1:3	1:1	1:2	1:3	1:1	1:2	1:3
DL-menthol: C_{10}	82.62 ± 1.25	63.24 ± 0.75	63.35 ± 0.77	74.61 ± 0.9	57.22 ± 1.02	52.54 ± 0.7	69.77 ± 1.2	54.48 ± 0.6	47.83 ± 1.2
DL-menthol: C_{12}	79.62 ± 0.9	60.46 ± 0.8	49.10 ± 0.85	73.03 ± 0.88	60.56 ± 0.84	46.08 ± 0.5	68.77 ± 1.04	52.74 ± 0.78	43.83 ± 1.5
C_{12}: C_{10}	69.14 ± 0.78	67.30 ± 1.03	69.17 ± 0.5	66.20 ± 0.8	61.12 ± 1.03	65.13 ± 0.45	64.47 ± 0.95	53.88 ± 0.45	51.29 ± 1.15

Table D.2: Distribution ratio of enoxacin between DES phase and aqueous phase

Mass ratio (DES/ water) / DESs	Distribution Ratio								
	Initial Concentration: 20 ppm			Initial Concentration: 10 ppm			Initial Concentration: 5 ppm		
	1:1	1:2	1:3	1:1	1:2	1:3	1:1	1:2	1:3
DL-menthol: C_{10}	4.75	1.72	1.73	2.94	1.34	1.11	2.31	1.20	0.92
DL-menthol: C_{12}	3.91	1.53	0.96	2.70	1.54	0.85	2.20	1.12	0.78
C_{12}: C_{10}	2.24	2.06	2.24	1.96	1.57	1.87	1.81	1.17	1.05

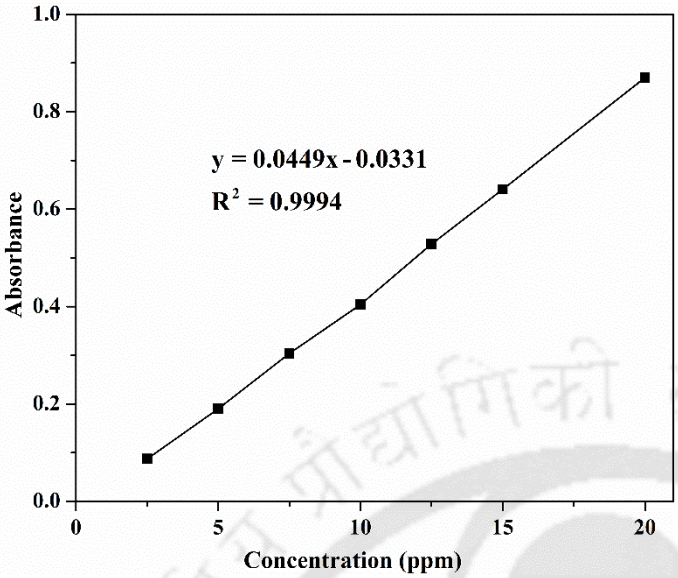

Figure D.1: Calibration plot of enoxacin solution in water at different concentrations. All the values were taken from the 50% diluted solution

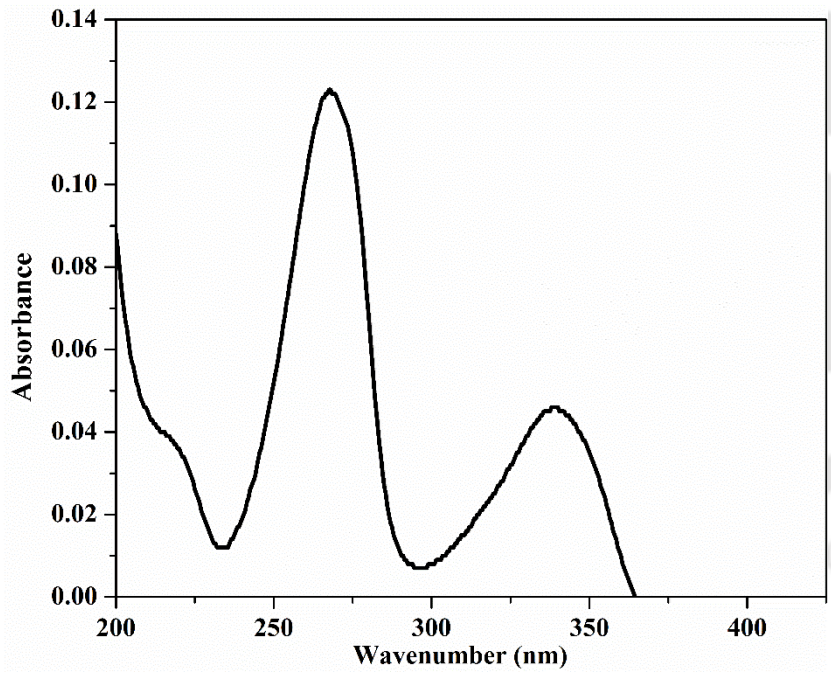

Figure D.2: UV-visible spectra of water phase after enoxacin extraction by DES1 at DES phase/ water phase mass ratio of 1:1 and at initial concentrations of 20 ppm

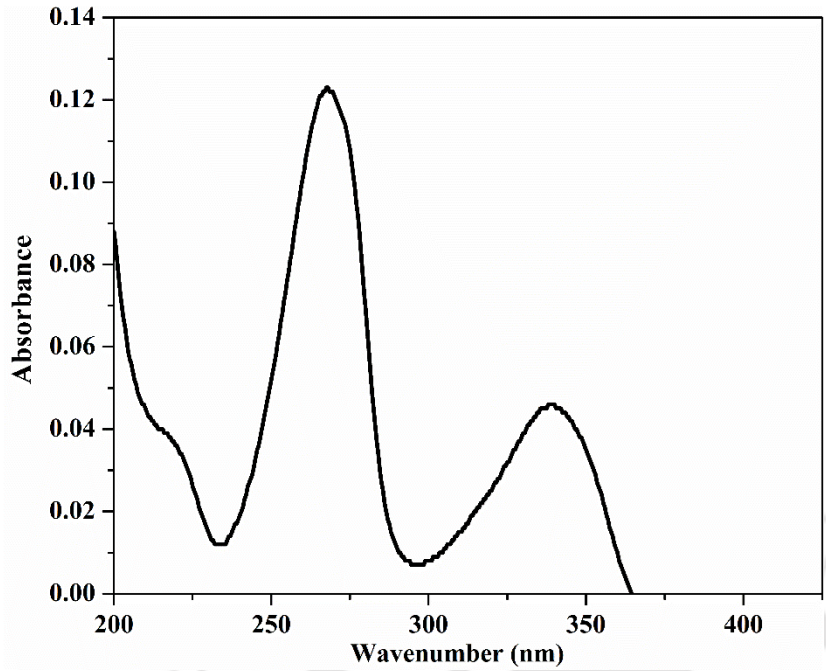

Figure D.3: UV-visible spectra of water phase after enoxacin extraction by DES1 at DES phase/ water phase mass ratio of 1:2 and at initial concentrations of 20 ppm

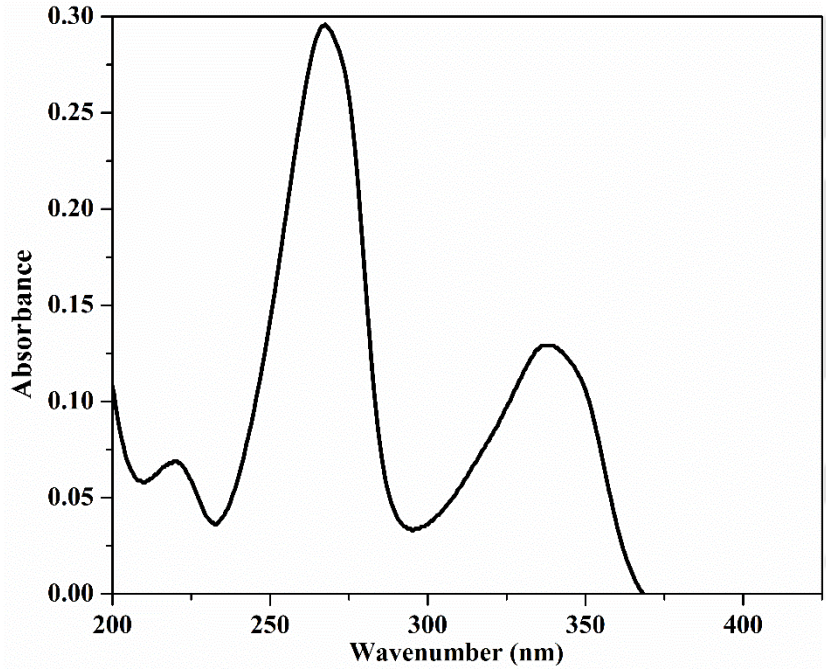

Figure D.4: UV-visible spectra of water phase after enoxacin extraction by DES1 at DES phase/ water phase mass ratio of 1:3 and at initial concentrations of 20 ppm

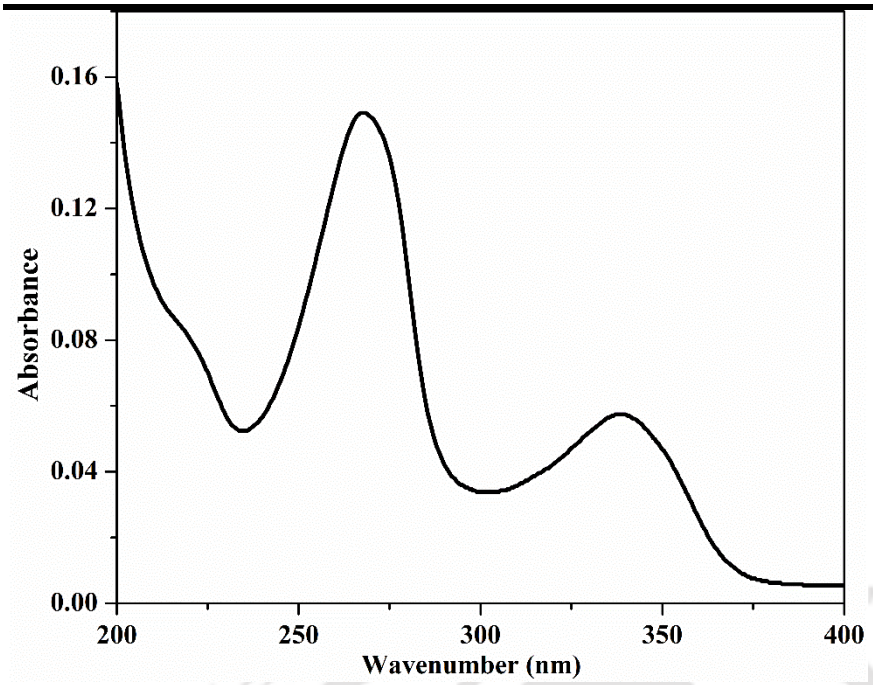

Figure D.5: UV-visible spectra of water phase after enoxacin extraction by DES2 at DES phase/ water phase mass ratio of 1:1 and at initial concentrations of 20 ppm

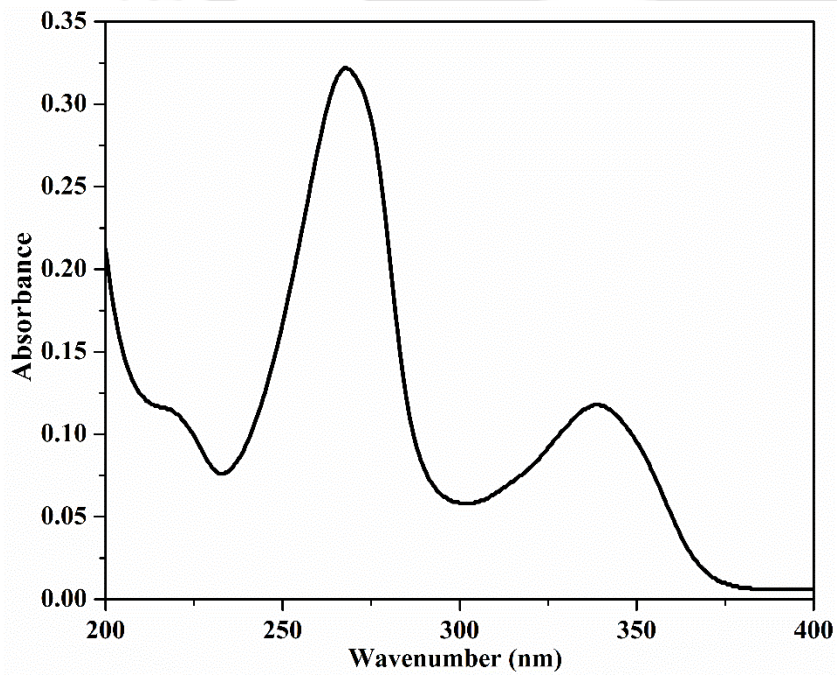

Figure D.6: UV-visible spectra of water phase after enoxacin extraction by DES2 at DES phase/ water phase mass ratio of 1:2 and at initial concentrations of 20 ppm

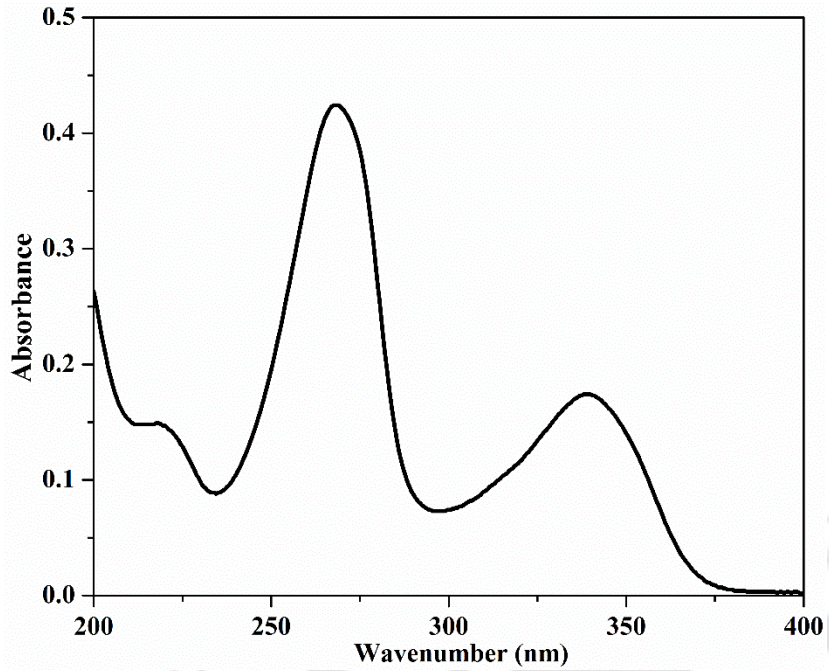

Figure D.7: UV-visible spectra of water phase after enoxacin extraction by DES2 at DES phase/ water phase mass ratio of 1:3 and at initial concentrations of 20 ppm

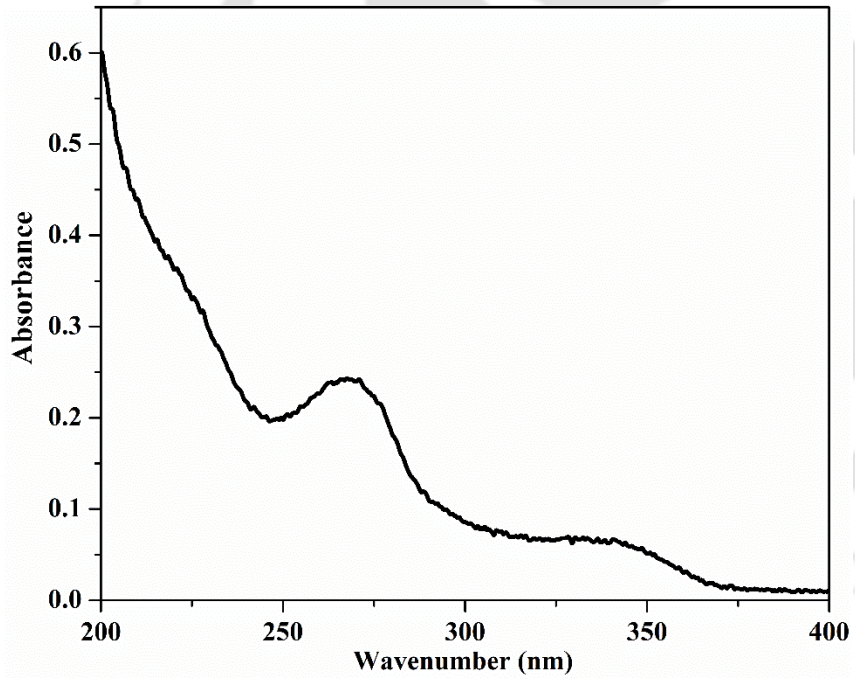

Figure D.8: UV-visible spectra of water phase after enoxacin extraction by DES3 at DES phase/ water phase mass ratio of 1:1 and at initial concentrations of 20 ppm

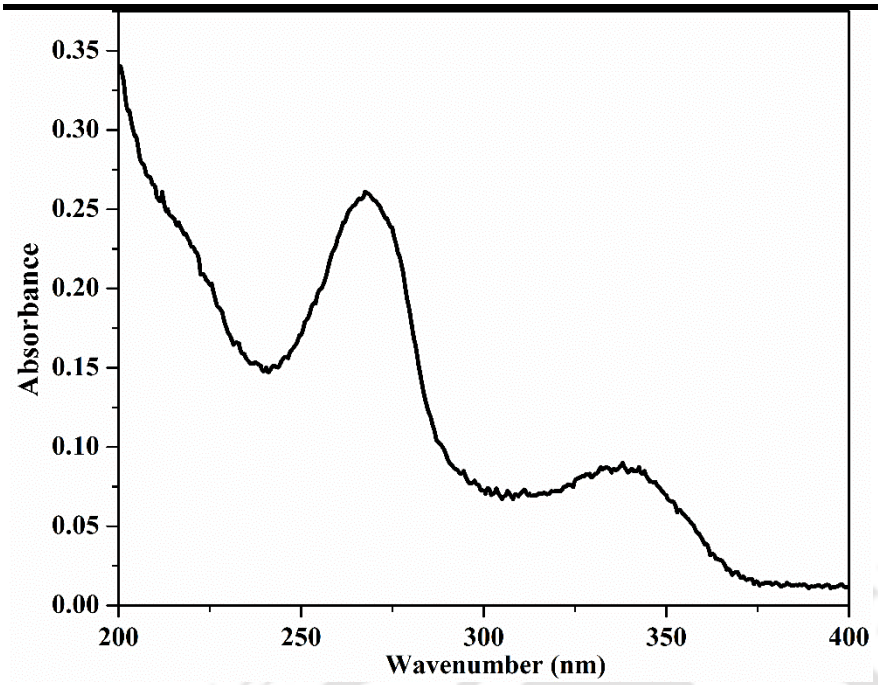

Figure D.9: UV-visible spectra of water phase after enoxacin extraction by DES3 at DES phase/ water phase mass ratio of 1:2 and at initial concentrations of 20 ppm

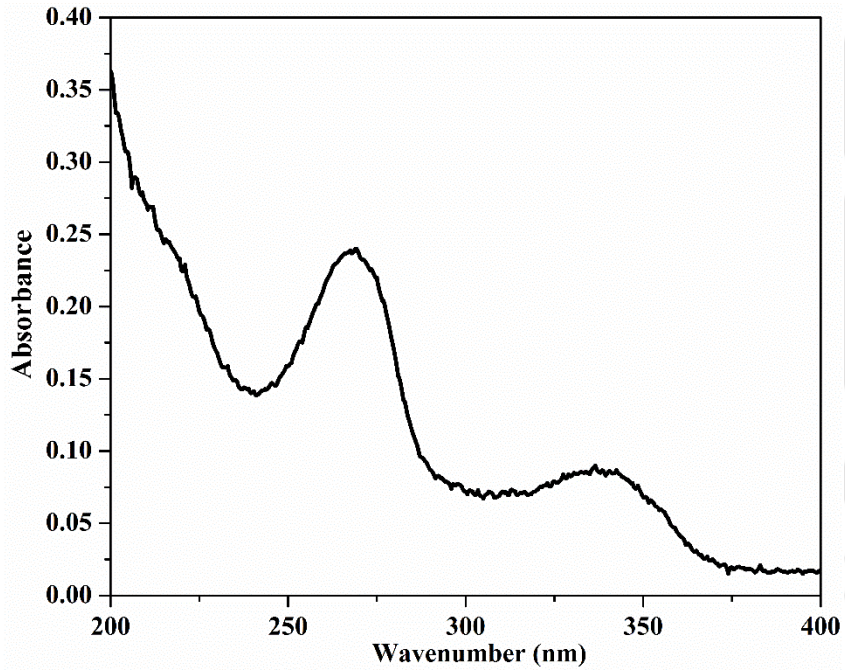

Figure D.10: UV-visible spectra of water phase after enoxacin extraction by DES3 at DES phase/ water phase mass ratio of 1:3 and at initial concentrations of 20 ppm

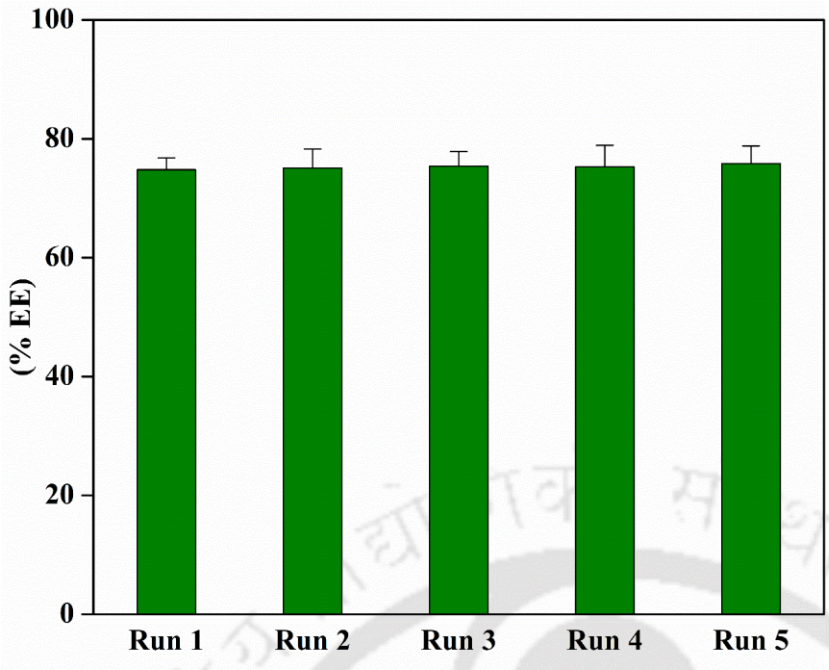

Figure D.11: Extraction and recycling performances of DL-menthol: decanoic acid (1:1) DES at a DES/water mass ratio of 1:1 and 10 ppm initial enoxacin concentration for various extraction cycles using AC as an adsorbent in DES phase at 25 °C for recycle process 1

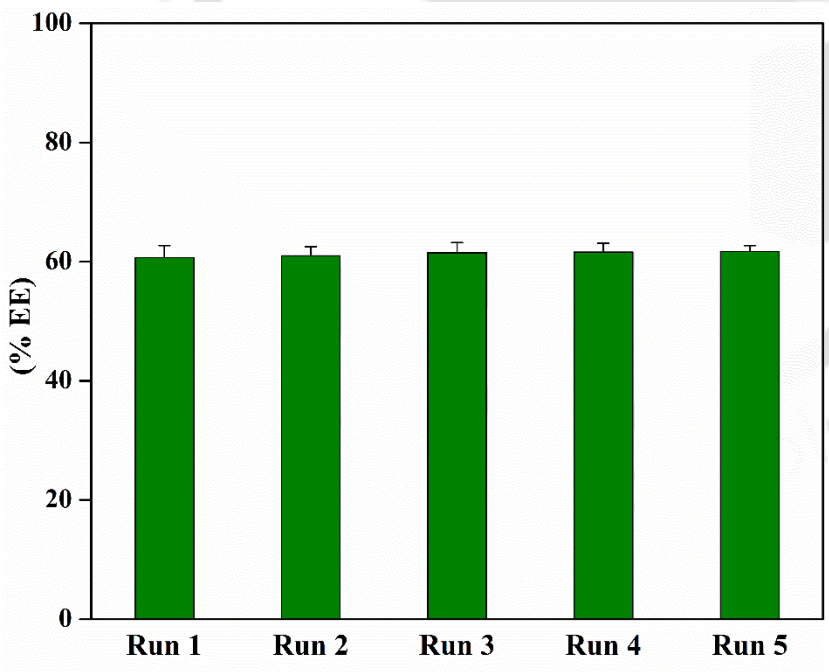

Figure D.12: Extraction and recycling performances of DL-menthol: decanoic acid (1:1) DES at a DES/water mass ratio of 1:2 and 20 ppm initial enoxacin concentration for various extraction cycles using AC as an adsorbent in DES phase at 25 °C for recycle process 1

E Appendix (Chapter-5)

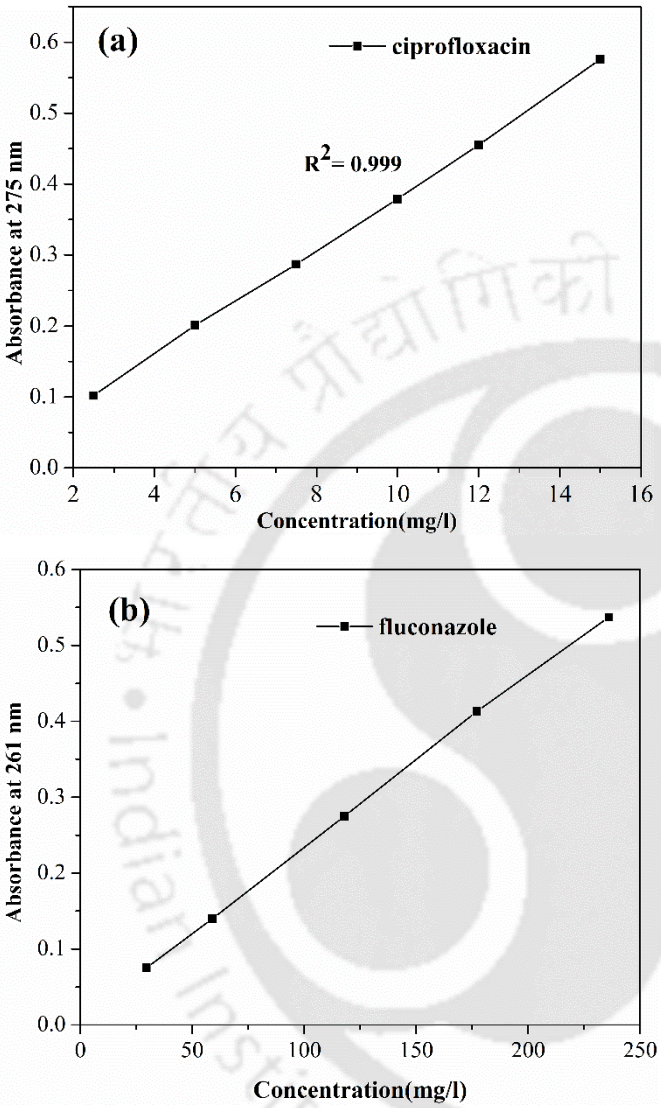

Figure E.1: Calibration plot of (a) ciprofloxacin and (b) fluconazole solution in water at different concentrations

List of Publications

Published Book

1. P.K. Naik, N. Kumar, N. Paul, T. Banerjee, Deep Eutectic Solvents in Liquid-Liquid Extraction: Correlation and Molecular Dynamics Simulation (1st ed.). CRC Press. (2022). https://doi.org/10.1201/9781003231158.

Journal Publications

1. **N. Paul**, P.K. Naik, B.D. Ribeiro, P.S. Gooh Pattader, I.M. Marrucho, T. Banerjee, Molecular Dynamics Insights and Water Stability of Hydrophobic Deep Eutectic Solvents Aided Extraction of Nitenpyram from an Aqueous Environment, *J. Phys. Chem. B.* 124 (2020) 7405–7420. https://doi.org/10.1021/acs.jpcb.0c03647.
2. **N. Paul**, T. Banerjee, Study on the Extraction of Acetamiprid and Imidacloprid from an Aqueous Environment Using Menthol-Based Hydrophobic Eutectic Solvents: Quantum Chemical and Molecular Dynamics Insights, *ACS Sustain. Chem. Eng*. 10 (2022) 4227–4246. https://doi.org/10.1021/acssuschemeng.2c00023.
3. **N. Paul**, G. Harish, T. Banerjee, Decontamination of enoxacin containing aqueous phase through hydrophobic deep eutectic solvents: solvent regeneration and quantum chemical insights, *J. Mol. Liq.*, 374 (2023) 121254.
4. **N. Paul**, T. Banerjee, Stability Mechanism of Menthol and Fatty Acid Based Hydrophobic Eutectic Solvents: Insights from Nonbonded Interactions, *ACS Sustain. Chem. Eng.*, 11 (2023) 3539−3556.
5. **N. Paul**, S. K. Singh, P.S. Gooh Pattader, T. Banerjee, Enhancement of the Extraction Performance of Ciprofloxacin and Fluconazole via Microchannel-based Solvent Extraction with Hydrophobic Deep Eutectic Solvent- a Combined Experimental and MD Simulation Study. (ready for submission)

Book Chapter

1. **N. Paul**, T. Banerjee, Micropollutants Extraction from Aqueous Systems using Ionic Liquids and Deep Eutectic Solvents, RSC Publications. (accepted)

Other Articles

1. A. Dutta, D. Kundu, S. Sharma, **N. Paul**, P.K. Naik, D. S. Silvestere, T. Banerjee, Physically cross-linked titania-supported novel eutectogels as solid-state electrolytes for supercapacitors: an experimental and quantum chemical investigation. (submitted in ACS Sustainable Chemistry & Engineering)

Conference Proceedings Conference Proceedings

1. **N. Paul**, T. Banerjee, Quantum Chemical studies on desulfurization of organosulfur compounds from fuel oil with extractive-oxidation by menthol based deep eutectic solvents, Advances in Chemical Engineering, Assam Engineering College, Guwahati, August 30, 2019.
2. **N. Paul**, T. Banerjee, Molecular Dynamics Simulation on the Extraction of pesticide from Aqueous Phase by Hydrophobic DES, Complex Fluids Symposium 2020, IIT Bombay and the Indian Society of Rheology, December 10-12, 2020.
3. **N. Paul**, Molecular Modeling Strategies for Hydrophobic Deep Eutectic Solvents, Scheme for Promotion of Academic and Research Collaboration (SPARC) Symposium, IIT Guwahati, Assam, India, March 10–13, 2021.
4. **N. Paul**, T. Banerjee, Molecular Dynamics Study of the Extraction of Thiamethoxam from an Aqueous Environment with Menthol- based Deep Eutectic Solvent, ASREEM-2021, Sardar Vallabhbhai National Institute of Technology, Surat (India) on August 06 – 08, 2021.
5. **N. Paul**, T. Banerjee, A Quantum Chemical Evaluation of the Extraction Mechanism of Imidacloprid from Aqueous Environment by Hydrophobic Eutectic Solvent, NERC, Assam Biotech Conclave-2022, IIT Guwahati, May 20-22, 2022.

Workshops and Short Term Courses

1. "Introduction to Gaussian: Theory and Practice" Workshop Organized by Gaussian Inc. USA and SCUBE Scientific Software Solutions, Kolkata, India, January 14-18, 2019.
2. Short Term Course titled "Ionic Liquids and Deep Eutectic Solvents with Nature", sponsored by Scheme for Promotion of Academic and Research Collaboration (SPARC), at Indian Institute of Technology Guwahati, Assam, India, March 10-13, 2021.

3. Invited Speaker on the Topic “Deep Eutectic Solvent: A new class of Green Solvent” in 6 Days Workshop on “Recent trends in Engineering on Emerging Technologies” organized by the Department of Chemical Engineering, NIT Agartala, October 17-22, 2022.